NOTICE

The quality of this microform is heavily dependent upon the quality of the original thesis submitted for microfilming. Every effort has been made to ensure the highest quality of reproduction possible.

If pages are missing, contact the university which granted the degree.

Some pages may have indistinct print especially if the original pages were typed with a poor typewriter ribbon or if the university sent us an inferior photocopy.

Reproduction in full or in part of this microform is governed by the Canadian Copyright Act, R.S.C. 1970, c. C-30, and subsequent amendments.

AVIS

La qualité de cette microforme dépend grandement de la qualité de la thèse soumise au microfilmage. Nous avons tout fait pour assurer une qualité supérieure de reproduction.

S'il manque des pages, veuillez communiquer avec l'université qui a conféré le grade.

La qualité d'impression de certaines pages peut laisser à désirer, surtout si les pages originales ont été dactylographiées à l'aide d'un ruban usé ou si l'université nous a fait parvenir une photocopie de qualité inférieure.

La reproduction, même partielle, de cette microforme est soumise à la Loi canadienne sur le droit d'auteur, SRC 1970, c. C-30, et ses amendements subséquents.

THE CONFORMATIONAL HETEROGENEITY OF PROTEINS

CINDY MARY–LYNN HUTNIK

Thesis submitted to
the School of Graduate Studies and Research
in partial fulfillment of the requirements for the degree of
Doctor of Philosophy in Biochemistry

University of Ottawa

ISBN 0-315-60041-1

UNIVERSITÉ D'OTTAWA
UNIVERSITY OF OTTAWA

" New opinions are always suspected, and usually opposed, without any other reason but because they are not already common"

John Locke
Essay on Human Understanding

ABSTRACT

THE CONFORMATIONAL HETEROGENEITY OF PROTEINS

Cindy Mary–Lynn Hutnik
Department of Biochemistry
University of Ottawa, 1989

Time–correlated single photon counting and steady–state fluorescence spectroscopy were used to investigate the conformational properties of select proteins. Specifically, the role of naturally associated metal ions in modulating the conformation of members from two families of metalloproteins was examined.

Two homologous bacterial copper–containing azurins were purified from *Pseudomonas fluorescens* (ATCC 13525) and *Pseudomonas aeruginosa* (ATCC 10145). The intrinsic fluorescence of the native Cu(II) single tryptophan–containing protein, as well as experimentally prepared Cu(I), Ni(II), Co(II) and metal–free derivatives demonstrated that the metal centre of these redox proteins played an important role in the conformational heterogeneity of the protein. Such an effect was strongly dependent on the nature of the metal ion.

From the calcium–binding superfamily, the single–tryptophan containing isotype III component of parvalbumin was purified from codfish. The previous notion that this protein was a Ca(II)/Mg(II)–specific protein was shown to be due to an experimental artefact arising from the use of the soluble chelator EGTA. The Ca(II)–specific conformational changes of cod III parvalbumin were compared with those of the highly homologous Ca(II)–binding tumour protein oncomodulin. Since native tumour oncomodulin was devoid of tryptophan, a site–specific mutant of oncomodulin with tryptophan in the identical position of the parvalbumin tryptophan was examined. The results showed that the ability of oncomodulin to function as a modulator (unlike parvalbumin) may be due to relatively subtle Ca(II)–specific conformational changes. Details of these changes were obtained by an examination of a number of oncomodulin mutant proteins in which the non–fluorescent phenylalanine, and the highly fluorescent tryptophan had been substituted into various positions of the two Ca(II)–binding loops. The results demonstrated that the binding of the first equivalent of Ca(II) induced greater than 90% of the conformational changes experienced by various probed positions, but that the second equivalent of Ca(II) played an important role in orienting the two Ca(II)–binding loops relative to each other.

To all my life's teachers.

ACKNOWLEDGEMENTS

Throughout my last four years at the National Research Council of Canada I have had the privilege of working with a fine group of enthusiastic and competent individuals. I owe a great deal of thanks to a number of the research officers at the Division of Biological Sciences from whom I have obtained advice, as well as to many members of the technical and clerical staffs, the draftspersons and the photographers. The appearance of the work of this thesis in published journals would not have been possible without the assistance of these people and for this, I extend my sincere appreciation.

In particular, there are three NRC employees to whom I offer my deepest gratitude. Dr. Arthur G. Szabo, my thesis supervisor, did an exceptional job in guiding me through the work of this thesis, while at the same time giving me a tremendous independence to use my own resources in tackling the various research problems. His trust in my work and his patience when posed with my incessant questions, are truly commendable. Simply put, without Dr. Szabo and his expertise, this thesis, and all of the opportunities which the work spawned, would not have been possible.

The work with the calcium–binding proteins involved my collaboration with Dr. John P. MacManus. His efficiency, his high standards of professional and moral conduct, and his avoidance of superfluous research endeavours have provided a tremendous example. I would like to thank Dr. MacManus for the unselfish sharing of his insights, expert research skills and advice, which have undoubtedly contributed to the quality of work with the calcium–binding proteins. In the final hours, the gracious offer by Dr. MacManus to read this thesis and offer comments was just another example of the frequent willingness of this internationally–recognized scientist to extend himself beyond the call of duty.

I would also like to extend a special thanks to Mr. Don T. Krajcarski for all of the practical guidance and assistance in the operation of the equipment, and the handling of the computer programmes for data analysis. Mr. Krajcarski is clearly an integral component of Dr. Szabo's internationally acclaimed fluorescence laboratory.

In addition to the above, a special thanks is in store for Dr. Jacinta Drew, whose friendship and encouragement helped make the transition to graduate school most enjoyable. This enjoyment was also derived from my association with a number of graduate students at the University of Ottawa with whom I could always count on for friendly discussions.

Finally, there remains three very special people to acknowledge. The first two are my parents, Irene and Joseph Hutnik. Without their pride, joy and seemingly infinite store of love there would have been no emotional inspiration, and hence no thesis. The third person is my soon–to–be husband, Marc St–Amand. His pride and support of my PhD pursuits, and his companionship have provided an immeasurable contribution to this work.

In addition to the above individuals, the financial support of the Natural Sciences and Engineering Research Council of Canada, and the University of Ottawa over the last four years is gratefully acknowledged. To all of the above, I extend my sincere appreciation for making the attainment of a PhD a fond and memorable experience.

TABLE OF CONTENTS

LIST OF TABLES

LIST OF FIGURES

LIST OF ABBREVIATIONS

A	absorbance
ADC	analogue–to–digital converter
ASC	ascorbate ion
CD	circular dichroism
CFD	constant fraction discriminator
CM–	carboxymethyl–
CN	cyanide ion
CRO	cathode ray oscilloscope
CW	continuous wave
DAS	decay–associated spectra
DEAE–	diethylaminoethyl–
DTT	dithiothreitol
EDTA	ethylenediaminetetraacetic acid
EGTA	ethylene glycol bis(β–aminoethyl ether)–N, N'–tetraacetic acid
EX–M	excitation monochromator
FPLC	fast phase liquid chromatography
FWHM	full width at half maximum
HPLC	high performance liquid chromatography
IRF	instrument response function
KDP	potassium dihydrogen phosphate
LED	leading edge discriminator
MCA	multichannel analyzer
MCP	microchannel plate
ML	mode–locker
NATA	N–acetyltryptophanamide
ND	neutral density
NMR	nuclear magnetic resonance
OD	optical density
Pae	*Pseudomonas aeruginosa*
Pfl	*Pseudomonas fluorescens*
PMT	photomultiplier tube
PV	parvalbumin
SDS–PAGE	sodium dodecyl sulfate–polyacrylamide gel electrophoresis
SVR	serial variance ratio
TAC	time–to–amplitude converter
TCA	trichloroacetic acid
TCSPC	time–correlated single photon counting
TFA	trifluoroacetic acid
TRIS	tris(hydroxymethyl)aminomethane
UV	ultraviolet
WSSR	weighted sum of the squares of residuals

LIST OF SYMBOLS

A_r	absorbance of reference
A_s	absorbance of sample
c_i	relative component concentration of the ith component
$D_c(t)$	trial convolution function
$D_l(t)$	instrument response function
D_r	integrated area under the reference emission spectrum
D_s	integrated area under the sample emission spectrum
$D_s(t)$	fluorescence decay curve
F_i	fractional fluorescence of the ith component
$F_s(t)$	δ–pulse response of sample or true decay
$[F^*]$	concentration of fluorophore in the first excited state
$H(t)$	excitation function
I_a	rate–intensity of absorbed photons
$I(\lambda,t)$	fluorescence intensity observed at wavelength λ and time t
k_f	rate constant for fluorescence emission
k_{ic}	rate constant for internal conversion
k_{isc}	rate constant for intersystem crossing
k_{nr}	nonradiative rate constant
k_p	rate constant for photoreaction
k_q	rate constant for deactivation by a quencher
$L(t)$	δ–pulse response of the detection system
$[Q]$	concentration of diffusional quencher
S_0	ground electronic state
S_1	first excited singlet electronic state
t	time
E	energy of a photon
$\alpha_i(\lambda)$	preexponential term of the ith component at wavelength λ
ϵ	molar absorptivity
$\eta_d(r)$	refractive index of solvent in which reference is dissolved
$\eta_d(s)$	refractive index of solvent in which sample is dissolved
λ	wavelength
λ_{em}	wavelength of emission
λ_{ex}	wavelength of excitation
λ_{max}	wavelength of maximum intensity
ν	frequency
τ_i	singlet lifetime of the ith component
τ_r	radiative lifetime
τ_s	singlet lifetime

Chapter 1

INTRODUCTION

1.1 Protein Structure, Function and Flexibility

"The processes of life are turned on and off by means of a universal control mechanism that depends on the ability of protein molecules to bend flexibly from one shape to another under external influences."

Daniel E. Koshland, Jr., 1973

Proteins are biological macromolecules which are fundamental in all aspects of cell structure and function. There are many different kinds of proteins, each specialized for a different biological function. Some of these functions include enzymatic catalysis, transport and storage, oxidation–reduction mediation, coordinated motion, mechanical support, immune protection, excitability, and the control of growth and differentiation. One of the central problems in biochemistry has been the understanding of the relationship between the biological function of proteins and their structure (Lehninger, 1979).

Structurally, proteins are polymers derived from twenty monomeric units known as amino acids. These amino acids covalently link to form amide bonds by elimination of the elements of water from the α–carboxyl group of one amino acid and the α–amino group of the next. Figure 1.1 depicts a general structural formula for an α–amino acid. The portion in the box is common to all amino acids while the "R" represents the location of one of the twenty distinct sidechains.

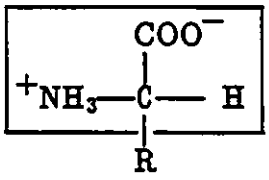

Figure 1.1: General structural formula for a zwitterionic α–amino acid in the naturally occurring L–configuration.

In its native state, each type of protein has a characteristic three–dimensional shape referred to as its conformation. Conformation is a general term which is often used to describe the combined effects of primary, secondary and tertiary levels of protein structure within a single polypeptide chain. The primary structure refers to the covalent backbone of the polypeptide chain and the sequence of its amino acid residues. Secondary structure refers to a regular, recurring arrangement in space of the polypeptide chain. Common secondary structural elements are known as the α–helix and the β–pleated sheet. Tertiary structure refers to how the polypeptide chain is bent or folded in three dimensions. Hydrogen and disulfide bonds linking different parts of the primary chain contribute to the stabilization of the secondary, and folded tertiary structures. As the word "conformation" refers to the spatial arrangement of substituent groups, a protein is described as conformationally heterogeneous if it is free to assume more than one structure without the breaking of bonds.

It is now generally accepted that an understanding of the dynamic ability of proteins to assume various conformations is essential to the understanding of the relationship between protein structure and function (Frauenfelder, 1989). As early as 1959, based primarily upon studies of deuterium–hydrogen exchange, it was suggested that a protein existed as a group of conformational states differing considerably in entropy (Linderstrom–Lang & Schellman, 1959). In 1966 the ability of oxygen to reach the binding site of the heme iron in hemoglobin and myoglobin, led Perutz and Mathews (1966) to conclude that these proteins must have flexible elements. However the view of the protein as a strongly fluctuating system (Gurd & Rothgeb, 1979) was challenged by the impact of the appearance of remarkably detailed, yet static X–ray crystallographic structures of proteins. These rigid

structures tempted many to cling to explanations of "lock–and–key" type mechanisms of protein function despite a growing amount of evidence in favour of protein conformational flexibility (Karplus & McCammon, 1981). As a result, it was not until the 1980's that protein flexibility was generally accepted as playing a crucial role in the biological function of proteins (Debrunner & Frauenfelder, 1982).

1.2 The Measurement of Protein Conformational Fluctuations

The characteristic times of motions within proteins at physiological temperatures range over more than 12 orders of magnitude, from below picoseconds to well above seconds (Frauenfelder, 1989). The measurement of these motions has been accomplished by many different spectroscopic and kinetic techniques (Peticolas, 1978; Gurd & Rothgeb, 1979; Williams, 1989), as well as by theoretical studies involving computer simulations (McCammon & Karplus, 1980; Levitt & Sharon, 1988). The ability of most proteins containing tyrosine and/or tryptophan to fluoresce, and the sensitivity of that fluorescence to the conformational state of the protein, has established fluorescence spectroscopy as a well–suited technique for the experimental determination of protein conformational heterogeneity.

1.2.1 Spectroscopy -- Absorption and Fluorescence

Spectroscopy is the study of the interaction of light with matter. Light is a form of energy known as electromagnetic radiation. Both the particle theory and

the wave theory of light are necessary to describe the properties of this energy (Jaffé & Orchin, 1966). In the particle theory, a beam of light is viewed as a stream of particles called photons. In the wave theory, a beam of light is viewed as orthogonal electric and magnetic fields moving through space as a wave motion, both fields being mutually perpendicular to the direction of wave propagation (Figure 1.2).

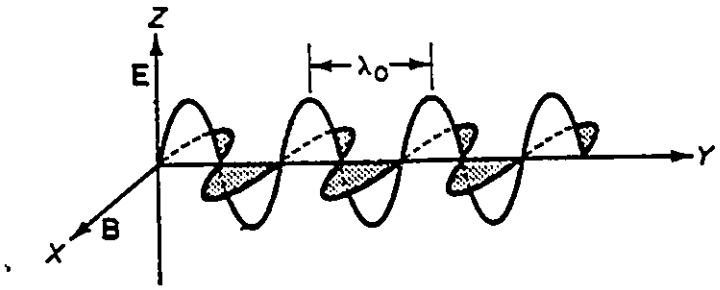

Figure 1.2: A plane wave of electromagnetic radiation at one instant in time. The magnetic field, B, is in the xy–plane and the electric field, E, is in the yz–plane. λ_o represents the wavelength of the electromagnetic radiation (Moore, 1983).

The energy E of a photon is related to the frequency ν of the electromagnetic wave by

$$E = h\nu \qquad (1.1)$$

where h is Planck's constant ($h = 6.626 \times 10^{-34}$ J.s). The energy of a photon can also be directly related to the wavelength λ of the light by

$$E = hc/\lambda \qquad (1.2)$$

where c is the speed of light in a vacuum ($c = 2.998 \times 10^8$ m.s^{-1}). A continuum of frequencies or wavelengths of light create what is called the electromagnetic spectrum which is divided into different regions based upon the energy of the radiation (Figure 1.3).

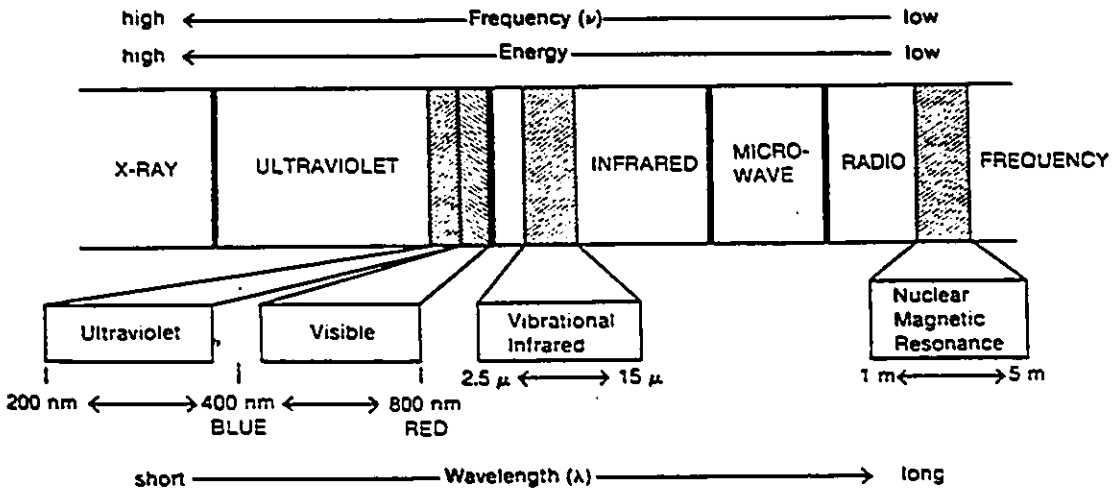

Figure 1.3: A portion of the electromagnetic spectrum (Pavia et al., 1979).

Measurement of the absorption or emission of radiation by molecules contains information about molecular energy levels. This is because molecules will absorb or emit energy only in discrete amounts or packets called quanta. The energy of the radiation quantum equals the energy difference ΔE between two energy levels in the molecule. Thus

$$\Delta E = E_2 - E_1 = h\nu. \qquad (1.3)$$

Whenever a molecule absorbs or emits a quantum of energy, it must make a

transition from one definite energy level E_1 to another E_2.

The transitions accompanying the absorption and emission of light by molecules are illustrated in Figure 1.4. As described above, a necessary condition for absorption of light by a molecule is that the molecule has two states with an energy separation E_2-E_1. However, this is not a sufficient condition for the absorption to occur. Selection rules exist which provide statements of which transitions are "allowed" and which are "forbidden". Allowed transitions are highly probable and will appear as lines in a spectrum. Forbidden transitions have low occurrence probabilities and give rise to weak spectral features, even though the energy levels of the appropriate separation are present. Absorption results when radiation causes an increase in energy of a system with which it interacts. The selection rules dictate that upon transition to an electronically excited state, the molecule has necessarily experienced a change in dipole moment. Further, the redistribution of electrons in the excited state must be assymetrical so that a net change in dipole does occur. In accordance with the Franck–Condon principle, this process of absorption is a single, almost instantaneous interaction occurring approximately in the time needed for one oscillation of the light wave ($\approx 10^{-15}$ sec) (Badley, 1976). The transitions occur without any significant change in either nuclear position or momentum. As a result, immediately after excitation, the newly formed molecular excited state has a nuclear geometry and solvent cage arrangement identical to the ground state (Werner, 1976). Measurement of light absorption across a wavelength spread will generate an absorption spectrum which will reflect the distribution of vibrational levels in electronically excited states (See Figure 1.4). Absorption spectra do not reveal anything about molecular dynamics as the information they provide reflects only the instantaneously averaged structure and environment in the solvent shell immediately adjacent to the absorbing species.

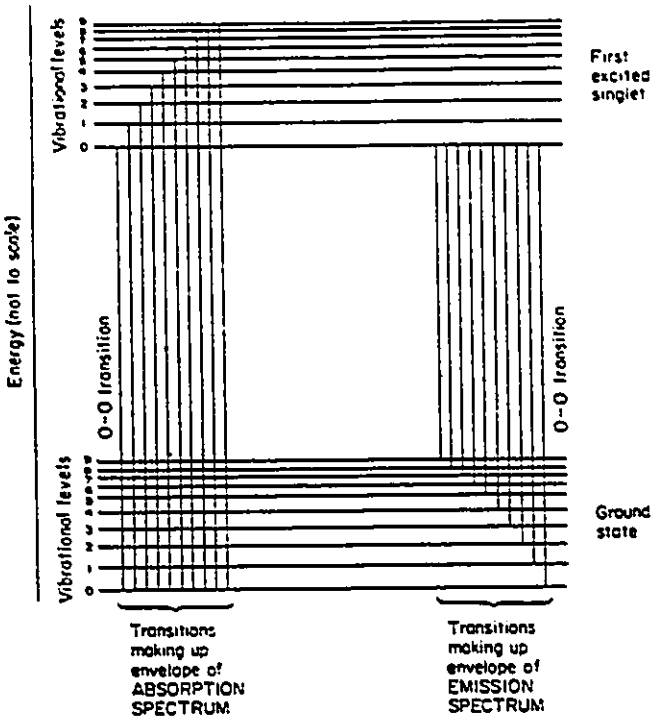

Figure 1.4: Energy level diagram illustrating transitions (vertical lines) between the ground, and first excited singlet electronic states. The horizontal lines define the vibrational levels of the molecule (Penzer, 1980).

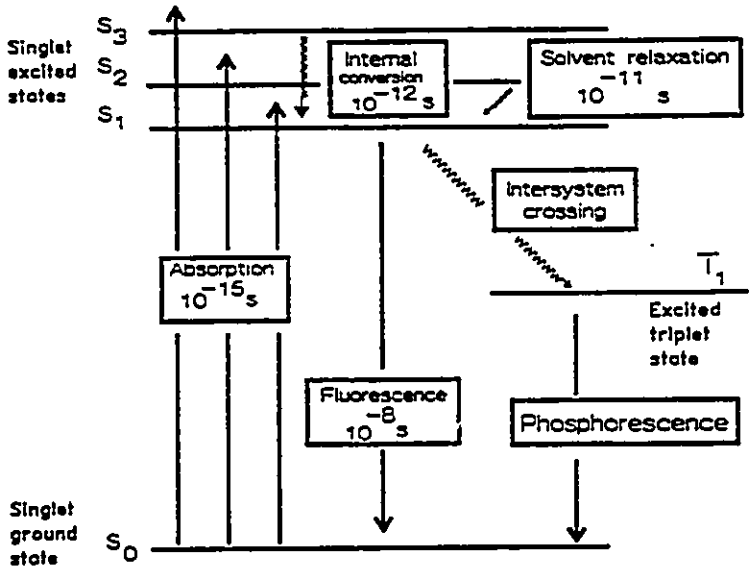

Figure 1.5: Jablonski diagram.

Once an excited electronic state has been formed by the absorption of light, a number of processes can compete for its deactivation. The Jablonski diagram in Figure 1.5 highlights some of these processes (Jablonski, 1935). The radiative emission of photons from electronically excited states is known as luminescence and represents one manner in which an excited molecule can return to the ground state. Under ordinary circumstances, return from an excited singlet state is known as fluorescence and is quantum mechanically "allowed" because the two electrons involved are paired and require no change in spin orientation. Phosphorescence is the emission which results from transition between states of different multiplicity, generally a triplet excited state returning to a singlet ground state. Such transitions are quantum mechanically "forbidden" because the electrons involved are unpaired and require a change in spin orientation. The low probability of phosphorescent transitions cause them to be characterized by relatively slow rates and weak emission.

Unlike absorption which involves a single transition process, fluorescence involves two processes, namely absorption and subsequent emission. Each process is practically instantaneous ($\approx 10^{-15}$ s). There exists a characteristic time lag of $\approx 10^{-8}$ s between the two processes during which the molecule lives in an electronically excited state (Lakowicz, 1983). During this time several molecular processes can occur, each of which can result in changes in the observed fluorescence. For example, this timescale coincides with the time taken for processes such as (i) rotational and/or translational diffusion, (ii) collision with quenchers, (iii) formation of excited–state complexes with solutes and/or solvents, and (iv) reorientation of the environment surrounding the altered dipole moment of the excited state. The singlet excited state lifetime will vary in the nanosecond

regime because it depends on competing non–radiative processes by which it can deactivate. Because the efficiencies of these non–radiative quenching mechanisms depend on the molecular environment, the fluorescence of an emitter can probe its immediate surroundings in a way that absorption cannot. If the fluorophore exists in a protein, the interaction of various protein moieties with the fluorophore can lead to non–radiative deactivation pathways which can compete with fluorescence to return the fluorophore to the ground state. These interactions may be determined by, and are sensitive to the different conformational states of the protein.

Changes in a number of fluorescence parameters can be used to assess the conformational heterogeneity of the fluorophore environment. These parameters include the intensity, the quantum yield, and the lifetime of the singlet state.

1.2.2 Fluorescence Intensity — Emission and Excitation Spectra

The intensity of the emitted light as a function of wavelength can be measured in two ways. An emission spectrum is the wavelength distribution of the fluorescence intensity measured with a single constant excitation wavelength. In Figure 1.4 it is shown that an emission spectrum thus reflects the distribution of vibrational levels in the electronic ground state. An excitation spectrum is the dependence of the fluorescence intensity at a single emission wavelength, as a function of excitation wavelength. For reasons which will be discussed below, a fluorescence excitation spectrum is usually very similar in shape to the fluorophore's absorption spectrum.

A number of general characteristics of fluorescence spectra are known (Pesce et al., 1971), although exceptions do exist and often infer unique behaviour of the system. Many of these characteristics result from a basic phenomenon known as "Stokes' shift". Stokes was the first to note that in solution, the emission of fluorophores relative to absorption invariably shifted to longer wavelength (ie. a red–shift to lower energy) (Stokes, 1852). Kasha's rule summarizes a common cause of Stokes' shift: no matter which excited singlet is initially attained, the molecule usually relaxes rapidly ($\approx 10^{-12}$ s) by a process of internal conversion (Figure 1.5) to the ground vibrational level of the lowest excited singlet state, S_1, from which the fluorescence transition initiates (Moore & Pearson, 1981).

Because the efficiency with which higher excited states relax to the first excited singlet state is very high, and emission occurs from the lowest vibrational level of the excited state, an excitation spectrum usually looks very similar to the fluorophore's absorption spectrum. Whatever the absorption wavelength, the first excited singlet is generated at a rate proportional to the absorbance at the excitation wavelength, λ_{ex}. Therefore fluorescence emission intensity is proportional to the absorbance at λ_{ex}. This internal conversion efficiency is also the reason why emission spectra are usually independent of λ_{ex}.

Stokes' shifts also result because of solvent relaxation (Figure 1.6). Although there is no significant displacement of nuclei during the instantaneous process of light absorption, the time ($\approx 10^{-15}$ s) is adequate for a redistribution of the electrons (Penzer, 1980). Usually fluorophores possess electronic excited states with dipole moments which are different from that of the ground state molecule (Lakowicz, 1983). In a polar solvent, in order to minimize the total excited state energy, the polar solvent cage surrounding the fluorophore undergoes a reorganization known as solvent dielectric relaxation. The timescale, which is

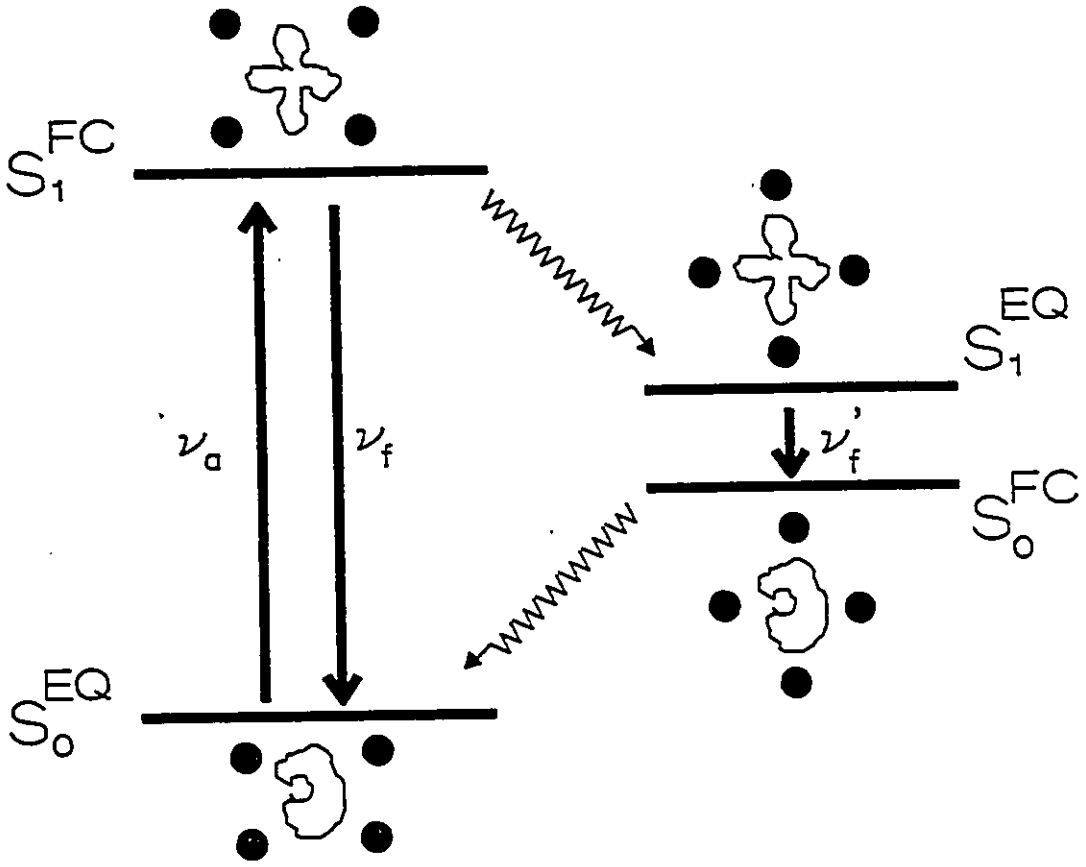

Figure 1.6: Schematic representation of Stokes' loss due to solvent relaxation. S_0 and S_1 represent the ground and first excited singlet states, respectively. The superscript "EQ" denotes a solvent equilibrated state and the superscript "FC" denotes a Franck–Condon non–equilibrated state. The energy of a transition is given in frequency, ν, where ν_a is the energy of absorption, ν_f is the energy of the fluorescence transition from unrelaxed S_1(FC) to relaxed S_0(EQ), and ν_f' is the energy of the fluorescence transition from relaxed S_1(EQ) to unrelaxed S_0(FC).

usually on the order of 10^{-11} s (Figure 1.5) in aqueous solvent (Pesce et al., 1971), will depend on the chemical and physical properties of the solvent. A polar solvent with strong solvating interactions, like water, will tend to cause larger shifts when compared to weak, non–polar solvents.

1.2.3 Fluorescence Quantum Yields

Fluorescence measurements can be made under both steady–state and transient conditions. Steady–state measurements are made by an illumination of the sample with a constant intensity of exciting radiation. Under these conditions a small, but constant fraction of the total fluorophore molecules will be maintained in the first excited singlet state under steady–state conditions. The following kinetic scheme 1.1 illustrates this situation:

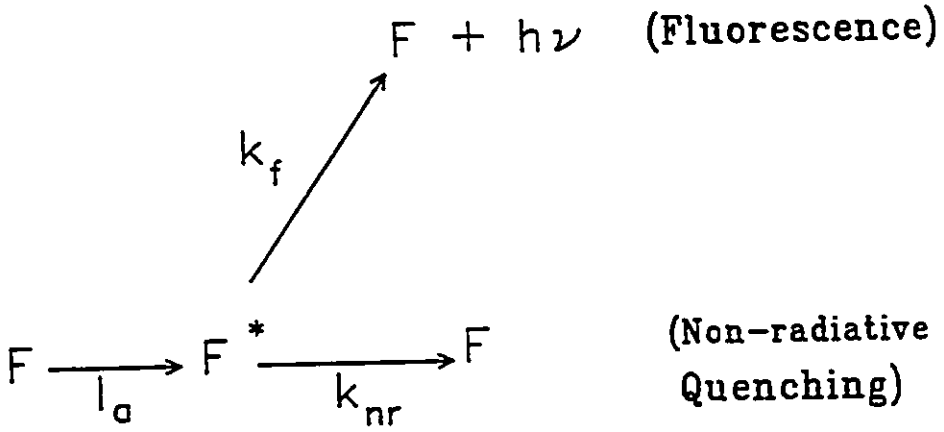

Scheme 1.1

where F is the ground–state fluorophore, F^* is the fluorophore in the first excited singlet state, I_a is the rate–intensity of the absorbed photons (i.e. the product of the

intensity of the exciting radiation times the rate constant for absorption), k_f is the radiative rate constant and k_{nr} is the nonradiative rate constant. The non–radiative rate constant is actually a sum of rate constants given by the following expression:

$$k_{nr} = k_{IC} + k_{ISC} + k_p + k_q[Q] \qquad (1.4)$$

where k_{IC} is the rate constant for internal conversion, k_{ISC} is the rate constant for intersystem crossing to the triplet state, k_p is the rate constant for photoreaction, k_q is the rate constant for deactivation by a quencher, Q, and [Q] is the concentration of the diffusional quencher. The rate of change in the concentration of F^* with time is given by the following expression:

$$\frac{d[F^*]}{dt} = I_a - (k_f + k_{nr})[F^*]. \qquad (1.5)$$

The quantum yield of fluorescence, ϕ_f, is defined as the ratio of the following rates:

$$\phi_f = \frac{\text{rate of emission of photons by } S_1}{\text{rate of absorption of photons by } S_0}$$

$$= \frac{k_f[F^*]}{I_a} \qquad (1.6)$$

where S_1 and S_0 are the first excited singlet and ground electronic states, respectively. Since under steady–state conditions ($d[F^*]/dt = 0$), the efficiency of fluorescence emission, i.e. the ϕ_f, can also be expressed as function of the competing

rate constants of excited state deactivation:

$$\phi_f = k_f/(k_f + k_{nr}). \qquad (1.7)$$

Since the variety of nonradiative deactivation processes are sensitive to changes in temperature and solvent composition, the ϕ_f is a sensitive measure of changes in the environment and interactions of the fluorophore.

1.2.4 Fluorescence Lifetimes

The lifetime of the excited singlet state, S_1, is defined as the average time the molecule spends in the excited state prior to return to the ground state, S_0. In terms of the parameters introduced in scheme 1.1, the singlet lifetime, τ_s, is defined as follows:

$$\tau_s = 1/(k_f + k_{nr}). \qquad (1.8)$$

As fluorescence emission is a random process, only a fraction of the excited molecules will emit their photons at $t = \tau_s$. In the absence of excited–state reactions, the decay of fluorescence after pulsed excitation follows first–order kinetics (Wong & Harris, 1989):

$$\frac{-\,d[F^*]}{dt} = (k_f + k_{nr})[F^*] \qquad (1.9)$$

where $[F^*]$ is the concentration of molecules in the excited singlet state. Integration

of equation 1.9 with respect to time leads to:

$$[F^*] = [F^*_o]\exp[-(k_f + k_{nr})t]$$
$$= [F^*_o]\exp[-t/\tau_s] \qquad (1.10)$$

where $[F^*_o]$ is the concentration of molecules in the excited state at t = 0. Thus the observed lifetime can also be defined as the time taken for the emission of the fluorophore to fall to 1/e of its initial value in the absence of further excitation. As the fluorescence intensity observed at wavelength λ and time t ($I(\lambda,t)$) results from the rate of return of F^* to the ground state, equation 1.10 can also be expressed as follows:

$$I(\lambda,t) = \alpha(\lambda)\exp[-t/\tau_s] \qquad (1.11)$$

where $\alpha(\lambda)$ is the preexponential term at wavelength λ. This monoexponential fluorescence decay function has been shown to be an adequate model describing the time dependent emission of a pure fluorophore in a non–interacting solvent (Hochstrasser, 1971). If the fluorescence decay results from a mixture of two or more fluorophores, then a multiexponential decay function of the following form is employed to adequately describe the decay kinetics:

$$I(\lambda,t) = \sum_{i=1}^{n} \alpha_i(\lambda)\exp[-t/\tau_i] \qquad (1.12)$$

where n is the number of components, $\alpha_i(\lambda)$ is the preexponential term of the ith

component at wavelength λ, and τ_i is the singlet lifetime of the ith component of the fluorescence. Multiexponential decay kinetics can also result from the presence of a single fluorophore in different environments. For example, a single tryptophan residue in a protein may possess multiexponential decay behaviour if the protein is conformationally heterogeneous (Brand et al., 1985). Donzel et al. (1974) have shown that it is possible to estimate the relative ground state concentrations of the fluorescent components from the preexponential terms, $\alpha_i(\lambda)$. Thus the lifetime and preexponential values obtained from an analysis of the decay can provide detailed information about the environment of the tryptophan probe in the different protein conformations.

In the absence of any nonradiative processes, the lifetime is called the intrinsic, or radiative lifetime τ_r, and is related only to the rate constant for fluorescence emission:

$$\tau_r = 1/k_f. \qquad (1.13)$$

The radiative lifetime can be determined through a measurement of the quantum yield of fluorescence and the singlet lifetime by application of the following simple relationship:

$$\phi_f = \tau_s/\tau_r. \qquad (1.14)$$

Equation 1.14 effectively combines results from both steady–state and transient or "time–resolved" fluorescence measurements. The utility of combining these measurements is that it allows both the radiative (k_f), and non–radiative (k_{nr}) rate

constants to be estimated through application of equations 1.14, 1.13 and 1.8. The rate information can contribute to a rationalization of the various photophysical and photochemical processes which may be occurring upon sample excitation.

Another utility derived by combining steady–state and time–resolved fluorescence data is seen in situations of fluorescence heterogeneity. As steady–state measurements provide an intensity–weighted average of all underlying decay processes, the number of decay processes will not be revealed in a steady–state measurement. In addition, the steady–state signal will be dominated not by the most populated state, but by the one which emits the most light. However, in combination with time–resolved measurements, detailed information about the population distribution of molecular species can be obtained. Also, by combining steady–state and time–resolved fluorescence data, it becomes possible to construct decay–associated spectra, or DAS. DAS represent the relative contributions of individual lifetime components, as a function of wavelength, to the total fluorescence (Knutson et al., 1982) thereby permitting a resolution of the underlying decay processes comprising the steady–state spectrum. Details regarding the construction of DAS are provided in Section 2.2.5.

1.3 Protein Fluorescence

Phenylalanine, tyrosine and tryptophan are amino acids which possess aromatic sidechains. The structures of these residues are given in Figure 1.7. It is the presence of these residues in proteins which cause proteins to fluoresce in the ultraviolet spectral range. Hence protein molecules containing one or more of these residues are provided with naturally "built–in" or intrinsic fluorophores which

can often function as convenient spectroscopic probes.

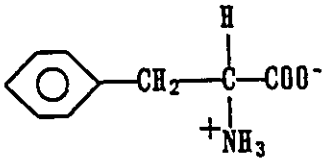

phenylalanine

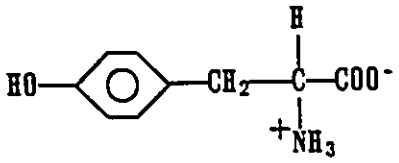

tyrosine

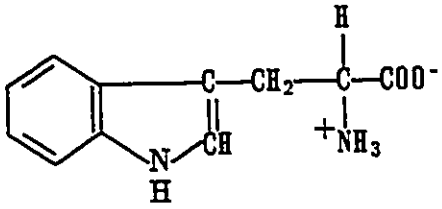

tryptophan

Figure 1.7: The aromatic amino acids.

The absorption spectra of these amino acids are shown in Figure 1.8. In most proteins, the maximum absorption is typically observed around 280 nm where both tyrosine and tryptophan make major contributions. Of the three aromatic residues, tryptophan is the least prevalent in proteins (Klapper, 1977); however, because of its high molar absorptivity, tryptophan tends to dominate the UV absorption spectrum when present in the protein sequence. The molar absorptivity, or extinction coefficient, is related to the probability that a molecule in the ground state will absorb a photon and be promoted to an electronically excited state. The molar absorptivity of a protein at 280 nm can roughly be estimated by summing the product of the number of each aromatic residue by its extinction coefficient at that

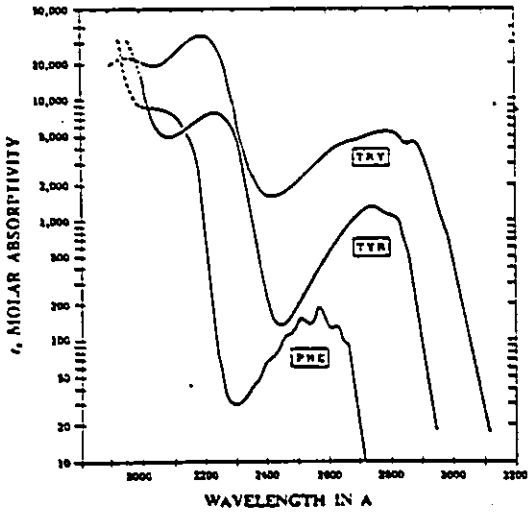

Figure 1.8: Ultraviolet absorption spectra of the aromatic amino acids (Wetlaufer, 1962).

wavelength (for phenylalanine, $\epsilon_{280nm} = 0.7 \pm 0.3\ M^{-1}cm^{-1}$; for tyrosine, $\epsilon_{280nm} = 1197 \pm 0\ M^{-1}cm^{-1}$; and for tryptophan, $\epsilon_{280nm} = 5559 \pm 12\ M^{-1}cm^{-1}$, (Sober, 1970).

As seen in Figure 1.8, phenylalanine has a negligible extinction coefficient at 280 nm. Furthermore, even if excitation is performed at shorter wavelengths where phenylalanine is excited, its ϕ_f is so low that under experimental conditions emission from this residue is rarely observed. Table 1.1 summarizes the spectroscopic properties of the aromatic amino acids at neutral pH. When present in a protein, phenylalanine makes a negligible contribution to protein fluorescence. In contrast, tryptophan tends to dominate protein fluorescence. This is due to a number of reasons. Examination of the absorption (Figure 1.8), and fluorescence emission spectra of the aromatic amino acids (Figure 1.9) reveals that the tryptophan spectra occur at the lowest energy (longest wavelength). The absorption spectrum of tryptophan overlaps the emission spectra of phenylalanine and tyrosine.

TABLE 1.1
SPECTROSCOPIC PROPERTIES OF THE AROMATIC AMINO ACIDS AT NEUTRAL pH

	ABSORBANCE[a]		FLUORESCENCE	
	λ_{max} (nm)	Absorbance ($M^{-1}cm^{-1}$)	λ_{max}[b] (nm)	Quantum yield
Phenylalanine	257.4	197	282	0.04[b]
Tyrosine	274.6	1420	303	0.135[c]
Tryptophan	279.8	5600	348	0.14[d]

[a]From CRC Handbook of Biochemistry.
[b]Teale & Weber, 1957.
[c]Chen, 1967.
[d]Eisinger, 1969.

On the basis of the observed sequence of singlet energies, the overlap of the absorption and emission spectra and the molar extinction, it was proposed (Teale & Weber, 1957), and subsequently observed (Vladimirov, 1957), that transfers of excited state energy can occur from phenylalanine → tyrosine → tryptophan as a result of dipolar resonance coupling. As the diameters of most proteins are generally comparable to the critical transfer distance of 10 – 18 Å (Weber, 1960; Vladimirov & Burstein, 1960), these transfers tend to be relatively efficient provided favourable orientations of the rings exist. It is for this reason that tryptophan residues tend to act as energy sinks for all excitation energy in proteins.

In addition, and in spite of the high absorbance at 280 nm, and the high fluorescence quantum yield of tyrosine zwitterion in aqueous solution ($\phi_f = 0.135$ (pH 7), Chen, 1967), the tyrosine emission from most proteins ranges from small to virtually undetectable (typical ϕ_f(Tyr) in proteins range from < 0.01 to 0.05, Kronman & Holmes, 1971). As a result, in a protein containing both Tyr and Trp,

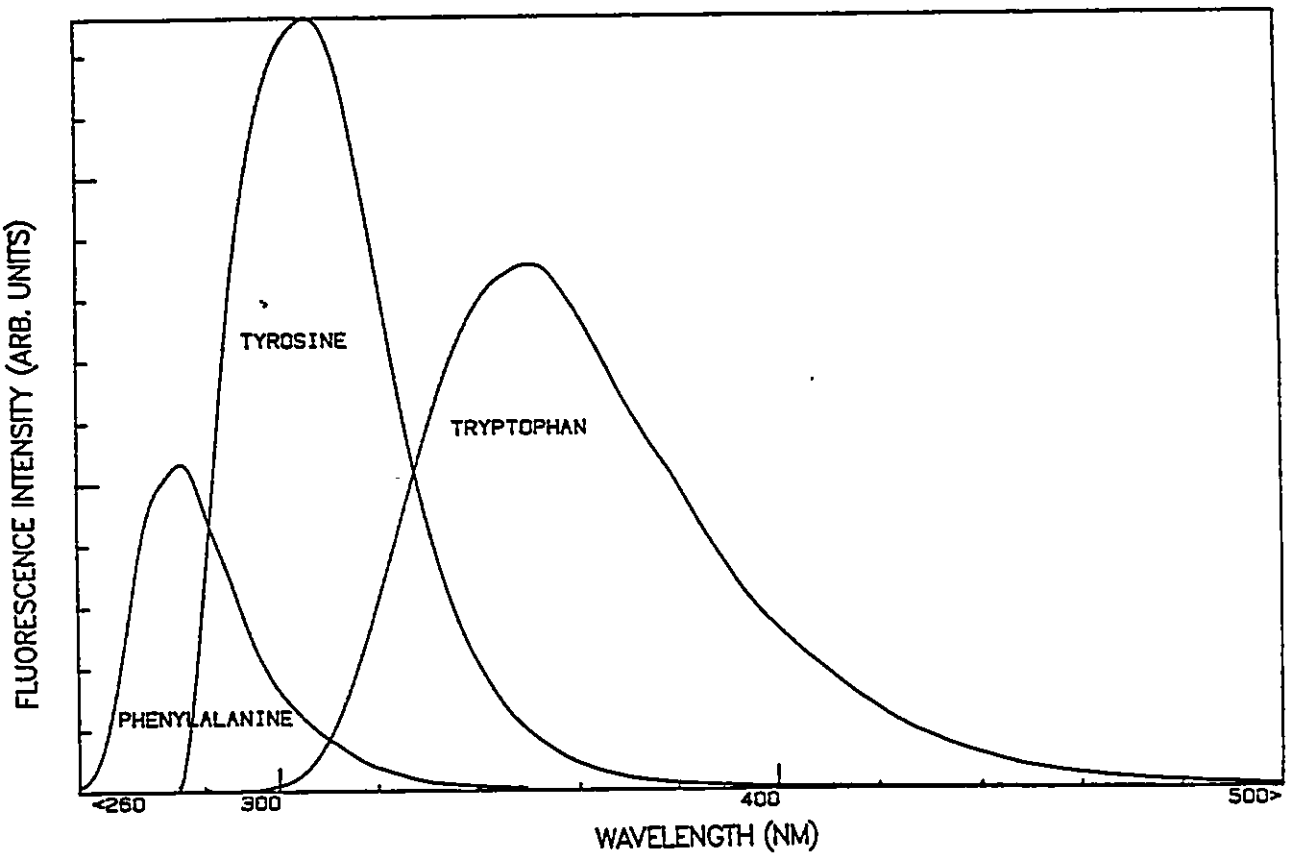

Figure 1.9: Fluorescence emission spectra of the aromatic amino acid zwitterions. As the absorbance of each solution was the same at the λ_{ex}, the relative areas under the spectra reflect the relative quantum yields of fluorescence of the amino acid zwitterions.

rarely is the Tyr fluorescence band visibly obvious, even with excitation at 280 nm (Kronman & Holmes, 1971; Teale & Weber, 1957). This latter condition is partly a consequence of the three–dimensional structure of the protein as denaturation will generally increase the emission due to tyrosine, yet even under these conditions its contribution will generally be less than that found for equimolar mixtures of the free residues in solution (Kronman & Holmes, 1971). Although it is difficult to assess the exact mechanism for quenching of tyrosyl fluorescence in particular proteins, a number of factors seem to contribute to the generally observed weak fluorescence of tyrosine. Tyrosine fluorescence can be quenched by nearby charged or neutral carboxyl and amino groups (Weber & Rosenheck, 1964). The formation of peptide bonds on either the α–carboxyl or the α–amino groups of tyrosine further decreases its ϕ_f (Cowgill, 1967). Hydrogen bonding in the ground state between the hydroxyl moiety on tyrosine and proton acceptors, such as the carbonyl groups of the peptide bond, and aspartic and glutamic acids, provides an effective quenching mechanism of tyrosine fluorescence (Chignell & Gratzer, 1968). Upon excitation, the pK_a of the tyrosine hydroxyl dramatically decreases from 10.3 to 4.2, allowing ionization to occur in the presence of strong proton acceptors, even at neutral pH (Shimizu & Imakuvo, 1977). The formation of tyrosinate, which has an emission maximum at 345 nm, is an effective quenching mechanism of tyrosine emission (Szabo et al., 1978). Finally, for reasons discussed above, tyrosine can often efficiently transfer its excitation energy to tryptophan resulting in the quenching of tyrosine fluorescence (Teale & Weber, 1957). Although tryptophan is also subject to a number of quenching influences within a protein (Creed, 1984; Privat et al., 1979; Ricci & Nesta, 1976), its dominating emission and unique photophysical properties cause it

to be the preferred intrinsic fluorophore in proteins. In the next section, a number of reasons are given describing why tryptophan is more informative than tyrosine as a probe of protein conformation.

1.3.1 Tryptophan — The Preferred Intrinsic Fluorophore

Tryptophan undergoes a large change in dipole moment in the excited state and for this reason, tryptophan, unlike tyrosine, is highly sensitive to the polarity of its surrounding environment. Environment–dependent Stokes' shifts of tryptophan emission are widely used in conformational studies (Burstein et al., 1973). Upon conformational changes in the protein, the tryptophan emission spectrum may not only undergo intensity changes, but changes in wavelength position and spectral shape are frequently observed. Such a situation tends not to occur for tyrosine emission owing to this residue's relative solvent insensitivity (Lakowicz, 1983). It is possible to selectively excite tryptophan, even in the presence of tyrosine. At wavelengths longer than 295 nm, the absorption in proteins is due primarily to tryptophan (Figure 1.8).

Compared to tyrosine, tryptophan tends to have a much lower occurrence in proteins (Klapper, 1977). The existence of a number of single tryptophan–containing proteins has allowed their conformational properties to be studied by fluorescence with a high degree of specificity in the absence of any chemical modification (Eftink & Ghiron, 1987; Lakowicz et al., 1986; Beechem & Brand, 1985; Ludescher et al., 1985; Brochon et al., 1974). A comprehensive survey of the time–resolved intrinsic fluorescence of a number of single tryptophan–containing proteins has been published by Grinvald and Steinberg (1976). With the exception

of apoazurin (a protein which will be examined in Chapter 3), all of the proteins were found to exhibit either double or triple exponential decay kinetics, with the longest lifetime component occurring in the range of 2 – 5 ns, the middle lifetime component occurring in the range of 0.03 – 4 ns, and the shortest lifetime component occurring in the range 0.03 – 1 ns (Grinvald & Steinberg, 1976). In many cases, the multiexponential decay from these single tryptophan–containing proteins was explained in terms of the existence of tryptophan in multiple environments corresponding to different protein conformations (Beechem & Brand, 1985). For example, the sensitivity to metal ion binding of the double exponential decay kinetics of the single tryptophan residue in human serum albumin was interpreted to arise from different metal ion–induced protein conformational states (Van Hoek et al., 1983; DeLauder & Wahl, 1971).

Thus the conformational properties of many proteins which contain single tryptophan residues can be conveniently studied using fluorescence spectroscopy. In addition, details regarding the control of protein conformation by non–fluorescent modulators, such as metal ions, can be obtained by using steady–state and time–resolved fluorescence spectroscopy.

1.4 Protein Function and Conformation — The Role of Metal Ions

In section 1.1 of this thesis, a number of biological functions performed by proteins were listed. Many of these functions have been shown to depend upon the specific association of one or more metal ions with the protein matrix. In some metalloproteins, such as those involved in oxidation–reduction reactions and oxygen transport, the metal ions directly function as the active centre in the protein. In

other metalloproteins, the controlled binding and release of metal ions allow the protein to provide the cell with biologically important metal ions in the right place, at the right time, and in the right amount. An example of the latter type of metalloprotein is provided by the albumins, as well as by members of the calcium–binding protein superfamily.

During the last two decades a number of studies have been conducted towards the goal of elucidating the impact of metal binding upon the protein structure, as well as the effects of the surrounding protein matrix upon the biochemical action of bound metal ions (Harrison, 1985a). In virtually all cases, the metal ions have been found to play an important role in the adoption and maintenance of the surrounding protein matrix in its biologically active conformation (Harrison, 1985a and b). In this thesis, the ability of metal ions to modulate the conformational properties of members from two families of metalloproteins is examined. Reasons for selecting these particular proteins will be discussed in section 1.5.

1.5 The Modulation of Protein Conformation by Metal Ions — The Present Study

In Chapter 3, the work on two single tryptophan–, copper–containing proteins is presented. These proteins, known as azurins, function as electron transferases in the bacterial electron transport chain (Wilson et al., 1975). As the single copper ion, and its oxidation state are central to the protein's function, the nature of the metal ion centre in modulating the protein conformation was examined. In addition, this chapter provides evidence in support of one side of a controversy which resulted from earlier work on the fluorescence properties of this

protein (Grinvald et al., 1975; Petrich et al., 1987).

In Chapter 4, the results of another single tryptophan–containing protein known as parvalbumin are presented. The parvalbumins are a subfamily of proteins belonging to the large superfamily of calcium–binding proteins. The results obtained with the isotype III component of cod parvalbumin, which has a single tryptophan residue in position–102, demonstrate how misconceptions regarding the metal ion binding properties of this protein may have arisen from the application of a well–known experimental method of protein decalcification. In the absence of the latter artefact, this chapter reveals detailed information regarding the role of calcium ions in modulating the conformational nature of this protein. Chapter 4 also serves as an important prelude to the work presented in Chapter 5.

In chapter 5, the calcium–specific conformational changes of cod III parvalbumin are compared with those of the highly homologous tumour protein, oncomodulin. Although parvalbumin–like in structure (MacManus et al., 1983), oncomodulin was found to exhibit certain calmodulin–like regulatory properties. Owing to the striking structural similarity of parvalbumin and oncomodulin, but yet the difference in their abilities to function as regulators of a number of enzymic and cellular processes, it was the purpose of this study to use a single tryptophan residue in position–102 of the amino acid sequence to probe for differences in the calcium–induced conformational responses of these proteins. As native oncomodulin was devoid of tryptophan, this study was made possible by an examination of a site–specific mutant with tryptophan in position–102.

In chapter 6, details regarding the calcium–specific conformational changes of oncomodulin are presented based upon an examination of a number of bacterially–expressed oncomodulin mutant proteins. In these mutants,

phenylalanine and tryptophan had been substituted into various positions of the two calcium–binding loops. The conformational impact of the binding of the first and second calcium equivalents is revealed.

1.6 References

Badley, R. A. (1976) In: Modern Fluorescence Spectroscopy, Ed.: E. L. Wehry (Plenum Press, New York) Volume 2, Chapter 3.

Beechem, J. M. & Brand, L. (1985) Time–resolved fluorescence of proteins. Ann. Rev. Biochem. 54, 43–71.

Brand, L., Knutson, J. R., Davenport, L., Beechem, J. M., Dale, R. E., Walbridge, D. G. & Kowalczyk, A. A. (1985) Time–resolved fluorescence spectroscopy. Some applications of associative behaviour to studies of proteins and membranes. In: Spectroscopy and the Dynamics of Molecular Biological Systems, (Academic Press, London) pp. 259–305.

Brochon, J. C., Wahl, P. & Auchet, J. C. (1974) Fluorescence time–resolved spectroscopy and fluorescence anisotropy decay of the *Staphylococcus aureus* endonuclease. Eur. J. Biochem. 41, 577–583.

Burstein, E. A., Vedenkina, N. S. & Ivkova, M. N. (1973) Fluorescence and the location of tryptophan residues in protein molecules. Photochem. Photobiol. 18, 263–279.

Chen, R. F. (1967) Fluorescence quantum yields of tryptophan and tyrosine. Anal. Lett. 1, 35–42.

Chignell, D. A. & Gratzer, W. B. (1968) Solvent effects on aromatic chromophores and their relation to ultraviolet difference spectra of proteins. J. Phys. Chem. 72, 2934–2941.

Cowgill, R. W. (1967) Fluorescence and protein structure. X. Reappraisal of solvent and structural effects. Biochim. Biophys. Acta 133, 6–18.

Creed, D. (1984) The photophysics and photochemistry of the near–UV absorbing amino acids — I. Tryptophan and its simple derivatives. Photochem. Photobiol. 39, 537–562.

Debrunner, P. G. & Frauenfelder, H. (1982) Dynamics of Proteins. Ann. Rev. Phys. Chem. 33, 283–299.

De Lauder, W. B. & Wahl, Ph. (1971) Fluorescence studies on human serum albumin. Biochem. Biophys. Res. Commun. 42, 398–404.

Donzel, B., Gauduchon, P. & Wahl, Ph. (1974) Study of the conformation in the excited state of two tryptophanyl diketopiperazines. J. Am. Chem. Soc. 96, 801–808.

Eftink, M. R. & Ghiron, C. A. (1987) Frequency domain measurements of the fluorescence lifetime of ribonuclease T_1. Biophys. J. 52, 467–473.

Eisinger, J. (1969) A variable temperature, U.V. luminescence spectrograph for small samples. Photochem. Photobiol. 9, 247–258.

Frauenfelder, H. (1989) New looks at protein motions. Nature 338, 623–624.

Grinvald, A., Schlessinger, J., Pecht, I. & Steinberg, I. Z. (1975) Homogeneity and variability in the structure of azurin molecules studied by fluorescence decay and circular polarization. Biochem. 14, 1921–1929.

Grinvald, A. & Steinberg, I. Z. (1976) The fluorescence decay of tryptophan residues in native and denatured proteins. Biochim. Biophys. Acta 427, 663–678.

Gurd, F. R. N. & Rothgeb, T. M. (1979) Motions in proteins. Adv. Protein Chem. 33, 74.

Harrison, P. M. (1985a) In: Metalloproteins. Part 1: Metal Proteins and Redox Roles, (MacMillan, London) Vol. 6.

Harrison, P. M. (1985b) In: Metalloproteins. Part 2: Metal Proteins with Non–Redox Roles, (Verlag, Basel) Vol. 7.

Hochstrasser, R. M. (1971) Some principles governing the luminescence of organic molecules. In: Excited States of Proteins and Nucleic Acids, Eds.: R. F. Steiner and I. Weinryb (Plenum Press, New York) Chapter 1, pp. 1–29.

Jablonski, A. (1935) Über den mechanismus des photolumineszenz von farbstoff–phosphoren. Z. Phys. 94, 38–46.

Jaffé, H. H. & Orchin, M. (1966) In: Theory and Applications of Ultraviolet Spectroscopy, (John Wiley and Sons, New York).

Karplus, M. & McCammon, J. A. (1981) The internal dynamics of globular proteins. CRC Crit. Rev. Biochem. 9, 293–349.

Klapper, M. G. (1977) The independent distribution of amino acid near neighbor pairs into polypeptides. Biochem. Biophys. Res. Commun. 78, 1018–1024.

Knutson, J. R., Walbridge, D. G. & Brand, L. (1982) Decay–associated fluorescence spectra and the heterogeneous emission of alcohol dehydrogenase. Biochem. 21, 4671–4679.

Koshland, D. E. Jr. (1973) Protein shape and biological control. Scientific American October, 52–64.

Kronman, M. J. & Holmes, L. G. (1971) The fluorescence of native, denatured and reduced–denatured proteins. Photochem. Photobiol. 14, 113–134.

Lakowicz, J. R. (1983) In: Principles of Fluorescence Spectroscopy, (Plenum Press, New York).

Lakowicz, J. R., Laczko, G., Gryczynski, I. & Cherek, H. (1986) Measurement of subnanosecond anisotropy decays of protein fluorescence using frequency–domain fluorometry. J. Biol. Chem. 261, 2240–2245.

Lehninger, A. L. (1979) In: Biochemistry, (Worth Publishers, New York) Second Edition, Chapter 3.

Levitt, M. & Sharon, R. (1988) Accurate simulation of protein dynamics in solution. Proc. Natl. Acad. Sci. USA 85, 7557–7561.

Linderstrom–Lang, K. U. & Schellman, J. A. (1959) Protein structure and enzyme activity. The Enzymes 1, 443–510.

Ludescher, R. D., Volwerk, J. J., de Haas, G. H. & Hudson, B. S. (1985) Complex photophysics of the single tryptophan of porcine pancreatic phospholipase A_2, its zymogen, and an enzyme/micelle complex. Biochem. 24, 7240–7249.

MacManus, J. P., Watson, D. C. & Yaguchi, M. (1983) The complete amino acid sequence of oncomodulin—a parvalbumin–like calcium–binding protein from Morris hepatoma 5123tc. Eur. J. Biochem. 136, 9–17.

McCammon, J. A. & Karplus, M. (1980) Simulation of protein dynamics. Ann. Rev. Phys. Chem. 31, 29–45.

Moore, J. W. & Pearson, R. G. (1981) In: Kinetics and Mechanism, (John Wiley and Sons, New York) Chapter 10.

Moore, W. J. (1983) In: Basic Physical Chemistry, (Prentice–Hall, New Jersey) p. 54.

Pavia, D. L., Lampman, G. M. & Kriz, G. S. Jr. (1979) In: Introduction to Spectroscopy, (Saunders College Publishing, Philadelphia) p 13.

Penzer, G. R. (1980) In: An Introduction to Spectroscopy for Biochemists, Ed.: S. B. Brown (Academic Press, London) Chapter 3.

Perutz, M. F. & Mathews, F. S. (1966) An x–ray study of azide methaemoglobin. J. Mol. Biol. 21, 199–202.

Pesce, A. J., Rosen, C.–G. & Pasby, T. L. (1971) In: Fluorescence Spectroscopy, (Marcel Dekker, New York).

Peticolas, W. L. (1978) Low frequency vibrations and the dynamics of proteins and polypeptides. Methods in Enzymology 61, 425–458.

Petrich, J. W., Longworth, J. W. & Fleming, G. R. (1987) Internal motion and electron transfer in proteins: A picosecond fluorescence study of three homologous azurins. Biochem. 26, 2711–2722.

Privat, J.–P., Wahl, P. & Auchet, J.–C. (1979) Rates of deactivation processes of indole derivatives in water–organic solvent mixtures — application to tryptophyl fluorescence of proteins. Biophys. Chem. 9, 223–233.

Ricci, R. W. & Nesta, J. M. (1976) Inter– and intramolecular quenching of indole fluorescence by carbonyl compounds. J. Phys. Chem. 80, 974–980.

Shimizu, O. & Imakuvo, K. (1977) New emission band of tyrosine induced by interaction with phosphate ion. Photochem. Photobiol. 26, 541–543.

Sober, H. A. (1970) In: CRC Handbook of Biochemistry, (The Chemical Rubber Co., Cleveland) Second Edition.

Stokes, G. G. (1852) On the change of refrangibility of light. Phil. Trans. R. Soc. London 142, 463–562.

Szabo, A. G., Lynn, K. R., Krajcarski, D. T. & Rayner, D. M. (1978) Tyrosinate fluorescence maxima at 345 nm in proteins lacking tryptophan at pH 7. FEBS Lett. 94, 249–252.

Teale, F. W. J. & Weber, G. (1957) Ultraviolet fluorescence of the aromatic amino acids. Biochem. J. 65, 476–482.

Van Hoek, A., Vervoort, J. & Visser, A. J. W. G. (1983) A subnanosecond resolving spectrofluorimeter for the analysis of protein fluorescence kinetics. J. Biochem. Biophys. Methods 7, 243–254.

Vladimirov, Y. A. (1957) Fluorescence of aromatic amino acids. Dokl. Akad. Nauk. SSSR 116, 780–783.

Vladimirov, Y. A. & Burstein, E. A. (1960) Luminescent spectra of aromatic amino acids and proteins. Biophysika 5, 385–392.

Weber, G. (1960) Fluorescence polarization spectrum and electronic energy transfer in tyrosine, tryptophan and related compounds. Biochem. J. 75, 335–345.

Weber, G. & Rosenheck, K. (1964) Proton–transfer effects in the quenching of fluorescence of tyrosine copolymers. Biopolymers Symp. 1, 333–344.

Werner, T. C. (1976) In: Modern Fluorescence Spectroscopy 2, Ed.: E. L. Wehry (Plenum Press, New York) Chapter 7, pp. 277–317.

Wetlaufer, D. B. (1962) Ultraviolet absorption spectra of proteins and amino acids. Adv. Protein Chem. 17, 303–390.

Williams, R. J. P. (1989) NMR studies of mobility within protein structure. Eur. J. Biochem. 183, 479–497.

Wilson, M. T., Greenwood, C., Brunori, M. & Antonini, E. (1975) Electron transfer between azurin and cytochrome c–551 from *Pseudomonas aeruginosa*. Biochem. J. 145, 449–457.

Wong, A. L. & Harris, J. M. (1989) Quantitative estimation of component amplitudes in multiexponential decay data: Application to time–resolved fluorescence spectroscopy. Anal. Chem. 61, 2310–2315.

Chapter 2

INSTRUMENTATION AND DATA ANALYSIS

2.1 Absorption and Steady–state Fluorescence Measurements

Absorption spectra were recorded on a Varian DMS 200 UV–VIS spectrophotometer, as well as on a Cary 219 spectrophotometer. The fluorescence excitation and emission spectra were measured on an SLM 8000C spectrofluorometer equipped with a Neslab Endocal RTE–5DD refrigerated circulating bath for temperature control. To assist in the understanding of how true excitation and emission spectra were measured, the component parts of a typical commerical spectrofluorometer are shown in Figure 2.1.

In a typical steady–state fluorescence experiment, a quartz cuvette containing the protein solution was placed in the sample chamber. The slits were manually adjusted on both the excitation and emission monochromators. The SLM 8000C software permitted the selection of the data acquisition parameters via an IBM–XT computer keyboard. These parameters included the excitation and emission wavelengths, the integration time during which photons were counted at each wavelength, as well as the wavelength step, the latter parameter indicating the wavelength intervals at which an intensity was measured. Buffer blanks lacking protein, were measured under identical conditions as the protein–containing solutions, and the resulting "blank" spectrum was subtracted from the "protein" spectrum using the SLM software. "True" spectra were then obtained by taking these blank–corrected spectra and applying additional correction factors which are described in detail in Section 2.1.1.

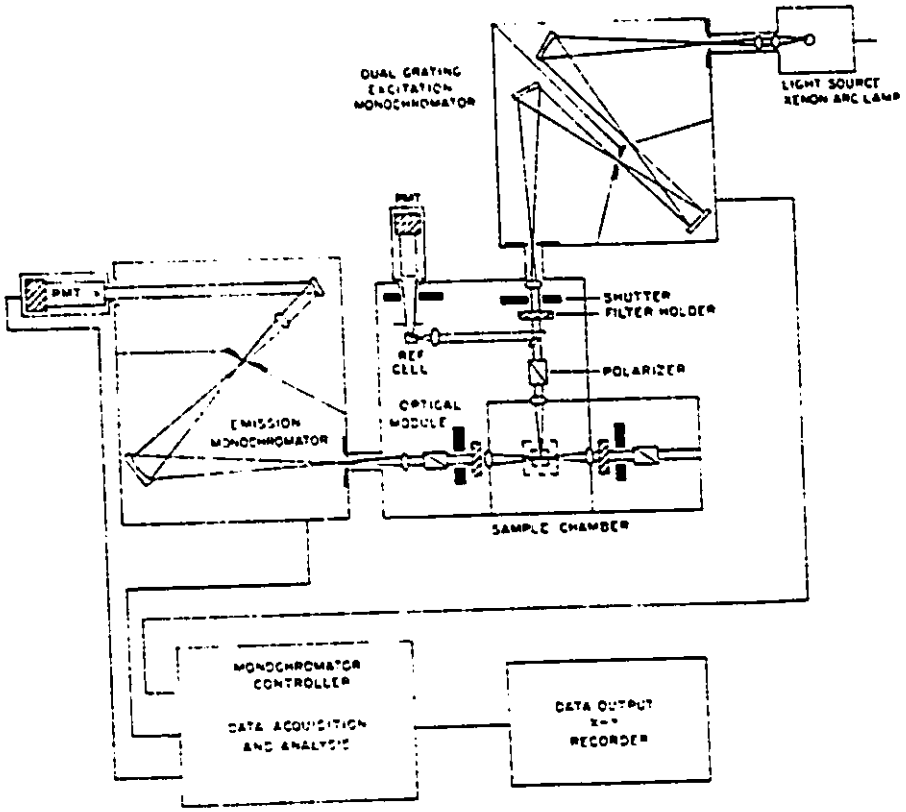

Figure 2.1: Schematic diagram of an SLM spectrofluorometer (Lakowicz, 1983).

2.1.1 Corrected Fluorescence Spectra

Spectra which were initially obtained, following the scanning of either excitation or emission wavelengths were "uncorrected". These spectra were composed of the true spectra of the fluorescent sample, distorted by the sensitivity characteristics of the excitation source, the fluorescence detector, and the monochromators. Most light sources have a non–uniform spectral output and are very sensitive to minor voltage fluctuations. In addition, the efficiency of the lamp output falls with time. The detector, which is a photomultiplier tube (PMT in Figure 2.1), has a wavelength–dependent sensitivity. The monochromators, which are used to select wavelengths, also have a wavelength–dependent sensitivity, as well as a polarization bias. Thus the shapes of the spectra recorded without any correction are different with individual instruments and with time.

In order to correct for intensity fluctuations of the xenon lamp excitation source, a beam splitter was placed in the excitation light path (Parker, 1958). This splitter reflected a small percentage of the excitation beam to a triangular reference cell which contained a concentrated solution of rhodamine 6G in ethylene glycol. The cell was oriented so that the hypotenuse faced the incident light. Rhodamine was selected because it is a stable fluorophore whose response is wavelength–independent (Miller, 1981). In the wavelength range 220 – 600 nm, concentrated solutions of rhodamine absorb greater than 99% of incident light. Fluorescent photons from the rhodamine were then detected by a reference photomultiplier, the electrical signal of which was proportional to the intensity of the exciting light. Variations in arc lamp intensity were then corrected by division of the sample intensity by that of the reference fluorophore as a spectrum was scanned.

Although the above method was sufficient to correct for intensity

fluctuations of the lamp, an additional correction was required for the variation of the polarization of the incident beam with excitation wavelength when measuring excitation spectra. This correction was required because of the polarization bias of both the excitation double monochromator and the beam splitter. As the beam splitter preferentially reflected vertically polarized light, the reference photomultiplier was unable to correct for the polarization variation with excitation wavelength.

Excitation correction factors took the form of a rhodamine excitation spectrum which was obtained in the following manner: a concentrated solution of rhodamine 6G in ethylene glycol was placed in a triangular cell in the sample compartment. The cell was oriented so that the hypotenuse faced the excitation beam. The excitation spectrum was measured through a Corning 2–62 filter at an emission wavelength of 640 nm, bandpass 4 nm. During the measurement, the "sample" photomultiplier signal was divided by the "reference" photomultiplier signal as described above. The quantum yield of fluorescence and emission maximum of concentrated solutions of rhodamine 6G at 640 nm are independent of excitation wavelength (Melhuish, 1955). The filter was used to select only fluorescent light. The spectrum was measured with a Special Optics depolarizer (model 80–1016) in the excitation path and a Glan–Taylor emission polarizer (Melles Griot, Irvine, CA) oriented at 35.3° to the vertical. Under these conditions, the variation of the fluorescence intensity was due only to the intensity variation of the excitation light with wavelength. The excitation correction factors generated in this way are shown in Figure 2.2. Corrected fluorescence excitation spectra were obtained by dividing the measured spectrum by these correction factors. In Figure 2.2, it can be seen that the correction factors in the range of 250 – 300 nm are

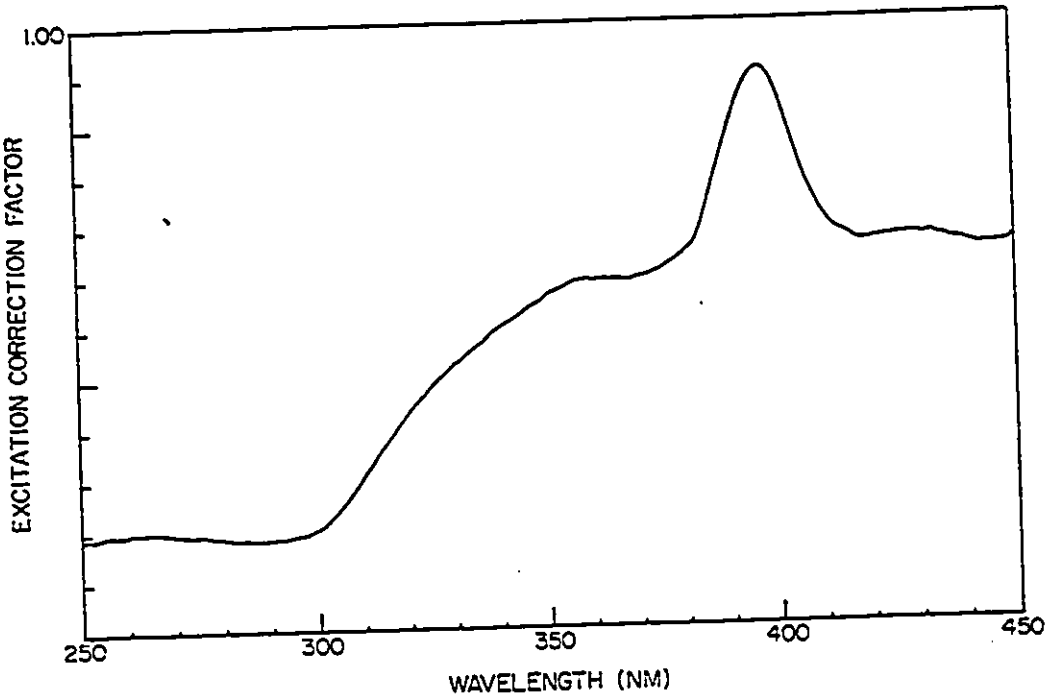

Figure 2.2: Excitation spectral correction factors.

relatively constant. Since the fluorescence excitation spectra of the proteins reported in this thesis were typically measured in the range 240 – 300 nm, correction due to the polarization of incident light had little effect upon the spectral shape and hence was optional.

All spectra were measured with a depolarizer in the excitation path and an emission polarizer oriented 35.3° to the vertical. This arrangement gave equal intensities of both the vertical and horizontal components of the emission (Spencer & Weber, 1970). A commonly used alternative arrangement involves the placement of a vertically oriented polarizer in the excitation path and an emission polarizer oriented at 54.7° to the vertical. However, as can be seen in the fluorescence emission spectrum of N–acetyltryptophanamide (NATA), a derivative of tryptophan (Figure 2.3), the former arrangement was more effective in reducing the extra 390 nm peak arising from the transmission properties of the monochromator (compare spectra B and C in Figure 2.3). In the experiments, Glan–Taylor polarizing prisms were used owing to good transmission properties down to 215 nm. Glan–Thompson polarizers were found to cut off the light sharply at wavelengths < 295 nm which was undesirable when measuring protein spectra. Finally, by ensuring that spectra measured on different days were collected with identical polarizer orientations, errors arising from the different transmission efficiencies of the polarizers were avoided. In general most polarizers transmit vertically polarized light with a higher efficiency at wavelengths < 350 nm, causing spectra recorded through a vertically oriented polarizer to be shifted to shorter wavelengths. The effect of the orientation of the emission polarizer on the spectrum of NATA is shown in Figure 2.4.

Just as uncorrected excitation spectra are composites of the true excitation

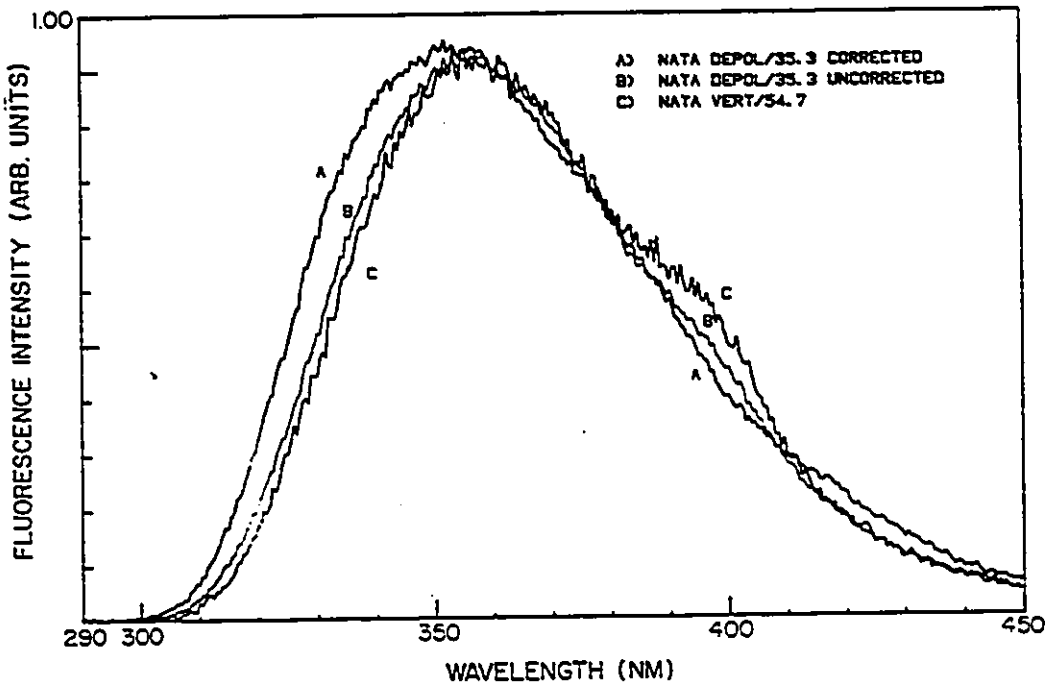

Figure 2.3: The effect of polarizer orientations and correction factors on the fluorescence emission spectrum of NATA. NATA was dissolved in 10 mM cacodylate buffer, pH 7 to a concentration yielding an optical density of 0.1 at the excitation wavelength, $\lambda_{ex} = 280$ nm. The excitation and emission bandpass were 4 nm and the spectra were recorded at 20°C. Spectra A and B were recorded with a depolarizer in the excitation path and an emission polarizer oriented at 35.3° to the vertical. Spectrum C was recorded with a vertically oriented excitation polarizer and an emission polarizer oriented at 54.7° to the vertical. Spectrum A has been corrected for the instrument response using the correction factors shown in Figure 2.5.

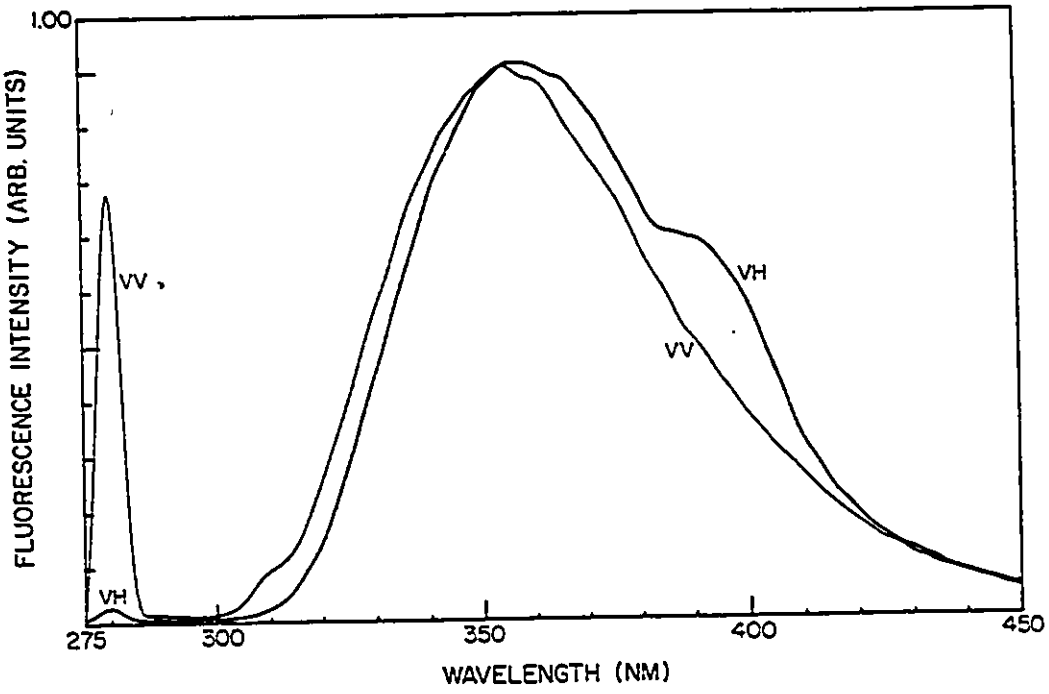

Figure 2.4: The effect of the orientation of emission polarizers on the fluorescence emission spectrum of NATA. The sample was prepared as described in Figure 2.3 except that a small amount of glycogen was added to increase scattering of the excitation radiation. The notation "VV" denotes the spectrum measured with vertical orientations of both the excitation and emission polarizers, while the notation "VH" denotes the spectrum measured through a vertically oriented excitation polarizer and a horizontally oriented emission polarizer.

spectra and the wavelength profile of the excitation source output and excitation monochromator, uncorrected emission spectra are composites of the true emission spectra and the wavelength dependence of the photomultiplier detector and emission monochromator. Although emission correction factors were supplied with the SLM 8000C software, these factors only began at 300 nm and were relatively featureless (Figure 2.5) owing to the assumption that a smooth function existed between recorded 50 nm intervals. As a result, the correction factors provided at 0.2 nm intervals had to be obtained by interpolation. In addition, the factors were measured using a vertically oriented excitation polarizer and an emission polarizer oriented at 54.7° which differed from the preferred set–up of a depolarizer in the excitation path and an emission polarizer oriented at 35.3°. More detailed correction factors extending to 270 nm were measured by synchronously scanning the excitation and emission monochromators with a quartz diffuser plate at an angle of 45° in the sample compartment (Kirby, 1971). This provided a lamp–excitation monochromator output spectrum distorted by the variation of emission monochromator throughput and photomultiplier tube sensitivity with wavelength. The emission correction factors were then determined by dividing the rhodamine excitation spectrum (true lamp) which was measured as described above by this latter spectrum. The emission correction factors are shown in Figure 2.5. Corrected emission spectra were obtained by multiplication of the uncorrected emission spectra by these correction factors. An example of the difference between an uncorrected and corrected spectrum of NATA is shown in Figure 2.3 (Spectra B and A, respectively).

In order to avoid inner filter effects, the optical density of the protein solutions at the excitation wavelength was always less than 0.1. Inner filter effects

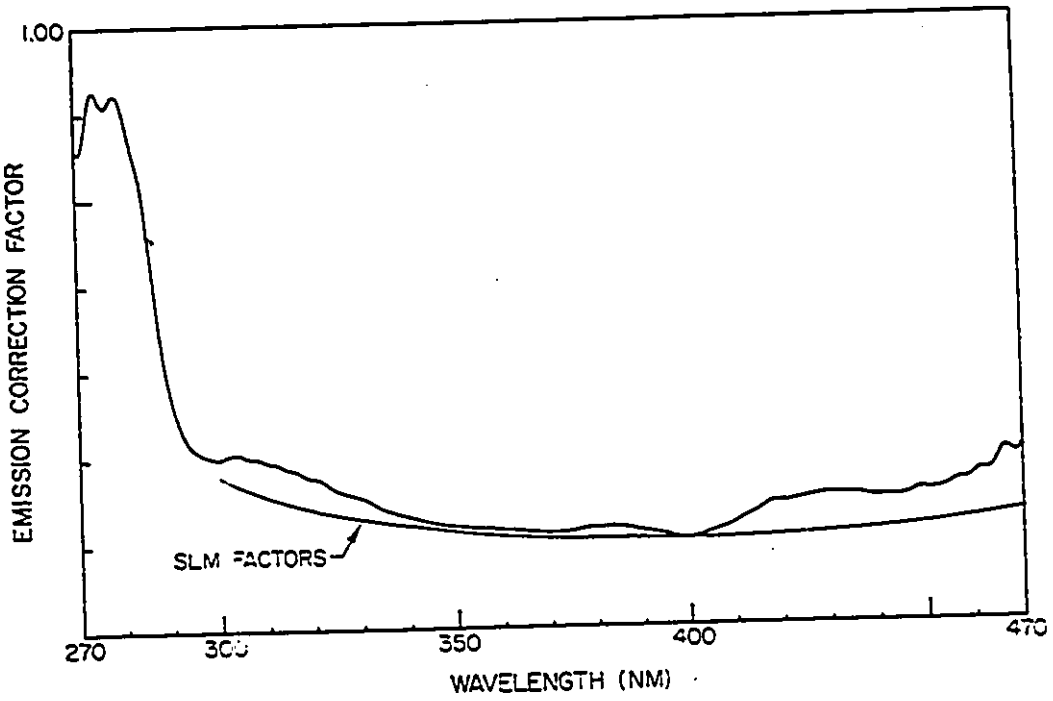

Figure 2.5: Emission spectral correction factors.

should be avoided as they result in non–linearity between the observed fluorescence intensity and the fluorophore concentration. Inner filter effects arise because, in most instruments, both excitation and emission optics focus on the centre of the sample and, to a first approximation, it is only luminescence generated at this focus which is detected (Penzer, 1980). To illustrate the influence of the inner filter effect, consider the following two conflicting effects of doubling the concentration of a fluorophore. One effect of doubling the fluorophore concentration is to double the number of potential emitters in the observed volume of solution. This would double the observed fluorescence intensity. A second effect is to double the number of absorbing species in the volume of solution through which the exciting beam must pass before reaching the focus. This effect would reduce the intensity of light incident on the observed volume of solution thereby tending to lower the observed fluorescence. It is only at low absorbances (≤ 0.1), i.e. dilute solutions, that the first effect will dominate allowing the emission intensity and fluorophore concentration to be almost proportional. At higher absorbance values, emission intensity can actually decrease as the concentration is increased. Thus it is especially important when measuring quantum yields of fluorescence that the absorbance values at the excitation wavelength be ≤ 0.1. When working with protein solutions, the low optical density coincided with relatively low sample concentrations (typically $5 - 40$ μM). This was desirable as it meant that only small amounts of sample were required for a given experiment, and further that chances of sample aggregation and light scattering were reduced. Fluorescence data could be collected with a minimum of 1.5 mL of solution in 1 cm–pathlength quartz cuvettes, or when the samples were particularly scarce, data could be obtained with a minimum volume of 750 μL in 0.5 cm–pathlength quartz cuvettes. The latter cells were held snugly in the

sample chamber by specially–constructed metal adapters. Finally, the fluorescence was collected with right angle illumination in order to further minimize effects of scatter and reflection of the exciting light (Kirby, 1971).

2.1.2 Quantum Yield Measurements

Absolute measurements of fluorescence quantum yields, ϕ_f are difficult to perform owing to the large number of effects that can influence the determination of the rates of both photon absorption and emission (See Section 1.2.3 for definition). Although different methods do exist (Crosby et al., 1972), no single method has been found to be ideal (Miller, 1981). As a result, it has become common practice to measure quantum yields relatively, i.e., by comparison with standard reference compounds. In such a manner, the fluorescence quantum yield, ϕ_f, can be calculated using the following equation (Demas & Crosby, 1971):

$$\phi_f(s) = \phi_f(r) \cdot \frac{1-10^{-A_r}}{1-10^{-A_s}} \cdot \frac{D_s}{D_r} \cdot \frac{I(\lambda_s)}{I(\lambda_r)} \cdot \left[\frac{\eta_d(s)}{\eta_d(r)}\right]^2 \qquad (2.1)$$

where "s" refers to the sample, "r" refers to the reference compound, A_s and A_r are the absorbances of the sample and reference compounds, respectively, at the excitation wavelength, D_s and D_r equal the integrated areas under the emission spectra of the sample and reference compounds, respectively, $I(\lambda_s)/I(\lambda_r)$ is the relative intensity of the exciting light at the two excitation wavelengths used to measure the sample and reference emission spectra, and $\eta_d(s)$ and $\eta_d(r)$ are the refractive indices of the solvent in which the sample and reference compounds, respectively, are dissolved. If the sample and reference compounds have spectra in

the same spectral region and if they are excited at the same excitation wavelength, λ_{ex}, under identical conditions of illumination, and if both compounds are dissolved in the same buffer, the last two terms, $I(\lambda_s)/I(\lambda_r)$ and $[\eta_d(s)/\eta_d(r)]^2$ become equal to 1 leading to a simplification of equation 2.1. Thus in order to calculate the relative quantum yield of a sample, all that is required is a measurement of the absorbance of both the sample and reference at the excitation wavelength, and a measurement of the integrated area under the fluorescence emission spectra of both compounds when excited at λ_{ex}. In order to avoid inner filter interferences, the absorbances of both sample and reference compounds should be low, preferably less than 0.1 at λ_{ex}. As described in Section 2.1.1, under such conditions the fluorophore concentration is almost proportional to the emission intensity (Penzer, 1980).

In the work reported in the following chapters, relative fluorescence quantum yields of tryptophan–containing proteins were measured at 20°C relative to N–acetyltryptophanamide (NATA, ϕ_f = 0.14, Eisinger, 1969). The ϕ_fs of tyrosine–containing proteins were measured at 20°C relative to L–tyrosine (ϕ_f = 0.135, Chen, 1967). The reference compounds were dissolved in the same buffer, at the same ionic strength, as the proteins which were measured. Both quantum yield standards were purchased from Aldrich Chemical Co., Milwaukee, Wisconsin. These standards were selected for a number of reasons: (i) they absorb and emit light in similar spectral regions as proteins, (ii) they are relatively easy to acquire in a highly purified form and, (iii) only small amounts are required to achieve the desired optical density. NATA was chosen instead of tryptophan because it is less photolabile (Evans et al., 1978). Prior to measurement the solutions of the reference compounds were bubbled with nitrogen gas for 10 minutes in order to

displace dissolved oxygen which is a known collisional quencher of fluorescence (Ware, 1962; Lakowicz & Weber, 1973).

2.2 Time–Resolved Fluorescence Measurements

The method of time–correlated single photon counting (TCSPC) was used in the time–resolved fluorescence decay experiments to measure the singlet lifetimes, τ_Ss. This method measures the time difference between the excitation of a sample and the detection of a fluorescent photon. The method relies on the concept that the probability distribution for emission of a single photon following excitation gives the actual intensity against time distribution for all photons emitted. By sampling the time of single photon emission following a large number of excitation pulses, the probability distribution is created (Phillips et al., 1985). A schematic diagram of the basic components of a time–correlated single photon counting instrument is shown in Figure 2.6.

In a time–correlated single photon counting experiment, the sample is repetitively excited with short pulses of light. The excitation source is highly attenuated by a neutral density (ND) filter so that the probability of a single photon being detected per exciting pulse is much less than one (Bollinger & Thomas, 1961). In order to ensure that the single emitted photon is randomly selected from all those emitted, the number of observed photons relative to excitation pulses is experimentally restricted. This prevents pulse pile–up errors which arise from multiple emission photon events biasing the data to shorter decay times (Coates, 1968). In order to prevent this distortion, a ratio of 1 fluorescent photon:100 excitation pulses is experimentally selected (Harris & Selinger, 1979). The resulting "single photon" response at the microchannel plate–photomultiplier tube detector (MCP) is routed through a discriminator to the START input of a

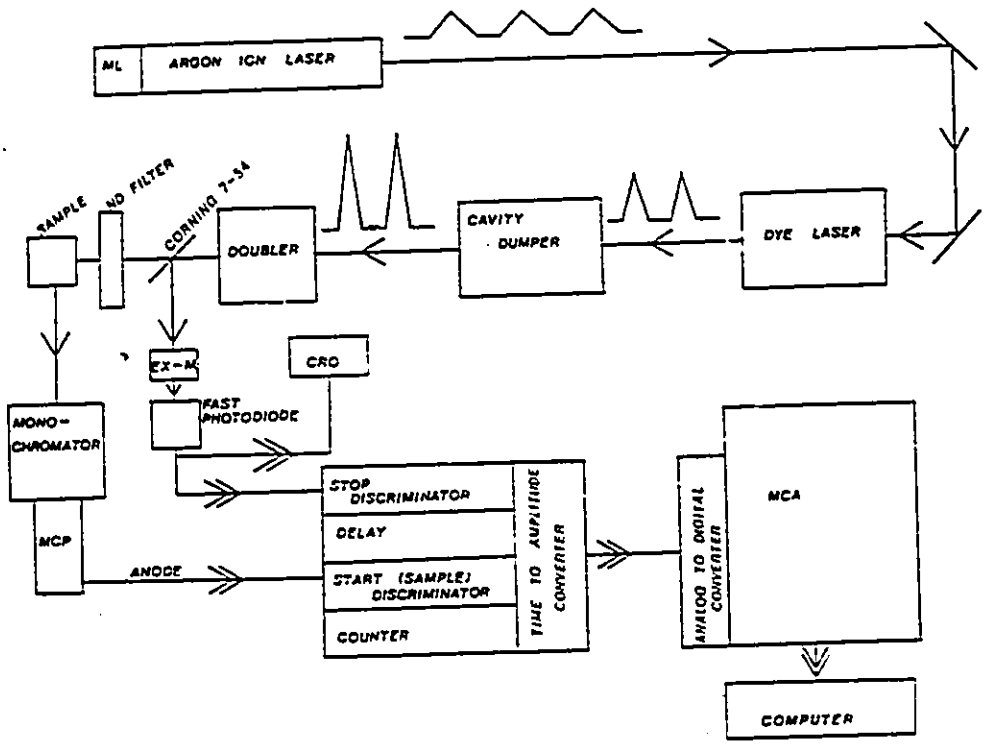

Figure 2.6: Components of the time–correlated single photon counting instrument. The abbreviated components are as follows: ML, mode–locker; ND filter, neutral density filter; EX–M, excitation monochromator; CRO, cathode ray oscilloscope; MCP, microchannel plate photomultiplier tube; MCA, multichannel analyzer.
⟶ corresponds to an optical signal and
⟶⟶ corresponds to an electronic signal.

time–to–amplitude converter (TAC) where a linear voltage–time ramp is initiated. The voltage ramp in the TAC is stopped by an electrical pulse from a fast photodiode which is generated at a fixed time exactly correlated with the time the sample is excited by the next optical pulse. The voltage reached in the TAC ramp is proportional to the time difference between the START and STOP pulses. The voltage output from the TAC of the single photon event is given a digital value in the analogue–to–digital converter (ADC) and a "count" is stored in the multichannel analyzer (MCA). Each channel of the MCA is assigned a particular time width (usually in picoseconds) such that each channel will represent a particular time difference value between excitation and single fluorescent photon detection. The histogram of the number of counts in a channel versus channel number in the MCA will represent the time–intensity profile of the sample (Knight & Selinger, 1973).

2.2.1 TCSPC Instrumental Details

The excitation source was a Spectra Physics argon ion laser (Model 2030, ceramic bore) equipped with a Spectra Physics 270 power supply. The argon ion laser is representative of a class of gas lasers that produce continuous wave (CW) output. In order to obtain the pulsed output from the laser, a Spectra Physics 342 mode–locker head was included. The argon ion laser operated at 81.6 MHz with a pulse–width of 175 ps FWHM and an average power of 470 mW at the 514.5 nm line. A Spectra Physics 314 closed loop water circulator was used to cool both the power supply and the argon ion laser tube.

The mode–locked argon ion laser was used to synchronously pump a Spectra Physics 375 dye laser. Synchronous pumping was achieved by matching exactly

(within 2 μM) the cavity lengths of the pump laser and the combination dye laser–cavity dumper (Canonica & Wild, 1985). The dye used was a 2 mM solution of Rhodamine 6G in ethylene glycol. This dye provided a tunable range of 570 – 640 nm. A Spectra Physics 376B dye laser circulator was used to circulate the dye at a pressure of 100 psi. The temperature of the dye was held constant at 30°C by passing through a heat exchanger connected to a Haake water circulator.

The output from the mode–locked argon ion synchronously–pumped dye laser was routed to a Spectra Physics 344 cavity dumper. The purpose of the cavity dumper was to reduce the pulse repetition rate in order to be within the time capabilities of the detection electronics and to increase the peak power. The cavity dumper consisted of an astigmatically compensated folded cavity formed with high reflecting mirrors and an acousto–optic Bragg diffractor centered at the focus of the cavity. With each pass through the acoustic cell, part of the cavity light was diffracted. The Bragg cell frequency effectively shifted each diffracted beam upward or downward in optical frequency by an amount equal to the radiofrequency signal set on the cavity dumper. The repetition rate, which was selectable from 1 Hz – 4 MHz was typically set at 816 kHz ($\approx$ 1200 ns interpulse separation). This operation rate was sufficiently low to allow the fluorescence from one excitation event to decay prior to the arrival of the next excitation pulse, while still allowing rapid data collection (Phillips et al., 1985). At 1200 ns intervals, the internally circulating diffracted beams were intercepted by a small prism and deflected out of the cavity. Typically, the power of the emerging light was greater than 50 mW at 590 nm. A 10 ps FWHM pulse width characterized the vertically polarized output pulses.

The output pulses from the cavity–dumped dye laser were passed to a frequency doubler. The frequency doubler was an angle–tuned second harmonic

generating KDP crystal (Cleveland Crystals, 25 mm length). The resulting UV light was vertically polarized. The UV output was passed through a 7–54 Corning filter to remove light at the fundamental wavelength which passed through the frequency doubling crystal.

Prior to reaching the sample, the UV light pulses were passed through an adjustable neutral density filter. The purpose of the neutral density filter was to adjust the intensity of the incoming light so that the ratio of detected photons to excitation pulses was 1:100. The reasons for selecting this fluorescence count rate were discussed in Section 2.2. The light was then passed to the sample which was placed in a thermostatted cell compartment which could hold up to four 1 cm cuvettes and could be rotated by the use of a Slo–Syn stepping motor. The emission wavelength was selected by a Jobin Yvon H–10 monochromator (4 nm bandpass, 0.50 mm slits) after passing through a Glan–Taylor polarizer set at 54.7° to the vertical.

After passing through the monochromator, the fluorescent photon was detected by a Hamamatsu 1564U–01 proximity–type microchannel plate (MCP) photomultiplier tube detector. The output of the MCP was amplified (Electronic Navigation Industries 500 AP amplifier), passed into a modified Tennelec TC 453 constant fraction discriminator (CFD) and directed to the START input of an Ortec 457 time–to–amplitude converter (TAC).

The 7–54 Corning filter which was used to remove fundamental light which passed through the KDP frequency doubling crystal was also used to reflect the visible light onto a Jobin Yvon H–10 monochromator and Texas Instruments TIED 56 fast photodiode. A small portion (10%) of the resulting electronic signal was directed to a Tektronix 7904 cathode ray oscilloscope in order to monitor the

performance of the laser system. The remaining signal from the photodiode was passed through an Ortec 436 leading edge discriminator and directed to the STOP input of the TAC. The ratio of STOP to START pulses was measured by an Ortec 9315 counter, using the negative output of the TAC for the number of START pulses, and an output of the excitation pulse leading edge discriminator for the number of STOP pulses.

A Wilkinson–type analogue–to–digital converter (ADC) built into the multichannel analyzer (MCA) received the positive output of the TAC and the resulting digitized signals were collected in 1024 channels of the MCA. The MCA, which was operated in the live–time mode, was a Nucleus Personal Computer Analyzer card installed in an IBM compatible AT–clone. The channel width was typically 20.5 ps/channel. The channel width was selected such that the total range was at least three times greater than the longest measured lifetime. This ensured a full representation of the sample decay curve. If the decay times were very short (approximately < 50 ps), the channel width could be adjusted to 10 ps/channel or less. To optimize the signal–to–noise ratio, a minimum of 10000 counts was usually collected in the peak of the sample decay curve giving a total of 10^6 counts in the total decay curve. This number of counts has been shown to render the data statistically significant (McKinnon et al., 1977). Each data set was transferred to a Digital VAX 11–750 for data analysis.

A buffer blank, lacking protein, was measured for each sample for the same accumulation time. By subtraction of the resulting "blank" intensity–time profile from that of the fluorescent sample, contributions due to scattered light were reduced (Chang et al., 1985). A "lamp–profile", also known as the instrument response function (IRF) was also measured by collecting for 60 s the scattered light

from a suspension of rabbit liver glycogen (Sigma) in 10 mM cacodylate buffer, pH 7.0, having an optical density of ≈ 0.1 at the excitation wavelength. Two IRFs were collected for every fluorescence decay curve that was to be analyzed; these IRFs were collected immediately preceeding and following the measurement of the fluorescent sample and the buffer blank. The purpose of measuring an IRF is outlined in Section 2.2.2.

2.2.2 Fluorescence Decay Data Analysis

If the pulse of light that excited the sample was a δ–pulse (a δ–pulse has zero width, with zero rise and fall time (Meserve, 1971)), and if the response of the detection system was infinitely fast, then the observed decay curve would represent the true decay, or δ–pulse response of the sample, $F_S(t)$. Instead, the measured fluorescence decay curve, $D_S(t)$, is distorted by the finite width of the instrument response function, $D_L(t)$, requiring the use of convolution integrals (*) for the determination of $F_S(t)$. The form of the observed decay, $D_S(t)$, when the excitation function, H(t), is not a δ–function can be deduced as follows: suppose that L(t) is the δ–pulse response of the detection system, and $D_L(t)$ is the measured time–intensity profile of the pump pulse, i.e., the instrument response function. $D_L(t)$ is then a convolution of H(t) and L(t),

$$D_L(t) = H(t) * L(t). \qquad (2.2)$$

The observed decay, $D_S(t)$ is then a convolution of $D_L(t)$ and the true decay, $F_S(t)$,

i.e.,

$$D_S(t) = D_L(t) * F_S(t)$$
$$= \int_0^t D_L(t') F_S(t-t') dt' \qquad (2.3)$$

where $D_S(t)$ represents the δ–function response of the sample distorted by convolution with both the pump pulse and the detector response, i.e., the measured decay curve. Thus the convolution integral can be solved for $F_S(t)$, if $D_S(t)$ and $D_L(t)$, measured under the same conditions of instrumental distortion, are known. Experimentally the instrument response function, $D_L(t)$ is determined by measuring the response of the system to scattered light generated by directing the excitation pulses onto a suspension of glycogen in buffer (as described in more detail in Section 2.2.1), under identical optical arrangements at the excitation wavelength. In Figure 2.7, a typical sample fluorescence decay curve ($D_S(t)$, solid line) and instrument response function ($D_L(t)$, dashed line) are shown.

A convolution of the instrument response function, $D_L(t)$ is performed with a number of trial functional forms of $F_S(t)$ using a non–linear least squares iterative convolution method based on the Marquardt algorithm (Marquardt, 1963; Bevington, 1969). With this method, the data points with the highest number of counts are more heavily weighted. If it is assumed that the instrument response function is independent of wavelength, then the above convolution procedure will yield a trial convolution function, $D_C(t)$ having parameters which correspond to those of the true decay function, $F_S(t)$. In the measurements reported in this thesis, this was a reasonable assumption as the MCP–PMT upon which the instrument response function depended, possessed a wavelength–independent response in a

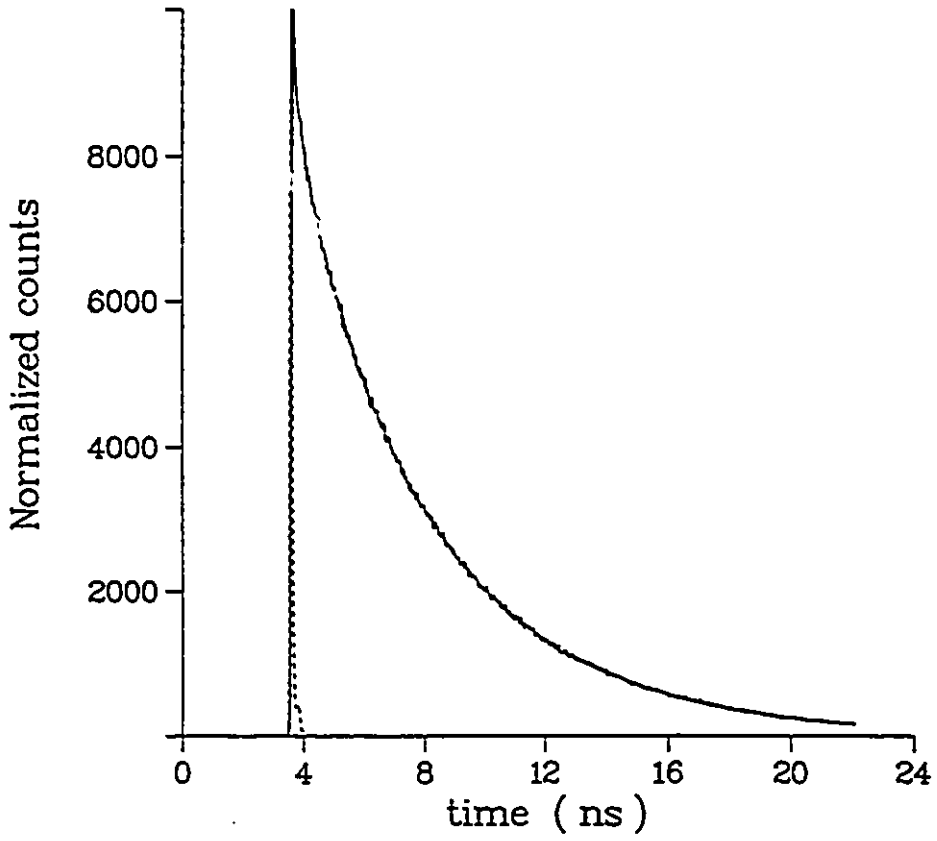

Figure 2.7: Typical normalized fluorescence time–intensity curves. The sample decay curve is given in the solid line and the instrument response function curve is given in the dashed line.

range of 300 – 800 nm (Yamazaki et al., 1985).

As described in Section 1.2.4, exponential functions represent adequate models by which the time–dependent emission of most fluorophores in dilute solution can be described. The form of these functions is given in equations 1.11 and 1.12.

The "best fit" between the experimentally measured decay curve, $D_S(t)$, and the mathematically convolved $D_C(t) = D_L(t) * F_S(t)$ curve was determined by a minimization of the weighted sum of the squares of the differences or residuals (WSSR) between the experimental points $D_S(t_i)$, and the calculated points $D_C(t_i)$. The WSSR is defined as follows:

$$\text{WSSR} = \sum_{i=1}^{n} \omega_i \, [D_S(t_i) - D_C(t_i)]^2, \qquad (2.4)$$

where n is the number of data points (or channels), t_i is the time at the ith time interval for which a measurement or computation is made, and ω_i is the weight given to the square deviation between $D_S(t_i)$ and $D_C(t_i)$ in the ith channel. In order to minimize WSSR, the greatest weight was given to points for which the variance of the experimental observation was small, i.e.,

$$\omega_i = 1/\sigma_i^2 = 1/D_S(t_i). \qquad (2.5)$$

Thus a weighted residual in a given channel i is defined simply as a function of $r(t_i)$

as shown in the following equation:

$$WSSR = \sum_{i=1}^{n} \left[\frac{[D_s(t_i) - D_c(t_i)]^2}{D_s(t_i)} \right] = \sum_{i=1}^{n} [r(t_i)]^2. \qquad (2.6)$$

The WSSR parameter is also equivalent to the statistical parameter chi–square, χ^2 = WSSR (O'Connor & Phillips, 1984). Since in the absence of systematic errors, the number of counts in a particular channel follows a Poisson distribution (Harris & Selinger, 1979), there are some rather strict limitations on the acceptable deviations of the experimental and fitted curves. If no systematic errors are present, the properly weighted residuals should have the properties of a set of independent random variables selected from a normal distribution with unit standard deviation. Based upon the determination of the weighted residuals, three different statistical parameters were examined in order to judge the quality of the fit between the experimental and calculated decay curves (McKinnon et al., 1977). These statistical parameters were (i) Sigma value, (ii) serial variance ratio and, (iii) WSSR/Sigma.

The sigma value is defined as the square root of the reduced chi–square (χ_r^2):

$$\text{Sigma} = (\chi_r^2)^{\frac{1}{2}} = \left[\frac{\chi^2}{n_2 - n_1 + 1 - p} \right]^{\frac{1}{2}} \qquad (2.7)$$

where n_1 and n_2 are the start and stop channels used for determination of the statistical parameters, p is the number of variable parameters in the trial function

D_c (two for a single exponential fit), and χ^2 is the WSSR as defined in equation 2.4. The value of Sigma should be close to 1; values much less than 1 are symptomatic of poor statistics whereas values much greater than 1 indicate a poor fit (Phillips et al., 1985). If all distorted data are rejected, Sigma values between 0.9 and 1.2 are generally acceptable. However, as it was possible to obtain acceptable Sigma values for poor fits, the Sigma values were used in combination with two other statistical parameters which are described below.

The serial variance ratio (SVR) is a statistic for testing the independence of a successive series of observations. Unlike the Sigma value, the SVR is able to provide a measure of the correlation between successive residuals (Durbin & Watson, 1951). The SVR is defined as follows:

$$SVR = \frac{\sum_{i=n_1+1}^{n_2} [r(t_i)-r(t_{i-1})]^2}{\sum_{i=n_1}^{n_2} [r(t_i)]^2} \cdot \frac{(n_2-n_1)}{(n_2-n_1-1)} \qquad (2.8)$$

An SVR value in the range of 1.7 to 2.0 is considered to correspond to a good statistical fit of the data (O'Connor & Phillips, 1984).

A more subjective, yet equally informative statistical parameter took the form of a plot of the weighted residuals ($r(t_i)$) divided by the Sigma value. Subjectively, the resulting plots were evaluated in terms of the randomness of the distribution of the points about zero. Weighted residual plots corresponding to single, double and triple exponential trial functions are shown in Figure 2.8. As can be seen, the majority of the points fall in a range of -1 to 1 which reflects the standard deviation. The complete randomness of the weighted residual plot

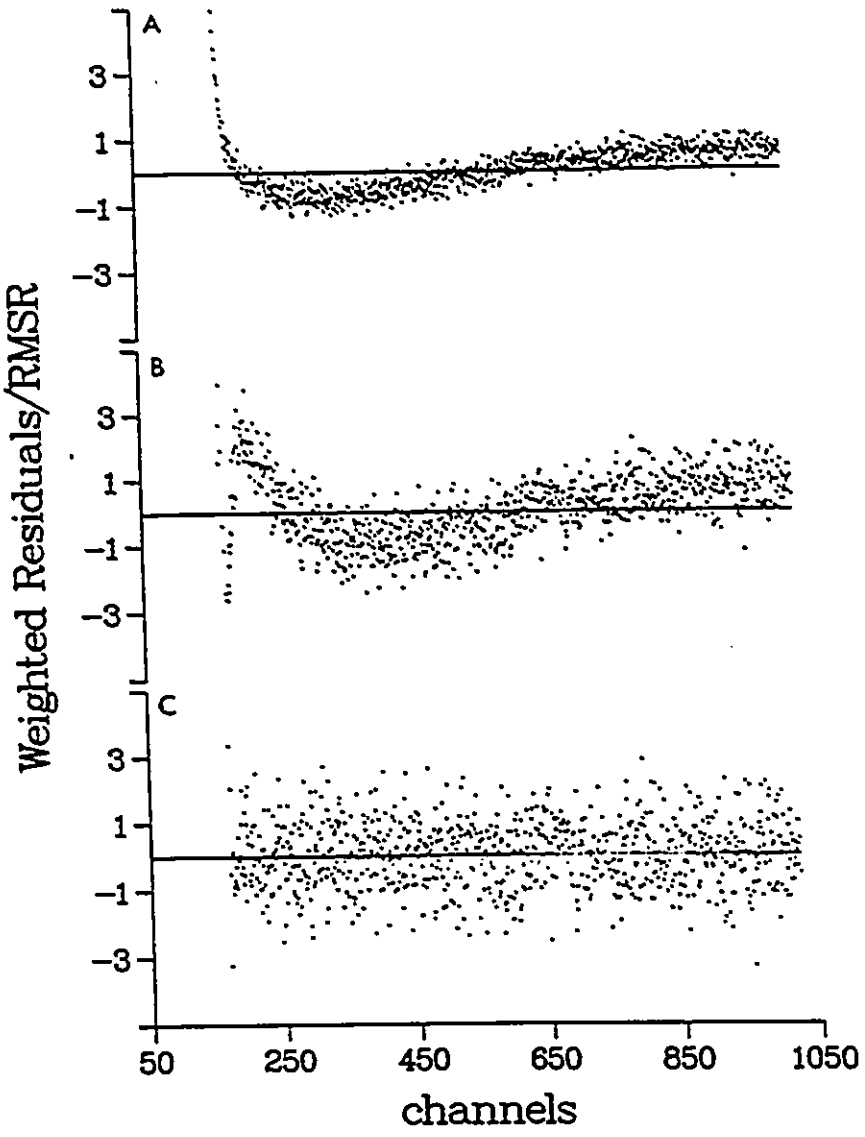

Figure 2.8: Weighted residual plots corresponding to the decay curve in Figure 2.7 fit to a (A) single, (B) double and (C) triple exponential decay function.

corresponding to a triple exponential trial function indicates that the experimental decay curve was best fit by this function.

2.2.3 Merits of the TCSPC System

A number of advantages exist by combining a mode–locked, synchronously–pumped and cavity–dumped dye laser excitation source with the method of time–correlated single photon counting. The "single photon" detection results in extremely high sensitivity. The excitation source has the desired properties of high intensity, high repetition rates variable from 80 – 4000 kHz (Szabo, 1988), complete polarization, wavelength tunability, wavelength–independent pulse shape, and very narrow pulse widths (10 ps) approximating ideal δ–pulses. The high intensity and high repetition rate allow rapid data collection and permit samples to be measured which have small quantum yield–optical density products (Ware et al., 1983). As the precision of the measured lifetimes depend upon excitation pulse stability and photomultiplier tube transit time (O'Connor & Phillips, 1984), the precision is optimized by the small 10 ps FWHM pulse width (which decreases instabilities proportionately) and the rapid transit time characteristic of the microchannel plate–photomultiplier tube (MCP–PMT). The wavelength–independence of the proximity type MCP–PMT eliminates distortions arising from time shifts between the instrument response function and the sample decay curve, and the low 10 Hz dark count rate results in very good signal–to–noise ratios. The stability and reliability of the pulse shape eliminate rising edge distortions. The stability of the excitation pulse and the wavelength–independence of the instrument response function permit routine analysis of the entire decay curve. Iterative convolution of

the appropriately weighted data results in a minimum variance in the estimated parameters.

With the system described in this thesis, multiexponential decays with up to four components have been shown tractable with lifetimes on the order of 20 ps being reproducibly measured (Szabo et al., 1989; Willis & Szabo, 1989; Holzwarth et al., 1983). Provided that the decay components are well–separated (avoiding parameter correlation), photophysical significance has frequently been assigned to multicomponent analyses (Birch & Imhof, 1985). However, Knutson et al. (1983) have shown that the limitation of the decay components being well–separated can be overcome by a simultaneous analysis of decay measurements at several different wavelengths. With this latter method it is possible to reliably recover the parameters of even closely–spaced decay components. Details regarding this method are given in the next section.

2.2.4 Global Decay Curve Analysis

The accuracy of the preexponential factors, α_is, and the lifetimes, τ_is, for a given sample is increased by the simultaneous analysis of multiple fluorescence decay curves (Knutson et al., 1983). In the work reported in the following chapters, a number of decay curves were generated by exciting the sample at one particular λ_{ex}, and subsequently monitoring the emission at a number of different λ_{em} spanning the emission spectrum. Upon establishing that the lifetimes were independent of wavelength through analysis of each individual decay curve, it was possible to link the lifetimes between the multiple decay curves and effectively decrease the number of degrees of freedom upon simultaneous analysis. As this global analysis provided a method for overdetermining the parameters, it allowed

for increased model testing sensitivity. When compared to single curve analysis, the global method was better able to resolve two closely spaced lifetimes, as well as to estimate the value of small preexponential factors (Knutson et al., 1983).

The results of a global analysis performed at one λ_{ex} and a number of λ_{em} provided the fractional contribution of each decay component to the total fluorescence at each λ_{em}. As described in Section 2.2.5, this information could directly be applied to determine the emission spectra of each of the components.

2.2.5 Decay Associated Spectra (DAS)

If the lifetime values of a particular sample are wavelength–independent, it is possible that the lifetimes may be associated with different emission spectra. By combining the time–resolved and steady–state fluorescence data, it is possible to construct decay–associated spectra, or DAS. DAS represent the relative contributions of individual lifetime components, as a function of wavelength, to the total fluorescence and were calculated based upon the following equation:

$$I_i(\lambda) = I_{SS}(\lambda)[\alpha_i(\lambda)\tau_i / \sum_i \alpha_i(\lambda)\tau_i] \qquad (2.9)$$

where $I_i(\lambda)$ is the emission intensity associated with the ith component, $I_{SS}(\lambda)$ is the total corrected steady–state intensity and $\alpha_i(\lambda)\tau_i / \sum_i \alpha_i(\lambda)\tau_i$ is the fractional fluorescence of the ith component at wavelength λ (Donzel et al., 1974). The DAS of tryptophan–containing proteins have been shown to be able to report on differences in tryptophan environments existing within the same protein (Knutson et al., 1982). In the case of single tryptophan–containing proteins, different DAS

associated with the various components would provide an indication of the different tryptophan environments in each of the various ground–state conformations. As shown in Chapters 4–6 in this thesis, changes in the DAS of particular components upon metal ion binding to parvalbumin and oncomodulin can be rationalized in terms of metal ion–induced conformational changes in the vicinity of the tryptophan probe.

2.3 References

Bevington, P. R. (1969) In: Data Reduction and Error Analysis for the Physical Sciences, (McGraw–Hill, New York).

Birch, D. J. S. & Imhof, R. E. (1985) Kinetic interpretation of fluorescence decays. Anal. Instr. 14, 293–329.

Bollinger, L. M. & Thomas, G. E. (1961) Measurement of the time dependence of scintillation intensity by a delayed coincidence method. Rev. Sci. Instr. 32, 1044–1050.

Canonica, S. & Wild, U. P. (1985) Single photon counting with synchronously pumped dye laser excitation. Anal. Instr. 14, 331–357.

Chang, M. C., Courtney, S. H., Cross, A. J., Gulotty, R. J., Petrich, M. W. & Fleming, G. R. (1985) Time–correlated single photon counting with microchannel plate detectors. Anal. Instr. 14, 433–464.

Chen, R. F. (1967) Fluorescence quantum yields of tryptophan and tyrosine. Anal. Lett. 1, 35–42.

Coates, P. B. (1968) The correction for photon "pile–up" in the measurement of radiative lifetimes. J. Phys. E. 1, 878–879.

Crosby, G. A., Demas, J. N. & Callis, J. B. (1972) Absolute quantum efficiencies. J. Res. Natl. Bur. Stds – A. Phys. Chem. 76A, 561–577.

Demas, J. N. & Crosby, G. A. (1971) The measurement of photoluminescence quantum yields. A review. J. Phys. Chem. 75, 991–1024.

Donzel, B., Gauduchon, P. & Wahl, Ph. (1974) Study of the conformation in the excited state of two tryptophanyl diketopiperazines. J. Am. Chem. Soc. 96, 801–808.

Durbin, J. & Watson, G. S. (1951) Testing for serial correlation in least squares regression. II. Biometrika 38, 159–178.

Eisinger, J. (1969) A variable temperature, U.V. luminescence spectrograph for small samples. Photochem. Photobiol. 9, 247–258.

Evans, R. F., Kuntz, R. R., Volkert, W. A. & Ghiron, C. A. (1978) Flash photolysis of N–acetyl–L–tryptophanamide: The relationship between radical yields and fluorescence quenching. Photochem. Photobiol. 27, 511–515.

Harris, C. M. & Selinger, B. K. (1979) Single–photon decay spectroscopy. II. The pile–up problem. Aust. J. Chem. 32, 2111–2129.

Holzwarth, A. R., Wendler, J., Schaffner, K., Sundstrom, V. & Gillbro, T. (1983) In: Picosecond and Biology, Eds.: T. A. M. Doust & M. A. West (Science Reviews, New York) p. 82.

Kirby, E. P. (1971) Fluorescence instrumentation and methodology. In: Excited States of Proteins and Nucleic Acids, Eds.: R. F. Steiner & I. Weinryb (Plenum Press, New York) Chapter 2A, pp. 31–56.

Knight, A. E. W. & Selinger, B. K. (1973) Single photon decay spectroscopy. Aust. J. Chem. 26, 1–27.

Knutson, J. R., Beechem, J. M. & Brand, L. (1983) Simultaneous analysis of multiple fluorescence decay curves: A global approach. Chem. Phys. Lett. 102, 501–507.

Knutson, J. R., Walbridge, D. G. & Brand, L. (1982) Decay–associated fluorescence spectra and the heterogeneous emission of alcohol dehydrogenase. Biochem. 21, 4671–4679.

Lakowicz, J. R. (1983) In: Principles of Fluorescence Spectroscopy, (Plenum Press, New York).

Lakowicz, J. R. & Weber, G. (1973) Quenching of protein fluorescence by oxygen. Detection of structural fluctuations in proteins on the nanosecond timescale. Biochem. 12, 4171–4179.

Marquardt, D. W. (1963) An algorithm for least–squares estimation of nonlinear parameters. J. Soc. Ind. Appl. Math. 11, 431–441.

McKinnon, A. E., Szabo, A. G. & Miller, D. R. (1977) The deconvolution of photoluminescence data. J. Phys. Chem. 81, 1564–1570.

Melhuish, W. H. (1955) The measurement of absolute quantum efficiencies of fluorescence. New Zealand J. Sci. Technol. 37, 142–149.

Meserve, E. T. (1971) Direct measurement of fluorescence lifetimes. In: Excited States of Proteins and Nucleic Acids, Eds.: R. F. Steiner & I. Weinryb (Plenum Press, New York) Chapter 2B, pp. 57–86.

Miller, J. N. (1981) Correction of excitation and emission spectra. In: Standards in Fluorescence Spectrometry, (Chapman & Hall, New York) Chapter 7, pp. 49–67.

O'Connor, D. V. & Phillips, D. (1984) In: Time–Correlated Single Photon Counting, (Academic Press, London).

Parker, C. A. (1958) Direct recording of fluorescence excitation spectra. Nature 182, 1002–1004.

Penzer, G. R. (1980) In: An Introduction to Spectroscopy, Ed.: S. B. Brown (Academic Press, London) pp. 70–114.

Phillips, D., Drake, R. C., O'Connor, D. V. & Christensen, R. L. (1985) Time correlated single–photon counting (TCSPC) using laser excitation. Anal. Instr. 14, 267–292.

Spencer, R. D. & Weber, G. (1970) Influence of brownian rotations and energy transfer upon the measurements of fluorescence lifetime. J. Chem. Phys. 52, 1654–1663.

Szabo, A. G. (1988) Laser instrumentation and data analysis in time–correlated photon counting fluorescence decay measurements in biochemical investigations. In: Time–Resolved Laser Spectroscopy in Biochemistry, Ed.: J. R. Lakowicz (SPIE Proceedings, Los Angeles) Volume 909, pp. 2–7.

Szabo, A. G., Willis, K. J., Krajcarski, D. T. & Alpert, B. (1989) Fluorescence decay parameters of tryptophan in a homogeneous preparation of human hemoglobin. Chem. Phys. Lett. 163, 565–570.

Ware, W. R. (1962) Oxygen quenching of fluorescence in solution: An experimental study of the diffusion process. J. Phys. Chem. 66, 455–458.

Ware, W. R., Pratinidhi, M. & Bauer, R. K. (1983) Performance characteristics of a small side–window photomultiplier in laser single–photon fluorescence decay measurements. Rev. Sci. Instr. 54, 1148–1156.

Willis, K. J. & Szabo, A. G. (1989) Resolution of tyrosyl and tryptophyl fluorescence emission from subtilisins. Biochem. 28, 4902–4908.

Yamazaki, I., Tamai, N., Kume, H., Tsuchiya, H. & Oba, K. (1985) Microchannel–plate photomultiplier applicability to the time–correlated photon–counting method. Rev. Sci. Instr. 56, 1187–1194.

Chapter 3

THE CONFORMATIONAL HETEROGENEITY OF AZURIN AND METALLO AZURIN DERIVATIVES

3.1 Introduction

The azurins comprise a homologous class (Ambler & Brown, 1967; Ryden & Lundgren, 1973) of blue copper–containing, low molecular weight ($M_r \simeq 14000$) proteins which function as redox partners in bacterial electron transfer (Brunori et al., 1974; Brunori et al., 1975; Wilson et al., 1975). Their study has been pursued not only to better understand the molecular basis of biological electron transfer (Wherland & Pecht, 1978; Brill, 1978), but also to determine what aspects of their structure give rise to their unique spectroscopic properties (McMillin & Tennent, 1979; Szabo et al., 1983; Tennent & McMillin, 1979; Ugurbil et al., 1977a; Tullius et al., 1978). Among the extraordinary spectroscopic properties is an unusually high extinction coefficient of the absorption transition near 600 nm (Fee, 1975). Studies have shown that the geometry and nature of the ligands at the active site are responsible for the protein's unique spectroscopic properties, as well as playing an influential role in the redox reactivity which is important for the protein's function (this has been summarized by Engeseth & McMillin, 1986). There is additional evidence to suggest that the structure around the copper site, which includes closely connected residues such as His–35 exhibits "fluxionality" (Adman et al., 1982). It has been suggested that this dynamic behaviour may offer an explanation for the electron transfer function of azurin (Adman et al., 1982; Adman et al., 1983; Canters et al., 1984).

The azurins from several bacterial strains have been sequenced (Ambler, 1971) and the X–ray crystallographic structures of two azurins from *Pseudomonas aeruginosa* and *Alcaligenes denitrificans* have been determined (Adman & Jensen,

1981; Norris et al., 1986). The X–ray crystallographic structure of *Pseudomonas aeruginosa* azurin is shown in Figure 3.1. The majority of the azurins contain 128 amino acid residues and only a single tryptophan residue at position 48 which, in all cases, is conserved. The position of the single tryptophan residue relative to the copper ion is highlighted in Figure 3.1; the purple–coloured indole side chain of tryptophan is indicated by the green arrow in this figure.

The presence of this single intrinsic fluorescent amino acid in the azurins has resulted in their use in a number of fluorescence spectroscopic studies (Grinvald et al., 1975; Mallinson et al., 1981; Munro et al., 1979). Upon excitation at 291 nm, the fluorescence emission maximum of the azurins is located at 308 nm (Burstein et al., 1977; Finazzi–Agro et al., 1973). As such, the fluorescence of Trp in azurin has the most blue–shifted emission maximum of any tryptophan–containing protein reported to date. This blue–shifted emission is clearly a consequence of the three dimensional structure of the protein since denaturation of azurin with 6 M guanidinium hydrochloride shifted the emission maximum to 351 nm (Szabo et al., 1983). In addition, the fluorescence behaviour was found to closely parallel that of 3–methylindole in methylcyclohexane solution and this similarity was attributed to the complete inaccessibility of Trp–48 in azurin to solvent molecules (Szabo et al., 1983). This was consistent with the crystallographic data which revealed that the Trp was located in the highly hydrophobic interior of an 8–stranded, β–barrel structure constituting the bulk of the azurin molecule (Adman & Jensen, 1981; Adman et al., 1978).

Previous time–resolved fluorescence studies have revealed double exponential decay behaviour for the Trp residue in holoazurin (Grinvald et al., 1975; Munro et al., 1979; Szabo et al., 1983), with the long decay time being quite similar to the

Figure 3.1: X–ray crystallographic structure of azurin from *Pseudomonas aeruginosa* (Adman & Jensen, Brookhaven Protein Data Bank). The peptide backbone is shown in white and the atomic sphere of the cupric ion is shown in blue. All sidechains have been removed except those of the following: His–35 (in two potential positions) and His–46 are shown in orange; Gly–45, Cys–112, His–117 and Met–121 are shown in yellow and Trp–48 is shown in purple. A green arrow is also shown pointing at Trp–48. The sidechains of His–46, Cys–112, His–117 and Met–121 are well–established as the copper ion–binding ligands, while the possible involvement of Gly–45 as a potential fifth ligand has also been suggested (Norris et al., 1986). The importance of His–35 and Trp–48 is discussed in the text.

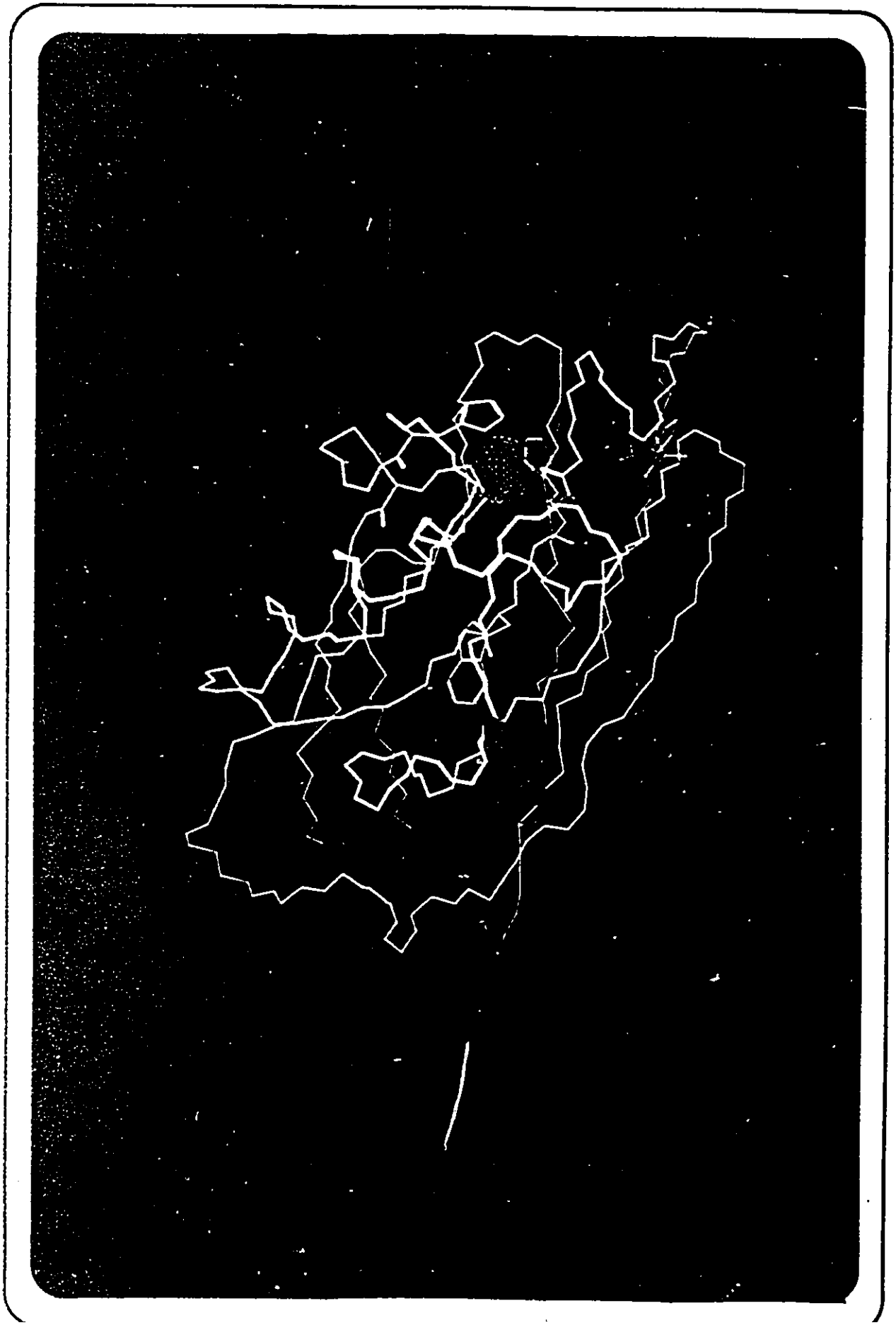

single decay time reported for the corresponding copper–less apoazurin. The time–resolved fluorescence results of several groups are summarized in Table 3.1.

TABLE 3.1

Comparison of the time–resolved fluorescence decay parameters measured by different groups for holo– and apoazurins.

SAMPLE	λ_{ex} (nm)	λ_{em} (nm)	τ_1 (ns)	τ_2 (ns)	α_1	α_2
Pae holoazurin[a]	295	>310	4.5	0.8	0.44	0.56
Pae apoazurin[a]	295	320–380	4.7			
Pae holoazurin[b]	300		4.15	0.75	0.50	0.50
Pae apoazurin[b]	300		4.79	0.88	0.60	0.40
Pfl holoazurin[c]	290	310	4.78	0.17	0.20	0.80
Pfl apoazurin[c]	290	310	4.86			
Pae? holoazurin[d]	292	325	4.15	0.102	0.03	0.97
Pae apoazurin[d]	292	325	5.16			

[a]The measurements were done by Grinvald et al., 1975. The samples were dissolved in 0.1 M phosphate buffer, pH ≈ 7. $A_{625}/A_{280} = 0.48$. *Pae* is an abbreviation for *Pseudomonas aeruginosa*.

[b]The measurements were done by Munro et al., 1979. The samples were dissolved in 0.05 M sodium phosphate/0.15 M NaCl, pH 7.4. $A_{625}/A_{280} = 0.5$.

[c]The measurements were done by Szabo et al., 1983. The samples were dissolved in 0.01 M cacodylate buffer, pH 5.3. $A_{620}/A_{280} > 0.47$. *Pfl* is an abbreviation for *Pseudomonas fluorescens*.

[d]The measurements were done by Petrich et al., 1987. The samples were dissolved in 0.05 M acetate buffer, pH 5.0. $A_{625}/A_{280} = 0.56$. The question mark indicates that some uncertainty exists regarding the source of this azurin (See section 3.4.3).

The initial interpretation was that the multiexponential decay behaviour of holoazurin was due to the protein's conformational heterogeneity (Grinvald et al., 1975; Szabo et al., 1983). In contrast to this interpretation, Petrich et al. (1987) reported that the long decay time component in holoazurin was due to an apoazurin contaminant. Because of the critical nature of this point in the interpretation of the fluorescence spectral data, it was necessary to establish definite biochemical criteria by which the homogeneity of azurin could be assessed. Once confidence in the purity of the samples was achieved, both steady–state and time–resolved fluorescence measurements on the homogeneous protein might confirm or refute the earlier interpretations (Szabo et al., 1983). Additional studies aimed at determining the influence of the metal ion centre on the protein's conformational properties could then also be assessed.

Earlier it had been shown that cobalt(II) and nickel(II) bind to apoazurin to form a metalloazurin complex (Ferris et al., 1979; Tennent & McMillin, 1979; Blaszak et al., 1982; Engeseth et al., 1984; Engeseth & McMillin, 1986) having the same amino acid residues as ligands as the native copper–containing azurin. Furthermore, it had been suggested that in the case of Co(II) and Ni(II) azurin, the metal–ligand cluster possessed a pseudotetrahedral structure not unlike the holoazurin. This implied that the protein structure restricted the metal–ligand complex from assuming its preferred planar geometry. It has been suggested that the nonplanar metallo ligand complex confers a more positive reduction potential on the metal, leading to a more favourable electron–transfer process (Gray & Solomon, 1981; Gray & Malmstrom, 1983). As different metals possess different sizes and different geometrical preferences (Ambler, 1971), they have the potential of providing useful information on the active site and the factors controlling the

electron–transfer process.

In this chapter several lines of evidence are presented which confirm the homogeneity of holoazurin samples isolated from *Pseudomonas fluorescens* (*Pfl*) and *Pseudomonas aeruginosa* (*Pae*). The pH and temperature dependence of both the steady–state and time–resolved fluorescence behaviour of these two homologous azurins is also presented. Additional information which characterizes the azurin isolated from *Pfl* (ATCC 13525), including its amino acid composition, is reported. Differences in the conformational heterogeneity of the homologous azurins are presented based upon the fluorescence properties. A refined procedure for the preparation of apoazurin is presented along with evidence which suggests that, under certain conditions, a non–reconstitutable, non–trypsin digestible apoazurin may exist. In order to obtain information on the role of the active site geometry on the conformational properties of azurin, the Co(II) and Ni(II) derivatives of *Pfl* azurin have been prepared. In this chapter, the time–resolved and steady–state fluorescence measurements of these metalloazurins are presented and discussed in terms of the conformational heterogeneity of the protein.

3.2 Materials and Methods

3.2.1 Materials

The bacterial cultures used were *Pseudomonas aeruginosa* (ATCC 10145) and *Pseudomonas fluorescens* (ATCC 13525). In addition, samples of *Pae* azurin were purchased from Sigma Chemical Company, St. Louis, Missouri. Whatman pre–swollen CM–52 carboxymethyl cellulose cation exchange resin was purchased from Mandel Scientific Co., Rockwood, Ontario. Buffalyte 3–10, used in isoelectric focusing, was purchased from Pierce Chemical Company, Rockford, Illinois. The

FPLC mono–P HR 5–20 column, isoelectric focusing pI markers, Polybuffer 74, Sephadex G–25 and Sephadex G–75SF were obtained from Pharmacia Canada Ltd., Dorval, Quebec. Potassium cyanide, thiourea, acetone, diethyl ether and cupric chloride were purchased from BDH Chemicals Ltd., Toronto, Ontario. Cupric nitrate, ferric chloride and cobaltous chloride were purchased from Fisher Scientific Co., Fair Lawn, New Jersey. Cupric sulfate, nickelous sulfate, sodium mono– and dibasic phosphates, ammonium acetate, sodium citrate, sodium nitrate, potassium dihydrogen phosphate, sodium acetate and ammonium hydroxide were purchased from Anachemia, Montreal, Quebec. Spectrapor membrane tubing (Mw cutoff 3500) was purchased from Spectrum Medical Industries, Los Angeles, California. Bovine pancreatic trypsin, L–ascorbic acid and L–histidine were obtained from Sigma Chemical Co., St. Louis, Missouri. Magnesium sulfate was purchased from J.T. Baker Chemical Co., Phillipsburg, New Jersey. The Difco bacto yeast extract was purchased from Difco, Detroit, Michigan. All buffers were prepared from reagent–grade chemicals and double glass distilled, deionized water and, in some cases, were passed through Chelex–100 (Bio–Rad Laboratories, Richmond, California) prior to use.

3.2.2 Purification of Azurin

Pseudomonas fluorescens was grown and harvested by Mr. P. Fleming, Division of Biological Sciences, NRC, and *Pseudomonas aeruginosa* was grown and harvested by Mr. D. Griffith, Division of Biological Sciences, NRC. In each case the cells were provided as a wet cell paste from which the extraction of azurin began as described in detail beginning in the next paragraph. However, prior to this, a comment regarding the bacterial growth medium is of importance. After the

purification of azurin from a number of different wet cell preparations, it became evident that the amount of cupric ion in the bacterial growth medium was an important factor in obtaining fully copper(II)–saturated azurin. The following growth medium was optimal in achieving azurin with a 1 copper(II):1 protein stoichiometry: 5 g/L sodium citrate, 5 g/L sodium nitrate, 0.5 g/L magnesium sulfate, 1 g/L potassium dihydrogen phosphate, 4 g/L Difco yeast extract, 10 mg/L ferric chloride, 10 mg/L cupric sulfate and approximately 4.5 mL of 1 N sodium hydroxide, the latter used to adjust the pH to 6.9 – 7.1.

The first step in the purification procedure involved the preparation of acetone–dried cells from the wet cell paste (Ambler & Wynn, 1973). The acetone–dried cells were prepared by dividing the wet cells into 250 g batches which were added to 2 L of CO_2(s)–cooled (–10° – 0°C) acetone. The mixture was blended for 1 – 2 min, and then stirred for another 10 min at –10°C. The mixture was then filtered through a Buchner funnel under aspiration and washed with 0.6 L cold acetone, followed by 250 mL of cold diethyl ether. The material which had been collected on the filter was transferred to a tray, finely divided and continuously evacuated in a desiccator at room temperature until constant weight was obtained (24 – 48 hours). A typical yield from 350 g of wet cells was 80 g of dried cell powder.

Following this, the method of Ambler and Wynn (1973) was used to purify azurin from the acetone–dried cells of *Pseudomonas fluorescens* (ATCC 13525) and *Pseudomonas aeruginosa* (ATCC 10145). The soluble proteins, which included azurin, were separated from the insoluble cellular material by centrifugation of a mixture of the acetone–dried powder in 50 mM ammonium acetate buffer, pH 6.5. The pH of the supernatant obtained after the centrifugation was adjusted to pH 4.1

and the precipitated proteins removed by additional centrifugation. The supernatant, which contained the azurin, was diluted with refrigerated water and passed through pads of CM–52 cellulose (2 x 9 cm) which had been formed on a Buchner funnel. The CM–52 cellulose cation exchange resin had been pre–equilibrated with 50 mM ammonium acetate buffer, pH 4.2. The filtrate was passed through successive pads until little coloured material was adsorbed to the final pad. As azurin was blue–coloured, the location of the protein throughout the purification could be conveniently monitored simply by visible observation. The pads were collected and poured into a 4 x 30 cm column and washed with 50 mM ammonium acetate buffer, pH 4.2 to remove unadsorbed proteins. The adsorbed proteins were then eluted from the column with 50 mM ammonium acetate buffer, pH 6.5. The coloured fractions were pooled, the pH adjusted down to 4.1, and then applied to a second CM–52 cellulose column (1.5 x 16 cm) which had been pre–equilibrated with 50 mM ammonium acetate buffer, pH 4.1. The blue–coloured azurin was separated from the red–coloured cytochromes by elution of the column with 50 mM ammonium acetate buffer, pH 4.2.

Although the eluted azurin fraction was bright blue in colour suggesting that the red–coloured cytochromes had been removed, the absorption spectrum of the sample revealed that cytochrome was still present. The presence of cytochrome was indicated by the characteristic Soret band at 410 nm (Figure 3.2). In order to remove the contaminating cytochrome, the procedure of Ambler and Wynn (1973) was modified as follows. After the CM–52 ion exchange chromatography, ammonium sulfate precipitation in 50 mM ammonium acetate buffer, pH 5.5 was used instead of DEAE–cellulose chromatography. To remove the contaminating

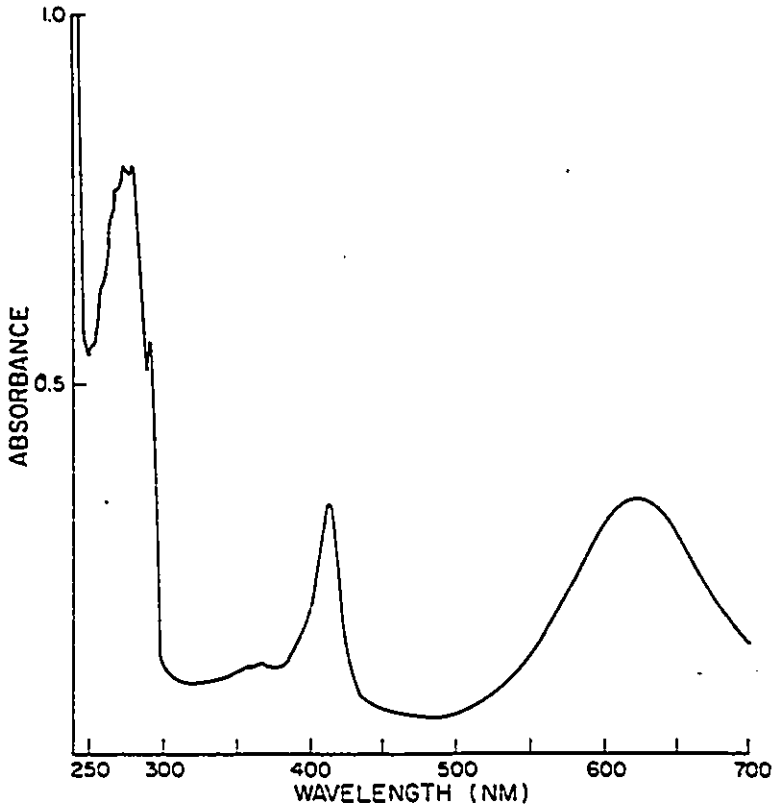

Figure 3.2: Absorption spectrum of the blue–coloured fraction obtained during the purification of *Pfl* azurin following elution from CM–52 cellulose with 50 mM ammonium acetate buffer, pH 4.2. The Soret band of contaminating cytochrome is observed at 410 nm. The 620 nm band is characteristic of the blue–coloured azurins and plays a diagnostic role in assessing the homogeneity of azurin. For homogeneity, the absorbance at 620 nm (A_{620}) divided by the absorbance at 280 nm (A_{280}) should be greater than 0.53 (See text). In the above spectrum, the spectral ratio (A_{620}/A_{280}) = 0.43 indicates that this is the spectrum of a non–homogeneous sample of azurin.

cytochrome, ammonium sulfate was gradually added at room temperature until the solution became turbid. After waiting approximately 2 to 5 minutes, the solution was centrifuged for 10 minutes at 9500 rpm. Both the supernatant and the pellet were monitored spectrophotometrically in order to locate the cytochrome (as indicated by a Soret band). This procedure was repeated until the absorption spectrum of the supernatant showed no sign of a Soret band at 410 nm. The solution was then saturated with ammonium sulfate and left at 4°C overnight. The precipitate was collected by centrifugation, redissolved in 1–2 mL of 50 mM ammonium acetate buffer, pH 5.0 and further purified by gel filtration on a Sephadex G–75SF column (2.2 x 100 cm, flowrate 8.0 mL/h) eluted with the same buffer. All blue–coloured fractions were collected and those having a spectral ratio (A_{620}/A_{280} for *Pfl*; A_{625}/A_{280} for *Pae*) greater than 0.53 were combined, concentrated on CM–52 and stored at –20°C. As will subsequently be shown, spectral ratios of 0.53 or higher correspond to homogeneous azurin samples. From 70 g of acetone–dried powder, typical yields of *Pfl* azurin were 10 – 20 mg, while consistently higher yields were obtained from *Pae*, typically 50 – 60 mg for the same amount of acetone–dried cells.

Several criteria were applied to assess the purity of the azurin samples. Molecular weight homogeneity was established by sodium dodecyl sulfate polyacrylamide gel electrophoresis (SDS–PAGE) on a 10–15% gradient using the Pharmacia PhastSystem. Charge homogeneity was established by both cationic disk polyacrylamide gel electrophoresis and isoelectric focusing in polyacrylamide gels (Righetti & Drysdale, 1971). The latter gels were run in a pH gradient of 3–10. Estimates of the isoelectric points were made by comparing the mobility of each sample with the mobility of pI marker proteins. Another test for homogeneity involved the stoichiometric determination of copper:protein by atomic absorption

spectroscopy and amino acid analysis. The amino acid analyses were performed by Dr. M. Yaguchi, Division of Biological Sciences, NRC and the copper content of the azurin samples was measured by M. Miedema, Division of Chemistry, NRC.

3.2.3 Preparation of Apoazurin

Apoazurin was prepared from holoazurin using two general procedures. The first method was a modified version of the KCN dialysis procedure that was first described by Yamanaka et al. (1963). Two – four mL of the holo samples (2 mg/mL) were initially dialyzed for 2 hours against 2.0 L of 100 mM phosphate buffer, pH 7 at room temperature. The samples were then dialyzed at room temperature against 1.0 L of 0.5 M KCN in 100 mM phosphate buffer, the pH being adjusted down to pH 8.5 with concentrated HCl after cyanide addition, in the fume hood. Judging by the lack of blue colour, the dialysis was considered complete after 20 minutes. The sample was then exhaustively dialyzed at 4°C against the desired storage buffer for the apoazurin samples. The second method used in the preparation of apoazurin involved reduction of the Cu(II) azurin to Cu(I) azurin by addition of ascorbate ion followed by dialysis against thiourea as described by Blaszak et al. (1983).

3.2.4 Metal Reconstitution of Apoazurin

Metal–reconstituted azurin samples were prepared in two ways. The first method involved dialysis of apoazurin samples ($\simeq 5 \times 10^{-5}$ M) against a 10–fold molar excess of the metal ion solution in 50 mM ammonium acetate buffer, pH 6.5 at 4°C. In some cases nitrogen gas was bubbled into the metal solutions during dialysis. Metal–reconstituted samples were also prepared by the addition of various aliquots of a metal ion solution to the apoazurin samples ($\simeq 5 \times 10^{-5}$ M) at different

metal:protein ratios. These solutions were then equilibrated at room temperature and monitored by absorption and fluorescence spectroscopy for reconstitution after various times.

3.2.5 Attempt to Further Purify Nonhomogeneous Holoazurin Samples Having Spectral Ratios Below 0.5

Holoazurin samples having spectral ratios (A_{620}/A_{280}) below 0.5 were treated with trypsin under the conditions of Ambler (1963). It had been shown that holoazurin was markedly resistant to trypsin digestion (Ambler & Brown, 1967) and thus if trypsin was added to a solution of holoazurin containing a protein contaminant, the trypsin could theoretically digest the contaminant while leaving the holoazurin molecule intact. A solution was prepared containing 14 mg of *Pfl* azurin in 6 mL of 50 mM ammonium acetate buffer, pH 8.5. To this was added 100 μL of a solution of bovine pancreatic trypsin. The enzyme solution consisted of 10 mg of trypsin dissolved in 1 mL of 50 mM ammonium acetate buffer, pH 3. The mixture of azurin and trypsin was incubated at room temperature for 7 hours. After the incubation, the pH of the solution was adjusted to pH 4.2. The solution was then applied to a CM–52 cellulose column (1 x 18 cm, 50 mM ammonium acetate buffer, pH 4.2) and eluted with the same buffer, pH 6.5. The blue–coloured fractions were pooled and then applied to a Sephadex G–25 column (1 x 30 cm) equilibrated and eluted in 50 mM ammonium acetate buffer, pH 5.0.

Pfl holoazurin samples with spectral ratios below 0.5 were also subjected to chromatofocusing using a Pharmacia FPLC system. Isoelectric focusing had revealed that the isoelectric point of *Pfl* holoazurin was approximately 6.5, and that of the corresponding apoprotein was approximately 6. As a result, the start buffer

selected for chromatofocusing was 0.025 M histidine–HCl, pH 7.2 and the eluting buffer was Pharmacia polybuffer 74–HCl, pH 5.0. Blue–coloured fractions were collected and their spectral ratios determined.

3.2.6 Reduction of Cu(II) Azurin to Cu(I) Azurin

Azurin samples were reduced according to the method of Corin and coworkers (1983). This method involved the catalytic reduction of the Cu(II) azurin by hydrogen. The blue–coloured solution of Cu(II) azurin was added to a 10–mL Amicon concentration cell fitted with a Millipore filter (0.25 μm pore size). A few milligrams of platinum black were added and the top sealed with a serological cap. Ultrahigh purity grade hydrogen gas, saturated with water, was passed over the stirred mixture and after 15 min, the colourless Cu(I) azurin solution was forced under slight hydrogen pressure into a 3 mL quartz cuvette that had been flushed with argon gas. The cuvette was sealed with a teflon cap and was ready for measurement. Spectrophotometric measurements revealed that less than 1% of the oxidized protein was present in the reduced samples, and when sealed in the cuvette, the protein remained reduced for up to 8 hours.

3.3 Results

3.3.1 Homogeneity of Protein Samples

The absorption spectrum of holoazurin from *Pfl*, illustrated in Figure 3.3, was virtually identical to spectra obtained from *Pae* holoazurin, although the 620 nm peak was generally slightly broadened in the latter. Removal of all of the cytochrome by ammonium sulfate precipitation was shown by the lack of any significant absorption near 410 nm.

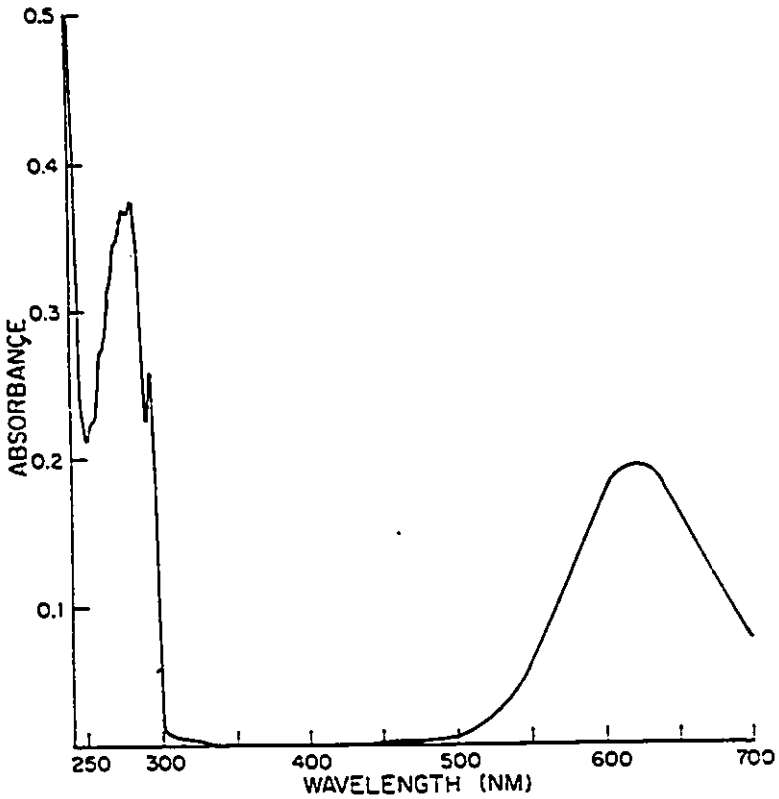

Figure 3.3: Absorption spectrum of *Pfl* holoazurin in 50 mM ammonium acetate buffer, pH 5; spectral ratio = 0.53. The lack of a Soret band near 410 nm illustrates that no cytochrome was present in this azurin sample.

Holoazurin samples of various spectral ratios were purified from *Pfl* and *Pae* and were compared by spectrophotometry and electrophoresis to commerically obtained *Pae* holoazurin samples. The absorption spectra of the *Pfl*, and the two *Pae* azurins were identical in the UV region and, in fact the only differences in the spectra were the ratios of the 620 (or 625 nm) bands to the 280 nm bands. Samples of each of these proteins were subjected to SDS–PAGE and the results are illustrated in Figure 3.4. In all cases single bands of identical mobility were observed, indicating no proteins of molecular weight different from azurin were present in the samples.

When the various protein samples were analyzed for their copper content by atomic absorption and also for their protein concentration by amino acid analysis, 100% of the expected copper was detected (i.e., a stoichiometry of 1 mole copper:1 mole protein) when the spectral ratios were above 0.50 (Table 3.2).

TABLE 3.2

Stoichiometry Determination of Copper to Protein by Atomic Absorption and Amino Acid Analysis[a]

sample	copper concn		protein concn (M)	% copper
	μg/L	M		
blank	<0.33	$<5.2 \times 10^{-9}$		
Pfl apo/CN	80 ± 0.7	$1.3 \times 10^{-6} \pm 0.01 \times 10^{-6}$	$5.74 \times 10^{-5} \pm 0.02 \times 10^{-5}$	2.3 ± 0.01
Pfl apo/ascorbate	220 ± 0.0	$3.5 \times 10^{-6} \pm 0.0$	$3.5 \times 10^{-5} \pm 0.05 \times 10^{-5}$	10.0 ± 0.1
Pfl holo, $R = 0.54$	5950 ± 106	$9.4 \times 10^{-5} \pm 0.17 \times 10^{-5}$	$9.2 \times 10^{-5} \pm 0.03 \times 10^{-5}$	102 ± 1.5
Pae holo, $R = 0.52$	3500 ± 0	$5.5 \times 10^{-5} \pm 0.0$	$5.5 \times 10^{-5} \pm 0.03 \times 10^{-5}$	100 ± 0.5
Pae holo, $R = 0.39$	4950 ± 35	$7.8 \times 10^{-5} \pm 0.06 \times 10^{-5}$	$11.5 \times 10^{-5} \pm 0.10 \times 10^{-5}$	68 ± 0.07
Pfl CN[b] + Cu(II) (reconstituted)	1748 ± 23	$2.8 \times 10^{-5} \pm 0.03 \times 10^{-5}$	$2.7 \times 10^{-5} \pm 0.08 \times 10^{-5}$	102 ± 1.9
Pfl ASC[c] + Cu(II) (reconstituted)	1810 ± 40	$2.9 \times 10^{-5} \pm 0.06 \times 10^{-5}$	$3.4 \times 10^{-5} \pm 0.07 \times 10^{-5}$	85 ± 0.02

[a]The samples were analyzed quantitatively by either graphite furnace atomic absorption spectrometry or inductively coupled plasma atomic emission spectrometry. Norleucine was added to the protein samples prior to amino acid analysis for concentration determination. Each value represents the mean of at least two individual samples, each done in duplicate, and the standard error of the mean is calculated. [b]The symbol CN denotes apoazurin preparation by the method of KCN dialysis as described under Methods. [c]The symbol ASC denotes apoazurin preparation by the ascorbate/thiourea method as described by Blaszak et al. (1983).

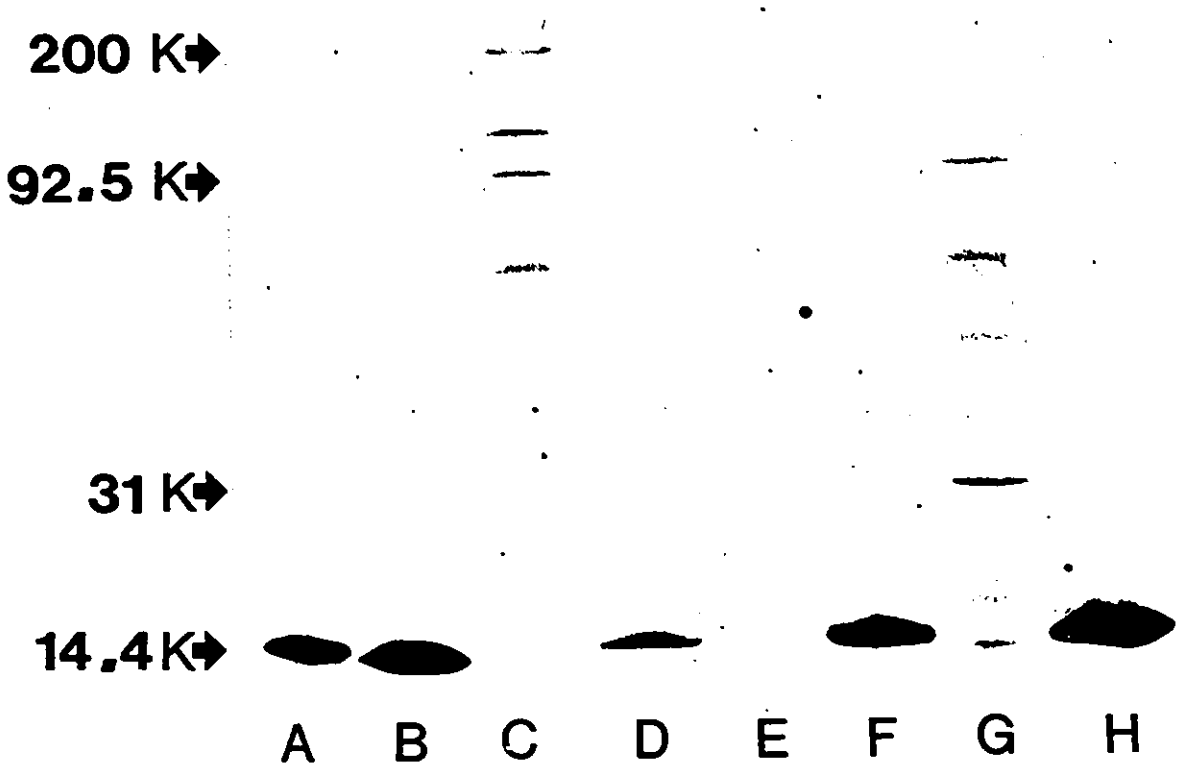

Figure 3.4: SDS–PAGE pattern of the following azurin samples: (lane A) *Pae* holo after G–75SF, spectral ratio = 0.30; (lane B) *Pfl* holo, spectral ratio = 0.55; (lane C) high molecular weight standards; (lane D) *Pae* holo before G–75SF, spectral ratio = 0.30; (lane E) sample buffer—control; (lane F) *Pae* holo, spectral ratio = 0.52; (lane G) low molecular weight standards; (lane H) duplicate sample as in lane A at double the concentration.

However, in the samples having spectral ratios less than 0.50, 1:1 stoichiometry was not obtained. Amino acid analysis results consistently revealed the same residue compositions, regardless of the spectral ratio.

Table 3.3 gives the amino acid compositions of the two homologous azurins.

TABLE 3.3

Amino Acid Composition of Holoazurin from *Ps. aeruginosa* and *Ps. fluorescens*

Amino Acid	*Pae* (ATCC 10145)	*Pfl* (ATCC 13525)
Ala	7	13
Arg	1	1
Asx	18	15
Cys	3	3
Glx	10	6
Gly	11	11
His	4	4
Ile	4	7
Leu	10	5
Lys	11	12
Met	6	6
Phe	6	6
Pro	4	3
Ser	10	11
Thr	10	12
Trp	1	1
Tyr	2	2
Val	10	10
TOTAL	128	128

The composition of *Pae* azurin was identical with that previously reported (Ambler, 1971). There have been no reports to confirm the composition of the *Pfl* azurin (ATCC 13525), but analyses from different preparations were reproducible.

The combination of the amino acid analyses, the copper stoichiometry, and SDS–PAGE results strongly indicated that a protein contaminant having a composition similar to holoazurin was present when the spectral ratios were less

than 0.50. In preparation for separation by chromatofocusing techniques, the protein preparations were subjected to isoelectric focusing to determine their isoelectric points. The isoelectric focusing results are shown in Figures 3.5 A and B. Several points were noted. The first was that the pI of *Pfl* azurin was higher than that of *Pae* azurin, and that the former protein, having a spectral ratio greater than 0.50, migrated as only a single band. The corresponding *Pfl* apoazurin, which was fully reconstitutable upon addition of Cu(II) also migrated as a single band but with a more acidic pI compared to that of the holo form. In contrast, samples of *Pae* azurin displayed additional bands with only one of the bands (marked "B" on Figure 3.5 B) appearing blue in colour prior to staining. In *Pae* holoazurin samples having spectra ratios less than 0.50, the bands which appeared second from the top of each gel upon staining, varied in intensity depending upon the spectral ratio. The intensity of this band progressively *decreased* as the spectral ratio *increased*, and the band could not be detected when the spectral ratio was 0.53, or higher. As seen faintly in a sample of *Pae* holoazurin, spectral ratio = 0.48, in Figure 3.5 B (middle gel marked "*Pae* holo"), this band was found to comigrate with *Pae* apo protein samples. A band appeared virtually at the top of the gel (pI < 3) in *Pae* azurin samples. The intensity of this band did not depend on the spectral ratio and was present in all *Pae* samples isolated by us, as well as in samples obtained from a commercial source. This band was evident even when the spectral ratios were greater than 0.56. However, this additional band was not detectable in the corresponding *Pae* apo samples. No such bands were ever detectable in the *Pfl* azurin samples. The stoichiometric determination of copper:protein by atomic absorption and amino acid analyses, showed that 1:1 stoichiometry was obtained in both *Pfl* and *Pae* holoazurin samples when the spectral ratio was 0.53 or higher.

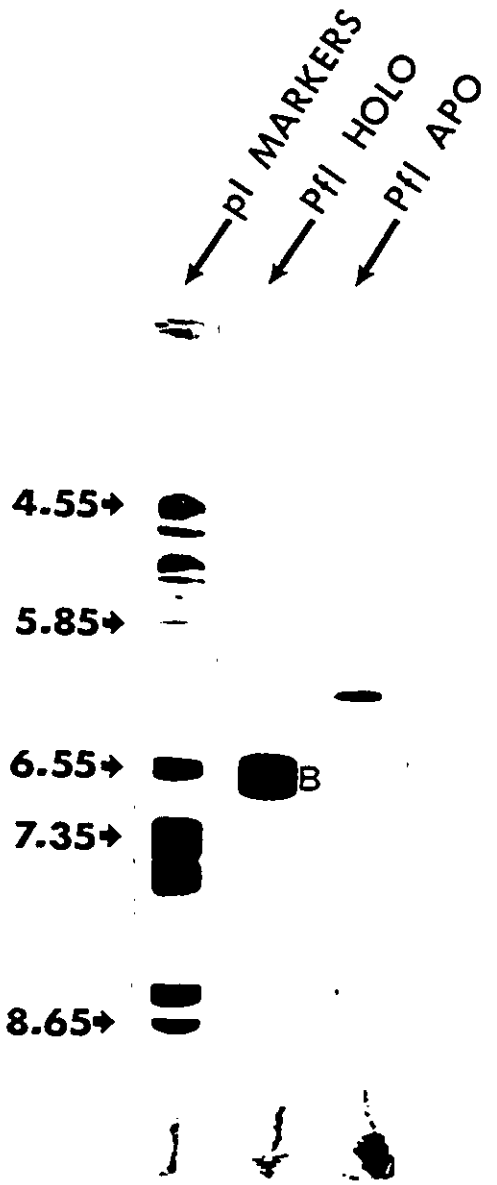

Figure 3.5 A: Polyacrylamide rod gels obtained upon isoelectric focusing of *Pseudomonas fluorescens* azurin samples in a gradient of pH 3–10 from top to bottom at a constant voltage of 250 V. The bands with a "B" located on the immediate right were blue–coloured prior to Coomassie staining and hence were assigned to blue copper–containing azurin. pI markers, holo– and apoazurin from *Pseudomonas fluorescens* (*Pfl*) are shown. The spectral ratio of the holoazurin was 0.55.

Figure 3.5 B: Polyacrylamide rod gels obtained as described in Figure 3.5 A. pI markers, holo– and apoazurin from *Pseudomonas aeruginosa* (*Pae*) are shown. The spectral ratio of the holoazurin was 0.48.

Thus the combination of the stoichiometry determinations, the amino acid compositions, SDS–PAGE and isoelectric focusing, provided strong evidence that *Pfl* holoazurin samples were homogeneous when the spectral ratios were greater than 0.53. Despite the appearance of the extra low pI (< 3) band upon isoelectric focusing of *Pae* holoazurin, these samples were also regarded as homogeneous when the spectral ratios were greater than 0.53 for reasons which will be discussed, and summarized in Section 3.4.1.

When the spectral ratios were less than 0.50, the stoichiometry determinations revealed that non–copper containing protein was present. The amino acid composition analyses, isoelectric focusing and SDS–PAGE showed that the non–copper containing contaminant had a composition very similar to that of apoazurin. Two attempts were made to separate holoazurin from this contaminant.

Earlier it had been reported (Ambler & Brown, 1967) that holoazurin was markedly resistant to trypsin digestion. Hence, it was thought that the non–holoazurin protein contaminant might be removed when samples were subjected to tryptic digestion, leaving the holoazurin intact. After treatment with trypsin the impure azurin samples were purified by ion exchange and gel chromatography. No significant improvement in the spectral ratio was achieved.

The holoazurin samples were also subjected to chromatofocusing and an elution profile was obtained in which two closely eluting bands were observed (Figure 3.6). Upon monitoring the spectral ratios, a distribution of ratios from 0.45 to 0.25 were obtained across the elution profile. The higher spectral ratios in the early eluting fractions were consistent with these fractions containing greater proportions of holoazurin, which were expected to be the first to elute owing to the

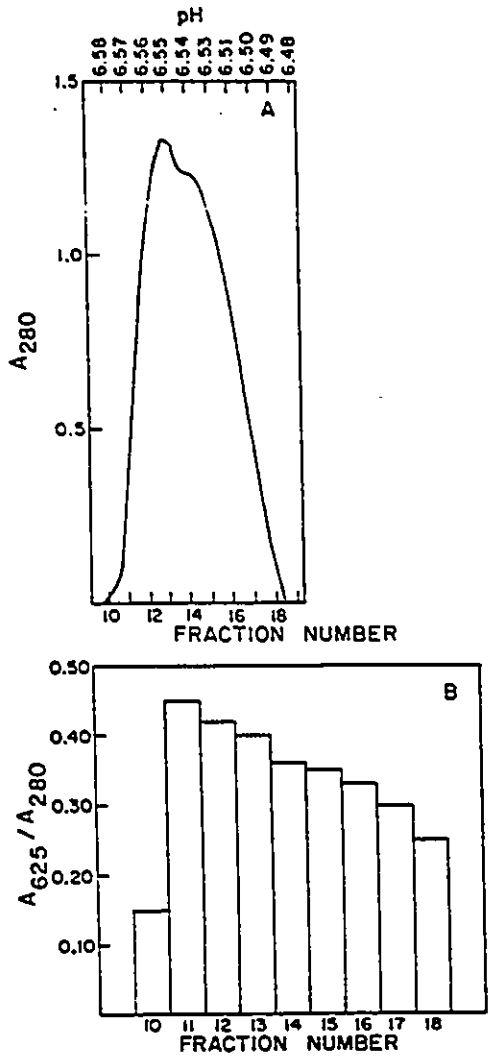

Figure 3.6: Data obtained following the chromatofocusing of *Pfl* holoazurin with spectral ratio = 0.30. In (A), the elution profile obtained upon monitoring the absorbance of the blue–coloured fractions at 280 nm shows two closely eluting bands. In (B), a histogram illustrating the spectral ratios of the various fractions is shown.

higher pI when compared to apoazurin (See Figure 3.5 A). Owing to the poor resolution of the peaks, homogeneous holoazurin from low spectral ratio samples was not achieved by chromatofocusing.

3.3.2 Preparation and Cu (II) Reconstitution of Apoazurin

Earlier reports (Blaszak et al., 1983), and the one of Petrich and coworkers (1987) suggested that it was difficult to produce an apoazurin preparation which could be fully reconstituted with copper. This problem was reinvestigated by treating holoazurin samples with different concentrations of KCN at different pH values ranging from 8.5 to 11. The critical criterion in choosing the best conditions was the ability to fully reconstitute the azurin with its original A_{620}/A_{280} spectral ratio. The second criterion was the maximal removal of copper as judged by atomic absorption analysis. In the apoazurin samples obtained, $\leq$ 2% copper was detected (Table 3.2). Figure 3.7 shows the titration of a *Pfl* apoazurin sample with aqueous Cu(II) from which an extinction coefficient for *Pfl* azurin of 5100 $M^{-1}cm^{-1}$ at 620 nm was calculated.

It was found that dialysis against lower concentrations of cyanide ion greatly increased the length of time required to remove the copper, from 20 minutes at 0.5 M KCN to over two days at 0.05 M KCN at pH 8.5. In addition, more than 10% of the copper remained bound to holoazurin under these latter conditions. If the pH of the solution was not adjusted down to pH 8.5 after 0.5 M KCN addition, the dialysis was found to take at least two hours and sometimes resulted in protein denaturation as witnessed by a loss of the characteristic azurin sharp peak at 292 nm in the absorption spectrum. The azurin spectrum could not be regenerated by addition of Cu(II) (aq) to these samples.

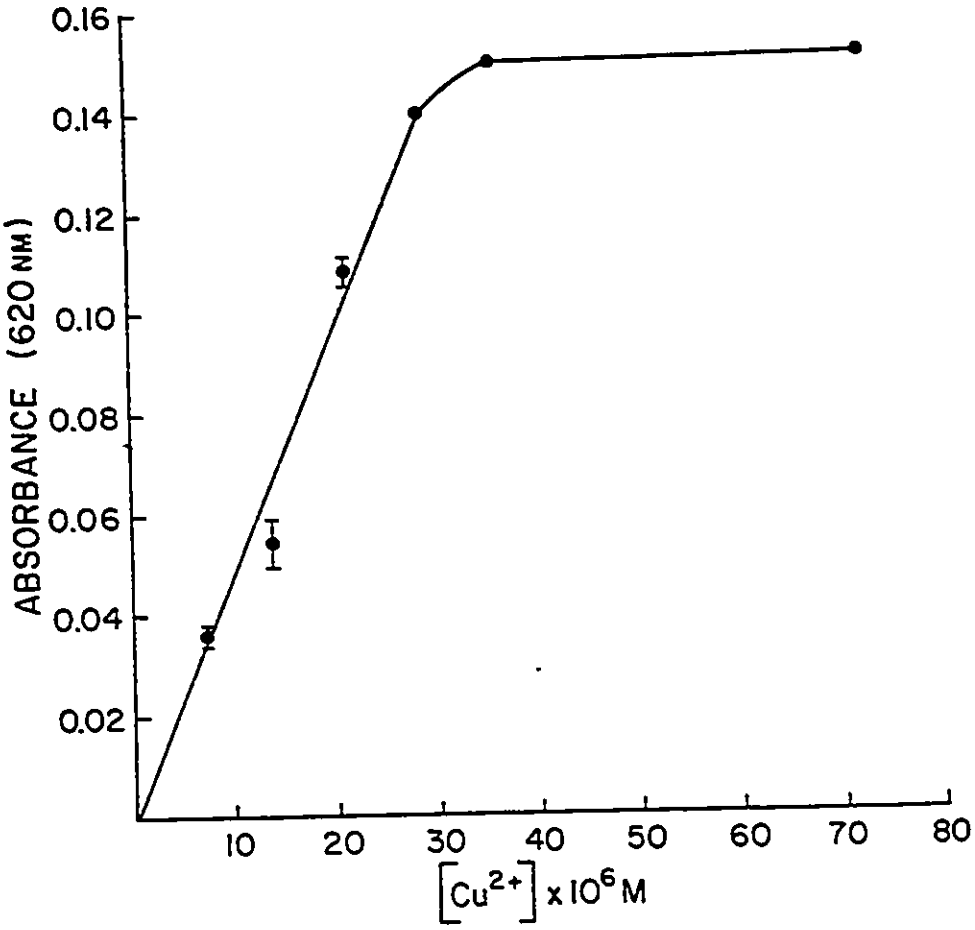

Figure 3.7: Plot of absorbance at 620 nm as a function of $CuCl_2$ concentration during the Cu(II) reconstitution of 3.6×10^{-5} M *Pfl* apoazurin. All solutions were in 50 mM ammonium acetate buffer, pH 6.5, and the values shown are the average values recorded after 6, 24, and 48 h of incubation at room temperature with duplicate samples. At the plateau a spectral ratio of 0.53 was obtained, and an extinction coefficient at 620 nm of 5100 $M^{-1}cm^{-1}$ was calculated for this *Pfl* holoazurin. Errors are reported as the standard error of the mean.

Upon preparation of the apoazurin by the method of Blaszak et al. (1983) using ascorbate ion and thiourea, it was found that no more than 90% of the original copper could be removed and full reconstitution could not be achieved (≈ 85% at best). In addition, there was evidence of absorbance at 310 nm which indicated that trace amounts of ascorbate ion, or an ascorbate decomposition product remained, even after exhaustive dialysis against ascorbate–free buffer.

The Cu(II) reconstitution of apoazurin was performed at a variety of pH values and in the presence of three different counterions, chloride, nitrate and sulfate. In some cases nitrogen was bubbled through the copper solutions during dialysis and the buffers were Chelex treated prior to addition of copper. These latter two precautions however, did not affect the final results. The nature of the counterion appeared to have no effect on the reconstitution as judged by the final spectral ratio. Neither did the pH of the solution have any effect on the final spectral ratio between pH 5 and pH 7. However, at pH > 8, a complete restoration of the spectral ratio could not be achieved. All further reconstitution experiments were conducted at pH 6.5.

3.3.3 Metallo Azurin Derivatives

The ultraviolet absorption spectra in the range of 250 – 295 nm of the Cu(II), Ni(II) and Co(II) azurins were indistinguishable, while in the visible region each derivative had its characteristic absorption bands centered at 620 nm for Cu(II) azurin, 360 nm and 445 nm for Ni(II) azurin, and 340 nm and 380 nm for Co(II) azurin (Figures 3.3 and 3.8).

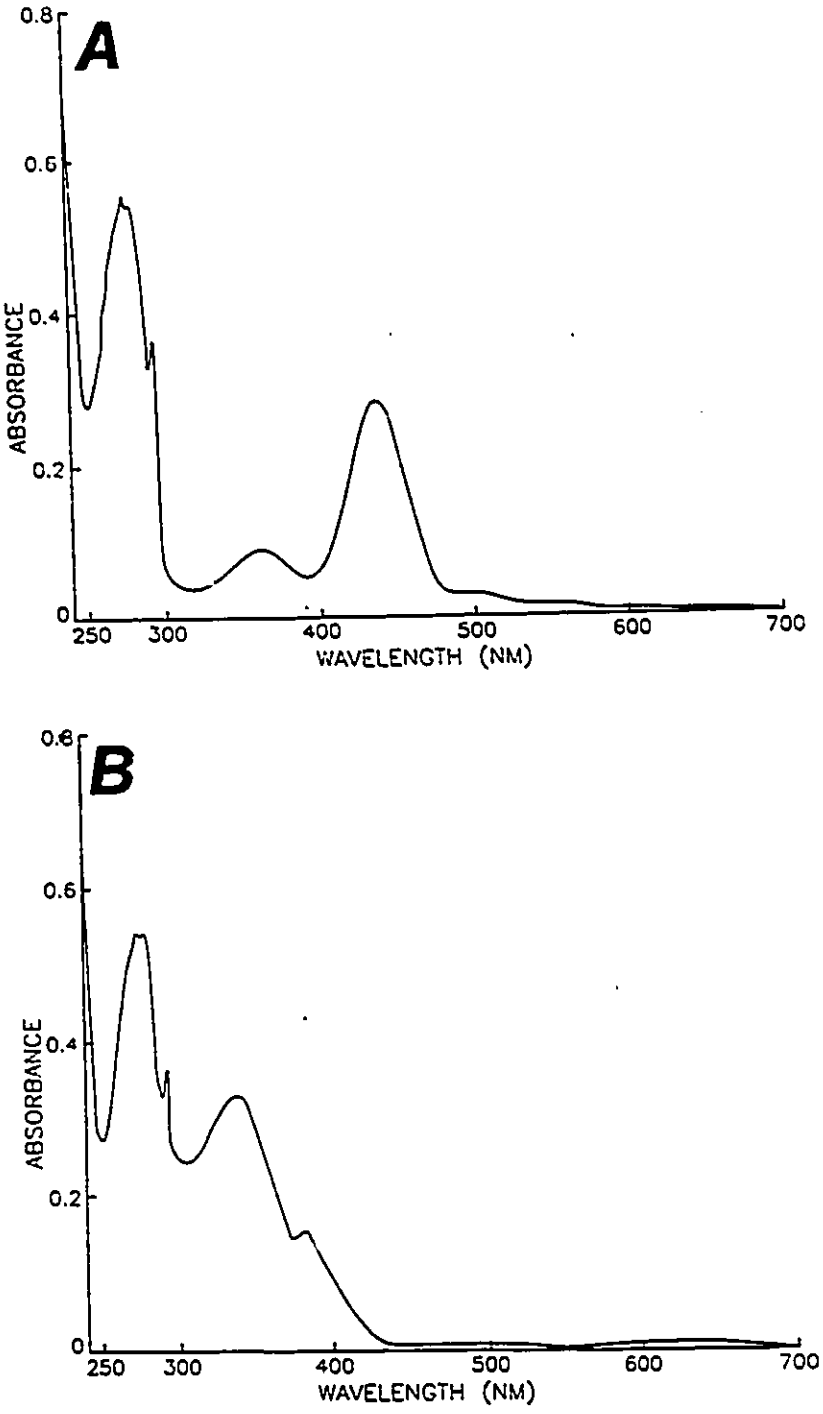

Figure 3.8: (A) UV–VIS absorption spectrum of *Pfl* Ni(II) azurin in 50 mM ammonium acetate buffer, pH 6.5. (B) UV–VIS absorption spectrum of *Pfl* Co(II) azurin in 50 mM ammonium acetate buffer, pH 6.5.

3.3.4 Steady–state and Time–resolved Fluorescence

The relative fluorescence quantum yields, ϕ_fs, measured in this work were 0.051 ± 0.002 for *Pfl* holoazurin and 0.018 ± 0.001 for *Pae* holoazurin. These quantum yields were measured at 20°C relative to apoazurin (ϕ_f (*Pfl* apoazurin) = 0.31, Szabo et al., 1983) as the latter was thought to be a better secondary standard than the usual standard, N–acetyltryptophanamide (NATA) owing to the blue–shifted emission spectrum of azurin. The effects of pH on the quantum yield of fluorescence for both holo– and apoazurin obtained from *Pfl* are shown in Figures 3.9 and 3.10. In both cases a sigmoidal curve was obtained displaying an inflection near pH 5.5 – 6. However, whereas the quantum yield remained relatively high at pH 8 for the holoazurin, it appeared to fall off at pH 8 for the corresponding apo protein. This trend was confirmed by continued titration which at pH 9 resulted in a relative fluorescence quantum yield equal to 42% of the pH 7 value for the apoprotein.

In addition to titration in 50 mM ammonium acetate buffer, concentrated solutions of *Pfl* holo– and apoazurin samples were also diluted into at least a 10–fold volume excess of the following buffers: 10 mM cacodylate buffer, pH 5, 5.5, 6, 6.5 and 7; 10 mM TRIS–HCl, pH 7 and 8; 10 mM carbonate buffer, pH 9. The measured quantum yields of fluorescence were within the error bars shown in Figures 3.9 and 3.10 which demonstrated that (i) the negligible buffering capacity of ammonium acetate buffer at high pH was not affecting the measurements and, (ii) different buffer ions had no particular effects on the measurements.

Upon the addition of Cu(II) ion to a solution of apoazurin, a 6–fold quenching of the Trp fluorescence was observed. The resulting quantum yield was

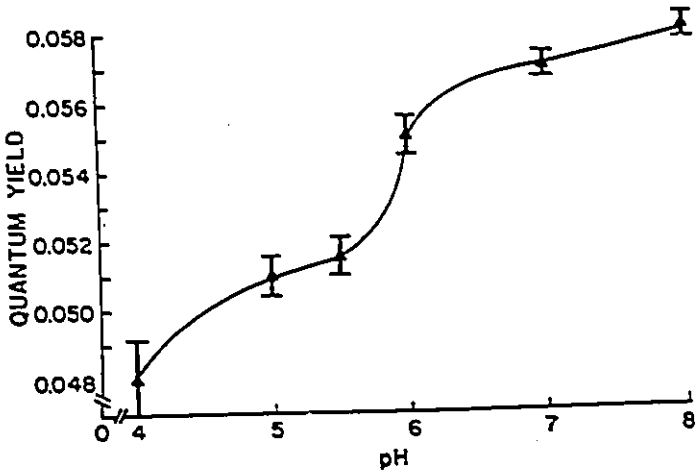

Figure 3.9: Effect of pH on the quantum yield of fluorescence of *Pfl* holoazurin in 50 mM ammonium acetate buffer. The sample absorbance at the excitation wavelength was always less than 0.1, and the quantum yields were calculated relative to previously determined values of *Pfl* apoazurin at 20°C (Szabo et al., 1983). Errors are reported as the standard error of the mean.

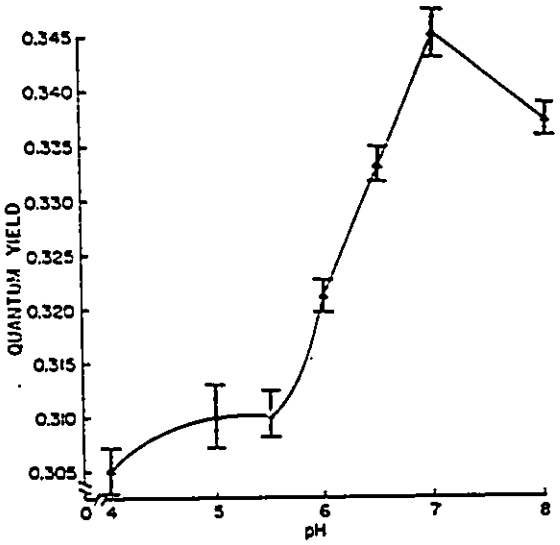

Figure 3.10: Effect of pH on the quantum yield of fluorescence of *Pfl* apoazurin (prepared by the modified cyanide ion dialysis method, See Section 3.2.3) in 50 mM ammonium acetate buffer. The sample absorbance at the excitation wavelength was always less than 0.1, and the quantum yields were calculated relative to previously determined values of *Pfl* apoazurin at 20°C (Szabo et al., 1983). Errors are reported as the standard error of the mean.

the same in the presence of either a 2–fold or a 10–fold molar excess of Cu(II). This amount of quenching corresponded to a 1 mole copper:1 mole protein sample. Addition of a 10–fold excess of Ni(II) resulted in a 2.2–fold quenching of the fluorescence, while addition of the same excess of Co(II) produced a 2.1–fold quenching. The steady–state fluorescence emission spectra, when normalized at 308 nm, were superimposable for all of the metallo–azurin forms. Figure 3.11 shows the relative quantum yield of fluorescence of each of the *Pfl* metallo azurin proteins as a function of metal:protein ratio. The data shown are the mean of three trials recorded after 48 hours. The ϕ_fs recorded after dialysis against a 10–fold molar excess of each metal ion are also shown in this figure. The 1:1 complex plateau values corresponded to relative fluorescence quantum yields of 0.15 ± 0.01 for Ni(II) azurin, 0.16 ± 0.01 for Co(II) azurin, and 0.055 ± 0.005 for Cu(II) azurin.

It is important to note that a plateau ϕ_f was achieved when either Cu(II), Co(II), or Ni(II) was added to apoazurin. When the copper solutions were also monitored by absorption spectroscopy, full restoration of the original spectral ratio was achieved, which suggested that this preparation of apoazurin was completely reconstitutable. Only small changes in the absorbances at 295 nm were observed. Atomic absorption and amino acid analysis revealed a 1 mole copper:1 mole protein complex had been formed (prior to these analyses the samples were either dialyzed against copper–free buffer or desalted by G–25 gel filtration).

When monitored after 6 hours of equilibration at room temperature, both Cu(II) azurin and Co(II) azurin had ϕ_fs which remained constant over the next 48 hours; however, the ϕ_f observed for Ni(II) azurin after 6 hours was higher than the ϕ_fs recorded after 24 and 48 hours which suggested that more than 6 hours was required to achieve full Ni(II) incorporation.

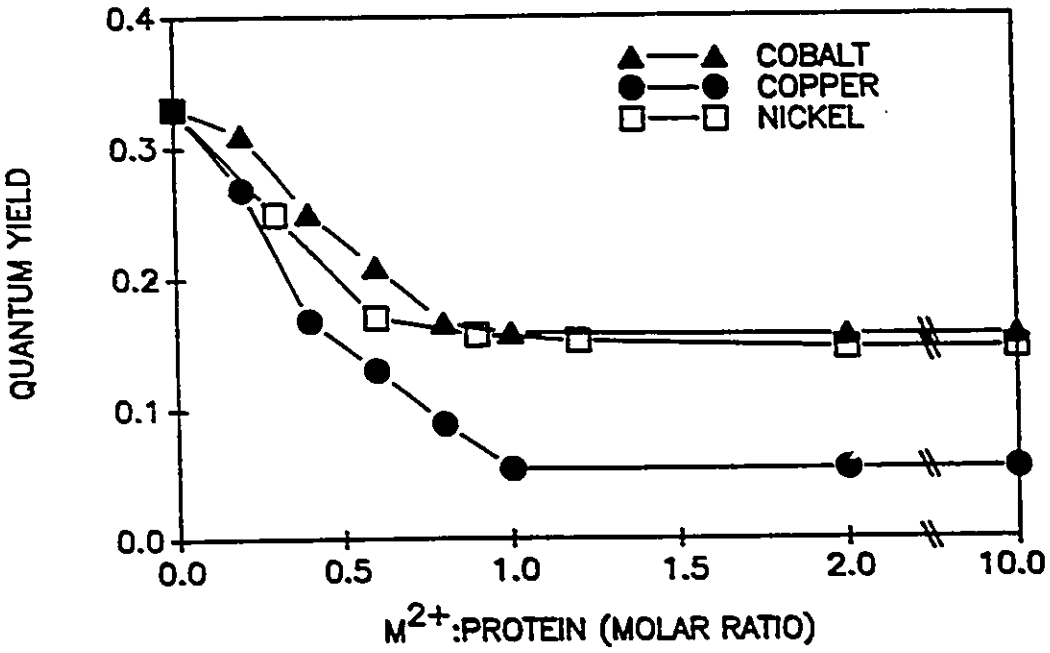

Figure 3.11: Effect of metal ion titration on the quantum yield of fluorescence of *Pfl* apoazurin in 50 mM ammonium acetate buffer, pH 6.5, 20°C. Note that in the case of the Co(II) derivative the absorbance at 292 nm of apoazurin (instead of the Co(II) azurin) was used as an approximation in the quantum yield calculation. This avoided interference caused by the visible absorbance of the Co(II)–chelate complex. All values shown are the mean of three determinations whose standard errors are within the size of the symbols.

The fluorescence decay results from the various holoazurin, reduced azurin, apoazurin, and metal–reconstituted azurin samples are given in Tables 3.4 and 3.5. A typical decay curve of holoazurin is shown in Figure 3.12 and weighted residual plots are shown in Figure 3.13. On the basis of the randomness of residuals, as well as the SVR and Sigma, all apoazurin samples were found to adequately fit single exponential decay kinetics with a decay time near 5 ns (Figure 3.13 A), whereas the best fit for reduced Cu(I) azurin, holoazurin, and Cu(II) reconstituted holoazurin samples having spectral ratios above 0.53 was found for a triple exponential decay function (Figure 3.13 E). All the copper–containing azurin samples had one long decay time component with a value near 5 ns. The fractional fluorescence of this component varied depending on the source of the holoazurin sample. In the case of *Pfl* holoazurin, F_1 was 0.78 while for *Pae* holoazurin, F_1 was 0.49 at 310 nm. The fractional fluorescence of this long decay time component in the reconstituted Cu(II) samples was virtually the same as the originally isolated protein. In the case of the reduced Cu(I) azurins, the fractional fluorescences of the long decay time components, F_1, were 0.87 and 0.46 for *Pfl* Cu(I) azurin and *Pae* Cu(I) azurin, respectively. The shortest decay time component observed in the Cu(II)–containing samples was approximately 100 ps. Consistent with the observed variation in fractional fluorescence of the long lifetime component, the fractional fluorescence of this short decay time component, F_3, significantly changed depending on the source of the azurin. Contrary to earlier reports (Szabo et al., 1983; Munro et al., 1979; Grinvald et al., 1975) and those published by Petrich et al. (1987), a third decay time component was required in order to obtain a satisfactory fit to the decay data. The value of this middle decay time component τ_2, varied depending on the source

TABLE 3.4

Fluorescence Decay Parameters[a]										
sample[b]	λ_{em} (nm)	τ_1 (ns)	τ_2 (ns)	τ_3 (ns)	F_1	F_2	F_3	α_1	α_2	α_3
Pfl apo[c]	310	5.10								
	320	5.20								
	330	5.04								
Pae apo[d]	310	5.11								
	330	5.14								
Pae apo[e]	310	5.08								
Pfl holo, pH 5.0	310	4.91	0.52	0.105	0.78	0.06	0.16	0.09	0.06	0.85
	330	4.95	0.50	0.106	0.79	0.04	0.17	0.09	0.04	0.87
Pfl Cu(II) azurin	310	4.94	0.52	0.097	0.83	0.04	0.13	0.11	0.05	0.85
	330	4.85	0.48	0.100	0.80	0.05	0.15	0.09	0.06	0.85
Pfl Cu(I)	310	4.98	0.37	0.063	0.87	0.03	0.10	0.09	0.04	0.86
	330	4.96	0.39	0.068	0.86	0.02	0.12	0.09	0.03	0.89
Pae holo, pH 5.0	310	4.89	0.36	0.098	0.49	0.08	0.44	0.02	0.05	0.93
	330	4.95	0.35	0.100	0.49	0.08	0.44	0.02	0.05	0.93
Pae Cu(II) azurin	310	4.80	0.36	0.097	0.51	0.09	0.41	0.02	0.05	0.92
Pae Cu(I)	310	4.76	0.47	0.061	0.46	0.09	0.46	0.01	0.02	0.96
	330	4.74	0.46	0.063	0.46	0.10	0.45	0.01	0.03	0.96
Pae holo, R = 0.40	310	5.01	0.12		0.96	0.04		0.37	0.63	
	330	5.03	0.15		0.96	0.04		0.42	0.58	

[a]The fluorescence decay parameters are the best-fit values, which are obtained from the exponential decay model. Each value is the mean of at least two determinations. The precision of the data per exponential decay was typically as follows: τ_1, ±0.01; τ_2, ±0.01; τ_3, ±0.001. Standard errors were typically as follows: τ_1, ±0.03; τ_2, ±0.03; τ_3, ±0.002. The lifetime value of 5.20 ns for *Pfl* apoazurin at 320 nm is slightly less accurate due to interference at this λ by the Raman scattering of water. τ_i is the symbol used for lifetime, F_i represents the fractional fluorescence for each respective component, and α_i represent the normalized preexponential terms. [b]All samples were in 50 mM NH_4OAc buffer, pH 6.5, unless otherwise stated. All samples were measured at 20 °C. All holoazurin and Cu(II)-reconstituted azurin samples had spectral ratios greater than 0.50 unless otherwise stated. λ_{ex} = 292 nm. [c]This apoazurin was prepared from *Pfl* holo having an original spectral ratio = 0.55. [d]This apoazurin was prepared from *Pae* holo having an original spectral ratio = 0.33. [e]This apoazurin was prepared from *Pae* holo having an original spectral ratio = 0.51.

TABLE 3.5

Fluorescence Decay Parameters of Apoazurin, Holoazurin, and M(II) Azurins[a]								
sample	λ_{em} (nm)	τ_1	τ_2	τ_3	F_1	F_2	F_3	ϕ[b]
holoazurin, pH 5	310	4.91	0.52	0.105	0.78	0.06	0.16	0.056
Cu(I) azurin	310	4.98	0.37	0.063	0.87	0.03	0.10	
apoazurin	310	5.10						0.330
Cu(II) azurin, reconstituted	310	4.94	0.52	0.097	0.83	0.04	0.13	0.055
Co(II) azurin	310	4.88	2.08	0.136	0.91	0.07	0.02	0.160
Ni(II) azurin	310	4.90	1.01	0.094	0.97	0.01	0.02	0.150

[a]Time-resolved measurements were performed in the presence of a 10-fold molar excess of each metal in 50 mM ammonium acetate buffer, pH 6.5 at 20 °C. All samples were prepared from protein purified from *P. fluorescens* having an original $A_{450}/A_{280} \geq 0.56$. The values presented are the mean of at least six determinants with standard errors as follows: for τ_1, ±0.005; for τ_2, ±0.01; for τ_3, ±0.001. [b]Fluorescence quantum yields of the various azurin samples were measured in 50 mM ammonium acetate buffer, pH 6.5 at 20 °C.

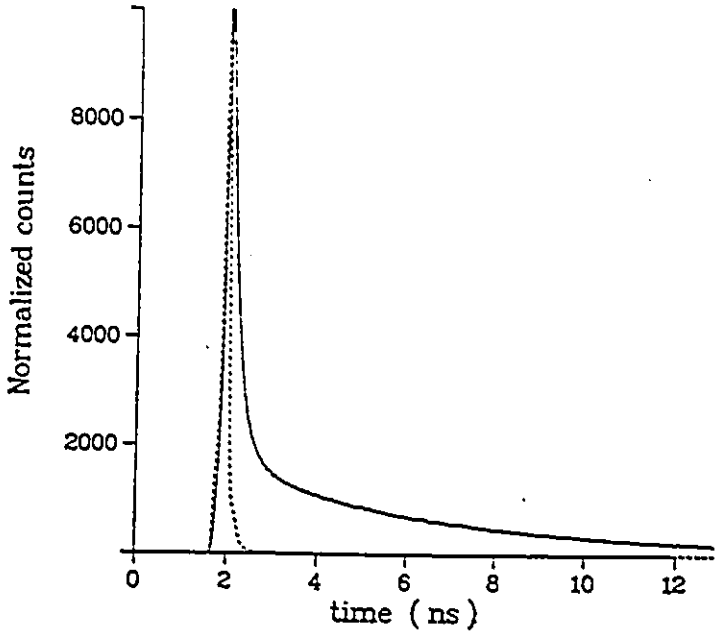

Figure 3.12: Typical normalized fluorescence time–intensity curves. The instrument response function curve (dotted line) and *Pfl* holoazurin decay curve were recorded with a channel width = 21.6 ps/channel; λ_{ex} = 292 nm; λ_{em} = 310 nm; emission bandpass = 4 nm.

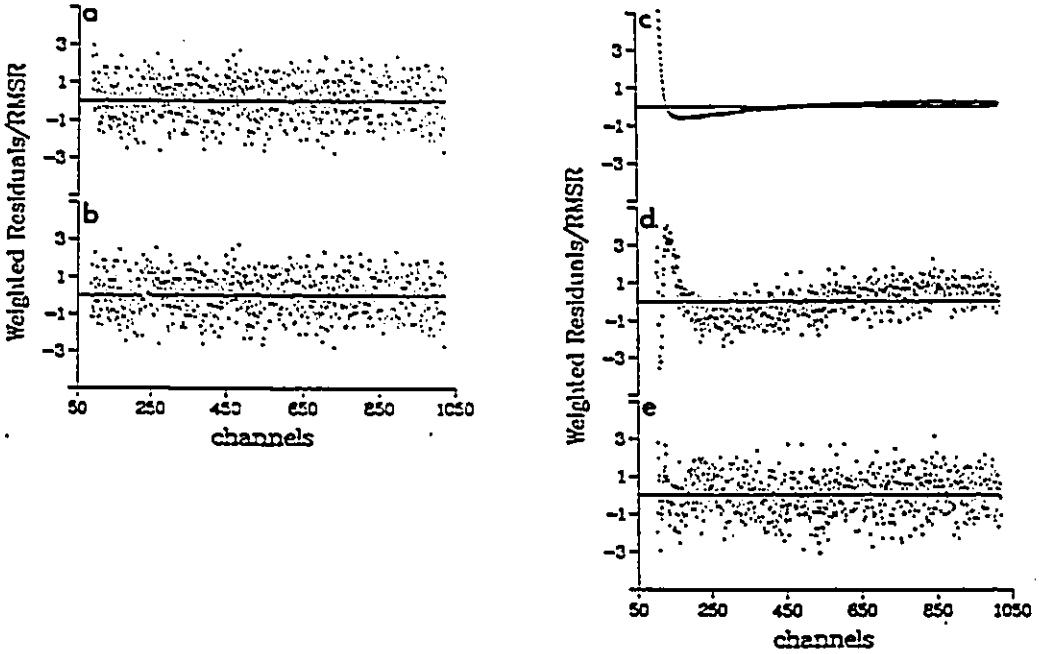

Figure 3.13: Weighted residual plots for the calculated best–fit emission decay function. Panels a and b correspond to those plots for *Pfl* apoazurin fitted to single– and double–exponential decay functions, respectively, and panels c – e correspond to those plots for *Pfl* holoazurin fitted to a single–, double–, and triple–exponential decay function, respectively.

of the azurin, being 0.52 ns in *Pfl* holoazurin and 0.36 ns in *Pae* holoazurin. In all cases the fractional fluorescence corresponding to this component, F_2 was relatively small (0.04–0.09).

Reduction of the Cu(II) azurins to Cu(I) azurins resulted in a decrease in the value of τ_3 for both *Pae* and *Pfl* azurins to a value of approximately 0.063 ns. In *Pfl* azurin, τ_1 increased slightly while the opposite was true in *Pae* azurin. A corresponding increase in F_1 was noted upon reduction of *Pfl* azurin but a decrease in F_1 was noted upon reduction of *Pae* azurin. τ_2 followed opposite trends: τ_2 decreased upon reduction of *Pfl* azurin but increased upon reduction of *Pae* azurin with only slight changes in the F_2 values.

In samples which had a spectral ratio of 0.4, the best–fit fluorescence decay kinetics were obtained with a double exponential model. The decay times were similar to those reported earlier, with the long decay time being again near 5 ns, while the short decay component had a value of 0.12 ns at 310 nm which was slightly longer than the shortest component found in the azurin samples with a spectral ratio > 0.53.

The pH dependence of the fluorescence decay parameters is highlighted in Table 3.6 and Figure 3.14 for *Pfl* holoazurin. The long and middle decay components, τ_1 and τ_2 were titratable between pH 5 and pH 7 whereas the shortest decay component, τ_3, was not affected by pH. The fractional fluorescence of the decay components hardly varied with pH.

The temperature dependence of the fluorescence decay parameters of *Pfl* holoazurin was determined and the data are given in Table 3.7. The long decay component, τ_1, gradually decreased with increasing temperature whereas the middle decay component, τ_2, followed the opposite trend. The shortest decay component,

TABLE 3.6

Influence of pH on Fluorescence Decay Parameters[a] of *P. fluorescens* Holoazurin[b] in 50 mM NH_4OAc Buffer, 20 °C

pH	λ_{em} (nm)	τ_1 (ns)	τ_2 (ns)	τ_3 (ns)	F_1	F_2	F_3
4	310	4.95	0.48	0.085	0.77	0.07	0.16
	330	4.97	0.50	0.107	0.77	0.04	0.19
5	310	4.91	0.52	0.105	0.78	0.06	0.16
	330	4.95	0.50	0.106	0.79	0.04	0.17
6	310	4.79	0.54	0.105	0.77	0.05	0.18
	330	4.82	0.53	0.102	0.78	0.04	0.18
7	310	4.71	0.55	0.101	0.77	0.05	0.18
	330	4.71	0.55	0.101	0.78	0.04	0.18
8	310	4.69	0.57	0.100	0.77	0.04	0.19
	330	4.70	0.60	0.102	0.78	0.03	0.19

[a]Each value is the mean of at least three determinations, and typical standard errors are as follows: τ_1, ±0.03; τ_2, ±0.03; τ_3, ±0.002. τ_i is the symbol used for lifetime, and F_i represents the fractional fluorescence for each respective component and is determined according to $F_i = \alpha_i\tau_i/\sum\alpha_i\tau_i$, where α_i is the preexponential of the corresponding ith exponential term. [b]Each holoazurin sample used had a spectral ratio greater than 0.52.

TABLE 3.7

Influence of Temperature on Fluorescence Decay Parameters[a] of *P. fluorescens* Holoazurin[b] in 50 mM NH_4OAc Buffer, pH 5.0

temp (°C)	λ_{em} (nm)	τ_1 (ns)	τ_2 (ns)	τ_3 (ns)	F_1	F_2	F_3
5	310	5.11	0.44	0.100	0.79	0.04	0.17
	330	5.14	0.45	0.101	0.80	0.03	0.17
10	310	5.01	0.46	0.099	0.79	0.06	0.15
	330	5.04	0.47	0.091	0.80	0.05	0.15
16	310	4.96	0.48	0.104	0.78	0.04	0.18
	330	4.98	0.48	0.097	0.79	0.04	0.17
20	310	4.91	0.52	0.105	0.78	0.06	0.16
	330	4.95	0.50	0.106	0.79	0.04	0.17
29	310	4.61	0.71	0.111	0.78	0.04	0.19

[a]Each value is the mean of at least three determinations, and typical standards error are the same as those in Table IV. [b]Each holoazurin sample used had a spectral ratio greater than 0.52.

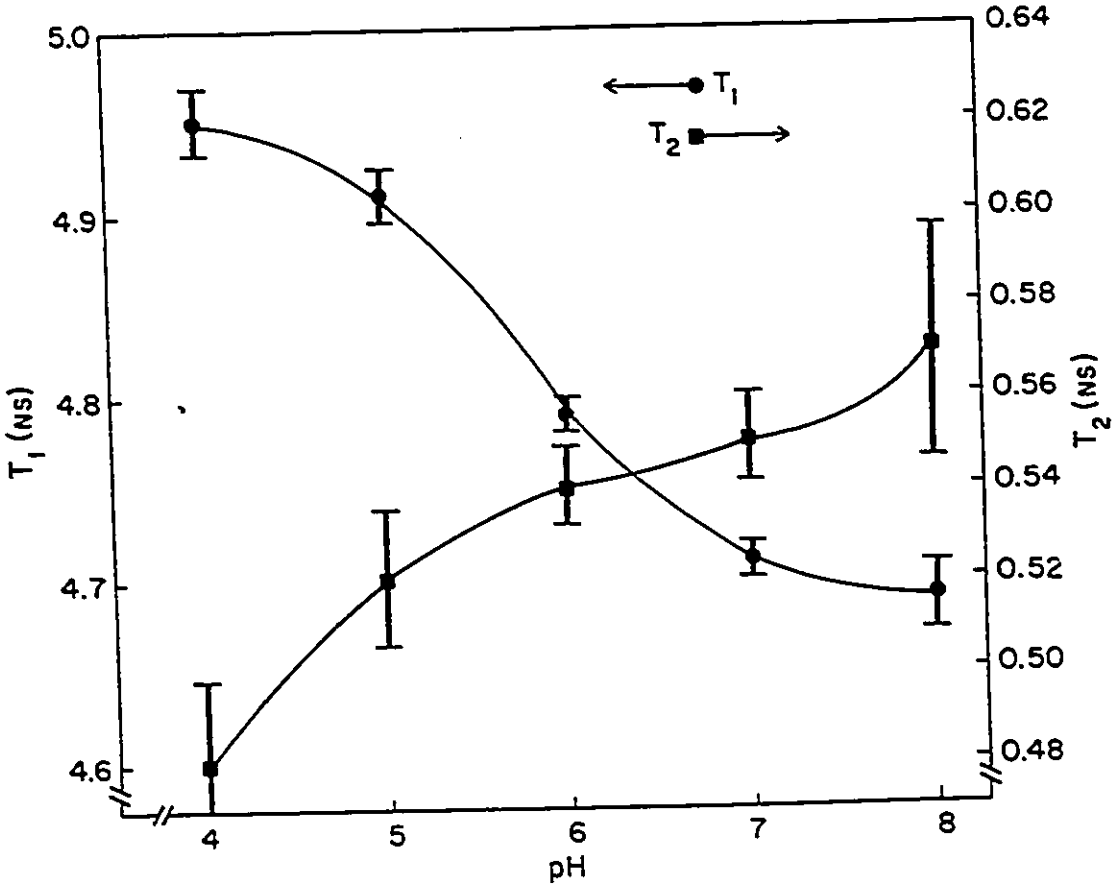

Figure 3.14: Plot of the variation of the long decay component, τ_1 (●), and the middle decay component, τ_2 (■), of *Pfl* holoazurin with pH. The left–hand ordinate is that for τ_1, and the right–hand ordinate is that for τ_2. The samples were excited at 292 nm, and the emission was monitored at 310 nm. Errors are reported as the standard error of the mean.

τ_3, was relatively unaffected by temperature changes. Again there was negligible change in the fractional contribution of each decay component to the total fluorescence with temperature.

The fluorescence decay parameters of the metal–reconstituted azurin samples were measured in the presence of excess metal to ensure that no dissociation of the metal–protein complexes had taken place. In the presence of Cu(II), Co(II) or Ni(II), the data were best fit by a sum of three exponentials. Figure 3.15 gives a typical decay curve for a M(II) azurin (Co(II) azurin in this case) while the residual plots corresponding to this curve are highlighted in Figure 3.16. The longest decay component was essentially identical in all M(II) azurins but possessed different contributions to the total fluorescence. The fractional fluorescence of the shorter decay components constituted only 3% of the total fluorescence in Ni(II) azurin and 9% in Co(II) azurin. However, the plots of weighted residuals showed satisfactory fits to the data could only be obtained when the data were fit with three exponential decay components (Figure 3.16). The shortest decay component was identical in Cu(II) and Ni(II) forms, while for Co(II) azurin, it was about 30% longer (0.13 ns). The fractional contribution of τ_3 to the total observed fluorescence was much less in the Co(II) and Ni(II) derivatives when compared to Cu(II) azurin.

3.4 Discussion

3.4.1 Homogeneity of Protein Samples

In 1967, Ambler reported that azurin samples having a spectral ratio ranging from 0.48 to 0.60 may be regarded as homogeneous on the basis of results from starch–gel electrophoresis, although some difficulty in removing all of the cytochrome which copurified with the azurin was reported (Ambler & Brown, 1967).

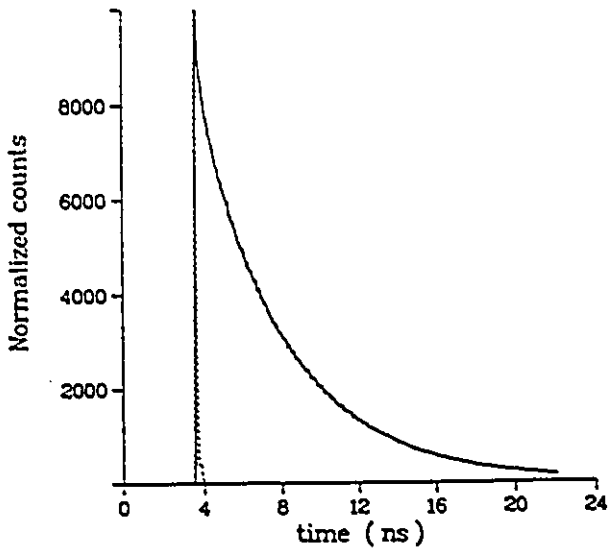

Figure 3.15: Typical normalized fluorescence time–intensity curves for a *Pfl* M(II) azurin derivative. The instrument response function curve (dotted line) and the Co(II) azurin decay curve were recorded with a channel width = 21.6 ps/channel, λ_{ex} = 292 nm, λ_{em} = 310 nm, bandpass = 4 nm.

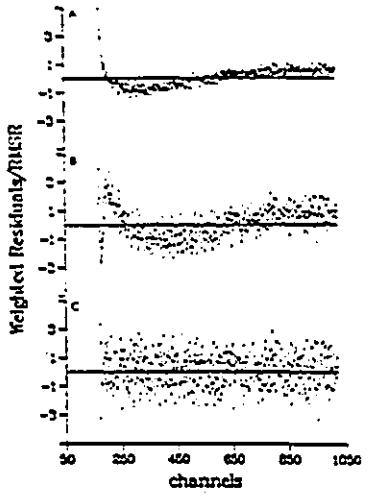

Figure 3.16: Weighted residual plots for the calculated best–fit emission decay function of the emission decay curve of Co(II) azurin shown in Figure 3.15. Panels A – C correspond to the plots for the fluorescence decay of Co(II) azurin fitted to single–, double–, and triple–exponential decay functions, respectively.

Since then, most workers either cite just the spectral ratio, or the spectral ratio plus SDS–PAGE when discussing azurin homogeneity (Blaszak et al., 1983; Canters et al., 1984; Blair et al., 1985; Szabo et al., 1983; Finazzi–Agro et al., 1970; Engeseth & McMillin, 1986; Petrich et al., 1987). In some cases, azurin with spectral ratios below 0.48 have been routinely used, and reports using azurin with spectral ratios as low as 0.4 have been published. Grinvald et al. (1975) used the rationale that if the apoazurin prepared from the corresponding holoazurin gave monoexponential decay kinetics, then the holoazurin used originally must be pure. In agreement with these workers, it was stated (Szabo et al., 1983) that holoazurin samples could not be initially contaminated with apoazurin since the addition of excess Cu(II) ion did not result in either an increase in absorbance of the 620 nm band or a decrease in the fluorescence intensity. However, no effort was made at that time towards correlating this spectral evidence with biochemical techniques capable of detecting protein heterogeneity.

This chapter includes biochemical evidence which establishes definite criteria by which homogeneity can be monitored. It is shown that homogeneous azurin samples, free from apoazurin or other protein contaminants, can be obtained for spectroscopic studies. The various electrophoretic results presented herein and the stoichiometry determination using amino acid and atomic absorption analyses show that a single UV–VIS absorption spectrum may provide satisfactory evidence as to whether an azurin sample was homogeneous.

When the spectral ratio was below 0.50, neither SDS–PAGE or the shape of the UV–VIS absorption spectrum revealed the obvious presence of another protein contaminant other than a diminished absorbance at 620 nm relative to that at 280

nm. Addition of either Cu(II) ion in a 25–fold molar excess or an oxidizing agent such as 20 μM $K_3Fe(CN)_6$ had no effect upon either the absorption spectrum or the steady–state fluorescence intensity. These observations provided evidence that the protein samples did not contain either a colourless, reconstitutable apoazurin or a colourless reduced Cu(I) azurin. The combined amino acid analyses and atomic absorption stoichiometry determination of holoazurins having spectral ratios < 0.50 suggested contamination by a copper–less protein. The reproducibility of the amino acid composition results, which in the case of *Pae* azurin matched the previously published sequence data (Ambler, 1971), as well as the detection of only single bands in SDS–PAGE suggested that any proteins present had compositions similar to holoazurin. This would be consistent with holoazurin being contaminated with a copper non–reconstitutable apoazurin when the spectral ratio was less than 0.50. The nature of this "nonreconstitutable" apoazurin is unknown at the present time. The most likely possibility is that the ligands responsible for Cu(II) binding have been altered either during the purification or during biosynthesis. The latter possibility is the preferred rationalization as the spectral ratios which were obtained depended upon the amount of cupric ion which was present in the bacterial growth medium (See Section 3.2.2).

The isoelectric focusing results strongly supported the suggestion of a non–reconstitutable apoazurin being present when spectral ratios were less than 0.50, since apoproteins could be distinguished from holoazurins as they migrated at more acidic pIs. In the samples whose spectral ratios were below 0.50, the intensity of the extra bands attributed to apoazurin increased as the spectral ratio decreased. Two preliminary attempts have been made to remove this putative, nonreconstitutable apoazurin from the holo samples by both trypsin digestion and

chromatofocusing. Trypsin digestion could not remove the non–reconstitutable apoazurin contaminant. Chromatofocusing revealed that two closely eluting proteins were present in holo samples having spectral ratios below 0.50. However, due to the poor resolution of the two peaks, appreciable amounts of the separate components were not obtained by this method.

In the isoelectric focusing of the *Pae* holo samples, an additional band, beside that ascribed to holoazurins, was observed. This band was noted in all samples of *Pae* azurin, independent of spectral ratio and independent of protein source (purified or commercially obtained). The band migrated to an extremely acidic position (pI less than 3.0). It is suggested that it may be due to artefacts arising from interactions with the ampholytes or represent non–protein particles which were also stained (Illingworth, 1972). Additional arguments which support this view follow. Samples with a spectral ratio of 0.53 containing this band were found to possess a 1 copper: 1 protein stoichiometry on the basis of amino acid and atomic absorption analyses. Amino acid analysis revealed a composition indistinguishable from that which has already been published (Ambler, 1971). Apo samples prepared from these holo samples were fully Cu(II) reconstitutable (as judged by A_{625}/A_{280}), and it was noted that the presence of this extra band diminished significantly upon copper removal. All of these observations, including single bands observed upon SDS–PAGE, support the idea that no other non–azurin protein could be present in the samples and that the extra band was most likely due to a complex between ampholyte and *Pae* azurin. The results also argue against the possibility of some other form of azurin sample accounting for these bands. The corresponding apo samples were found to obey monoexponential fluorescence decay kinetics. At the level of resolution obtainable with the instrumentation employed, no other protein

has been reported which displays such behaviour. It is difficult to imagine that a protein (azurin derivative or oxidized apo) with such a markedly different pI would have an amino acid composition essentially identical with that of the azurin of interest and have identical fluorescence properties. Finally, it was interesting to note that this additional band was not observed when the *Pfl* holoazurin was run under identical conditions. This suggests that this latter protein does not form a similar complex with ampholytes.

Provided that the spectral ratio was above 0.53 and no absorbance at 410 nm (attributed to cytochrome) was observed, neither the biochemical tests nor the spectral results could detect any spurious protein contamination. Such criteria would also rule out contamination by an "apoazurin". Since it was possible to obtain spectral ratios above 0.50, even when a Soret band was detectable, it is important that an entire UV–VIS absorption spectrum, as illustrated in Figure 3.3, be reported when purity is being attested.

3.4.2 Preparation of a Reconstitutable Apoazurin

The method first reported for the preparation of apoazurin involved dialysis against potassium cyanide (Yamanaka et al., 1963). More recently, Blaszak et al. (1983) stated that the use of this method yielded an apoprotein which gave variable kinetics for Cu(II) uptake, depending upon the number of times the protein was exposed to cyanide solution. They suggested that it was likely that Yamanaka et al. failed to reduce the pH after addition of 0.5 M KCN (pH 10.5). The initial apo preparation results obtained in the present work support this view, and in addition, when the solution was dialyzed overnight at high pH (10.5), changes in the absorption spectrum at 280–300 nm suggested protein denaturation. By careful

control of the pH after cyanide addition, apoazurin retaining less than 2% of its original copper could be obtained. Further, this apoazurin was 100% Cu(II)–reconstitutable upon addition of aqueous Cu(II).

The preparation of apoazurin according to the method of Blaszak et al. (1983) was also attempted. These samples did not show full Cu(II) reconstitutability, and significant amounts of copper remained in the original samples. Frequently, spectral interference was caused by the presence of ascorbate ion or an ascorbate decomposition product. Petrich et al. (1987) also reported that traces of ascorbate ion or a yellow impurity remained in the apoazurin samples even after dialysis when the protein was prepared by this method.

As judged by the final spectral ratio and recovery of the fluorescence decay parameters, the full reconstitution of apoazurin could be achieved in the range of pH 5 – 7. However, in contrast to the work of Tennent and McMillin (1979), it was not possible to achieve full reconstitution at pHs above 7.5. The examination of the pH dependence of the quantum yield of apoazurin (Figure 3.10) showed a marked decrease in the quantum yield at pHs above 7 which was not seen in the holoform. These results may suggest the apoazurin was less stable at these high pH values.

3.4.3 Fluorescence Behaviour of Homogeneous Cu(II) Azurin

On the basis of the evidence presented in this chapter, the holoazurin samples used in the fluorescence study were considered homogeneous. The decay data obtained for those holo samples having a spectral ratio above 0.53 were best fit by a sum of three exponential decay components, instead of a sum of two exponentials as previously reported (Szabo et al., 1983; Grinvald et al., 1975; Munro, et al., 1979; Petrich et al., 1987). Double exponential decay was observed

when the spectral ratios were below 0.50. In these latter cases, the fraction of the fluorescence of the long–lived 5 ns component was considerably greater, consistent with the presence of a non–reconstitutable apoazurin. In all apoazurin samples, single–exponential decay behaviour with a decay time near 5 ns was observed at all emission wavelengths. This confirmed earlier published values (See Table 3.1). The lack of reconstitutability was not reflected in a heterogeneity of Trp fluorescence in the apoprotein preparations. This suggests that if there were any conformational changes associated with the inability to take up Cu(II), they were not "sensed" by the Trp residue. The results also suggest that in the absence of copper, the Trp in the two homologous azurins existed in comparable molecular environments.

Contrary to earlier work (Szabo et al., 1983; Petrich et al., 1987), the fluorescence decay of the holoazurin or Cu(II)–reconstituted samples obeyed triple–exponential decay kinetics. The fact that the fluorescence decay parameters could be recovered on Cu(II) reconstitution of the apoprotein strongly implies that the component with the intermediate decay time was not due to any experimental artefact. The observation of three exponential decay components was highly reproducible. It is difficult to account for the difference between these results and those reported by Petrich et al. (1987) (See Table 3.1), who found only double–exponential decay behaviour for holoazurin. In their work they proposed that the long decay component found in holoazurin was due to an apoazurin impurity. However, the long decay time value reported by Petrich et al. for *Pae* apoazurin (5.16 ± 0.19 ns) was significantly different from that found in the corresponding holoazurin (4.15 ± 0.53 ns). For this long decay component of *Pae* holoazurin, the fractional fluorescence amounted to 55% of the total. A value similar to that is reported herein. The large error on a decay component comprising

55% of the total fluorescence is surprising.

In comparing the decay parameters obtained from the two homologous azurins, it can be seen that the largest difference was observed in the fractional contribution of the longest and shortest lifetime components to the total observed fluorescence. As the residues in the vicinity of the active copper sites in azurin are highly conserved (Ambler, 1971), this suggests that the less highly conserved amino acids have an influence upon the conformational distribution of these two proteins. The secondary structure of *Pfl* holoazurin has been examined by Fourier transform infrared spectroscopy (Surewicz et al., 1987) and was shown to be quite similar at that level to the structure of *Pae* azurin, based on the known X–ray data of the latter (Adman & Jensen, 1981; Adman et al., 1978). This requires that the Trp fluorescence was sensitive to subtle structural or dynamic differences in the two proteins.

The lack of exact agreement in detail of the Trp fluorescence decay behaviour in holoazurin between different laboratories may be due to one of several factors. One may be the homogeneity of the various azurin preparations. When the spectral ratios were below 0.50, only two decay components were observed. As apoazurin was on average 6 times more fluorescent than the corresponding holoform, even a small fraction could potentially "mask" a weak component if it were present.

Another source of variability may be the confusion associated with the taxonomic numbering of the various *Pseudomonas* species and strains. Initial reports of the amino acid sequence of *Pfl* azurin were later corrected by the realization that the protein was that of *Pae* rather than *Pfl* (Ambler & Brown, 1967; Ambler & Wynn, 1973). To complicate matters further, seven biotypes of *Pfl* exist (Stanier et al., 1966) while only a few of the associated azurins have been sequenced.

Petrich et al. (1987) reported using a bacterial strain whose ATCC number 13525 corresponds to *Pseudomonas fluorescens* biotype A, not *Pseudomonas aeruginosa* as they indicate.

3.4.4 Conformational Heterogeneity Versus an "Apo-Like" Contaminant

It is clearly shown in this chapter, from the electrophoretic results and the determination of the copper to protein stoichiometry by atomic absorption and amino acid analysis, that the holoazurin samples did not contain any apoazurin contamination as long as the spectral ratio was 0.53, or greater. When the gels were heavily loaded with azurin samples used for the fluorescence studies, no trace of any apoazurin could be detected. Instead, the combination of the electrophoretic experiments and the results obtained suggest a conformational heterogeneity of the holoazurin molecule as proposed earlier (Szabo et al., 1983).

The possible existence of a number of conformations of the azurin molecule and the pH dependence of their interconversion has already been proposed. NMR measurements showed that in *Pae* azurin, His–35 slowly exchanged between its protonated and nonprotonated forms (Hill & Smith, 1979; Ugurbil & Bersohn, 1977; Ugurbil et al., 1977b). It was also found that two forms of His–83 were in fast exchange and that the X–ray structure of *Pae* azurin crystals grown at pH 5.5 – 5.8 clearly showed that the imidazole group of His–83 juts out into the solution whereas that of His–35 lies in a crevice near the surface (Adman & Jensen, 1981; Adman et al., 1978). The position of His–35 is highlighted in orange in Figure 3.1. Structural and kinetic data collectively suggested that the fast reaction of imidazole protonation could be coupled to a slower conformational change involving His–35 (Corin et al., 1983).

In the earlier work from this laboratory it was proposed that the two fluorescence decay components observed in holoazurin resulted from two different conformational states of the copper–ligand complex. The long decay time component (5 ns) was assigned to a conformer with the copper–ligand complex in a more tetrahedral structure and at some distance from Trp–48 (Szabo et al., 1983). In this case fluorescence quenching by interaction with the copper–ligand complex would not be important. The short decay time component was assigned to a conformer in which the copper–ligand complex had a flattened tetrahedral structure bringing potential quenching groups closer to the Trp residue. Obviously, the observation of a third decay time component in the holoazurin samples requires a revision of this former assignment.

From the fluorescence results, the longest lifetime was essentially the same for the two homologous holoazurins. In addition, it was similar to the single decay time observed for apoazurin (4.9 ns vs 5.1 ns). This decay time component of the holoazurins was titratable between pH 5 and pH 7, decreasing with increasing pH (pH 4, 4.95 ns versus pH 8, 4.70 ns). As was proposed earlier, this long decay component is assigned to a protein conformation in which the interactions of the Trp with the Cu(II) binding site are not important. The pH behaviour of this decay time component suggests that it may be attributed to a conformer whose structure was influenced by a titratable histidine residue. Both Canters et al. (1984) and Corin et al. (1983) have suggested the protonation–deprotonation of His–35 (pK = 5.9 ± 0.4), a nonliganded residue lying adjacent to the ligand His–46 (See Figure 3.1), leads to conformational changes of the protein. The decrease in the value of the long decay time component with increasing pH rules out any close interaction of the surface histidine residues 35 and 83 with the Trp. If there were such an

interaction, it would be expected that the fluorescence decay time should increase as the histidine becomes increasingly deprotonated since a proton–transfer quenching process from histidine to tryptophan would be eliminated (Masotti et al., 1988). The results then are most consistent with alteration of the protein conformation with protonation or deprotonation of His–35, which alters the interaction of the Trp with other parts of the protein structure leading to a reduction of the fluorescence decay time.

The increase in quantum yield (20% between pH 4 and pH 8) (Figure 3.9) is difficult to rationalize in terms of the fluorescence decay parameters (Table 3.6). The fractional fluorescence of the long decay component remained constant with increasing pH. There are two possible explanations to account for this behaviour. Either there is a nonfluorescent conformer which becomes fluorescent at higher pH, or the radiative lifetime of the Trp residue in the holoprotein changes with pH. A rationalization which favours this latter alternative is presented below.

The quantum yield of the apoazurin also was titratable between pH 5 and pH 7, although the inflection appeared at a slightly higher pH (Figure 3.10). This suggests that the same protonation–deprotonation of a His residue may be influencing the Trp fluorescence, even in the absence of the copper centre. In contrast to that of the holoazurin, the fluorescence decay time of the apoazurin remained constant with pH, lending support to the proposal that the radiative lifetime changed with pH.

The remaining two lifetimes observed in the holoazurin must be the result of an influence by the copper–ligand complex on the conformers, since they are absent in the apoprotein. The decay time of the shortest component, τ_3, remained essentially constant, not being influenced by temperature, pH, or even the different

amino acid compositions of the proteins. The major difference was its contribution to the total fluorescence observed in the two homologous azurins ($F_3 \simeq 16\%$ *Pfl* vs $F_3 \simeq 44\%$ *Pae*). On the other hand, the middle lifetime component, τ_2, was affected by pH, temperature and amino acid differences, but its contribution to the total fluorescence was not that much different in the two homologous azurins.

It is proposed that the two shorter decay components represent conformations wherein the copper–ligand complex is closer to the tryptophan residue. These decay components may be due to local conformational differences of the tryptophan residue with respect to a proximate ligand complex. The greater effect of pH on the intermediate decay time suggests that the protein conformational changes resulting from protonation of His–35 influence the local interactions of the tryptophan with the copper–ligand complex.

In this discussion, considerable emphasis has been put on the effect of protonation of the histidine residues on the conformational states of the protein. However, the photophysical origin of the quenching of the tryptophan excited state leading to the short decay times remains speculative. When the copper is reduced from Cu(II) to Cu(I), changes in the decay times and fractional fluorescence values are observed. The shortest decay time becomes even shorter on reduction, changing from 0.10 ns in the Cu(II) form to 0.06 ns in the Cu(I) form. It may be that the short decay time results from an electron–transfer mechanism from the excited state of the tryptophan to the copper centre. However, such a possibility cannot be distinguished from other excited state deactivation processes. For example, the quenching may result from an interaction between the charge–transfer excited state of tryptophan (Meech & Phillips, 1983) and the electronic structure of the copper–ligand complex. Another possible quenching mechanism may involve either

the ligand histidines or ligand cysteine or methionine in a special interaction with Trp–48. It may be that upon reduction of the copper, the proximity of the ligand complex to the tryptophan is altered leading to a more efficient deactivation process. It is interesting that the changes observed upon reduction of *Pae* azurin are different from those observed in *Pfl* azurin (Table 3.4). No rationalization for these differences can be given at present.

The assignment of the three decay components to three different conformational states of the protein leads to the question of estimating the relative concentrations of these components. It can readily be shown according to equations presented by Donzel et al. (1974) that the relative ground state concentrations can be estimated from the preexponential terms. For example,

$$\frac{c_j}{c_k} = \frac{\alpha_j \tau_j}{\alpha_k \tau_k} \cdot \frac{\phi_k}{\phi_j} \qquad (3.1)$$

where c_j, c_k are the relative concentrations of the jth and the kth decay components, respectively and α, τ, and ϕ are the normalized preexponential term, decay time and quantum yield of fluorescence of the corresponding components. If it is assumed that τ_r is the same for each component, and given $\phi_i = \tau_i/\tau_r$, then equation 3.1 reduces to

$$\frac{c_j}{c_k} = \frac{\alpha_j}{\alpha_k} \cdot \qquad (3.2)$$

According to equation 3.2, the normalized preexponential terms (Table 3.4) represent the relative concentration of each component, where $c_1 + c_2 + c_3 = 1$.

The relative concentration of the long decay time component was 9% and 2% of the total protein for *Pfl* and *Pae* azurins, respectively, while the shortest decay time component dominated the component concentrations, being 85% and 93% of the total for *Pfl* and *Pae* azurins, respectively. The relative concentration of the intermediate decay time component was virtually the same for both azurins, being 6% and 5%, for *Pfl* and *Pae* azurins, respectively.

Using these relative concentration values and the value of the radiative lifetime determined earlier (τ_r = 15.5 ns; Szabo et al., 1983), it was possible to calculate an expected steady–state quantum yield for each of the proteins. The calculations were made using the following equation:

$$\phi_f = c_1 \frac{\tau_1}{\tau_r} + c_2 \frac{\tau_2}{\tau_r} + c_3 \frac{\tau_3}{\tau_r}. \qquad (3.3)$$

The calculated quantum yields using the decay parameters were 0.036 and 0.014 for *Pfl* and *Pae* holoazurin, respectively. These calculated quantum yields were approximately 75% of the measured values. It is expected that there should be a closer correspondence between the measured quantum yield and that calculated (note that the quantum yield accuracy was better than 5%), hence one of the assumptions must be incorrect (Donzel et al., 1974). The most likely possibility was that τ_r for the holoazurin was different from that of the apoazurin, owing perhaps to an electronic perturbation of the Trp–48 excited singlet state by the copper–ligand complex. With the measured quantum yield values of 0.051 and 0.018 for *Pfl* and *Pae* holoazurin, respectively, a value of τ_r for each protein was calculated using equation 3.3. This calculated value of τ_r was 11.0 ns and 11.7 ns for *Pfl* and *Pae*

azurins, respectively. These values are significantly different from that determined for apoazurin. They are not unreasonable since radiative lifetimes similar to this have been reported for several indole derivatives in nonpolar environments (Meech & Phillips, 1983). This difference between the estimated radiative lifetimes for the apo– and holoazurins suggests the interesting speculation of whether τ_r for the 5 ns component was different from that of the other two components.

If it was assumed that τ_r for the two short decay components were similar and the τ_r for the long decay component was the value obtained from apoazurin (15.5 ns), then it was possible to estimate the former value. If this was the case, the value of the relative concentrations were not represented by equation 3.2, but were related according to:

$$\frac{c_1}{c_2} = \frac{\alpha_1}{\alpha_2} \cdot \frac{15.5}{\tau_r'} \qquad (3.4)$$

$$\frac{c_1}{c_3} = \frac{\alpha_1}{\alpha_3} \cdot \frac{15.5}{\tau_r'} \qquad (3.5)$$

where 15.5 ns is the radiative lifetime of the long decay time component and τ_r' is the radiative lifetime of the two short decay components. With $c_1 + c_2 + c_3 = 1$ and equations 3.3, 3.4 and 3.5, values of τ_r' equal 10.2 ns for *Pfl* and 11.6 ns for *Pae* holoazurin, respectively were calculated. Following these calculations, the values of the relative component concentrations were recalculated according to equations 3.4 and 3.5. When this was done, the relative concentrations for *Pfl* holoazurin were $c_1 = 0.13$, $c_2 = 0.07$, and $c_3 = 0.81$, while for *Pae* holoazurin they were $c_1 = 0.02$, $c_2 = 0.05$, and $c_3 = 0.93$. This suggestion that the different conformers have different

radiative lifetimes would be consistent with the conformer model. In the conformers with the short decay times, the electronic interaction of the copper–ligand complex with Trp–48 might lead to a shorter radiative lifetime.

Over the temperature range studied (5–29° C) there were only small changes in the measured decay parameters. Importantly, the fractional fluorescence values remained constant. Using these parameters and the radiative decay times calculated for long decay and short decay components, it was possible to calculate the relative concentrations of each component at each of the measured temperatures according to equations 3.4 and 3.5. It was found that there was hardly any change in the relative concentrations over the temperature range studied. The decrease in value of the long decay time was considerably less than that seen for other tryptophan–containing proteins or peptides. This was in keeping with the relatively stable structure of azurin.

As indicated above, the fluorescence quantum yield of *Pfl* holoazurin increased with pH, yet the fractional fluorescence values remained constant and the decay time of the major fluorescent component, the long decay time component, decreased with increasing pH. If it was assumed that this component had a radiative lifetime equivalent to that of apoazurin, 15.5 ns, then again the radiative lifetimes of the short decay components (assuming they were equal) could be calculated. These values are tabulated in Table 3.8. Using the various parameters, it was possible to calculate the relative concentrations of each component, and the fractional quantum yield at each pH value. These values for the long decay component are also tabulated in Table 3.8. The relative concentration of the long decay component increased from a value of 0.115 at pH 4 to 0.148 at pH 8. The fractional quantum yield increased from 0.037 to 0.045 between the same pH range,

TABLE 3.8

Summary of pH Effect on Radiative Rate Constants of the Short Decay Time Components, Relative Concentration of the Long Decay Component, and Fractional Quantum Yield of This Component in *Pfl* Holoazurin

pH	τ_r' (ns)[a]	c_1[b]	ϕ_1[b]
4	9.9	0.12	0.037
5	10.2	0.13	0.041
6	8.7	0.14	0.043
7	8.1	0.14	0.044
8	7.4	0.15	0.045

[a] Radiative decay time of the short decay time components calculated according to the text. [b] The relative concentration, c_1, and fractional quantum yield, ϕ_1, of the long decay time component.

easily accounting for the change in total quantum yield observed. This result is significant in another respect since it shows that the relative concentrations of the various decay components, or conformers, is affected by pH. The decrease in radiative lifetime of the short decay components is rationalized in the following way. Upon an increase in the pH, the histidine residues become neutral, leading to changes in the conformational distribution and a more effective electronic perturbation of the tryptophan excited state by the copper–ligand complex.

3.4.5 Metal Derivatives of Azurin

It has already been demonstrated that different metals, including Ni(II) and Co(II), all coordinate at the copper binding site in azurin (Tennent & McMillin, 1979; Blaszak et al., 1982; Engeseth et al., 1984; Engeseth & McMillin, 1986). In addition, by using a variety of spectrophotometric assays, it has been shown that

even after exhaustive dialysis or gel filtration, the metal derivatives retained "significant quantities of metal ions" (Tennent & McMillin, 1979).

Consistent with these findings, plateau quantum yields were observed when the metal to apoazurin stoichiometry was 1:1. No further change in fluorescence was seen when there was either a 2– or 10–fold molar excess of metal ion. This same apoazurin could be fully Cu(II)–reconstituted as judged by the A_{620}/A_{280} spectral ratio and the 1:1 copper to protein stoichiometry established by amino acid and atomic absorption analysis. These results indicated that the various samples had become fully metal incorporated with a 1:1 stoichiometry and that no free apoazurin was present. Excess metal ion did not alter the quantum yields or lifetimes observed for any of the native, reconstituted or metal–incorporated azurins allowing measurements to be made in the presence or absence of excess cations.

3.4.6 Quenching of Fluorescence by Metal Incorporation

In agreement with Tennent and McMillin (1979), a reduction of the quantum yield of fluorescence upon the addition of metal ions to apoazurin was observed in the order Cu(II) > Co(II) >> Ni(II) when the actual A_{292} values of the samples were used. All the normalized emission spectra of the various metal derivatives were superimposable upon that of apoazurin. However, earlier Tennent and McMillin (1979) reported that Co(II) azurin had a σ S(Cys) → Co(II) electronic transition near 330 nm. The absorption band corresponding to this transition is clearly seen in Figure 3.8 B. The overlap of this band with the 292 nm band of apoazurin resulted in a significantly higher absorbance measurement at λ_{ex} for the Co(II) derivative. In order to make the appropriate comparison with the quantum yields of the other metallo derivatives (where the quantum yield is essentially that

of the Trp residue), the quantum yield of the Trp residue in the Co(II) derivative of azurin was determined using the absorbance of the original apoazurin solution. When this was done, the relative reduction in the quantum yields of fluorescence was different, occurring as Cu(II) > Co(II) = Ni(II).

Engeseth and McMillin (1986) have reported metal ion binding energies of azurin and various metal–substituted derivatives. Their results suggested that Ni(II) was much less strongly bound than the Cu(II) to azurin on the basis of the comparison of enthalpies of denaturation. They suggested that Ni(II) suffered the greatest loss in ligand field stabilization energy when bound to the protein and thus a thermodynamic effect may dictate the lack of selectivity. The steady–state fluorescence measurements revealed that Ni(II) required more time than either Cu(II) or Co(II) in order for the protein to reach its final quantum yield. These data do not indicate whether the affinity of Ni(II) for the binding site was less, or whether all of the metals had comparable binding affinities but differed in their ability to induce protein conformational changes necessary for incorporation of the metal ions.

The mechanism by which the metal ion (especially Cu(II)) quenches the Trp fluorescence has been of some interest and it has been suggested that the fluorescence quenching reaction is an electron–transfer process from the excited state of Trp to the liganded copper atom (Petrich et al., 1987). This quenching mechanism, if operative, would suggest a correlation between the quenching efficiency and the relative redox potentials of the metal ions. Both Co(II) and Ni(II) have negative reduction potentials (–0.283 V and –0.236 V, respectively), while the reduction potential for Cu(II) is positive (+0.153 V) (Glasstone, 1942; Atkins, 1978). This implies that both Co(II) and Ni(II) would not efficiently

quench Trp fluorescence via an electron–transfer process from the excited Trp chromophore. Despite this point, the fluorescence quantum yield of the azurin was considerably reduced when these metals were bound to the protein. It appears therefore the quenching efficiency of the Trp is not primarily related to the reduction potential of the metal. This was reinforced by the comparatively similar quantum yield and lifetime behaviour of Cu(II) and Cu(I) azurins despite significant differences in the reduction potential of these two oxidation states of copper (+0.153 V, Cu(II) versus +0.521 V, Cu(I), Atkins, 1978). It cannot be ruled out, however, that in this latter case a limiting electron–transfer rate constant may have been realized at the reduction potential of Cu(II).

It was possible to calculate a fluorescence quantum yield of the metallo derivatives from the preexponential terms and the decay times of each decay component using equation 3.3 if it was assumed that the radiative lifetime, τ_r, was the same for each component. In section 3.4.4 it was found that the calculated quantum yield for Cu(II) azurin was *lower* than the measured value. It was suggested that the two short decay components in this case had a lower τ_r value (10.2 ns for *Pfl* holoazurin) than the long decay time (5 ns) component (τ_r = 15.5 ns). It was proposed that the shorter radiative lifetime arose because of an electronic perturbation of the Trp excited state by the copper–ligand complex.

When the quantum yield of the Ni(II) derivative was estimated from the decay parameters, a value of $\phi_f = 0.153$ was calculated when the radiative lifetime value of each component was considered to be the same, with a value of 15.5 ns. A value of $\phi_f = 0.156$ was calculated when the long decay time component had a τ_r = 15.5 ns and the other two decay components had τ_r = 10.2 ns. The measured quantum yield of 0.15 agreed quite well with either of these two calculated values.

In the case of the Co(II) derivative, the calculated quantum yield was 0.176 if all components were given the same τ_r = 15.5 ns and was 0.184 when values of τ_r = 15.5 and 10.2 ns were used. These values were both higher than the measured quantum yield of 0.16. However, the measured value may be lower due to the fact that the quantum yield was calculated with the A_{292} of the starting apoazurin solution as an estimate of the Trp absorbance in order to avoid interference by the 330 nm peak of the Co(II)–chelate complex.

As was the case for Cu(II) azurin, the long decay time components of approximately 4.9 ns in both the Co(II) and Ni(II) derivatives of azurin are assigned to a conformer where the tryptophan is distant from the metal–ligand complex. The other two components are assigned to conformational states in which the distance and/or orientation of the Trp residue relative to the ligand centre are different. The significant differences in the decay parameters of these two shorter components in the various derivatives suggest that the geometrical constraints placed upon the metal centre influence the Trp fluorescence to a considerable extent. Tennent and McMillin (1979) presented evidence that the Co(II) azurin–ligand complex existed in a distorted tetrahedral structure. The results reported in this thesis suggest that the Co(II)–ligand structure is heterogeneous and the relationship of these structures to the single Trp residue is reflected in fluorescence behaviour unique to this derivative.

In the case of Ni(II) azurin, the fluorescence decay components have similar values to those of the Cu(II) derivative, except for τ_2 and the preexponential terms. This suggests that in the Ni(II) and Cu(II) azurins the structure of the metal complex is similar, varying primarily in the relative concentration of the conformational components. The relative concentrations of the two short

components in the Ni(II) derivative are very low when compared to that of the long decay component and significantly less than the relative concentrations of these two components in Cu(II) azurin. It implies that the Ni(II) protein structure is most similar to the apoazurin structure. The work of Engeseth and McMillin (1986) is interesting in this respect since they reported that the calorimetric scans of Ni(II) azurin resembled that of apoazurin, having two well–separated thermal transitions. The work of Engeseth and McMillin is very relevant to these studies since they suggest that apoazurin also exists in two conformational states. It is rather surprising that if this were the case, the fluorescence decay behaviour of tryptophan in apoazurin did not reflect that heterogeneity. In view of the results presented in section 3.3 showing that some azurin samples contain non–metal reconstitutable components, verification of the calorimetric scans on azurin samples known to be homogeneous would be appropriate.

Obviously, metal complexes in protein centres are varied and complex. This suggests that the approach of comparing metalloproteins with small model compounds requires care in interpretation. For example, it has been shown, on the basis of the hydrolysis of tetrabromide adducts, that the divalent transition metal ions have an increased stability in tetrahedral complexes as one progresses from Co(II) to Zn(II) (Bianchi & Paoletti, 1984). However, it was found that Cu(II) azurin was more stable than either Ni(II) or Zn(II) azurin, which was rationalized as being due to a particularly low–symmetry structure of the metal binding site in azurin (Engeseth & McMillin, 1986). Because of a pseudo Jahn–Teller effect, Cu(II)/Cu(I) in the binding site may achieve stabilization by virtue of a distortion from idealized tetrahedral symmetry. It has also been demonstrated that the extinction coefficient of the band near 620 nm in the absorption spectrum of

holoazurin is approximately 100 times larger than that, apparent in the same spectral region, of most small model Cu(II) complexes (Fee, 1975). This suggests the Cu(II)–protein combination possesses a structural arrangement which is entirely unique among Cu(II) coordination complexes.

3.5 Chapter Summary and Conclusions

Homologous azurins from *Pseudomonas fluorescens* (ATCC 13525) and *Pseudomonas aeruginosa* (ATCC 10145) were examined by a number of electrophoretic techniques, and their copper to protein stoichiometry was determined by atomic absorption and amino acid analysis. Provided that the spectral ratio (A_{620}/A_{280}) was at least 0.53, and there was no evidence of a Soret band in the absorption spectrum, then these criteria can be used to judge the homogeneity of the azurin sample. If the spectra ratio was less than 0.50, evidence suggested a non–reconstitutable, non–trypsin digestible apoazurin was present. The fluorescence decay of these homogeneous holoazurins included three components, not two as previously reported (Szabo et al., 1983). The decay times were nearly the same for the azurins from the different sources, with one decay time near 5 ns, another between 0.5 and 0.4 ns, and a third at 0.10 ns. The fractional fluorescence of each component varied with the azurin measured. These three decay components were suggested to originate from three different protein conformational states. It was possible to estimate the relative concentrations of these three conformers, and it was shown that they were different for the two proteins. In addition, it was suggested that the radiative rate constant of tryptophan, when it is proximate to the copper–ligand complex, was affected by pH owing to structural changes of the protein with pH. Furthermore, the distribution of conformational states also

changed with pH. The pH study suggested an influence by a group which titrates between pH 5 and pH 7. The fluorescence of the corresponding apoazurins, prepared by a refined procedure, obeyed monoexponential decay kinetics. When taken together, these results confirm that the multiexponential decay behaviour originates from conformational heterogeneity, and not from contamination by an apo form (Petrich et al., 1987).

Nickel(II) and cobalt(II) derivatives of *Pseudomonas fluorescens* azurin were prepared and their steady–state and time–resolved fluorescence monitored. Like the copper(II)–containing native protein, the fluorescence decay of both metallo derivatives was best fit to a sum of three exponentials. However, comparison of the lifetimes and fractional fluorescence of each of the components in these derivatives to those in the oxidized and reduced native proteins revealed significant differences. The structures of the Cu(II) and Ni(II) conformers may be comparable, but their proportions are different. The Co(II) derivative is the most different in terms of the interactions of these components with the tryptophan residue. These results suggested that the presence of a metal center in azurin imparts a conformational heterogeneity which is strongly dependent on the nature of the metal center.

Although this fluorescence study cannot determine the geometry of ligands in the coordination sphere, it very clearly reveals that the geometric constraints placed upon the centre by various metal ions are quite different. The possible participation of a fifth ligand, contributed by Gly–45 (Norris et al., 1986), highlights the complexity that may be involved. The fluorescence results also indicate that the nature of the metal centre can alter the conformational heterogeneity of the protein. It is this effect upon conformation by the redox–altered geometry at the active centre which most probably mediates the electron–transfer process.

As suggested in section 1.4, and as supported by the results in this chapter, metal ions are capable of exerting a profound influence upon the conformational properties of proteins to which they associate. In the next three chapters, the dramatic influence of the biologically ubiquitous calcium ion on the conformational properties of two proteins known as parvalbumin and oncomodulin is examined.

3.6 References

Adman, E. T., Canters, G. W., Hill, H. A. O. & Kitchen, N. A. (1982) The effect of pH and temperature on the structure of the active site of azurin from *Pseudomonas aeruginosa*. FEBS Lett. 143, 287–292.

Adman, E. T., Canters, G. W., Hill, H. A. O. & Kitchen, N. A. (1983) The redox properties of azurin from *Pseudomonas aeruginosa* as studied by high frequency proton NMR. Inorg. Chim. Acta 79, 127–128.

Adman, E. T. & Jensen, L. H. (1981) Structural features of azurin at 2.7 A resolution. Isr. J. Chem. 21, 8–12.

Adman, E. T., Stenkamp, R. E., Sieker, L. C. & Jensen, L. H. (1978) A crystallographic model for azurin at 3 A resolution. J. Mol. Biol. 123, 35–47.

Ambler, R. P. (1963) The amino acid sequence of *Pseudomonas* cytochrome c–551. Biochem. J. 89, 349–378.

Ambler, R. P. (1971) In: Recent Developments in the Chemical Study of Protein Structures, Eds.: A. Previero, J. F. Pechere and M. A. Coletti–Previero (Inserm, Paris) pp 289–305.

Ambler, R. P. & Brown, L. H. (1967) The amino acid sequence of *Pseudomonas fluorescens* azurin. Biochem. J. 104, 784–825.

Ambler, R. P. & Wynn, M. (1973) The amino acid sequences of cytochromes c–551 from three species of *Pseudomonas*. Biochem. J. 131, 485–498.

Atkins, P. W. (1978) In: Physical Chemistry, (Oxford University Press, Oxford) p. 355.

Bianchi, A. & Paoletti, P. (1984) Stabilita di bromocomplessi tetraedrici dei metalli da Mn(II) a Zn(II). Chim. Ind. M. 66, 649.

Blair, D. F., Campbell, G. W., Schoonover, J. R., Chan, S. I., Gray, H. B., Malmstrom, B. G., Pecht, I., Swanson, B. I., Woodruff, W. H., Cho, W. K., English, A. M., Fry, H. A., Lum, V. & Norton, K.A. (1985) Resonance raman studies of blue copper proteins: Effect of temperature and isotopic substitutions. Structural and thermodynamic implications. J. Am. Chem. Soc. 107, 5755–5766.

Blaszak, J. A., McMillin, D. R., Thornton, A. T. & Tennent, D. L. (1983) Kinetics of copper (II) uptake by apoazurin in complexing media. J. Biol. Chem. 258, 9886–9892.

Blaszak, J. A., Ulrich, E. L., Markley, J. L. & McMillin, D. R. (1982) High–resolution proton nuclear magnetic resonance studies of the nickel (II) derivative of azurin. Biochem. 21, 6253–6258.

Brill, A. S. (1978) Activation of electron transfer reactions of the blue proteins. Biophys. J. 22, 139–142.

Brunori, M., Greenwood, C. & Wilson, M. T. (1974) A temperature–jump study of the reaction between azurin and cytochrome c–551 from *Pseudomonas aeruginosa*. Biochem. J. 137, 113–116.

Brunori, M., Parr, S. R. & Greenwood, C. (1975) A temperature–jump study of the reaction between azurin and cytochrome c oxidase from *Pseudomonas aeruginosa*. Biochem. J. 151, 185–188.

Burstein, E. A., Permyakov, E. A., Yashin, V. A., Burkhanov, S. A. & Finazzi–Agro, A. (1977) The fine structure of luminescence spectra of azurin. Biochim. Biophys. Acta 491, 155–159.

Canters, G. W., Hill, H. A. O., Kitchen, N. A. & Adman. E. T. (1984) The assignment of the ^1H nuclear magnetic resonance spectrum of azurin. Eur. J. Biochem. 138, 141–152.

Corin, A. F., Bersohn, R. & Cole, P. E. (1983) pH dependence of the reduction–oxidation reaction of azurin with cytochrome c–551: Role of histidine–35 of azurin in electron transfer. Biochem. 22, 2032–2038.

Donzel, B., Gauduchon, P. & Wahl, Ph. (1974) Study of the conformation in the excited state of two tryptophanyl diketopiperazines. J. Am. Chem. Soc. 96, 801–808.

Engeseth, H. R. & McMillin, D. R. (1986) Studies of thermally induced denaturation of azurin and azurin derivatives by differential scanning calorimetry: Evidence for copper selectivity. Biochem. 25, 2448–2455.

Engeseth, H. R., McMillin, D. R. & Otvos, J. D. (1984) Comparative Cd–113 nuclear magnetic resonance studies of Cd(II)–substituted blue copper proteins. J. Biol. Chem. 259, 4822–4826.

Fee. J. A. (1975) Copper proteins. Systems containing the "blue" copper center. Structure and Bonding 23, 1–60.

Ferris, N. S., Woodruff, W. H., Tennent, D. L. & McMillin, D. R. (1979) Native azurin and its Ni(II) derivative: A resonance raman study. Biochem. Biophys. Res. Commun. 88, 288–296.

Finazzi–Agro, A., Giovagnoli, C., Avigliano, L., Rotilio, G. & Mondovi, B. (1973) Luminescence quenching in azurin. Eur. J. Biochem. 34, 20–24.

Finazzi–Agro, A., Rotilio, G., Avigliano, L., Guerrieri, P., Boffi, V. & Mondovi, B. (1970) Environment of copper in *Pseudomonas fluorescens* azurin: Fluorometric approach. Biochem. 9, 2009–2014.

Glasstone, S. (1942) In: An Introduction to Electrochemistry, (Van Nostrand, Princeton) p. 243.

Gray. H. B. & Malmstrom, B. G. (1983) On the relationship between protein–forced ligand fields and the properties of blue copper centers. Comments Inorg. Chem. 2, 203–209.

Gray, H. B. & Solomon, E. I. (1981) In: Copper Proteins, Ed.: T. G. Spiro (Wiley, New York) Vol. 1, pp. 1–39.

Grinvald, A., Schlessinger, J., Pecht, I. & Steinberg, I. Z. (1975) Homogeneity and variability in the structure of azurin molecules studied by fluorescence decay and circular polarization. Biochem. 14, 1921–1929.

Hill, H. A. O. & Smith, B. E. (1979) Characteristics of azurin from *Pseudomonas aeruginosa* via 270–MHz ^{1}H nuclear magnetic resonance spectroscopy. J. Inorg. Biochem. 11, 79–93.

Illingworth, J. A. (1972) Anomalous behaviour of yeast isocitrate dehydrogenase during isoelectric focusing. Biochem. J. 129, 1125–1130.

Mallinson, R., Carter, R. & Ghiron, C. A. (1981) Acrylamide quenching studies with azurin B. Biochim. Biophys. Acta 671, 117–122.

Masotti, L., Cavatorta, P., Szabo, A. G., Farruggia, G. & Sartor, G. (1988) In: Fluorescent Biomolecules, Eds.: D. Jameson & E. Gratton (Plenum Press, New York) In Press.

McMillin, D. R. & Tennent, D. L. (1979) In: ESR and NMR of Paramagnetic Species in Biological and Related Systems, Eds.: I. Bertini & R. S. Drago (D. Reidel, Dordrecht) pp. 369–379.

Meech, S. R., Phillips, D. & Lee, A. G. (1983) On the nature of the fluorescent state of methylated indole derivatives. Chem. Phys. 80, 317–328.

Munro, I., Pecht, I. & Stryer, L. (1979) Subnanosecond motions of tryptophan residues in proteins. Proc. Natl. Acad. Sci. USA 76, 56–60.

Norris, G. E., Anderson, B. F. & Baker, E. N. (1986) Blue copper proteins. The copper site in azurin from *Alcaligenes denitrificans*. J. Am. Chem. Soc. 108, 2784–2785.

Petrich, J. W., Longworth, J. W. & Fleming, G. R. (1987) Internal motion and electron transfer in proteins: A picosecond fluorescence study of three homologous azurins. Biochem. 26, 2711–2722.

Righetti, M. & Drysdale, J. W. (1971) Isoelectric focusing in polyacrylamide gels. Biochim. Biophys. Acta 236, 17–28.

Ryden, L. & Lundgren, J. O. (1979) Homology relationships among the small blue proteins. Nature 261, 344–346.

Stanier, R. Y., Palleroni, N. J. & Doudoroff, M. (1966) The aerobic pseudomonads: A taxonomic study. J. Gen. Microbiol. 43, 159–271.

Surewicz, W. K., Szabo, A. G. & Mantsch, H. H. (1987) Conformational properties of azurin in solution as determined from resolution–enhanced fourier–transform infrared spectra. Eur. J. Biochem. 167, 519–523.

Szabo, A. G., Stephanik, T. M., Wayner, D. M. & Young, N. M. (1983) Conformational heterogeneity of the copper binding site in azurin. Biophys. J. 41, 233–244.

Tennent, D. L. & McMillin, D. R. (1979) A detailed analysis of the charge–transfer bands of a blue copper protein. Studies of the nickel(II), manganese(II), and cobalt(II) derivatives of azurin. J. Am. Chem. Soc. 101, 2307–2311.

Tullius, T. D., Frank, P. & Hodgson, K. O. (1978) Characterization of the blue copper site in oxidized azurin by extended x–ray absorption fine structure: Determination of a short Cu–S distance. Proc. Natl. Acad. Sci. USA 75, 4069–4073.

Ugurbil, K. & Bersohn, R. (1977) Nuclear magnetic resonance study of exchangeable and nonexchangeable protons in azurin from *Pseudomonas aeruginosa*. Biochem. 16, 3016–3023.

Ugurbil, K., Maki, A. H. & Bersohn, R. (1977a) Study of the triplet state properties of tyrosines and tryptophan in azurins using optically detected magnetic resonance. Biochem. 16, 901–907.

Ugurbil, K., Norton, R. S., Allerhand, A. & Bersohn, R. (1977b) Studies of individual carbon sites of azurin from *Pseudomonas aeruginosa* by natural–abundance carbon–13 nuclear magnetic resonance spectroscopy. Biochem. 16, 886–894.

Wherland, S. & Pecht, I. (1978) Protein–protein electron transfer. A Marcus theory analysis of reactions between c type cytochromes and blue copper proteins. Biochem. 17, 2585–2591.

Wilson, M. T., Greenwood, C., Brunori, M. & Antonini, E. (1975) Electron transfer between azurin and cytochrome c–551 from *Pseudomonas aeruginosa*. Biochem. J. 145, 449–457.

Yamanaka, T., Kijimoto, S. & Okunuki, K. (1963) Some properties of *Pseudomonas* blue protein and its apo–protein. J. Biochem. 53, 256–259.

Chapter 4

THE CONFORMATIONAL HETEROGENEITY OF PARVALBUMIN AND ITS SPECIFIC CONTROL BY CALCIUM

4.1 Introduction

The parvalbumins are low molecular weight ($M_r \simeq 12000$), acidic, soluble proteins which are ubiquitous in the vertebrate world (Pechère, 1974). They are especially plentiful in the white skeletal muscle of fish and amphibia (Blum et al., 1977). Based upon amino acid sequence data, as well as the X–ray crystallographic structure of carp parvalbumin, these proteins have been found to represent a subfamily of the large superfamily of calcium–binding proteins (Kretsinger, 1980). The parvalbumin subfamily is further subdivided based upon two evolutionarily distinct lineages, the α–lineage and the more acidic β–lineage (Goodman & Pechère, 1977).

Over the last fifteen years these proteins and their metal binding properties have been the subject of considerable research. Interpretation of the early thermodynamic and kinetic experiments suggested that the parvalbumins were involved in muscular contraction/relaxation and were Ca^{2+}/Mg^{2+} specific proteins (Pechère et al., 1977; Birdsall et al., 1979). A Ca^{2+}/Mg^{2+} specific protein is one which binds both Ca^{2+} and Mg^{2+}, with the affinity for Ca^{2+} being usually 10^2–10^3 fold greater than the affinity for Mg^{2+}. In contrast, a Ca^{2+}–specific protein is one which will not bind Mg^{2+} to any significant degree owing to a K_{Ca} affinity constant at least 6 orders of magnitude greater than the magnesium affinity constant, K_{Mg}. The generally held belief that parvalbumins are Ca^{2+}/Mg^{2+} specific proteins has been described by Henzl and Birnbaum (1988) as forming part of an "evolved paradigm". In accordance with this paradigm, the two metal ion binding sites of the parvalbumins are believed to possess features which allow them

to bind both Ca^{2+} and Mg^{2+}. In addition, indistinguishable conformational changes are believed to occur when the protein binds either of these two metal ions (MacManus et al., 1984). Such features are absent in those proteins which are Ca^{2+}–specific. However several inconsistencies exist in the literature. Equivalent conformational responses of parvalbumin upon Ca^{2+} or Mg^{2+} binding have been reported (Cox et al., 1979; MacManus et al., 1984). In other studies it was found that distinct changes occurred only in the presence of Ca^{2+} (Birdsall et al., 1979). Birdsall and coworkers (1979) suggested global conformational differences existed, while Moeschler et al. (1980) reported that the differences were confined to the vicinity of the metal–binding sites. Others have suggested that parvalbumin does not bind Mg^{2+}, which is surprising for a putative Ca^{2+}/Mg^{2+} specific protein (Cave et al., 1979b; Daures, 1977). However Mg^{2+} binding, as well as the associated binding constants have been measured (Birdsall et al., 1979; Moeschler et al., 1980). These contradictions were noted by White (1988) who suggested that the conclusions were formulated from a variety of experimental approaches leading to conflicting and inconsistent conclusions regarding basic features of metal binding to these proteins.

Of the 40 parvalbumins of known structure (Maeda et al., 1984; Gerday, 1982; Blum et al., 1977; Closset & Gerday, 1976), only two contain a single tryptophan. These parvalbumins, which are members of the β–lineage, have been isolated from two members of the genus *Gadus*, namely cod and whiting (Bhushana Rao et al., 1969; Closset, J.I., 1976). The presence of this single Trp residue has prompted a number of fluorescence studies on the isotype IIIb component of whiting (Permyakov & Burstein, 1984; Permyakov et al., 1982; Permyakov et al., 1980; White, 1988; Castelli et al., 1988), as well as on the isotype III component of cod

(Permyakov et al., 1987; Eftink & Hagaman, 1985; Horrocks & Collier, 1981). The purpose of the present study was to locate the position of the single Trp residue in highly purified cod III parvalbumin and to use it as a specific probe of protein conformation. In particular, the ability and manner in which Ca^{2+} and Mg^{2+} affect the conformation of the protein was investigated. The reported ability (Parello et al., 1979) of the frequently used soluble chelator EGTA to affect the metal–binding was also investigated. Analysis of the time–resolved fluorescence decay and the construction of DAS (decay–associated spectra) revealed distinct conformational states in the Ca^{2+}–loaded (holo) and metal–free (apo) proteins. In contrast, Mg^{2+}–binding did not significantly influence the spectral properties of the apo protein. Circular dichroism showed that the metal–binding effects were not limited to the vicinity probed by the single Trp residue. The results demonstrate that cod III parvalbumin undergoes Ca^{2+}–specific conformational changes.

4.2 Materials and Methods

4.2.1 Materials

Sodium dihydrogen phosphate, sodium hydrogen phosphate, sodium chloride and potassium chloride were obtained from Fisher Scientific Company, Fair Lawn, New Jersey. SpectraPor dialysis tubing (Mw cutoff 3500) was obtained from Spectrum Medical Industries, Los Angeles, California. Sodium cacodylate, EDTA, piperazine and DL–dithiothreitol were supplied by Sigma Chemical Company, St. Louis, Missouri. TRIS buffer was obtained from Boehringer Mannheim, W. Germany. Glycerol and trichloroacetic acid (TCA) were purchased from Anachemia, Montreal, Quebec. Calcium chloride and magnesium chloride were purchased from Thiokol/Ventron, Danvers, Massachusetts. Sephadex G–75SF and

DEAE–Sephacel were purchased from Pharmacia Canada Ltd., Dorval, Quebec and Whatman DEAE–52 was purchased from Mandel Scientific Company, Rockwood, Ontario. N–acetyltryptophanamide (NATA) was purchased from Aldrich Chemical Company, Milwaukee, Wisconsin. Electrophoretically pure (>99.9%) acrylamide, Chelex–100 resin (100–200 mesh), Bio–Lyte 3/5 carrier ampholytes and molecular weight standards were purchased from Bio–Rad Laboratories, Richmond, California. $^{45}CaCl_2$ was obtained from New England Nuclear, Boston, Massachusetts. All buffers were prepared using reverse osmosis quality water purified by the Milli–Q Water System, Millipore Canada Ltd., Mississauga, Ontario.

4.2.2 Parvalbumin Purification

Cod III parvalbumin was purified from 500 g of frozen fillets by the method of Horrocks and Collier (1981) with the following modifications. After the extraction of the soluble proteins from the muscle into Tris buffer as detailed by Horrocks and Collier (1981), the high molecular weight proteins were separated from the low molecular weight proteins by cold ($0 - 4^{\circ}C$) acetone fractionation. The acetone precipitation was conducted in two steps. Acetone was added to a final concentration of 54% (v/v) dropwise at $0 - 4^{\circ}$ C with stirring, followed by additional stirring for 15 minutes at 0° C. This solution was centrifuged for 75 minutes at 9500 rpm in a Sorvall RC–5B Refrigerated Superspeed Centrifuge. The supernatant was made 80% in acetone (v/v) and after centrifugation the pellet was redissolved in 100 mL of 20 mM sodium phosphate buffer, pH 7.30 containing 24 mM NaCl. This solution was gently agitated overnight, centrifuged, and divided into two 50 mL portions. In two separate applications, the 50 mL protein solutions

were loaded onto a Sephadex G–75SF column (2.5 cm x 100 cm), eluted at a flow rate of 3 mL/minute and collected in 5 mL fractions. The spectrophotometric absorbances of the fractions were monitored at 280 nm (the wavelength maximum of Trp/Tyr–containing proteins) to generate an elution profile. The fractions containing the low molecular weight parvalbumins were identified by both their peak position and their calcium binding activity as measured by the $^{45}Ca(II)$ chelex competition assay (Waisman & Rasmussen, 1983) (Figure 4.1).

These fractions were pooled and dialyzed overnight at 4° C against 0.0162 M piperazine buffer, pH 5.70 in preparation for DEAE–52 cellulose chromatography. After combining the fractions from gel filtration of the two 50 mL samples, a total volume of 170 mL was applied to the ion exchange column. The DEAE–52 cellulose column (3 cm x 42 cm) was eluted with a linear NaCl gradient (500 mL x 500 mL, 0–0.10 M NaCl) and fractions collected. Fractions containing the parvalbumins were identified based on their absorbance at 280 and 260 nm (to monitor differential Phe/Trp content), the protein–dye binding assay (to monitor total protein, Bradford, 1976), and calcium–binding activity (Figures 4.2 and 4.3).

At this stage of the purification, the protein appeared homogeneous with respect to size as established by sodium dodecyl sulfate polyacrylamide gel electrophoresis (SDS–PAGE) on a 8–25% gradient using the Pharmacia PhastSystem. A single band was observed as seen in Figure 4.4, Lane E. However, upon isoelectric focusing in 7.5% polyacrylamide rod gels (Righetti & Drysdale, 1971), 5% ampholytes, pH gradient 3–5, two bands appeared in fractions across the elution profile. An example of these 2 bands in a fraction is seen in Figure 4.5, in the third gel marked "Sephacel Load". Thus it was evident that another purification step was required. This two component mixture of proteins was

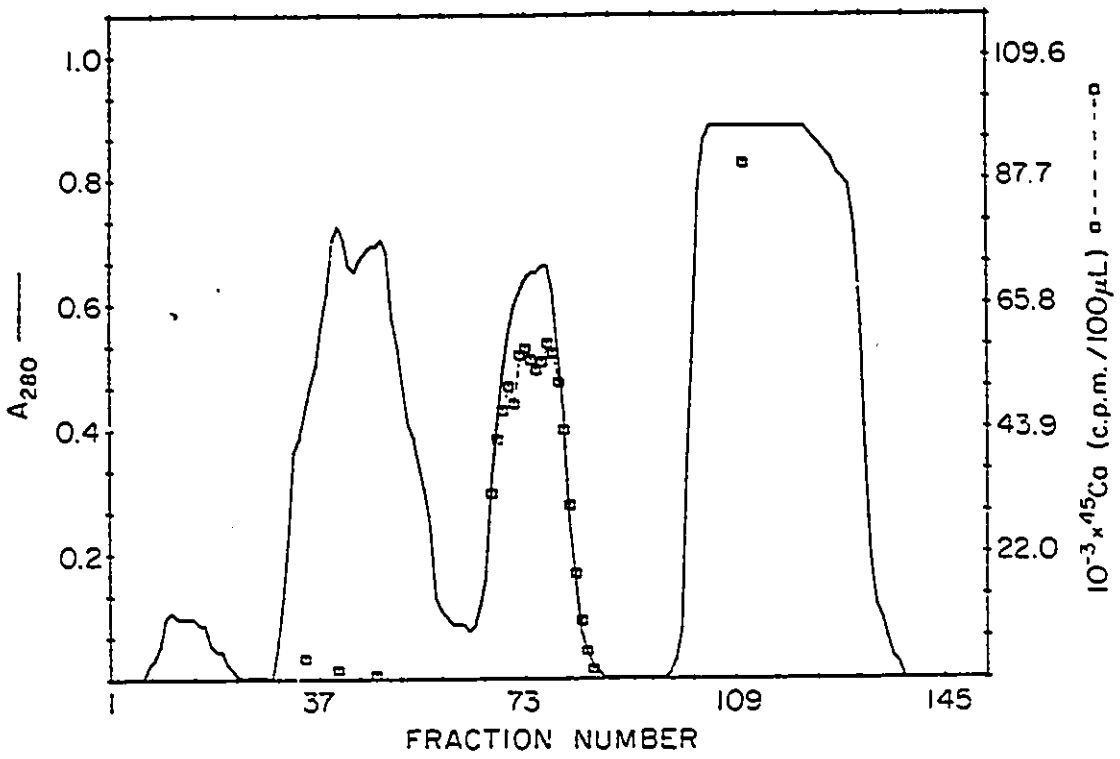

Figure 4.1: Elution profile of soluble cod muscle proteins eluted from a Sephadex G–75SF gel filtration column following acetone fractionation. The column was equilibrated and eluted with 20 mM sodium phosphate buffer, pH 7.3 containing 24 mM NaCl. The solid line represents the absorbance values of the fractions measured at 280 nm while the dashed line represents the calcium–binding activity. The coincidence of protein and calcium–binding activity in the third peak from the left identified the corresponding fractions as parvalbumin–containing.

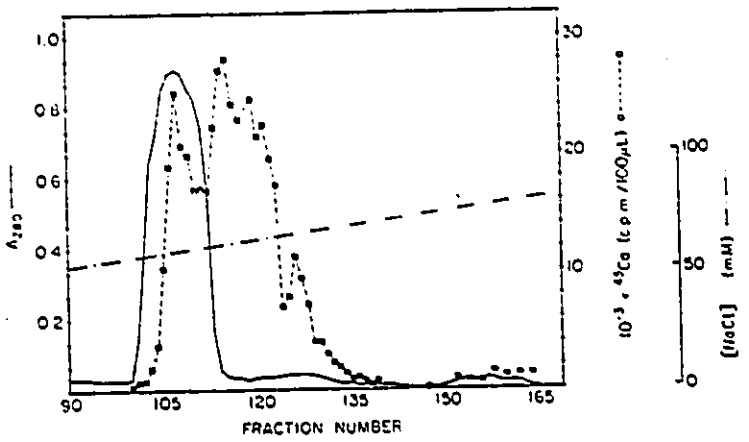

Figure 4.2: Elution profile of the low molecular weight, calcium–binding proteins eluted from a DEAE–52 cellulose ion exchange column with a linear NaCl gradient. The column had been preequilibrated in 0.0162 M piperazine buffer, pH 5.70. The solid line represents the absorbance values of the fractions measured at 280 nm, while the dashed line represents the calcium–binding activity. The dashed–dotted line displays the NaCl gradient. The high absorbance at 280 nm and the calcium–binding activity in fractions 104–111 identified the presence of a Trp–containing, calcium–binding protein.

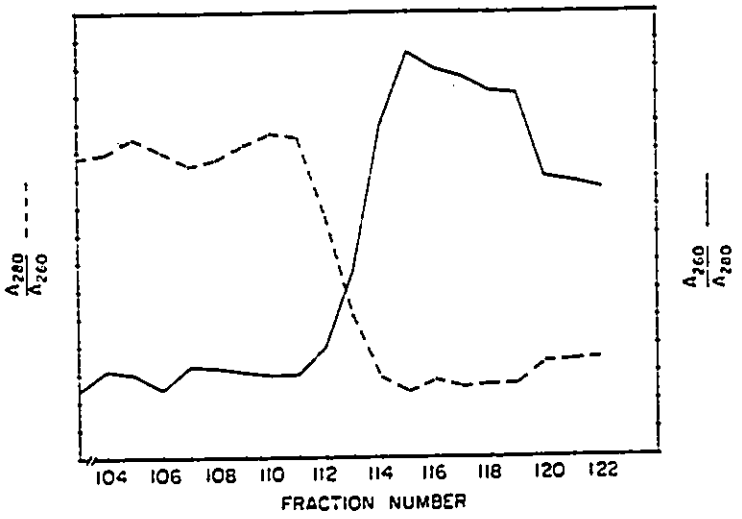

Figure 4.3: Absorbance ratios of the calcium–binding fractions obtained after DEAE–52 cellulose chromatography. The high A_{280}/A_{260} ratios corresponding to fractions 104–111 identified these fractions as containing a Trp–containing protein.

Figure 4.4: SDS–PAGE pattern of cod muscle protein extract obtained at various steps in the purification of cod III parvalbumin. Lane A, soluble extract; Lane B, 54% acetone pellet; Lane C, G–75 load; Lane D, DEAE 52–load; Lane E, peak DEAE–52 fraction (106); Lane F, DEAE–Sephacel load; Lane G, peak DEAE–Sephacel fraction; Lane H, molecular weight standards.

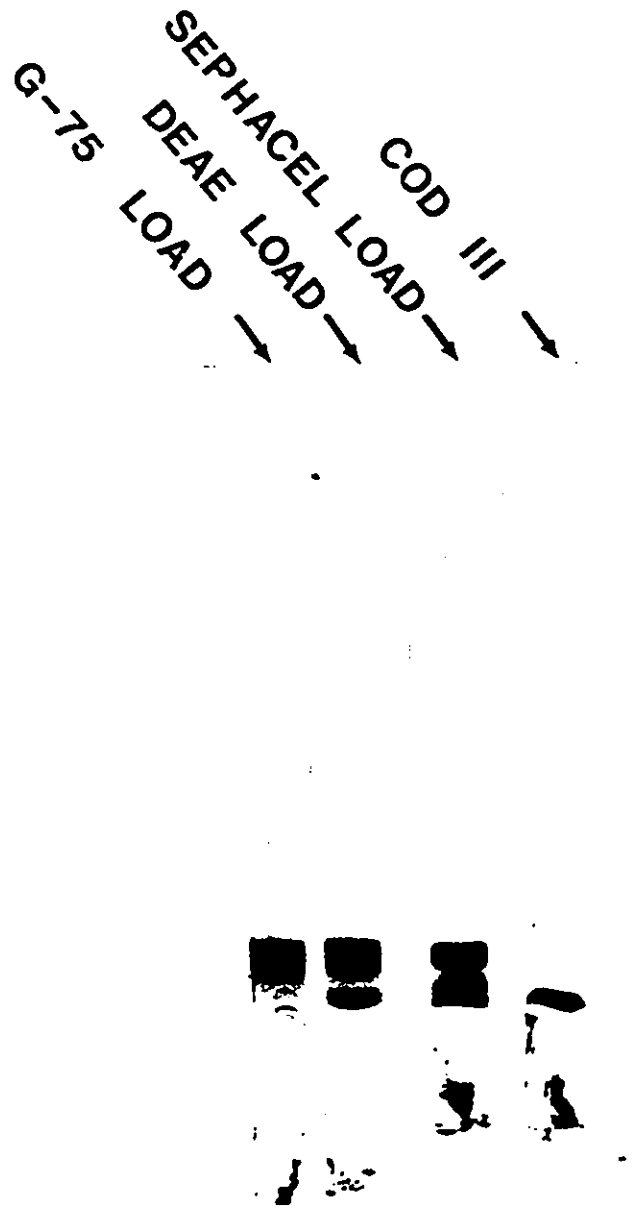

Figure 4.5: Polyacrylamide rod gels obtained upon isoelectric focusing of cod muscle extract at various stages of parvalbumin purification in a gradient of pH 3–5 from top to bottom at a constant voltage of 250 V. The gels show that the additional purification step on DEAE–Sephacel was required to achieve homogeneous cod III parvalbumin.

purified further as follows.

Pooled fractions from the DEAE–52 cellulose ion exchange column were dialyzed overnight at 4° C against 20 mM TRIS, pH 8 containing 1 mM dithiothreitol (DTT) and applied to a DEAE–Sephacel column (0.9 cm x 30 cm) equilibrated in the same buffer. The protein was then eluted with a linear NaCl gradient (250 mL x 250 mL, 0–0.30 M NaCl), fractions collected and monitored by measuring A_{280} and calcium–binding activity. Of the three peaks obtained in the resulting elution profile, peak #2 in Figure 4.6 was found to contain homogeneous, calcium–binding protein as judged by SDS–PAGE, isoelectric focusing, amino acid analysis and tryptic peptide sequence analysis. The fractions in this peak were pooled and the protein concentration estimated using $\epsilon_{280} = 7180\ M^{-1}cm^{-1}$ (Closset & Gerday, 1976). Typically, 70–80 mg of cod III parvalbumin was purified from 500 g of fish muscle.

4.2.3 Apoprotein Preparation

Calcium–loaded native (holo) parvalbumin was decalcified by precipitation with trichloroacetic acid (TCA) (Haiech et al., 1981). Calcium removal was also accomplished by addition of an excess of EGTA at neutral pH. The EGTA–treated samples were examined spectroscopically both in the presence of the chelator and following chelator removal by G–25 Sephadex gel filtration or dialysis. Calcium content following apo (metal–free) protein preparation or metal reconstitution was measured by atomic absorption spectroscopy on a Pye–Unicam SP 191 instrument.

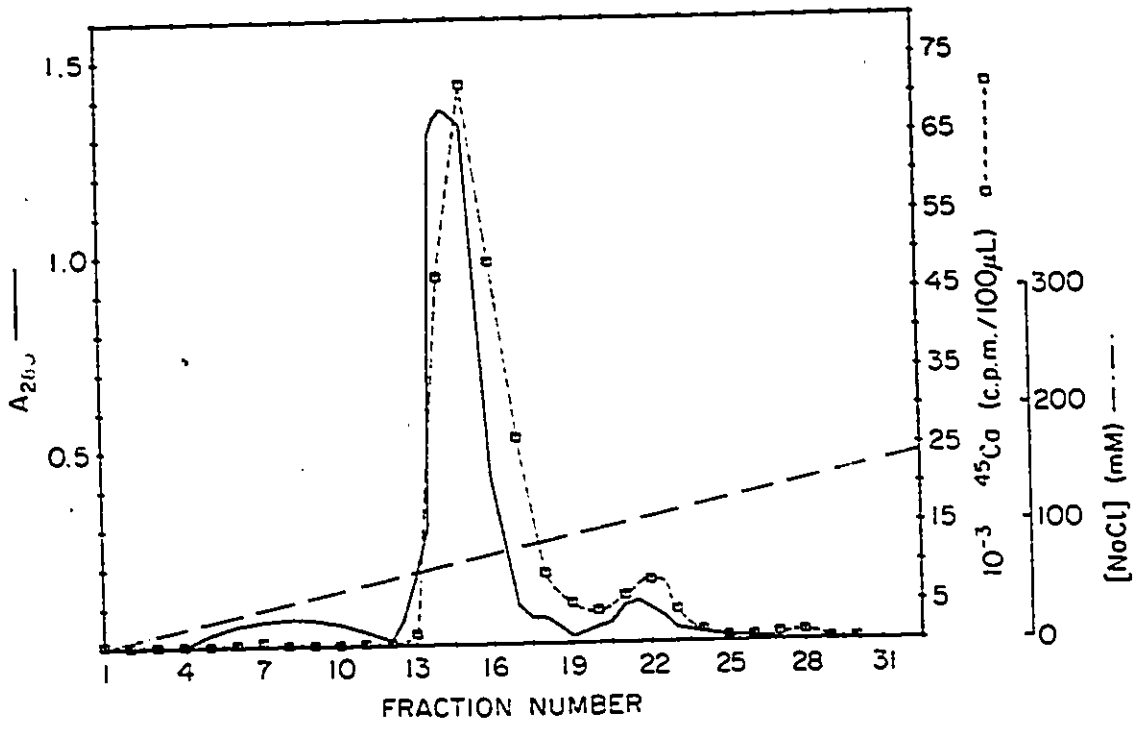

Figure 4.6: DEAE–Sephacel purification of cod III parvalbumin. The protein obtained following gel filtration and ion exchange on DEAE–52 cellulose was applied to DEAE–Sephacel which had been preequilibrated with 20 mM TRIS, pH 8 containing 1 mM dithiothreitol. The protein was eluted with a linear NaCl gradient (0–0.3 M) in the same buffer (dashed–dotted line). Fractions were collected and monitored for protein content by measuring A_{280} (solid line), A_{260} and calcium–binding activity (dashed line). Fractions 14–16 were found to be homogeneous as judged by SDS–PAGE, isoelectric focusing, amino acid composition determination and tryptic peptide mapping.

4.2.4 Amino Acid Composition and Partial Sequence Determination

Partial sequencing of holo cod III parvalbumin was performed according to methods previously described (MacManus et al., 1985). These methods involved HPLC separation of tryptic fragments of the protein on a Syncropak RP–P C18 reverse phase HPLC column (Synchrom Inc., Linden, Indiana) using a 0.1% trifluoroacetic acid (Pierce, Rockford, Illinois)/acetonitrile (Burdick & Jackson Laboratories, Muskegon, Michigan) elution system. Only one Trp–containing peptide from HPLC was obtained and hence this peptide was sequenced. The amino acid compositions of both the holo and apo–TCA parvalbumins were determined and the latter was used to estimate an extinction coefficient for the decalcified protein. The tryptic fragments were generated and purified by Dr. J. P. MacManus, and the amino acid compositions and sequence were determined by Dr. M. Yaguchi, both at the Division of Biological Sciences, NRC.

4.2.5 Additional Spectroscopic Details

Titration data were obtained with the aid of a macro programme for the SLM 8000C spectrofluorometer. Aliquots (2 μL) of a 1 mM $CaCl_2$ solution (in 10 mM cacodylate, 150 mM KCl, 1 mM dithiothreitol, pH 7) were added with continuous stirring to 1.5 mL of apoprotein (in the same buffer). The protein concentrations were 20–40 μM. Typically, sixty additions resulted in plateau values being recorded in the titration curves. The circular dichroism spectra were measured on a JASCO J–600 spectropolarimeter with quartz cells (0.1 cm or 1.0 cm pathlength) at 20° C. All spectroscopy was done with protein samples dissolved in 10 mM cacodylate buffer containing 150 mM KCl and 1 mM dithiothreitol, pH 7.0.

4.3 Results

4.3.1 Protein Homogeneity

A modification of the procedure of Horrocks and Collier (1981) was used to purify the isotype III component of cod parvalbumin. The major modification was the inclusion of an additional chromatographic step following ion exchange on DEAE–52 cellulose. This involved ion exchange on a DEAE–Sephacel column, with protein elution accomplished by a shallow NaCl gradient. Examination of the elution profile revealed three peaks (Figure 4.6) when fractions were monitored at A_{280}, with only the latter two exhibiting calcium–binding activity. Electrophoresis of the major peak revealed single bands both upon SDS–PAGE (Figure 4.4, Lane G) and isoelectric focusing (Figure 4.5, fourth gel labelled "COD III"). Determination of the amino acid composition yielded results identical to previous determinations (Closset & Gerday, 1976). The amino acid composition of the corresponding apo (metal–free) parvalbumin was used to determine the extinction coefficient at 280 nm. A value of $\epsilon_{280} = 7095\ M^{-1}cm^{-1}$ was calculated. HPLC of tryptic fragments of the protein showed only one Trp–containing peptide to be present (based on absorbance at 280 nm). On the basis of these criteria the protein was considered homogeneous for spectroscopic use.

4.3.2 Location of the Single Tryptophan Residue

Sequence analysis was performed on the only Trp–containing peptide found in the tryptic digest of homogeneous cod III parvalbumin. By alignment with existing parvalbumin sequences, this 20 amino acid residue peptide was found to

represent the C–terminal peptide. The results revealed the following sequence:

$$^{88}\text{A–G–D–S–D–G–D–G–A–I–G–V–D–E–}^{102}\text{W–A–V–L–V–}^{107}\text{K.}$$

As the penultimate amino acid in the protein is lysine, the C–terminus (position 108) was cleaved by trypsin and hence was undetermined. The sequence established the location of the single tryptophan residue in position 102 of a 108 amino acid cod III parvalbumin sequence, the total number of residues in the protein being determined by composition analysis.

4.3.3 Spectral Results and Apoprotein Preparation

The absorption spectrum of holo native cod parvalbumin had a maximum at 280 nm and a sharp subsidiary peak at 289 nm (Figure 4.7). A considerable amount of structure was especially evident in the absorption spectrum below 280 nm. Decalcification resulted in a complete loss of the 289 nm subsidiary peak of the absorption spectrum, as well as a reduction in spectral definition (Figure 4.7). TCA–precipitation of holo cod III parvalbumin resulted in greater than 96% decalcification as judged by atomic absorption spectroscopy; typically 0.03 mol Ca^{2+}/mol protein was measured.

The corrected steady–state fluorescence emission spectrum had a λ_{max} = 321 nm in the absence of added Ca^{2+}(aq) (Figure 4.8, Spectrum 1). The corrected steady–state fluorescence emission spectrum showed that Ca^{2+} removal prompted a substantial red–shift (λ_{max}= 321 nm for holo versus λ_{max}= 337 nm for apo), a broadening of the spectrum and a quenching of the Trp fluorescence (Figure 4.8, Spectrum 3). Upon decalcification the quantum yield decreased from 0.14 ± 0.01 to 0.09 ± 0.01 when excited at 295 nm, 20° C, pH 7.

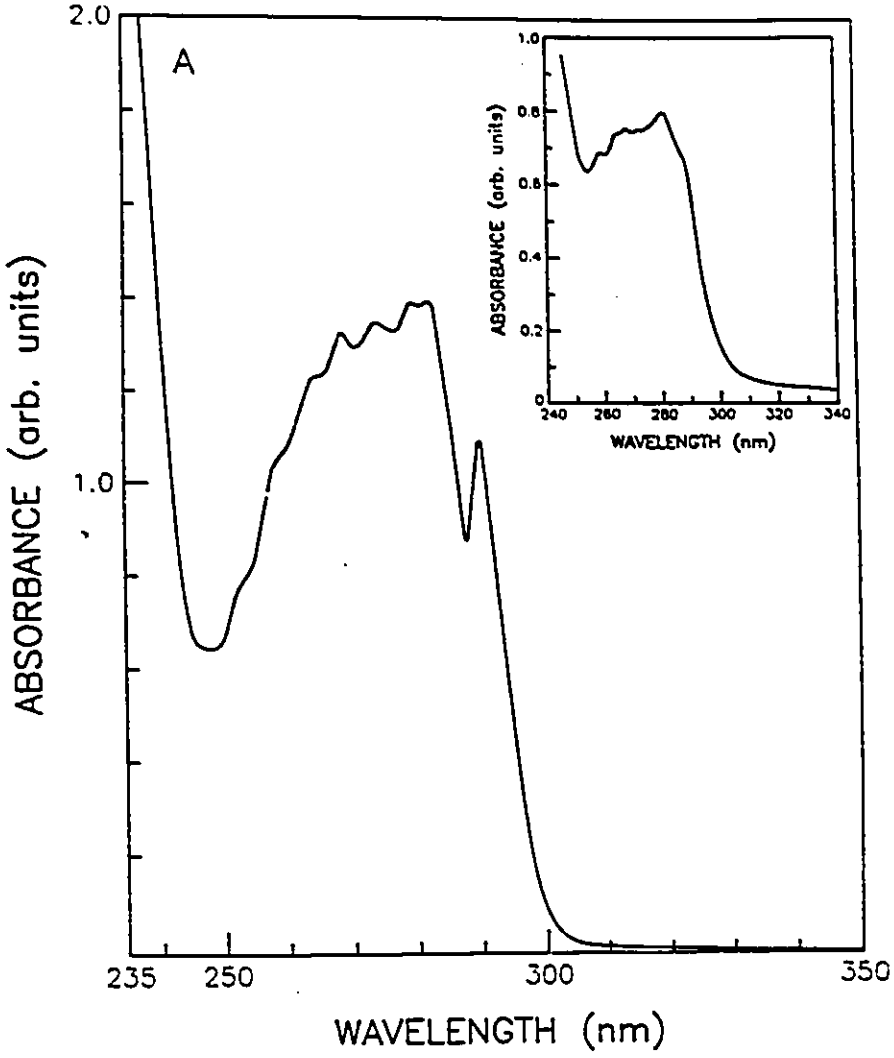

Figure 4.7: Ultraviolet absorption spectrum of homogeneous holo cod III parvalbumin + 1 μM $CaCl_2$ in 10 mM cacodylate, 150 mM KCl, 1 mM dithiothreitol, pH 7. Phenylalanine vibronic structure is evident in the region of 260–280 nm. In addition, the sharp ^1L_b electronic transition of tryptophan is evident at 289 nm. INSET: Spectrum of apo–TCA parvalbumin in the same buffer without Ca^{2+}. Decalcification resulted in a reduction in the defined spectral structure due to phenylalanine, as well as a complete loss of the 289 nm subsidiary peak of tryptophan.

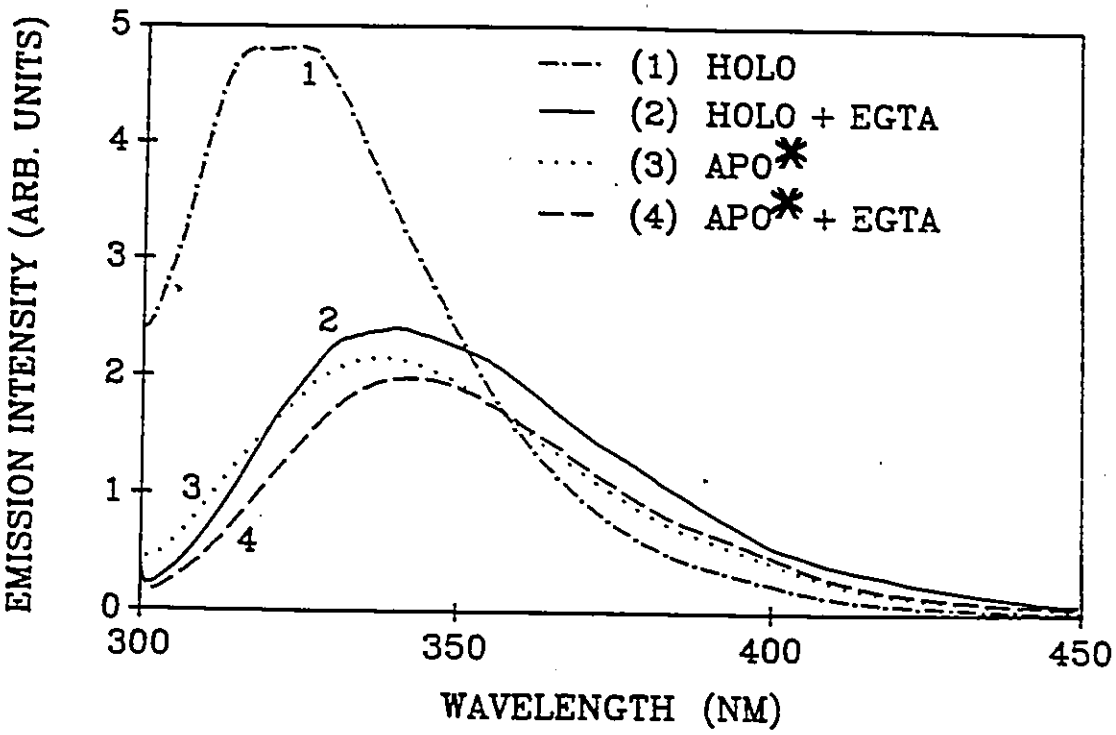

Figure 4.8: Corrected steady–state fluorescence emission spectra of EGTA–treated and untreated holo– and apo–TCA cod III parvalbumin. The protein concentration was approximately 20 μM in 10 mM cacodylate, 150 mM KCl, 1 mM DTT, pH 7, 20oC. λ_{ex} = 295 nm, concentration of EGTA = 1.2 mM. The asterisk (*) emphasizes that "APO" refers to the decalcified protein that has been prepared by TCA precipitation; atomic absorption measurements of the protein after this treatment typically gave 0.03 mol Ca^{2+}/mol protein.

Addition of ≈ 30–fold molar excess of EGTA to holo cod III parvalbumin resulted in a greater red–shift of the emission spectrum compared to the spectrum of the apo–TCA protein (λ_{max} = 343 nm (holo + EGTA, Figure 4.8, Spectrum 2) vs λ_{max} = 337 nm (apo–TCA, Figure 4.8, Spectrum 3)). The tryptophan fluorescence was quenched, but not to the same extent as that observed with the TCA–treated sample (Figure 4.8, Compare spectra 2 and 3.). When EGTA was added to an apo–TCA treated parvalbumin, a 4–8 nm red–shift was observed, as well as a slight decrease in the fluorescence intensity (Figure 4.8, Spectrum 4).

When the holo sample was sequentially titrated with EGTA, a monophasic quenching of the Trp fluorescence was observed (Figure 4.9). At a molar ratio of 2 EGTA:1 protein, the amount of fluorescence quenching was only 57% of the maximum amount of quenching observed in the presence of a 10–fold excess of EGTA at pH 7. Following gel filtration or dialysis to remove the excess EGTA and/or Ca–EGTA complexes, the amount of Ca^{2+} remaining in the EGTA–treated samples was determined by atomic absorption spectroscopy. Results showed that 0.40 ± 0.1 mol Ca^{2+}/mol protein remained in the EGTA–treated sample. The fluorescence spectra of the sample following gel filtration were the same as that observed prior to that treatment.

4.3.4 Metal Ion Addition to Parvalbumin

The corrected fluorescence emission spectrum of holo cod III parvalbumin showed a 5 nm blue–shift (Compare spectra 1 and 2 in Figure 4.10) and shape change upon addition of excess Ca^{2+} (λ_{max} = 316 nm). Addition of the same excess of Ca^{2+} to the apo–TCA precipitated protein restored the wavelength

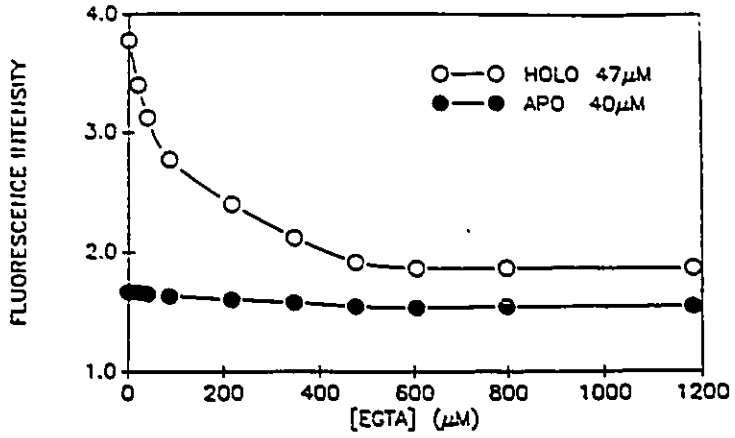

Figure 4.9: EGTA titration of holo and apo–TCA cod III parvalbumin in 10 mM cacodylate, 150 mM KCl, 1 mM DTT, pH 7, 20°C. λ_{ex} = 295 nm; λ_{em} = 325 nm.

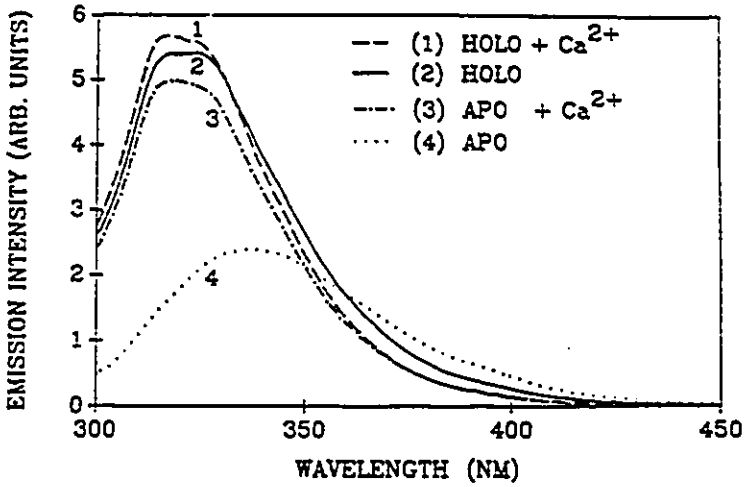

Figure 4.10: Corrected steady–state fluorescence emission spectra of holo– and apo–TCA cod III parvalbumin in the absence and presence of excess Ca^{2+} (aq). The ϕ_f (holo + Ca^{2+}) = 0.14 ± 0.01 and ϕ_f (apo + Ca^{2+}) = 0.13 ± 0.01. The protein concentration was approximately 20 μM to which 1–2 μL of a concentrated $CaCl_2$ stock solution was added to yield a final concentration [Ca^{2+}] = 2.5 mM. λ_{ex} = 295 nm.

position of the spectrum (λ_{max} = 316 nm), narrowed the spectrum and restored 93% of the fluorescence intensity as judged by quantum yield measurements (Figure 4.10, Spectrum 3). Ca^{2+} titration of an apo–TCA sample revealed progressive changes in the spectrum, with a plateau obtained at a molar ratio of 2 mol Ca^{2+}: 1 mol protein (Figure 4.11). A slight break in the titration curve was observed at a molar ratio of 1 mol Ca^{2+}: 1 mol protein. These results demonstrated the reversibility of conformational changes in the region of the protein probed by Trp–102 upon the addition and removal of Ca^{2+}.

As the parvalbumins are generally accepted as Ca^{2+}/Mg^{2+} specific proteins (See section 4.1), it was anticipated that the addition of excess Mg^{2+}(aq) to the decalcified protein would promote spectral changes comparable to those which were observed upon the addition of Ca^{2+}(aq). However, such changes were not observed. Addition of excess Mg^{2+} to holo cod III parvalbumin resulted in a 4% decrease in the fluorescence intensity of the spectrum (corrected for dilution factor) and a negligible wavelength shift, and negligible spectral broadening (Figure 4.12, Compare spectra 1 and 2). Addition of the same excess of Mg^{2+} ion to apo–TCA parvalbumin produced a spectrum which in no way resembled that of the holo + Mg^{2+} or holo + Ca^{2+}. In fact, addition of a 250–fold excess Mg^{2+} to apo–TCA protein caused only a slight (2–4 nm) blue–shift (λ_{max} = 335 nm) relative to the apo–TCA spectrum, no intensity changes (identical quantum yields were measured in the absence and presence of excess Mg^{2+}) and no spectral narrowing (Figure 4.12, Spectrum 3). However addition of excess Mg^{2+} to EGTA–treated parvalbumin produced a significant blue–shift (λ_{max} = 326 nm), increase in fluorescence intensity and spectral narrowing (Figure 4.13, Spectrum 3). This EGTA–treated parvalbumin also responded to an excess of Ca^{2+} in a qualitatively

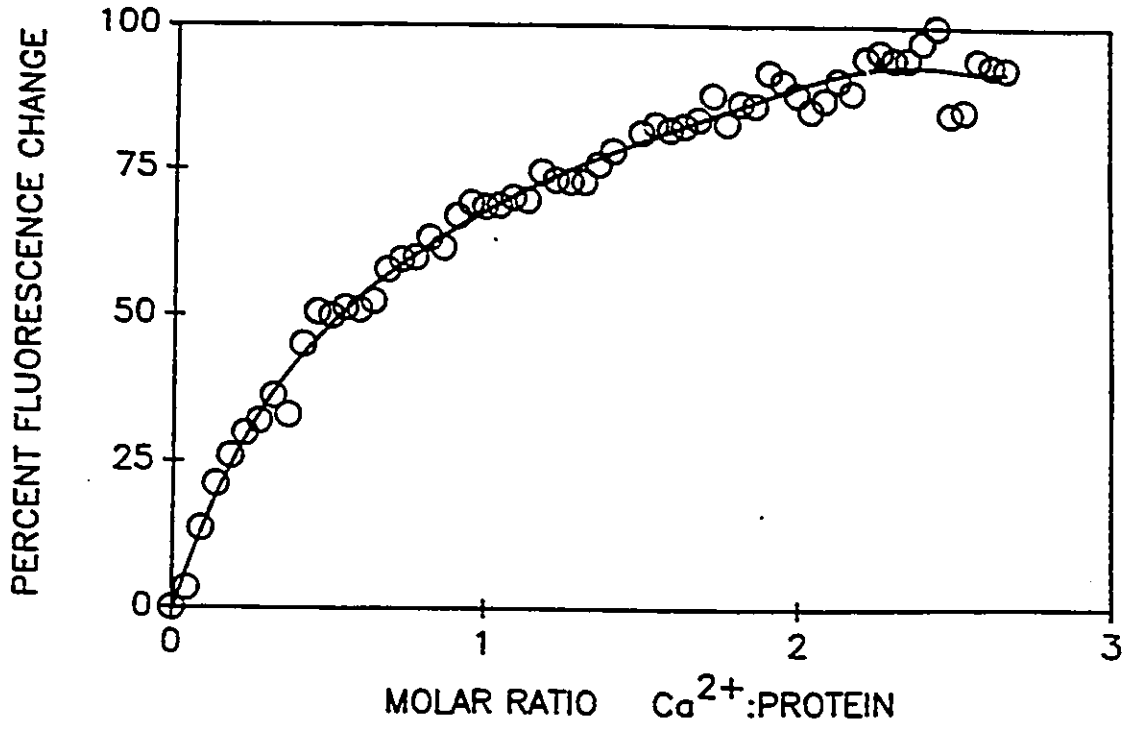

Figure 4.11: Ca^{2+} titration of TCA–treated parvalbumin plotted in terms of the difference between the fluorescence intensity at 325 nm at each metal ion ratio and the initial fluorescence intensity of the apoprotein. The line drawn through the data points was the "best–fit" line obtained upon 5th order polynomial regression analysis.

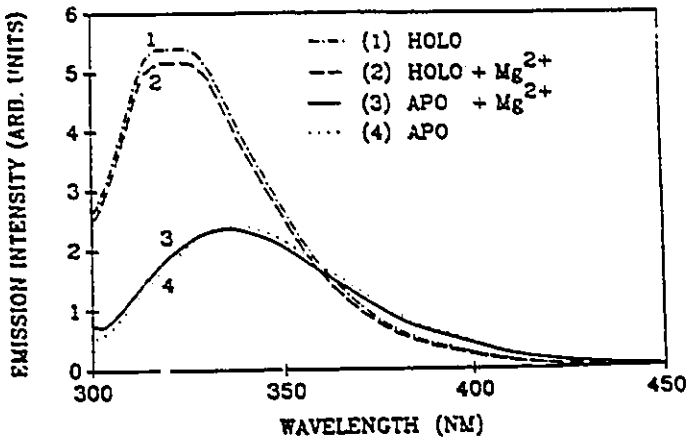

Figure 4.12: Corrected steady–state fluorescence emission spectra of holo– and apo–TCA cod III parvalbumin in the absence and presence of excess Mg^{2+}(aq). The protein concentration was approximately 20 μM to which 1–2 μL of a concentrated $MgCl_2$ stock solution was added to yield a final concentration $[Mg^{2+}] = 5$ mM. $\lambda_{ex} = 295$ nm.

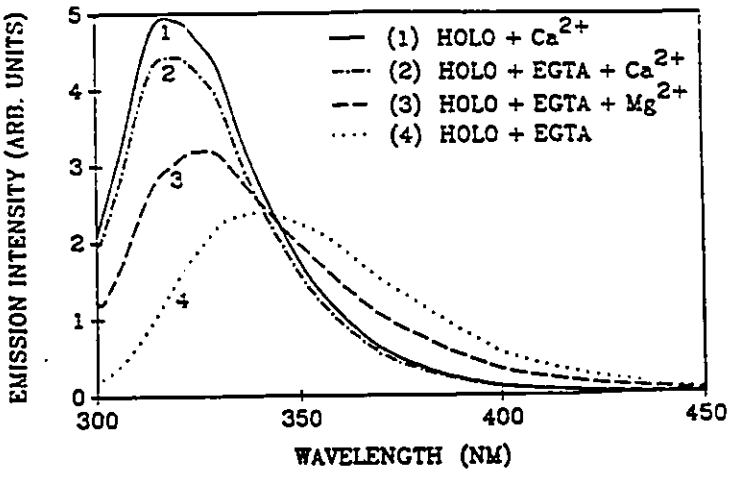

Figure 4.13: Corrected steady–state fluorescence emission spectra of holo cod III parvalbumin, holo + 1 mM EGTA, holo + 1 mM EGTA + 6 mM $CaCl_2$, holo + 1 mM EGTA + 6 mM $MgCl_2$. The holo protein was in a buffer composed of 10 mM cacodylate, 150 mM KCl, 1 mM DTT, pH 7. The protein concentration was approximately 20 μM. $\lambda_{ex} = 295$ nm.

similar manner as the apo–TCA treated sample.

Circular dichroism (CD) was used as an independent method to assess the apparent inability of apo–TCA cod III parvalbumin to respond to Mg^{2+}. It was hoped that the CD spectra would reveal if the metal–induced conformational responses (or lack of) were confined to the region probed by Trp–102, and thus if the conclusions were specific to a fluorescence study. Circular dichroism is a form of absorption spectroscopy which measures the difference in the absorbance of right– and left–handed circularly polarized light by chiral molecules. Empirical studies have shown that far UV CD spectra of proteins are sensitive to mainly the secondary structure of the molecules (Johnson, 1988), and near UV CD spectra are sensitive to the average environment of the aromatic amino acid residues (Bayley, 1980). The CD spectra of the various apo–TCA treated derivatives supported the fluorescence results. Both the near and far UV CD revealed that addition of Ca^{2+} to the apo–TCA treated protein restored the majority of the spectral features associated with the holoprotein, but addition of Mg^{2+} had only a minor effect on the apoprotein spectra (Figures 4.14 A and B) Thus the near UV CD results directly corresponded to the fluorescence results which suggested that the region probed by Trp–102 was affected in a reversible manner, by the binding of Ca^{2+}, but not Mg^{2+}. In addition, the far UV CD results suggested that these conformational affects may not be confined to the region probed by Trp–102 as more global changes in the secondary structure of cod III parvalbumin were induced by Ca^{2+}–, but not Mg^{2+}–binding. However, the possible contribution from aromatic residues in the far UV CD may have also influenced the latter results.

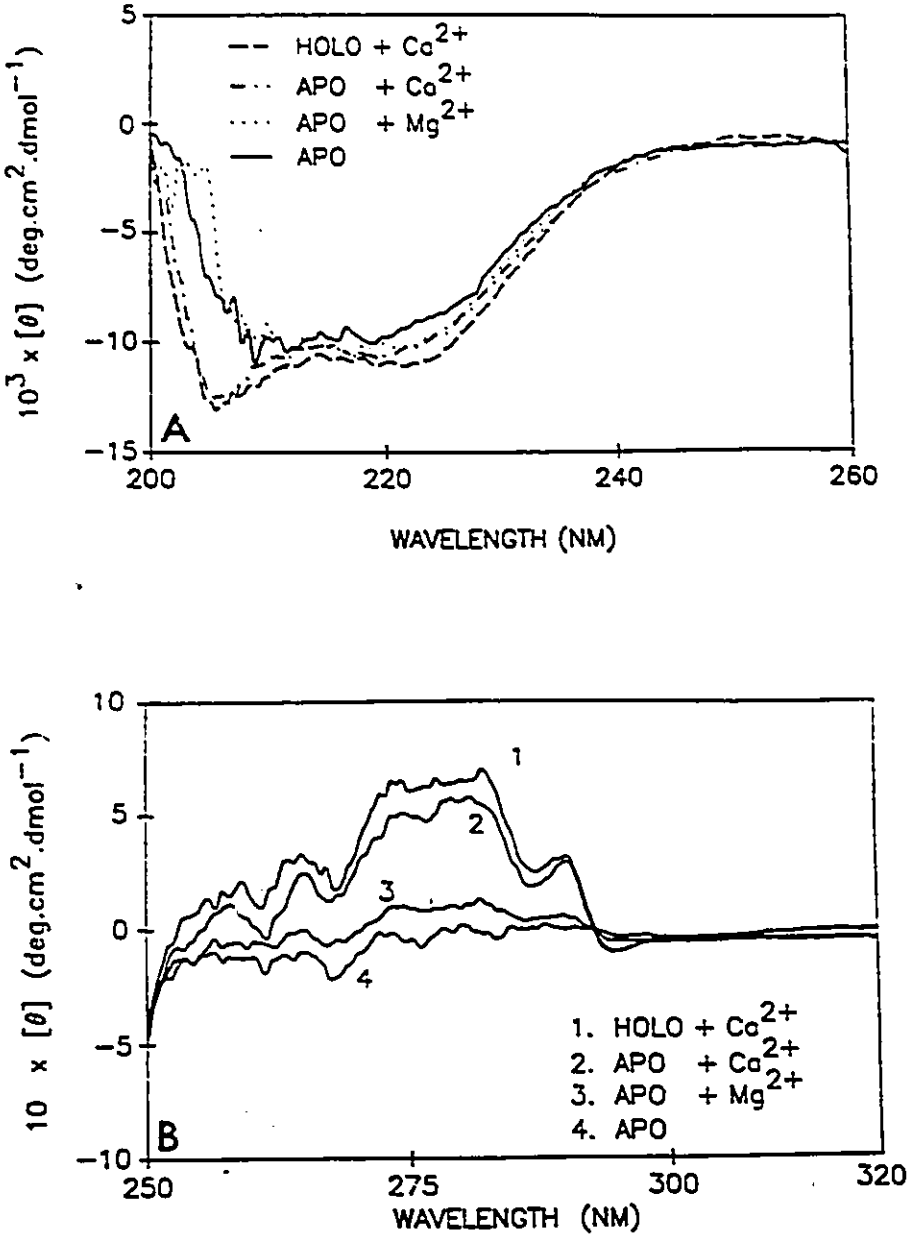

Figure 4.14: Near and far UV circular dichroism spectra of cod III parvalbumin holo–, apo– and metal derivatives. (A) Far UV CD, [protein] ≈ 20 μM. (B) Near UV CD, [protein] ≈ 150 μM. The metal ions were added to a final concentration of 5 mM.

4.3.5 Time–Resolved Fluorescence

Multi–exponential kinetics described the fluorescence decay of both holo and apo cod III parvalbumin. The results of decays from several emission wavelengths were analyzed by global analysis (Knutson et al., 1983) and are given in Table 4.1.

TABLE 4.1

Various steady-state and time-resolved fluorescence decay parameters of holo- and apo-TCA-cod III parvalbumin λ_{ex} = 295 nm, 20°C

Sample[a]	Φ_T	λ_{max}^{ss}[b]	SVR[c]	τ_1(ns)[d]	τ_2(ns)	τ_3(ns)	λ_{max}^{1}[e]	λ_{max}^{2}	λ_{max}^{3}	F_1[f]	F_2	F_3	c_1[g]	c_2	c_3	τ_r(ns)[h]
Holo	0.14 ± 0.01	336	1.92	3.33 ± 0.03	1.34 ± 0.02	-	335	336	-	0.88	0.12	-	0.96	0.04	-	22.9
Apo	0.09 ± 0.01	337	1.85	4.39 ± 0.02	2.17 ± 0.02	0.361 ± 0.004	335	330	330	0.59	0.37	0.04	0.31	0.42	0.28	26.1

[a]Both protein samples were in 10 mM cacodylate, 150 mM KCl, 1 mM dithiothreitol, pH 7.0. In addition, 1 mM $CaCl_2$ was added to the holo sample to ensure complete occupancy of the metal-binding sites.

[b]λ_{max}^{ss} represents the wavelength of maximum intensity in the corrected steady-state fluorescence emission spectrum.

[c]Serial variance ratio (SVR) is a statistical parameter reflecting the goodness of fit. An SVR = 2 corresponds to a perfect statistical fit. The SVR values shown reflect the statistics obtained upon global analysis of 10 data sets.

[d]The errors quoted for the lifetime values represent the standard errors for lifetime recovery from a given global set.

[e]λ_{max}^{i} represents the wavelength (in nm) of the maximum intensity emission of the various components when excited at 295 nm. These values are obtained from the DAS.

[f]F_i and c_i denote the fractional fluorescences and relative concentrations, respectively, of the various decay time components at 330 nm. The c_i's were calculated using equations described in detail elsewhere.

[g]τ_r represents the radiative lifetime and was calculated assuming that it was the same for all of the decay components in a given protein sample. A detailed description of its calculation can be found elsewhere.

This latter analysis was possible owing to the wavelength independence of the lifetimes. The lifetime data were combined with the steady–state fluorescence data to generate decay–associated spectra (DAS, Figure 4.15 A and B) which permitted a resolution of the contribution of each decay component to the total fluorescence

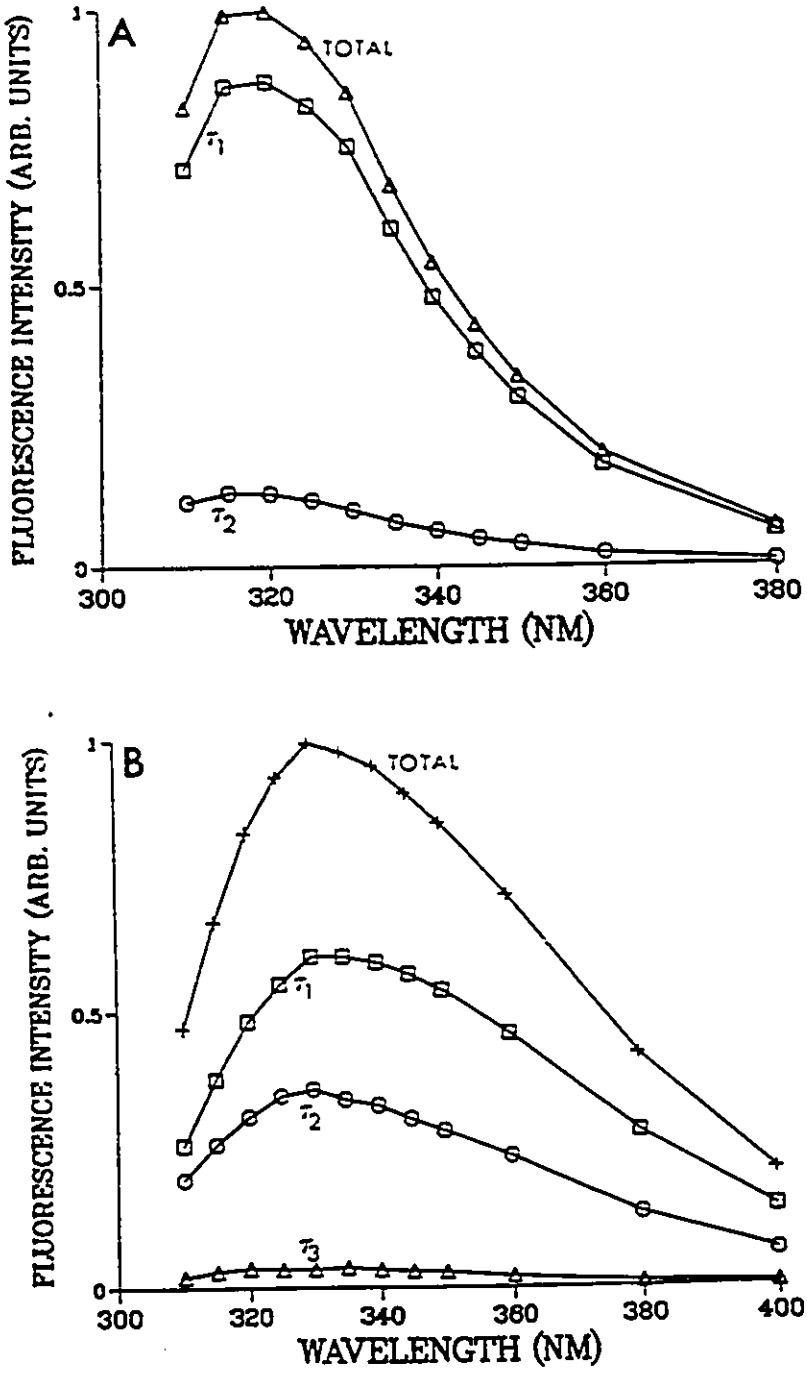

Figure 4.15: Decay–associated spectra for (A) holo cod III parvalbumin and (B) apo–TCA cod III parvalbumin. Spectra sum to the corresponding corrected steady–state spectral intensities normalized to a value of one unit at the emission maximum. Standard errors are within the contours of the plotted symbols.

(Knutson et al., 1982). In the holo sample, two decay components were observed having lifetimes τ_1 = 3.55 ns and τ_2 = 1.54 ns. The DAS showed that the longest decay component dominated the fluorescence (≈ 90%) and calculations revealed that the relative concentration of this component was 76% (See Table 4.1). The relative component concentrations are proportional to the normalized preexponential terms if it is assumed the radiative lifetime of each component is the same and static quenching is absent (details of these calculations are described in Section 3.4.4 of this thesis). For holo parvalbumin, the λ_{max} of the spectrum of the longest decay time component (τ_1 = 3.55 ns) was 320 nm, while the spectrum of the shorter decay time component (τ_2 = 1.54 ns) had a λ_{max} of 316 nm (Figure 4.15 A). Decalcification resulted in an increase in the lifetimes of the two components, τ_1 and τ_2, and a substantial red–shift of the spectra corresponding to both the longest (τ_1 = 4.39 ns; λ_{max} = 335 nm) and middle (τ_2 = 2.17 ns; λ_{max} = 330 nm) decay time components. Also, an additional short 361 ps component (λ_{max} = 330 nm) with a relative concentration of 28%, but only a fractional fluorescence of 4% was required to adequately describe the decay kinetics of the apo parvalbumin. The relative concentrations of the other two decay components experienced a significant alteration upon decalcification (See Table 4.1), with a substantial decrease in the concentration of the 4 ns decay component (31% apo vs 76% holo), and an almost 2–fold increase in the 2 ns component (41% apo vs 24% holo). Addition of Ca^{2+}(aq) to the apo–TCA parvalbumin resulted in decay kinetics indistinguishable from those of the original native holoprotein.

4.4 Discussion

4.4.1 Protein Homogeneity

Protein homogeneity is a fundamental requirement when using the intrinsic fluorescence of proteins to study their conformational and dynamic nature. Satisfaction of this requirement avoids ambiguous interpretation of the spectroscopic data. A frequently used method by which protein homogeneity is judged is that of SDS–PAGE, but it is inadequate as a definitive test because although molecular weight homogeneity may be indicated, SDS–PAGE permits no assessment of purity based upon molecular charge. In the purification of the isotype III component of cod parvalbumin, isoelectric focusing indicated that the protein which appeared homogeneous by SDS–PAGE (Figure 4.4, Lane E (single band)), still required another purification step (Figure 4.5, third gel labeled "Sephacel load" (two bands)). After DEAE–Sephacel chromatography, a rigorous assessment of protein purity was made by SDS–PAGE, isoelectric focusing, the determination of the amino acid composition, and tryptic peptide analysis. Atomic absorption spectroscopy detected 2.1 ± 0.1 mol Ca^{2+}/mole protein in the final purified sample. Collectively these analyses showed that homogeneous cod III parvalbumin had been obtained.

4.4.2 Location of the Single Tryptophan Residue

Previous amino acid composition determination (Closset & Gerday, 1976) and absorption spectroscopy (Bhushana Rao et al., 1969) revealed that the isotype III of cod parvalbumin contained tryptophan. The only reported attempt to sequence this protein placed the single Trp residue in position 109 of an anomalously long 113–residue protein (Elsayed & Bennich, 1975). Subsequently the amino acid

sequence of the only other parvalbumin known to contain Trp, whiting IIIb, was determined which located the Trp in position 102 (Joassin & Gerday, 1977). Based upon inference, the Trp in cod III parvalbumin was assigned to position 102 but had never been established (Horrocks & Collier, 1981; Eftink & Hagaman, 1985). In order to be more definite in the interpretation of the fluorescence data, a Trp–containing, 20 amino acid residue segment of the homogeneous cod III parvalbumin was sequenced and the location of the single Trp was established to be position 102. In Figure 4.16 the approximate location of the single Trp residue relative to the two Ca^{2+}–binding sites is shown based upon the coordinates of the crystal structure of carp parvalbumin (Kumar, Lee and Edwards, Brookhaven Protein Data Bank). The binding sites are known as the CD– and EF–loops for reasons which will be described in detail in section 5.1. The indole ring of the Trp is located approximately 11.6 Å equidistant from the two Ca^{2+} ions and is surrounded by a number of phenylalanine residues within the hydrophobic core.

4.4.3 Apoprotein Preparation — Problems with EGTA

Treatment of calcium–binding proteins with the soluble chelators EGTA and EDTA has frequently been employed to create "apo" (Ca^{2+}–free) proteins, despite several reports of the method's inefficiency. Although some have reported greater than 95% decalcification of parvalbumins with EDTA at pH 7 (Cox et al., 1979), others have reported that the calcium cannot be removed unless the pH is above 8 (the apparent binding constant of Ca^{2+} to EDTA is approximately 100–fold higher at pH > 8 compared to the highest reported affinity constant of Ca^{2+} in any parvalbumin) (Birdsall et al., 1979; White, 1988). At neutral pH, others have found that EGTA/EDTA are effective in complete protein decalcification only in the

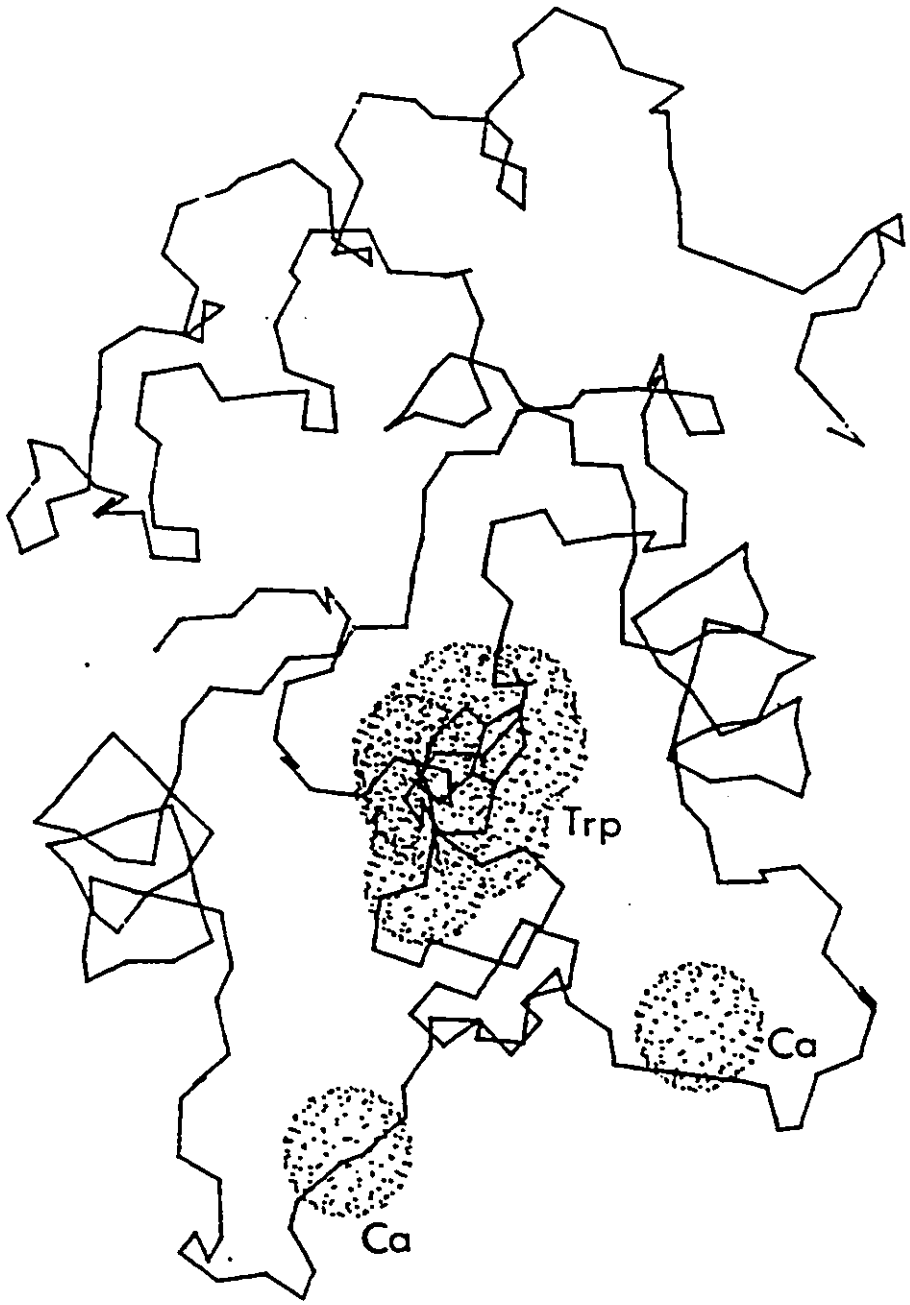

Figure 4.16: X–ray crystallographic structure of the peptide backbone of carp pI 4.25 parvalbumin in which phenylalanine in position 102 has been replaced with a tryptophan. The atomic spheres of the Trp and the two Ca^{2+} are also shown. The CD–binding site is located at the bottom–left and the EF–binding site is located at the bottom–right.

presence of 8 M urea (Sykes, personal communication).

Treatment of cod III parvalbumin with excess EGTA at neutral pH did not remove all of the Ca^{2+} from the protein solution. Atomic absorption spectroscopy revealed 0.4 ± 0.1 mol Ca^{2+}/mol protein remained after gel filtration or dialysis to remove Ca–EGTA complexes. It has been suggested that at neutral pH, EGTA can selectively remove one of the Ca^{2+} ions of parvalbumin (Nelson et al., 1976) and that under these conditions, it is the Ca^{2+} bound to the EF–loop (See Figure 4.16). It was reasoned that this Ca^{2+} existed closer to the surface and had a water molecule as one of its liganding groups (Kretsinger & Nockolds, 1973). The monophasic fluorescence quenching upon EGTA titration of cod III parvalbumin in the present study (Figure 4.9) suggests either a single site is responsible for the major fluorescence change, or that both sites in this parvalbumin have comparable affinities for Ca^{2+} and contribute equally to the fluorescence change. These alternatives cannot be distinguished from each other at the present time.

The fact that atomic absorption of this EGTA–treated protein detected 0.4 ± 0.1 mol Ca^{2+}/mol of protein, even after gel filtration and/or dialysis, deserves comment. The error of the atomic absorption results was shown to be less than 5% when measuring calcium standards or the native holo cod III protein. Thus the measurement of Ca^{2+} in the EGTA treated samples was considered reliable. The best rationalization of the results was that the Ca^{2+} had been removed from both metal binding sites but Ca–EGTA complexes remained associated with the protein despite gel filtration and dialysis. Thus the 0.40 mol Ca^{2+}/mol protein is a measure of the amount of Ca–EGTA complexes associated with the protein structure. Other workers have shown that apoparvalbumins interact strongly with these chelators (Lehky et al., 1977; Parello et al., 1979; Cave et al., 1979b). This

problem of a tight association between EGTA/EDTA and protein is not limited to the Ca^{2+}–binding proteins as Csopak et al. (1972) found that zinc–containing alkaline phosphatase also formed tight complexes with EDTA. In addition, the association does not seem to be dependent upon the presence of Ca^{2+} because further alteration of the spectral properties was observed upon EGTA addition to a sample of completely decalcified TCA–treated cod III parvalbumin. This demonstrates that even EGTA alone may interact with the protein (Figure 4.8).

The evidence presented above for the formation of a Ca^{2+}–EGTA–protein ternary complex has important implications for the interpretation of the Ca^{2+}–binding data presented by others. For example, it suggests that conclusions regarding cooperativity, or the lack thereof, of Ca^{2+} binding would be strongly influenced by the existence of this ternary complex. In addition, the interaction of EGTA with the protein makes it exceedingly difficult to obtain an accurate measurement of binding constants. The use of an EGTA–Ca^{2+} buffer system is one of few methods available to achieve solution concentrations of Ca^{2+} below 10^{-8} M. Such low concentrations of Ca^{2+} are necessary to accurately measure high affinity binding constants. However, the interaction of EGTA with the protein alters the binding properties in such a way to make any measurements invalid. Indeed, in the type of data presented in this report, it is difficult to relate the metal ion status of the protein to its spectral properties if EGTA is present, and no direct measurements of Ca^{2+} content are performed.

For example, Castelli et al. (1988) interpreted their fluorescence lifetime and quenching studies of the single Trp residue in whiting parvalbumin in terms of a two component mixture of apoparvalbumin and Ca_2–parvalbumin at substoichiometric levels of Ca^{2+}. Their studies were done at pH 9 and EGTA was used to achieve

decalcification. They postulated a mechanism of positive cooperativity where $K_2 >> K_1$ (K_1 and K_2 are the stoichiometric equilibrium constants for the first and second moles of Ca^{2+} bound to parvalbumin). Although similar results were reported using NMR (Cave et al., 1979a), Castelli et al. (1988) stated that their interpretation was not unequivocal. For example, a mechanism of independent binding was also possible provided that $K_1 \approx K_2$ and that the Trp fluorescence changes were due only to the filling of one specific site. However they dismissed this latter possibility of independent binding stating that it was highly unlikely a Ca_1–parvalbumin would have the same lifetime values at different wavelengths as those observed for an equimolar mixture of apoparvalbumin and Ca_2–parvalbumin.

At pH 7, the results in the present study with cod parvalbumin showed that at a ratio of 2 moles of EGTA:1 mole of protein, only a fraction of the total quenching response was apparent (Figure 4.9). Fluorescence quenching was observed even after addition of the first aliquot of EGTA. Thus it is unlikely that the requirement of an excess of EGTA to obtain plateau fluorescence values was due to a portion of the EGTA being lost by the formation of complexes with free Ca^{2+} ions in solution. Eftink and Wasylewski (1989) found at least 4 moles of EDTA/mole cod parvalbumin were required to achieve any change in a number of fluorescence parameters, including the fluorescence intensity, the integrated area under the emission spectrum, or the λ_{max}. Plateau quenching values were not achieved until 8–10 moles EDTA/mole protein were present at pH 8. However, the probable contamination of the cod III parvalbumin by the isotype II in the study by Eftink and Wasylewski (1989) could account for the lag of a fluorescence response upon EDTA addition. Nonetheless the requirement for a 10–fold excess to achieve plateau fluorescence values is consistent with the data presented in this report. As

the study of Castelli et al. (1988) was done with stoichiometric amounts of EGTA, there remains uncertainty as to whether the protein was completely decalcified and further, whether ternary complexes of EGTA–Ca(II)–protein were present and affecting the spectral signals. This could explain the contradiction of results between Castelli et al. (1988) and Permyakov et al. (1980). The latter group proposed a mechanism of positive cooperativity between the two binding sites of whiting parvalbumin (Permyakov et al., 1980). However, in contrast to the conclusions of Castelli et al. (1988), they proposed a sequential mechanism of Ca^{2+} binding wherein a distinct Ca_1–parvalbumin was formed upon titration, and $K_1 >> K_2$.

However, the use of EGTA may not be the only reason for the reported differences. There is spectral evidence to suggest that there are differences between the proteins used by various groups. The λ_{max} of the whiting parvalbumins studied by Castelli et al. (1988) and Permyakov et al. (1985) were significantly different (See Table 4.2). It has been shown by Permyakov et al. (1980) that the Trp emission properties in whiting parvalbumin were independent of pH in the range of 7–9. Hence it is unlikely that differences in solution pH can explain the differences in the emission spectra measured by the two groups. Another possibility might be the effect of ionic strength on emission. The spectra of Castelli et al. (1988) were measured in the presence of 1 M KCl or KI. Iodide ion is a known quencher of Trp fluorescence, particularly at high concentrations. However, at least in the presence of high concentrations of iodide, it is expected that the spectrum would be shifted to shorter wavelengths and thus it is unlikely KI could account for the broad, red–shifted spectrum which was measured. The spectra of cod parvalbumin reported in the present study were measured in the presence of 150 mM KCl, the

TABLE 4.2

Comparison of fluorescence lifetime data of tryptophan-102 in cod III parvalbumin and whiting IIIb parvalbumin.

Protein	Temperature (°C)	λ_{max}^{25} (nm)	τ_1(ns)	τ_2(ns)	τ_3(ns)	F_1	F_2	F_3	Reference
cod III PV[a]	20								
Holo		316	3.55	1.54	-	0.88	0.12	-	
Apo[b]		327	4.39	2.17	0.361	0.59	0.37	0.04	Hutnik this report
cod III PV[c]	25								
Holo		315	4.20	1.71	-	0.604	0.396	-	Eftink & Hagaman, 1985
cod III PV[d]	25								
Holo		316	4.61	2.22	-	0.83	0.17	-	
Apo[e]		336	4.21	1.43	-	0.72	0.28	-	Eftink & Wasylewski, 1989
whiting IIIb PV[f]	20								
Holo		320	3.5	2.0	-	0.80	0.20	-	
Apo[g]		346	4.0	1.0	-	0.55	0.45	-	Permyakov et al., 1981
whiting IIIb PV[h]	20								
Holo		330[j]	4.380	-	-	-	-	-	
Apo[i]		348[j]	4.26	1.28	-	0.86	0.14	-	Castelli et al., 1988

[a] In 10 mM cacodylate buffer containing 150 mM KCl, 1 mM dithiothreitol, pH 7 (holo protein with 1 μM $CaCl_2$).
[b] Prepared by TCA-precipitation (See Methods section).
[c] In phosphate buffer, pH 7.
[d] In 50 mM Tris-HCl, pH 8.0 (holo protein with 10 mM $CaCl_2$).
[e] Prepared by addition of 10 mM EDTA to approximately 3×10^{-5} M protein.
[f] In 50 mM Tris-HCl, pH 8.0.
[g] Prepared by addition of excess EDTA.
[h] In 20 mM borate buffer containing 1 M KCl, 0.1 mM dithiothreitol, pH 9.0.
[i] Prepared by addition of EDTA to a final concentration equal to 3-4.5 times the protein concentration.
[j] λ_{max} measured in the presence of 1 M KI, 20 mM borate, 0.1 mM dithiothreitol, pH 9.0.

latter representing physiological ionic strength. The λ_{max} was 316 nm. Because the single Trp residue in cod and whiting parvalbumins is located in the same position, and the amino acid composition of the two proteins differs by only 3 amino acids (Horrocks & Collier, 1981), it is likely the Trp in the two proteins would share very similar fluorescence properties. Therefore, large discrepancies would more likely be due to how the protein was treated during purification and whether, in fact, the protein was homogeneous. Thus differences in protein preparation, coupled

with the use of EGTA makes the interpretation of other workers' data extremely difficult and contributes to the confusion regarding the metal ion binding properties of these proteins.

The results in the present report obtained with EGTA and Mg^{2+} provide a clear example of the large influence the use of the chelator can have upon experimental results and conclusions. The absorption, CD and fluorescence emission spectra revealed that decalcification resulted in drastic changes in the Trp region of the protein and further, that greater than 93% of these changes could be reversed upon Ca^{2+}, but not Mg^{2+}, addition to a solution of the apoparvalbumin. It is suggested that changes in the fluorescence spectrum of the EGTA–treated protein upon the addition of Mg^{2+} that were observed in this thesis, as well as reported by Permyakov et al. (1987), were most likely due to the specific binding of Ca^{2+}, as opposed to Mg^{2+} to the metal–binding sites. The addition of excess Mg^{2+} to a solution containing 20 μM protein and 1 mM EGTA may cause a displacement of Ca^{2+} from Ca^{2+}–EGTA complexes. The free Ca^{2+} ions would then be available to bind to the metal binding sites of the protein and promote the spectral changes observed. This explanation is preferred over the possibility that trace amounts of Ca^{2+} ions still present in the protein could permit a Mg^{2+} response in the presence of an excess of the latter. When excess Mg^{2+} was added to apo–TCA samples containing 0, 0.5, 1 and 2 mol Ca^{2+}/mol protein, no response to Mg^{2+} was observed. Clearly in the absence of chelator, only Ca^{2+} induced distinct and reversible changes in the conformation of this parvalbumin. It is suggested that the generally held belief that indistinguishable conformational changes occur upon either Ca^{2+} or Mg^{2+} binding to this protein may be the result of an experimental artefact arising from the existence of an EGTA–Ca^{2+}–protein complex.

4.4.4 The Ca^{2+}–Specific Conformational Changes of Cod III Parvalbumin

Ca^{2+} titration of apo–TCA cod III parvalbumin (Figure 4.11) showed that fluorescence intensity changes occurred over the range of 0–2 moles Ca^{2+}/mole protein, with a plateau occurring upon occupation of both sites. However, upon titration it was found that at a molar ratio of 1:1, virtually the full wavelength shift (from 337 nm to 316 nm) was complete, even though the intensity changes were not. In fact, EGTA treatment was also capable of producing the full wavelength shift, but only partial quenching. Thus depending upon which fluorescence parameter is selected, different conclusions can be derived. In the absence of a direct measurement of Ca^{2+} content, the spectroscopic data can lead to ambiguous interpretations.

It is interesting that substoichiometric levels of Ca^{2+} could produce spectral changes typically interpreted as being indicative of a conformational change leading to a transfer of the single Trp residue from a rigid hydrophobic interior to the protein surface (Permyakov et al., 1985). Based upon the work of others (Nelson et al., 1976; Coffee et al., 1974; Iio and Hoshihara, 1984), removal of Ca^{2+} from the EF–loop is thought to induce the bulk of the conformational changes associated with parvalbumin. In addition, it has been suggested that the EF–binding site is much more flexible than the CD–site, with the former being able to expand or contract relative to the Ca^{2+}–coordinating positions (Williams et al., 1984). The results reported here with cod parvalbumin support this fact insofar that full Ca^{2+} reconstitution is not required to recover the majority of the spectral changes. Although no attempt was made in the present study to estimate the binding constants in cod parvalbumin, the results suggest that the affinities of Ca^{2+} for the

two sites are different. A slight break in the Ca^{2+} titration curve was observed at a molar ratio of 1:1 (Figure 4.11). The full wavelength shift was complete when only one equivalent of Ca^{2+} was present which would imply that binding to one site was responsible for this effect, while binding of the second equivalent of Ca^{2+} was required to achieve the final conformation, and hence the final fluorescence intensity. The two binding constants estimated in whiting parvalbumin have been found to be different by two orders of magnitude (Permyakov et al., 1980) and thus it is possible similar differences may exist in cod parvalbumin owing to the virtual identity of the amino acid compositions.

Time–resolved fluorescence of the holo and apo–TCA forms of cod III parvalbumin permitted a detailed assessment of the conformational differences. The data of both holo and apo–TCA parvalbumin revealed that the tryptophan residue, and hence the protein, existed in more than one conformationally distinct state. In Table 4.2, the time–resolved fluorescence results of the single Trp residue in cod parvalbumin are compared to the results of other groups who have measured the fluorescence of both cod and whiting parvalbumins. Although the data base is small, most results (including those presented in this chapter) suggest that the fluorescence of Trp–102 in the holo (Ca^{2+}–bound) parvalbumin decays in a double exponential manner. The only contradictory report is that of Castelli et al. (1988) who found the decay of whiting parvalbumin to be monoexponential. Although it is not possible to rule out that pH and ionic strength may account for the discrepancy (as has already been suggested by Eftink & Wasylewski (1989)), it is also possible that differences in instrumention may be responsible for different resolution capabilities. Although the lifetimes which were measured for holo cod III parvalbumin in the present study are among the shortest (τ_1 = 3.55 ns; τ_2 = 1.54

ns), there is relatively good agreement among the various reported values for both the lifetimes (τ_i's) and fractional fluorescences (F_i's). Perhaps the differences are reflecting the nature of the instrumentation used (TCSPC vs multifrequency phase/modulation fluorometry), as well as different buffer solutions and degrees of protein homogeneity.

The results reported herein distinctly show that, upon decalcification, three instead of two components were required to adequately describe the measured fluorescence decay. This is consistent with the idea that Ca^{2+}–free loops have a greater degree of conformational freedom compared to the Ca^{2+}–bound state (Herzberg et al., 1987). The decay–associated spectra (DAS) of the various components show that in the absence of Ca^{2+}, the spectra of both the longest and middle decay components were substantially red–shifted relative to the same two components of holo parvalbumin. Similar results were reported by both Permyakov et al. (1985) and Eftink & Wasylewski (1989). However, unlike Eftink & Wasylewski (1989) the results presented in this chapter, similar to those of Permyakov et al. (1985), show a substantial change in the fractional contribution of the first and second components upon decalcification. The second component becomes relatively more dominant in the absence of Ca^{2+} (F_2 = 37% in apo versus F_2 = 12% in holo). In addition, the cod parvalbumin results in this chapter reveal a 4% contribution to the total fluorescence by a third component with a lifetime of only 361 ps. The DAS revealed that both the apo and holo proteins possess conformational heterogeneity. In the case of the holo protein, the two components possessed spectra typical of Trp located in a relatively hydrophobic, less solvent exposed environment, with the short decay component having the most blue spectrum. This is supported by the sharp subsidiary peak at 289 nm in the

absorption spectrum (Figure 4.7). A similar feature was observed in the absorption spectrum of azurin (Figure 3.3) for which the X–ray crystallographic structure and similarity of the fluorescence emission spectrum to that of 3–methylindole in methylcyclohexane solution confirmed the inaccessibility of its single Trp to solvent molecules (See Section 3.1). The DAS of the apoparvalbumin revealed two conformational states in which the Trp was relatively more solvent exposed (supported by the loss of the 289 nm peak in the absorption spectrum). Thus the presence or absence of Ca^{2+} does not by itself impart conformational heterogeneity in the protein, but definitely determines the conformational distribution of the various states as judged by the degree of exposure of the Trp to the external solvent. In the absence of Ca^{2+}, additional conformational freedom is evident as judged by the appearance of an additional component which disappears upon Ca^{2+} reconstitution. This latter observation suggests that the third component does not reflect an irreversibly denatured form of the protein resulting from experimental conditions.

Some differences do exist between the various reports. In both the apo and holo forms of cod parvalbumin, the DAS revealed that the second component (τ_2) had a blue–shifted spectrum relative to τ_1 (See Figure 4.15 and Table 4.1). Similar results were reported with the phase–resolved spectra of cod parvalbumin (Eftink & Wasylewski, 1989). This would suggest that the Trp corresponding to τ_2 was in a relatively more solvent shielded environment (blue–shifted spectrum) compared to τ_1. However the opposite situation was reported for whiting parvalbumin (Permyakov et al., 1985). Using external quenchers such as Cs^+ and I^-, both Permyakov et al. (1985) and Castelli et al. (1988) found that the component with the shorter lifetime was more readily quenched than the component with the longer

lifetime. In addition they report that the short lifetime component had a red–shifted spectrum. This suggests that the DAS are capable of detecting differences between the cod and whiting parvalbumins which is surprising in view of the near identity in amino composition and the identical position of the tryptophan residue. Alternately, the differences in the results may be due to the quality of the data and resolution capabilities of the instrumentation. It is interesting that unlike Castelli et al. (1988) and Permyakov et al. (1985), the cod III parvalbumin time–resolved data reported herein showed no dependency of lifetime upon emission wavelength. This condition has been shown to be necessary to render global analysis valid (Knutson et al., 1982).

Eftink and Wasylewski (1989) have analyzed their data on cod III parvalbumin in terms of a continuous distribution of lifetimes and also as sums of discrete exponentials. It is beyond the scope of this thesis to comment on the validity of analyzing fluorescence decay data in terms of the former model. However, either analysis model shows that cod III parvalbumin is a conformationally heterogeneous protein, capable of existing in at least two or more conformational states. These would correspond to a discrete component analysis. This does not preclude the presence of a large number of conformational substates (distribution analysis). The identification of discrete conformational states of cod III parvalbumin implies their influence on its function, which at the present time remains undetermined.

The removal of Ca^{2+} resulted in a quenching of the Trp fluorescence quantum yield from 0.14 to 0.09. However, decalcification resulted in an increase in the lifetime values of both the first and second decay components, as well as the detection of a third short component. Permyakov et al. (1985) also found a

quantum yield decrease despite an increase in the mean lifetime of the single Trp in whiting parvalbumin. This contrasts the results of Castelli et al. (1988) who reported a 45% decrease in quantum yield, and a 35% decrease in the weighted fluorescence lifetime. Reasons for discrepancies in the lifetime data have been discussed above. However, in all cases it is clear that changes in the quantum yield upon decalcification cannot be accounted for in the lifetime data. Given that $\phi_f = \tau_s/\tau_r$, the results can be rationalized in two different ways. One possibility is that the Trp in parvalbumin may be experiencing a greater degree of static quenching in the absence of Ca^{2+} which would decrease the ϕ_f. Such a situation has been reported for the single tyrosine residue in octopus calmodulin (Kilhoffer et al., 1980). However it is not possible to offer an explanation for the source of such a mechanism. A second possibility is that the radiative lifetime, τ_r is changing upon decalcification. This proposal has also been suggested by Castelli et al. (1988). It is possible to calculate the τ_r from the measured fluorescence parameters (see Section 3.4.4 for details) using equations 3.2 and 3.3. Upon calculation the following results were obtained: τ_r (holo) = 22 ns and τ_r (apo) = 26 ns. The longer radiative lifetime in the apo parvalbumin is consistent with studies on model indole compounds. It was found that the radiative rate constant decreased (and hence τ_r increased) upon transfer of indole from a nonpolar to a more polar environment (Privat et al., 1979). Such a situation is suggested for the Trp in parvalbumin upon decalcification. The single Trp in cod parvalbumin is situated at the start of the F–helix, lying just outside of the EF–loop. Based on the crystal structure of troponin C, it has been suggested that decalcification of EF–hand structures in calcium–binding proteins results in an increase in interhelical angles within a given binding domain (Herzberg & James, 1985). Thus it is possible that in cod III

parvalbumin the electronic environment of the indole nucleus of Trp–102 may be significantly perturbed by the interaction with the dipole of either the F– or E–helix, the orientation of which is expected to change upon decalcification.

4.5 Chapter Summary and Conclusions

The single tryptophan containing isotype III parvalbumin from codfish (*Gadus callarius*) was purified by a modified procedure and was shown to be homogeneous by a number of biochemical analyses. Sequence analysis established the location of the single tryptophan in position 102 of the 108–amino acid primary sequence. Atomic absorption spectroscopy showed that trichloroacetic acid precipitation was more effective in parvalbumin decalcification compared to the more commonly used method of EGTA treatment. Magnesium induced changes in the EGTA–treated, but not the TCA–treated parvalbumin, as judged by the steady–state fluorescence spectrum. Steady–state fluorescence and circular dichroism spectra showed that calcium, but not magnesium, induced a conformational response in the TCA–treated protein. The fluorescence decay of the calcium–loaded native (holo) cod III parvalbumin was best described by two decay time components. By contrast, three decay time components were necessary to describe the fluorescence decay of the metal–free (apo) protein. The decay–associated spectra of each temporal component were obtained and revealed differences in the polarity of the tryptophan–102 environment in the different conformational states, as well as in the absence and presence of Ca^{2+}. Collectively, these results demonstrate that it is possible for a parvalbumin to display a calcium–specific response.

The results of this chapter present some doubt regarding the generally accepted notion that identical perturbations result upon Ca^{2+} and Mg^{2+} binding to

parvalbumins. The observation of dramatic Ca^{2+}–specific conformational changes in a non–modulatory parvalbumin leads to the question of whether in fact large Ca^{2+}–specific conformational changes are at the root of the observed modulatory properties of other proteins such as calmodulin and oncomodulin (Henzl & Birnbaum, 1988; MacManus et al., 1984). The combination of spectroscopy with protein engineering may offer some answers to the questions concerning metal specificity, conformational change and function of these and other calcium–binding proteins (MacManus et al., 1989). This question is directly addressed in Chapter 5 where a site–specific mutant of the modulatory protein oncomodulin is compared with cod III parvalbumin in terms of its Ca^{2+}–induced conformational properties.

4.6 References

Bayley, P. (1980) Circular dichroism and optical rotation. In: An Introduction to Spectroscopy for Biochemists, Ed.: S. B. Brown (Academic Press, New York) Chapter 5, pp. 148–234.

Bhushana Rao, K. S. P., Focant, B., Gerday, C. & Hamoir, G. (1969) Low molecular weight albumins of cod white muscle (*Gadus callarias* L.). Comp. Biochem. Physiol. 30, 33–48.

Birdsall, W. J., Levine, B. A., Williams, R. J. P., Demaille, J. G., Haiech, J. & Pechère, J.–F. (1979) Calcium and magnesium binding by parvalbumin. A proton magnetic resonance spectral study. Biochimie 61, 741–750.

Blum, H. E., Lehky, P., Kahler, L., Stein, E. A. & Fischer, E. H. (1977) Comparative properties of vertebrate parvalbumins. J. Biol. Chem. 252, 2834–2838.

Bradford, M. M. (1976) A rapid and sensitive method for the quantitation of microgram quantities of protein utilizing the principle of protein–dye binding. Anal. Biochem. 72, 248–254.

Castelli, F., White, H. D. & Forster, L. S. (1988) Lifetime and quenching of tryptophan fluorescence in whiting parvalbumin. Biochem. 27, 3366–3372.

Cave, A., Pages, M., Morin, P. & Dobson, C. M. (1979a) Conformational studies on muscular parvalbumins cooperative binding of calcium (II) to parvalbumins. Biochimie 61, 607–613.

Cave, A., Parello, J., Drakenberg, T., Thulin, E. & Lindman, B. (1979b) Mg^{2+} binding to parvalbumins studied by ^{25}Mg and ^{113}Cd NMR spectroscopy. FEBS Lett. 100, 148–152.

Closset, J. I. (1976) Parvalbumins of white muscles of Gadidae — I. Extraction and purification of the parvalbumins of the whiting (*Gadus merlangus* L.), of the coalfish (*G. virens* L.) and of the haddock (*G. aeglefinus* L.). Comp. Biochem. Physiol. 55B, 531–535.

Closset, J. I. & Gerday, C. (1976) Parvalbumins of white muscles of Gadidae — II. Properties and existence of two evolutionary lineages. Comp. Biochem. Physiol. 55B, 537–542.

Coffee, C. J., Bradshaw, R. A. & Kretsinger, R. H. (1974) The coordination of calcium ions by carp muscle calcium binding proteins A, B and C. Adv. Exp. Med. Biol. 48, 211–233.

Cox, J. A., Winge, D. R. & Stein, E. A. (1979) Calcium, magnesium and the conformation of parvalbumin during muscular activity. Biochimie 61, 601–605.

Csopak, H., Falk, K.–E. & Szajn, H. (1972) Effect of EDTA on *Escherichia coli* alkaline phosphatase. Biochim. Biophys. Acta 258, 466–472.

Daures, M.–F. (1977) Thesis, USTL, Montpellier.

Eftink, M. R. & Hagaman, K. A. (1985) Fluorescence quenching of the buried tryptophan residue of cod parvalbumin. Biophys. Chem. 22, 173–180.

Eftink, M. R. & Wasylewski, Z. (1989) Fluorescence lifetime and solute quenching studies with the single tryptophan containing protein parvalbumin from codfish. Biochem. 28, 382–391.

Elsayed, S. & Bennich, H. (1975) The primary structure of allergen M from cod. Scand. J. Immunol. 4, 203–208.

Gerday, Ch. (1982) Soluble calcium–binding proteins from fish and invertebrate muscle. Mol. Physiol. 2, 63–87.

Goodman, M. & Pechère, J.–F. (1977) The evolution of muscular parvalbumins investigated by the maximum parsimony method. J. Mol. Evol. 9, 131–158.

Haiech, J., Klee, C. B. & Demaille, J. G. (1981) Effects of cations on affinity of calmodulin for calcium: Ordered binding of calcium ions allows the specific activation of calmodulin–stimulated enzymes. Biochem. 20, 3890–3897.

Henzl, M. T. & Birnbaum, E. R. (1988) Oncomodulin and parvalbumin. A comparison of their interactions with europium ion. J. Biol. Chem. 263, 10674–10680.

Herzberg, O. & James, M. N. G. (1985) Structure of the calcium regulatory muscle protein troponin–C at 2.8 A resolution. Nature 313, 653–659.

Herzberg, O., Moult, J. & James, M. N. G. (1987) Conformational flexibility of troponin C. In: Calcium–binding Proteins in Health and Disease, (Academic Press, New York) pp. 312–321.

Horrocks, W. D. Jr. & Collier, W. E. (1981) Lanthanide ion luminescence probes. Measurement of distance between intrinsic protein fluorophores and bound metal ions: Quantitation of energy transfer between tryptophan and terbium(III) or europium(III) in the calcium–binding protein parvalbumin. J. Am. Chem. Soc. 103, 2856–2862.

Iio, T. & Hoshihara, Y. (1984) Static and kinetic studies on carp muscle parvalbumins. J. Biochem. 96, 321–328.

Joassin, L. & Gerday, C. (1977) The amino acid sequence of the major parvalbumin of the whiting (*Gadus merlangus*). Comp. Biochem. Physiol. 57B, 159–161.

Johnson, W. C. Jr. (1988) Secondary structure of proteins through circular dichroism spectroscopy. Ann. Rev. Biophys. Biophys. Chem. 17, 145–166.

Kilhoffer, M. C., Gerard, D. & Demaille, J. G. (1980) Terbium binding to octopus calmodulin provides the complete sequence of ion binding. FEBS Lett. 120, 99–103.

Knutson, J. R., Beechem, J. M. & Brand, L. (1983) Simultaneous analysis of multiple fluorescence decay curves: A global approach. Chem. Phys. Lett. 102, 501–507.

Knutson, J. R., Walbridge, D. G. & Brand, L. (1982) Decay–associated fluorescence spectra and the heterogenous emission of alcohol dehydrogenase. Biochem. 21, 4671–4679.

Kretsinger, R. H. (1980) Structure and evolution of calcium–modulated proteins. CRC Crit. Rev. Biochem. 8, 119–174.

Kretsinger, R. H. & Nockolds, C. E. (1973) Carp muscle calcium–binding protein. II. Structure determination and general description. J. Biol. Chem. 248, 3313–3326.

Lehky, P., Comte, M., Fischer, E. H. & Stein, E. A. (1977) A new solid–phase chelator with high affinity and selectivity for calcium: Parvalbumin–polyacrylamide. Anal. Biochem. 82, 158–169.

MacManus, J. P., Hutnik, C. M. L., Sykes, B. D., Szabo, A. G., Williams, T. & Banville, D. (1989) Characterization and site–specific mutagenesis of the calcium–binding protein oncomodulin produced by recombinant bacteria. J. Biol. Chem. 264, 3470–3477.

MacManus, J. P., Szabo, A. G. & Williams, R. E. (1984) Conformational changes induced by binding of bivalent cations to oncomodulin, a parvalbumin–like tumour protein. Biochem. J. 220, 261–268.

MacManus, J. P., Watson, D. C. & Yaguchi, M. (1985) Rat skin calcium–binding protein is parvalbumin. Biochem. J. 229, 39–45.

Maeda, N., Zhu, D. & Fitch, W. M. (1984) Amino acid sequences of lower vertebrate parvalbumins and their evolution: Parvalbumins of boa, turtle, and salamander. Mol. Biol. Evol. 1, 473–488.

Moeschler, H. J., Schaer, J.–J. & Cox, J. A. (1980) A thermodynamic analysis of the binding of calcium and magnesium ions to parvalbumin. Eur. J. Biochem. 111, 73–78.

Nelson, D. J., Opella, S. J. & Jardetzky, O. (1976) ^{13}C Nuclear magnetic resonance study of molecular motions and conformational transitions in muscle calcium binding parvalbumins. Biochem. 15, 5552–5560.

Parello, J., Reimarsson, P., Thulin, E. & Lindman, B. (1979) Na^+ Binding to parvalbumins studied by ^{23}Na NMR. FEBS Lett. 100, 153–156.

Pechère, J.–F. (1974) Isolement d'une parvalbumine du muscle de lapin. C. R. Acad. Sci. Paris 278, 2577–2579.

Pechère, J.–F., Derancourt, J. & Haiech, J. (1977) The participation of parvalbumins in the activation–relaxation cycle of vertebrate fast skeletal–muscle. FEBS Lett. 75, 111–114.

Permyakov, E. A. & Burstein, E. A. (1984) Some aspects of studies of thermal transitions in proteins by means of their intrinsic fluorescence. Biophys. Chem. 19, 265–271.

Permyakov, E. A., Ostrovsky, A. V., Burstein, E. A., Pleshanov, P. G. & Gerday, C. (1985) Parvalbumin conformers revealed by steady–state and time–resolved fluorescence spectroscopy. Arch. Biochem. Biophys. 240, 781–791.

Permyakov, E. A., Ostrovsky, A. V. & Kalinichenko, L. P. (1987) Stopped–flow kinetic studies of Ca(II) and Mg(II) dissociation in cod parvalbumin and bovine α–lactalbumin. Biophys. Chem. 28, 225–233.

Permyakov, E. A., Yarmolenko, V. V., Burstein, E. A. & Gerday, C. (1982) Intrinsic fluorescence spectra of a tryptophan–containing parvalbumin as a function of thermal, pH and urea denaturation. Biophys. Chem. 15, 19–26.

Permyakov, E. A., Yarmolenko, V. V., Emelyanenko, V. I., Burstein, E. A., Closset, J. & Gerday, C. (1980) Fluorescence studies of the calcium binding to whiting (*Gadus merlangus*) parvalbumin. Eur. J. Biochem. 109, 307–315.

Privat, J. P., Wahl, P. & Auchet, J. C. (1979) Rates of deactivation processes of indole derivatives in water–organic solvent mixtures — Application to tryptophyl fluorescence of proteins. Biophys. Chem. 9, 223–233.

Righetti, P. & Drysdale, J. W. (1971) Isoelectric focusing in polyacrylamide gels. Biochim. Biophys. Acta 236, 17–28.

Waisman, D. M. & Rasmussen, H. (1983) A reexamination of the chelex competitive calcium binding assay. Cell Calcium 4, 89–105.

White, H. D. (1988) Kinetic mechanism of calcium binding to whiting parvalbumin. Biochem. 27, 3357–3365.

Williams, T. C., Corson, D. C. & Sykes, B. D. (1984) Calcium–binding proteins: Calcium(II)–lanthanide(III) exchange in carp parvalbumin. J. Am Chem. Soc. 106, 5698–5702.

Chapter 5

COMPARISON OF METAL ION–INDUCED CONFORMATIONAL CHANGES IN PARVALBUMIN AND ONCOMODULIN

5.1 Introduction

Oncomodulin is a low molecular weight ($M_r \approx 11700$) calcium–binding protein that was first detected in the soluble extracts of Morris rat hepatomas (MacManus, 1979). It is an oncodevelopmental protein which has been found to occur in approximately 85% of a variety of human and rodent tumours, as well as in extraembryonic structures during normal prenatal development (MacManus et al., 1985). The primary structure has shown that oncomodulin belongs to the large superfamily of calcium–binding proteins which includes troponin C, calmodulin, parvalbumin, vitamin D dependent CaBP, S–100 and calbindin 9K (MacManus et al., 1983a; MacManus et al., 1983b). Specifically, all of these proteins possess what are known as "EF–hand calcium–binding sites". The name "EF–hand" is derived from the calcium–binding structure in parvalbumin that is formed by two of its six helices (the E–helix and the F–helix), and the peptide loop connecting these two α–helices (Kretsinger, 1980). The hallmark of an EF–hand site is that the two helices are positioned perpendicular to each other in a manner resembling the outstretched index finger (E–helix) and thumb (F–helix) of a right hand, with the curled second finger representing the joining Ca^{2+}–binding loop (Strynadka & James, 1989). Two of the 32–residue helix–loop–helix EF–hand patterns, linked by a β–bridge and helix–helix contacts, form a single domain that binds two calcium ions (Godzik & Sander, 1989).

Functionally, oncomodulin has been found to exhibit certain calmodulin–like regulatory properties. For example, oncomodulin has been shown to activate certain calmodulin–dependent enzymes such as cyclic nucleotide phosphodiesterase (MacManus, 1981; Mutus et al., 1985b), calcineurin (Mutus et al., 1988) and nuclear

protamine phosphokinase (MacManus & Whitfield, 1983). Oncomodulin has also been shown to mimic calmodulin by stimulating DNA synthesis in Ca^{2+}–deprived cells (Boynton et al., 1982). Currently the physiological target of oncomodulin remains unknown, although glutathione reductase has recently been considered a possibility owing to the inhibitory effect of oncomodulin on this enzyme (Palmer et al., 1989).

Although oncomodulin, in some limited way, resembles calmodulin functionally, it has been found to more closely resemble other members of the family in terms of structure, namely the β–parvalbumins. On comparison of the amino acid sequences of rat oncomodulin and rat muscle parvalbumin, 55/108 residues were identical, with an additional 33/108 residues resulting from possible single base–pair substitutions (MacManus et al., 1983b). Both proteins possess six stretches of α–helices, lettered A through F. The proteins are analogous in that the first two helices (A and B) flank a non–functional binding loop, whereas the latter four helices flank two functional Ca^{2+}–binding loops known as the CD– and EF–binding sites. Despite extensive homology, the two proteins have been shown to be immunologically dissimilar (MacManus & Whitfield, 1983). In addition, unlike both calmodulin and oncomodulin, parvalbumin has never been shown to possess any calcium–dependent modulator properties (Heizmann, 1984; Wnuk et al., 1982).

Although it is not known what confers this ability, it has been suggested that Ca^{2+}–specific conformational changes may play a role. For example, Ca^{2+}–binding to calmodulin is known to induce conformational changes that bring a hydrophobic area to the protein surface thereby facilitating protein–protein interactions (Klee & Vanaman, 1982; Tanaka & Hidaka, 1980). Ca^{2+}–binding to

oncomodulin has also been shown to induce specific conformational changes both in the vicinity of the metal–binding sites (MacManus et al., 1984) and at a site located on the opposite face of the protein (Mutus et al., 1985a). The parvalbumins have also been shown to undergo conformational changes upon the binding of Ca^{2+}, which in some cases have been found to be Ca^{2+}–specific (Moeschler et al., 1980; Birdsall et al., 1979). In Chapter 4 of this thesis, the detailed nature of Ca^{2+}–specific conformational changes in the isotype III parvalbumin from codfish is described. Based upon this information, a higher affinity for Ca^{2+} than for Mg^{2+} may not be as important physiologically as the structural alterations to the protein produced upon Ca^{2+}–binding. For example, labelling of both parvalbumin and oncomodulin at Cys–18 in the AB loop with the fluorescent reagent *N*–dansylaziridine has revealed that both proteins were insensitive to Mg^{2+} binding. On the other hand, one mole of Ca^{2+}/mole of protein could effect the Cys–18–attached probe on oncomodulin, but not on parvalbumin (Mutus et al., 1985a). The second equivalent of Ca^{2+} did not affect the Cys–18–attached probe in either proteins. This latter observation suggests that binding to the stronger EF–site (Williams et al., 1987) may have a greater conformational significance compared to the weaker CD–site.

The purpose of this study was to compare Ca^{2+}–induced conformational changes at an identical site lying closer than Cys–18 to the two metal–binding sites in oncomodulin and parvalbumin. This was accomplished by comparing the intrinsic fluorescence of tryptophan, which occurs naturally in position 102 of cod III parvalbumin (see Chapter 4) and in a site–specific mutant of oncomodulin in which the phenylalanine in position 102 has been replaced with tryptophan. X–ray crystallography of carp parvalbumin (Kumar, Lee & Edwards, Brookhaven Protein Data Bank) and oncomodulin (Ahmed et al., 1989) has revealed that position 102 is

equidistant (≈ 11 Å) from both metal–binding sites and lies within the hydrophobic protein interior. By examining the effect of Ca^{2+}–binding upon the fluorescence properties of the identically located Trp probe in the two proteins, differences emanating from the metal–binding sites and accounting for the differential modulator ability may be revealed.

5.2 Materials and Methods

Materials. All materials were the same as described in Section 4.2.1. In addition, concentrations of the oncomodulin mutant protein were determined using the Pierce bicinchoninic acid (BCA) protein assay reagent (Pierce, Rockford, Illinois). This method relies upon the ability of the highly sensitive BCA reagent to combine with the well–known biuret reaction permitting the spectrophotometric quantitation of protein in aqueous solution (Redinbaugh & Turley, 1986). Standard curves were generated using a series of native tumour oncomodulin concentrations, the latter which were estimated using the known molar extinction coefficient, $\epsilon_{276nm} = 3159\ M^{-1}cm^{-1}$ (MacManus & Whitfield, 1983).

Methods. Cod III parvalbumin was purified from frozen fish fillets and judged to be homogeneous as described in Section 4.2.2. The mutagenesis, plasmid characterization by DNA sequencing and expression of recombinant oncomodulin were performed by Dr. D. Banville at the Biotechnology Research Institute in Montreal, Quebec and the F102W[1] oncomodulin mutant protein was purified to

[1]The notation "Letter–Number–Letter" is read as follows: the first letter represents the IUPAC–IUB established one–letter amino acid code of the native residue, the number identifies the position of the native residue, and hence the position of the point mutation, and the second letter is the code for the amino acid which is being substituted by mutagenesis in the place of the native residue.

homogeneity by Dr. J. MacManus, Division of Biological Sciences, NRC. In addition to the DNA sequencing, verification that the mutagenesis was performed at the correct position was obtained by examination of a tryptic peptide map. The tryptic peptide map of the recombinant oncomodulin with the putative F102W mutation was obtained by HPLC. Three peptides were found to have absorbance at 280 nm. As the elution times of two of the peptides coincided with the established elution times of the two tyrosine–containing peptides in native oncomodulin, the additional peptide detected in the F102W mutant was further analyzed for its amino acid content. This peptide was shown by amino acid analysis (of both hydrochloric and methane sulphonic acid hydrolysates) to have the required composition of residues 97–108 (MacManus et al., 1983a) with the phenylalanine missing, and one tryptophan added. Details regarding these procedures are outlined elsewhere (MacManus et al., 1989; Hutnik et al., 1989).

The calcium–loaded (holo) proteins were decalcified by precipitation with trichloroacetic acid (TCA) (Haiech et al., 1981). As already described for cod III parvalbumin in Chapter 4, this method was satisfactory in achieving greater than 96% decalcification. In addition, reversible calcium reconstitution in both cod III parvalbumin and the F102W oncomodulin mutant protein was observed. Calcium content following apo (metal–free) protein preparation was measured by inductively coupled plasma atomic absorption spectrometry by S. Willie, Division of Chemistry, NRC.

The steady–state and time–resolved spectroscopic data were collected as described in Chapter 2 and Section 4.2.5 of this thesis. All spectroscopy was done with protein samples dissolved in 10 mM cacodylate buffer containing 150 mM KCl, pH 7.0. Initially, 1 mM dithiothreitol was added to the cod III parvalbumin solutions. However, as no discernible differences were apparent in its absence, it

was subsequently omitted.

5.3 Results and Discussion

5.3.1 Comparison of Composition and Structure

The recent solution of the X–ray crystallographic structure of oncomodulin (Ahmed et al., 1989) has revealed a striking similarity between oncomodulin and carp pI 4.25 parvalbumin (Kumar, Lee and Edwards, Brookhaven Protein Data Bank). Figure 5.1 shows a superimposition of the peptide backbones and the location of a substituted tryptophan residue superimposed upon the native phenylalanine residue in position 102 relative to the two Ca^{2+}–binding sites. While some differences in the backbone can be seen near the amino terminus (N 1), the main chains are remarkably similar.

The complete primary sequence of cod III parvalbumin has not been definitely determined. One attempt at sequencing an anomalously long 113–residue protein has been published (Elsayed & Bennich, 1975). As described in Chapter 4, the C–terminal twenty amino acid segment was sequenced and the single Trp residue was definitely located at position 102. Determination of the amino acid compositions of the remaining tryptic fragments and comparison to the published sequences of the anomalous cod III parvalbumin (Elsayed & Bennich, 1975) and whiting parvalbumin (Joassin & Gerday, 1977), allowed the estimation of a "best guess" amino acid sequence of cod III parvalbumin. In Figure 5.2, a comparison of the known sequence of the oncomodulin mutant F102W and the estimated cod III parvalbumin (PV) is shown. Examination of the 20 amino acid C–terminal segments reveals that although the net charge on the segment is the same (– 4), F102W has a greater number of both charged (8 in F102W vs 6 in PV) and polar

Figure 5.1: Superimposition of the peptide backbones of carp pI 4.25 parvalbumin in red and oncomodulin in yellow. Amino (N 1) and carboxyl (C 108) termini are labelled, as well as the α–carbon of residue–102 in which a tryptophan sidechain has been superimposed upon the native phenylalanine sidechain in oncomodulin. The location of the other aromatic amino acid residues in oncomodulin are also shown. The ionic spheres of the two calcium ions are shown in blue, located in the CD–loop (bottom–left) and the EF–loop (bottom–right).

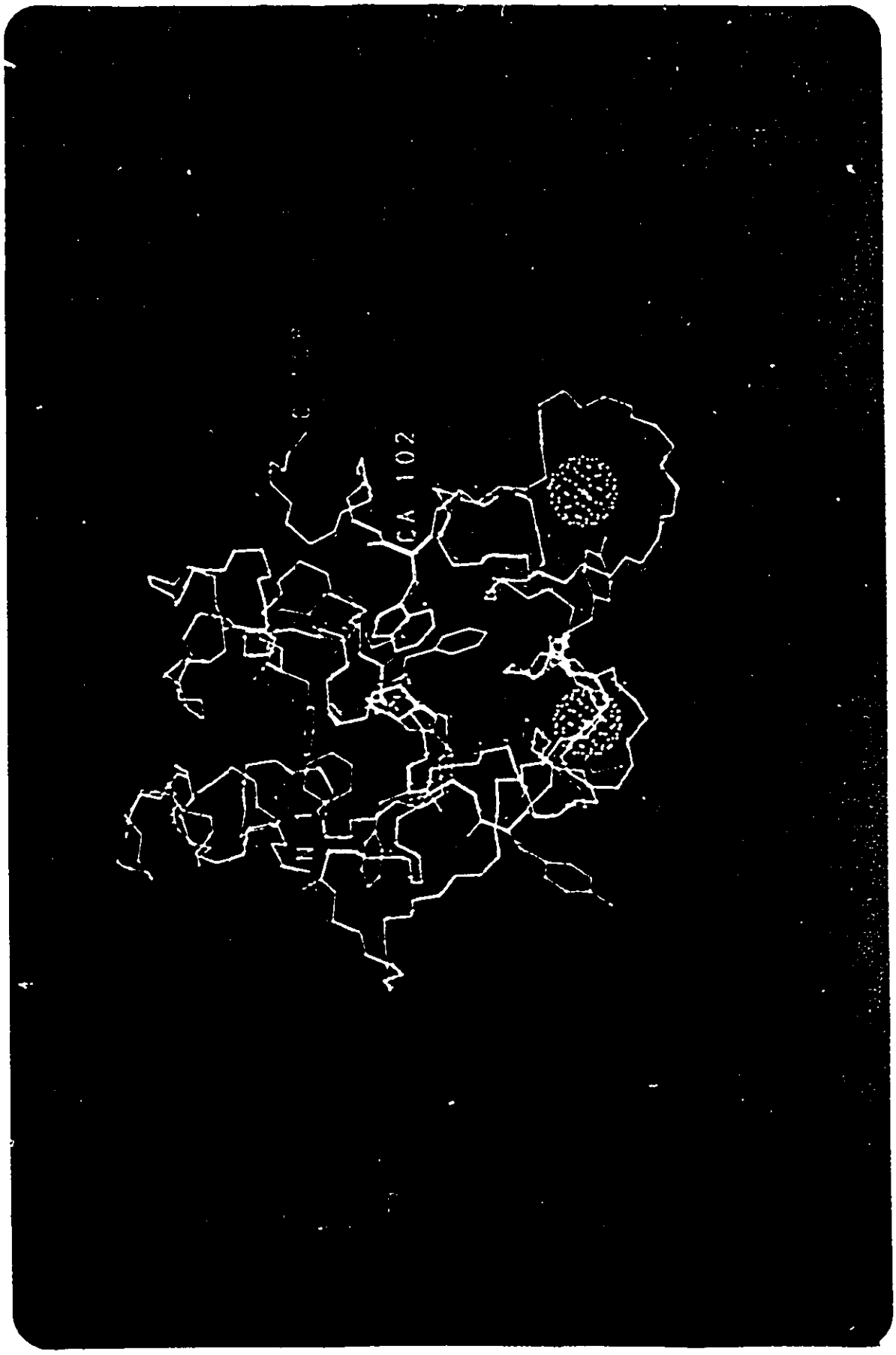
CA 102

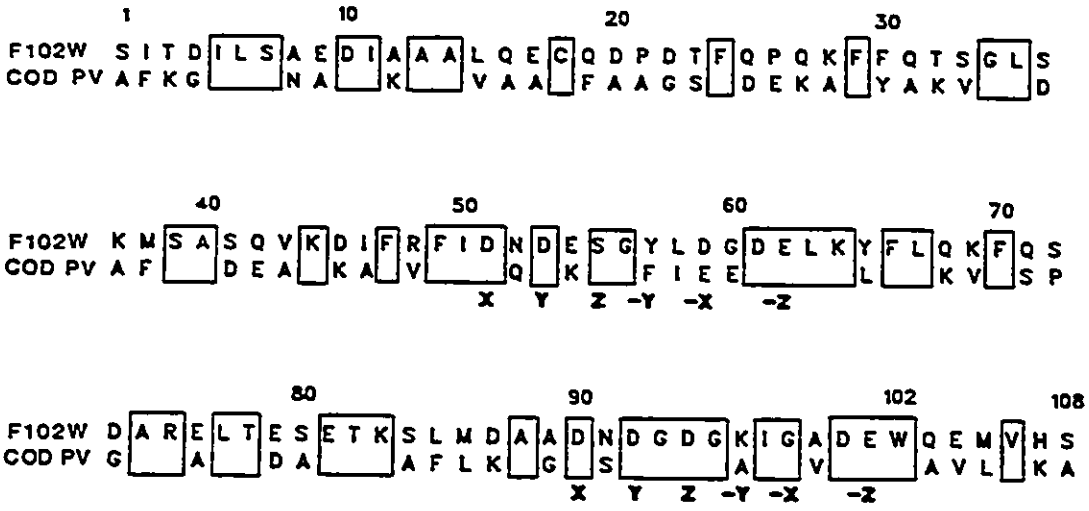

Figure 5.2: Comparison of the amino acid sequences of the oncomodulin mutant F102W (top sequence) and the estimated amino acid sequence of cod III parvalbumin (bottom sequence). The C–terminal twenty amino acid sequence of the parvalbumin was determined while the remaining tryptic fragments were placed by determination of their amino acid composition and comparison to other published parvalbumin sequences of cod III parvalbumin (Elsayed & Bennich, 1975) and whiting IIIb parvalbumin (Joassin & Gerday, 1977). The boxes indicate identity in both proteins and the one–letter amino acid code is used (IUPAC–IUB Commission on Biochemical Nomenclature). X, Y, Z, –X, –Y and –Z refer to the metal ion binding ligands (Kretsinger, 1980). The best guess of the cod III parvalbumin sequence was made by Dr. J.P. MacManus.

residues (5 in F102W vs 2 in PV). Examination of the entire sequences shows that F102W possesses a larger number of acidic residues (24 in F102W vs 19 in PV).

5.3.2 Spectral Comparison of Holo (Ca^{2+}–Containing) Proteins

The shape of the absorption spectra of the holo proteins were very similar (Figure 5.3 A) indicating that the aromatic amino acid residues resided in comparable molecular environments. These spectra are consistent with the amino acid compositions of the proteins. Cod III PV has 4 more phenylalanine (Phe) residues and one less tyrosine (Tyr) compared to F102W. As a result, in the spectrum of cod III PV, the vibronic structure associated with Phe (in the region 260–280 nm) is more evident, as well as the ^1L_b electronic transition of Trp, the latter appearing as a sharp subsidiary peak in the spectrum of both holo proteins. The location of the sharp subsidiary peak of the two proteins is different, with the PV peak at 289 nm occurring 4 nm to the blue of the F102W peak, the latter occurring at 293 nm. It has been shown that the local electrostatic potential of Trp is an important determinant of both the magnitude and position of the absorption transitions (Ilich et al., 1988). The differences in the wavelength positions of these transitions in F102W and PV are the first indication that the proximity of point charges with respect to the indole rings may be different. An alternative possibility which explains the red–shift of the ^1L_b absorption transition in F102W is the involvement of the indole N–H in hydrogen bond formation with a nearby protein moiety (Catalan et al., 1986). However the first possibility is the preferred explanation because of the fluorescence measurements which are presented below.

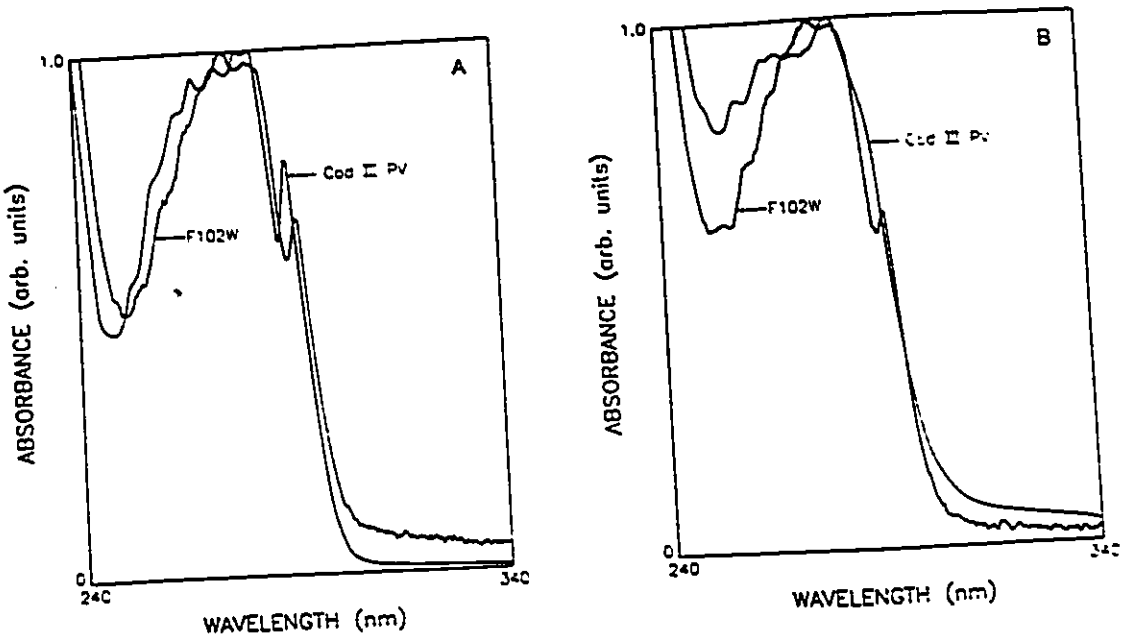

Figure 5.3: Ultraviolet absorption spectra of (A) holo and (B) apo ccd III parvalbumin and F102W oncomodulin mutant proteins, slits = 0.5 nm. The proteins were in 10 mM cacodylate buffer containing 150 mM KCl, pH .7. The parvalbumin solution also contained 1 mM dithiothreitol.

When the proteins were excited at 295 nm, the corrected steady–state emission spectra originating from the single Trp residue (Figure 5.4, Spectra 1 and 2) were comparable in shape, as well as in the wavelength position of the maximum fluorescence intensity (F102W λ_{max} = 319 nm and cod III PV λ_{max} = 320–325 nm). However, the fluorescence emission spectrum of PV was broader, possessing a 9 nm greater bandwidth at half height (48 nm in PV vs 39 nm in F102W). The slightly shorter wavelength position of the F102W fluorescence spectrum, and the slightly longer wavelength position of the absorption spectrum (Figure 5.3 A) were consistent with the idea that the electronic polarizability of the Trp in F102W, as well as its dipolar environment, may be considerably different when compared to cod III PV. Electronic transitions of Trp in less polar media have been shown to shift the absorption spectrum to longer wavelengths (Demchenko, 1986). In contrast, in an environment of low polarity, fluorescence spectra generally occur at shorter wavelengths (Lakowicz, 1983). Collectively these results suggest that the Trp in F102W resides in a relatively less polar environment when compared to cod III PV.

A nearest neighbour analysis relative to position–102 in oncomodulin and cod III parvalbumin supported the spectral results. Using the crystal structures of oncomodulin and carp pI 4.25 parvalbumin, all residues within a 6 Å radius of the CZ position of Phe–102 were located. The nearest neighbours relative to Trp–102 in cod III parvalbumin were then identified using the estimated primary sequence of cod III parvalbumin in Figure 5.2. The assumption was made that the identical positions in carp pI 4.25 and cod III parvalbumins would function as nearest neighbours relative to position–102. These residues are listed in Table 5.1, along with the hydropathy indices for each amino acid according to the scale of Kyte and

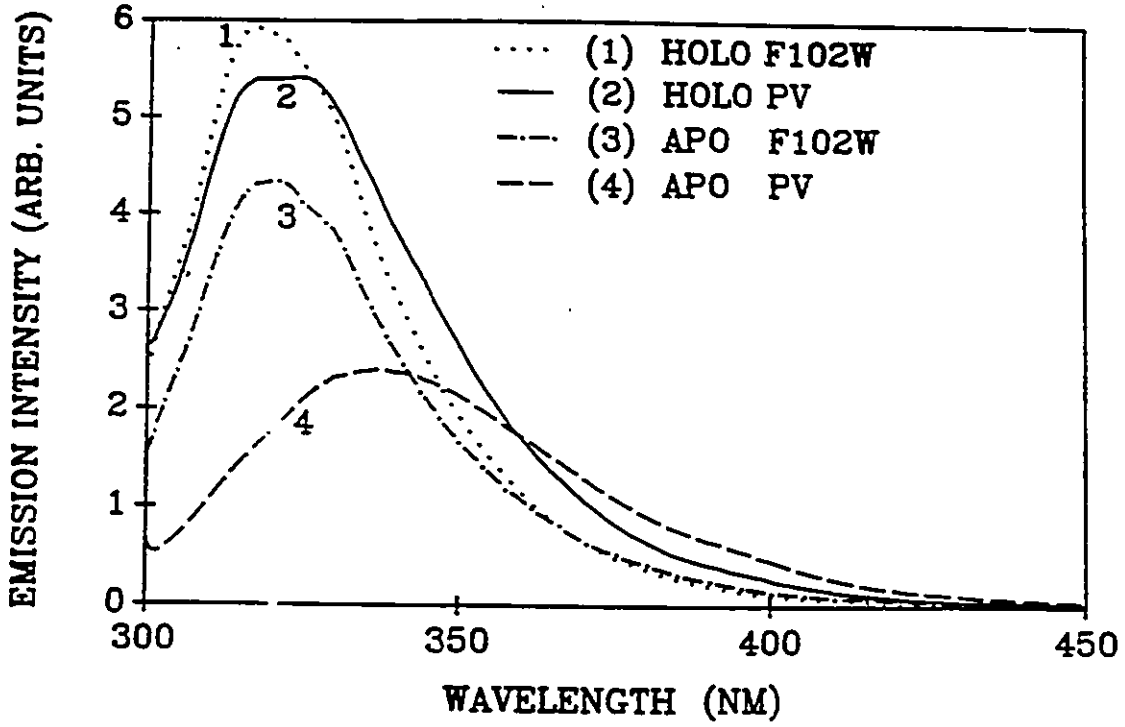

Figure 5.4: Corrected steady–state fluorescence emission spectra of holo– and apo–TCA cod III parvalbumin and F102W oncomodulin mutant, slits = 4 nm. The protein concentration was approximately 20 μM. λ_{ex} = 295 nm. In order to ease in the comparison of spectral shapes, the spectra of holo– and apo–TCA cod III parvalbumin have been multiplied by 2.

TABLE 5.1

Nearest neighbouring amino acid residues located within a radius of 6 Å relative to position–102 in oncomodulin and cod III parvalbumin. The nearest neighbours in cod III parvalbumin were identified by an examination of the crystal structure of carp pI 4.25 parvalbumin and comparison to the estimated primary sequence of cod III parvalbumin in Figure 5.2. The indices of hydropathy were obtained from Kyte and Doolittle (1982). The higher total hydropathy index for oncomodulin suggests that the immediate environment of position–102 is relatively more hydrophobic when compared to the environment in cod III parvalbumin.

Oncomodulin		Cod III Parvalbumin	
Residue	Hydropathy Index	Residue	Hydropathy Index
Phe–30	2.8	Tyr–30	– 1.3
Leu–35	3.8	Leu–35	3.8
Val–43	4.2	Ala–43	1.8
Lys–44	– 3.9	Lys–44	– 3.9
Ile–46	4.5	Ala–46	1.8
Phe–47	2.8	Phe–47	2.8
Ile–50	4.5	Ile–50	4.5
Leu–58	3.8	Ile–58	4.5
Phe–66	2.8	Phe–66	2.8
Leu–85	3.8	Phe–85	2.8
Ile–97	4.5	Ile–97	4.5
TOTAL	33.6	TOTAL	24.1

Doolittle (1982). The 40% larger total hydropathy index of the nearest neighbours in oncomodulin supports the spectral findings which indicate the environment of Trp–102 in F102W was more hydrophobic relative to the environment in cod III parvalbumin.

A striking difference was observed for the quantum yield of fluorescence (ϕ_f), with the ϕ_f of holo PV (0.14 ± 0.01) being only 60% that of holo F102W (0.24 ± 0.01). As hydrogen bonding of the indole N–H represents an efficient nonradiative

deactivation process (Privat et al., 1979), the blue–shifted ^1L_b transition in PV argues against hydrogen bonding accounting for the difference in ϕ_fs in the two proteins. Frequent contact with one or more highly polar groups, especially carbonyl groups, of the protein matrix is a common mechanism of fluorescence quenching via collisional or dynamic interactions (Ricci & Nesta, 1976). Further, it is known that such internal quenching by molecular carbonyls is reduced in non–polar environments (Privat et al., 1979). Even though F102W possesses a greater number of polar residues when compared to cod III PV, the local polar environment of the Trp may be different in terms of the proximity of one or more polar groups. Nearby peptide bonds could be involved in such an interaction. However, even if the position of polar groups were completely identical in the two proteins relative to the Trp residue, differences in the conformational heterogeneity of the proteins could alter both the collisional frequencies and the collisional geometries, resulting in large differences in the ϕ_fs (Axelsen & Prendergast, 1989). The higher ϕ_f for F102W suggests that the Trp residue in this protein is less likely exposed to solvent molecules (Schauerte & Gafni, 1989) compared to the Trp in cod III PV. In any given protein, it is difficult to identify the specific interaction(s) responsible for the quenching of Trp fluorescence, given the broad range of potential quenching mechanisms that have been suggested for Trp in proteins. Proton and electron transfer (Chen et al., 1987), exciplex formation (Lumry & Hershberger, 1978), ground–state complexation (Skalski et al., 1980), as well as charge transfer (Tournon et al., 1972) have been postulated as potential quenching mechanisms of Trp. These mechanisms have been proposed to involve Trp and a number of possible protein moieties including the terminal carboxylic and amino groups, peptide bonds, the carboxylic/carbonyl groups of Asp and Glu, the amino groups of

Lys and Arg, as well as a whole range of potential solvent interactions (for a review, see Creed, 1984). Despite the inability to identify the precise photophysical source of the quenching in the two proteins, the results unequivocally demonstrate differences in the local environment of the Trp.

The large difference in ϕ_f is not accounted for in the fluorescence decay measurements. Time–resolved fluorescence revealed that the fluorescence decays of both holo PV and holo F102W were best described by two components. The assignment of the decays to a double–exponential (two component) model was based upon the examination of a number of statistical parameters which were generated following the comparison of the experimental decay curve (shown in Figure 5.5 for holo cod III PV) with a calculated decay curve, the latter being generated based upon a sum of discrete exponentials as described in Section 1.2.4. Among these statistical parameters were the serial variance ratio (SVR) and the Sigma value, the merits of which have been discussed in Section 2.2.2. The adequacy of the exponential decay fitting was also judged by the inspection of weighted residual plots, which were generated based upon the difference (or residuals) between the experimental and calculated decay curves at each measured time interval. An adequate "fit" between the experimental and calculated decay curves would correspond to a randomness in the residual plots. In Figure 5.6, the weighted residual plots corresponding to the decay curve in Figure 5.5 are shown. In Figure 5.6 A, the non–random distribution of residual points, and the low SVR = 0.46, indicated that a single exponential decay function was not adequate to describe the fluorescence decay of holo cod III PV. However, the random residuals in Figure 5.6 B, and the SVR = 1.94 indicated that the double exponential decay function was adequate. As only a marginal improvement was gained in fitting the

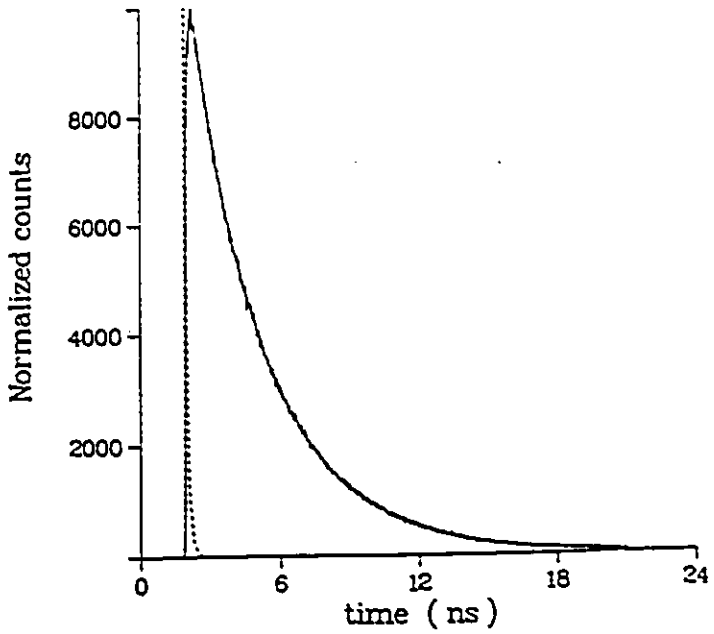

Figure 5.5: Typical normalized fluorescence time–intensity curves. The instrument response function curve (dotted line) and the holo cod III parvalbumin decay curve were recorded with channel width = 21.6 ps/channel, λ_{ex} = 295 nm, λ_{em} = 345 nm, and emission band–pass = 4 nm.

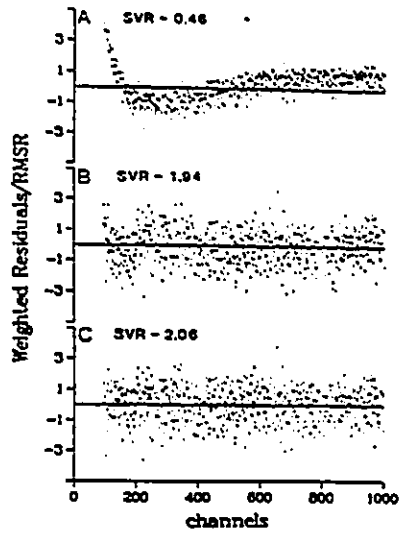

Figure 5.6: Weighted residual plots for the calculated best–fit emission decay curve for the experimentally measured decay curve shown in Figure 5.5. Panels A–C correspond to the plots for holo cod III parvalbumin fitted to single–, double–, and triple–exponential decay components, respectively. The serial variance ratios (SVRs) are also shown. An SVR $\simeq$ 2 is considered to be a satisfactory parameter value indicative of randomness of residuals (See Section 2.2.2).

data to a triple exponential function (Figure 5.6 C), the double exponential function was accepted. The fluorescence decay curve shown in Figure 5.5 was measured by exciting the sample at 295 nm and measuring the emission at 345 nm. In order to improve the accuracy of estimating the preexponential factors and lifetime values which are determined in a discrete exponential component analysis of fluorescence decay, a simultaneous analysis of multiple fluorescence decay curves was performed (Knutson et al., 1983). These different decay curves were measured at different emission wavelengths between 305–360 nm, all with an excitation wavelength = 295 nm. The results are summarized in Table 5.2. Upon global analysis, the lifetime values of the two components were found to be similar for the two holo proteins (τ_1 (PV) = 3.55 ns vs τ_1 (F102W) = 4.19 ns; τ_2 (PV) = 1.54 ns vs τ_2 (F102W) = 1.89 ns). Global analysis also permitted decay–associated spectra (DAS) of the components to be obtained. Figure 5.7 and Table 5.2 show that the λ_{max} for the various components are virtually identical for the two holo proteins, with λ^1_{max} (PV) = 320 nm versus λ^1_{max} (F102W) = 319 nm, and λ^2_{max} (PV) = 316 nm versus λ^2_{max} (F102W) = 313 nm. From the DAS in Figures 5.7 A and 5.7 B it can be seen that the fractional fluorescences (F_is) are virtually identical for the two proteins. For example, at 320 nm, F_1 = 0.88 for holo PV vs F_1 = 0.92 for holo F102W and F_2 = 0.12 for holo PV vs F_2 = 0.08 for holo F102W. If the reasonable assumptions are made that the radiative lifetime of each component is the same and that static quenching is absent, it is possible to calculate the relative component concentrations (c_is) owing to their proportionality to the normalized preexponential terms (See Section 3.4.4, equation 3.2). As each lifetime component is assigned to the Trp residue in a different conformation, the relative component concentrations reflect the relative occurrence of the various conformational states. As the most highly

TABLE 5.2

Steady-state and time-resolved fluorescence parameters of holo- and apo-TCA-cod III parvalbumin and the F102W oncomodulin mutant. λ_{ex} = 295 nm; 20°C.

Sample	ϕ_f	λ_{max}^{ss}[a] (nm)	SVR[b]	τ_1[c] (ns)	τ_2 (ns)	τ_3 (ns)	λ_{max}^{1}[d] (nm)	λ_{max}^{2} (nm)	λ_{max}^{3} (nm)	F_1[e]	F_2	F_3	C_1[e]	C_2	C_3	τ_r[f] (ns)
Holo PV	0.14 ± 0.01	321	1.92	3.55 ± 0.03	1.54 ± 0.02	-	320	316	-	0.88	0.12	-	0.76	0.24	-	22
Holo F102W	0.24 ± 0.01	319	1.80	4.19 ± 0.01	1.89 ± 0.02	-	319	313	-	0.92	0.08	-	0.83	0.17	-	16
Apo PV	0.09 ± 0.01	337	1.85	4.39 ± 0.02	2.17 ± 0.02	0.361 ± 0.006	335	330	330	0.59	0.37	0.04	0.31	0.41	0.28	26
Apo F102W	0.19 ± 0.01	319	1.84	4.11 ± 0.01	2.00 ± 0.02	0.222 ± 0.011	320	315	315	0.79	0.21	0.01	0.60	0.32	0.08	17

a λ_{max}^{ss} represents the wavelength of maximum intensity in the corrected steady-state fluorescence emission spectrum.

b SVR represents the serial variance ratio. It is a statistical parameter reflecting the goodness of fit. An SVR = 2 corresponds to an ideal statistical fit of the data (see Section 2.2.2). The SVR values shown reflect the statistics obtained upon global analysis of 10 data sets.

c The errors quoted for the lifetime values represent the standard errors for lifetime recovery from a given global set.

d λ_{max}^{i} represents the wavelength of the maximum intensity emission of the various components when excited at 295 nm. These values are obtained from the DAS.

e F_i and C_i denotes the fractional fluorescence and relative concentrations, respectively, of the various decay time components at 320 nm. The c_i's were calculated based upon their proportionality to the normalized preexponential times.

f τ_r represents the radiative lifetime and was calculated assuming that it was the same for all of the decay components in a given protein sample.

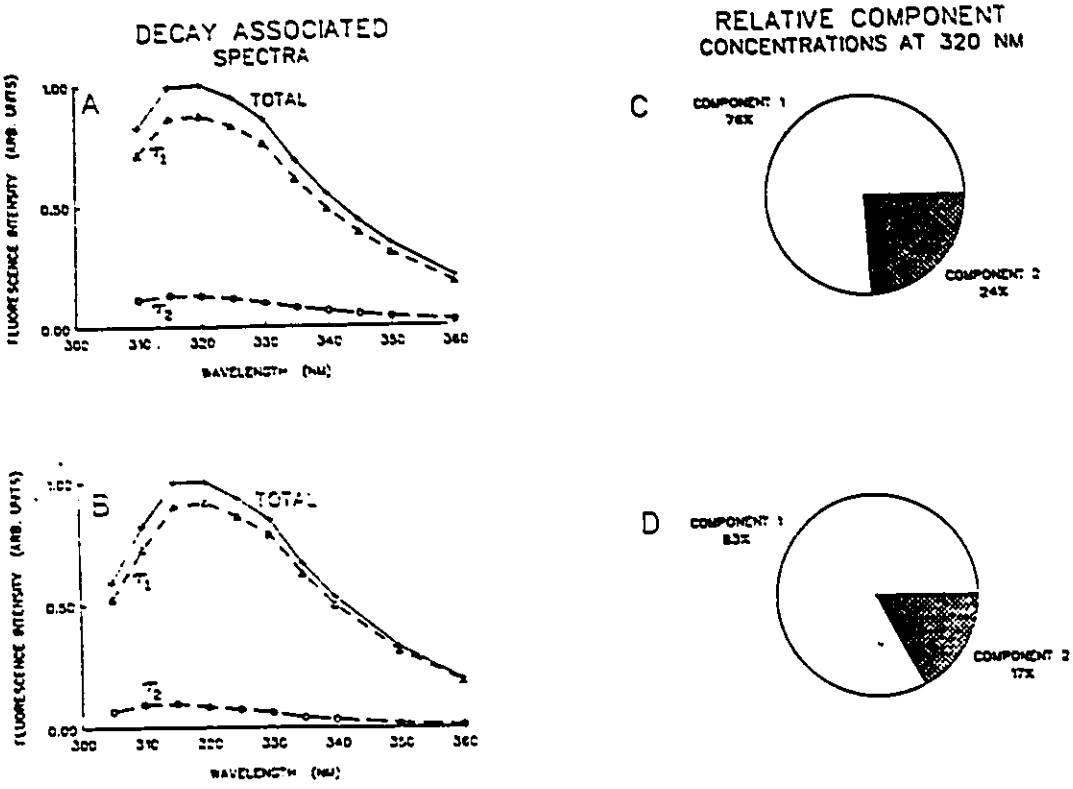

Figure 5.7: Decay–associated spectra for (A) holo cod III parvalbumin and (B) holo F102W oncomodulin mutant. The spectra sum to the corresponding corrected steady–state spectral intensities normalized to a value of one unit at the emission maximum. Standard errors are within the contours of the plotted symbols. The relative component concentrations at 320 nm of (C) holo cod III parvalbumin and (D) holo F102W are also shown.

fluorescent component may not be present in the highest concentration, this information provides some insight into the local environment of the Trp fluorophore in the various conformations. The relative component concentrations at 320 nm for holo cod III PV and holo F102W are depicted in Figures 5.7 C and 5.7 D. Both proteins are virtually identical in that the longest lived component dominates the fluorescence and is associated with the conformation which exists in the highest concentration (≈ 80%, See Table 5.2). The only significant difference between the Trp residue in the holo proteins is the ϕ_f.

In Section 1.2.4 of this thesis, equation 1.14 defined a simple relationship between the quantum yield of fluorescence (ϕ_f) and the singlet and radiative lifetimes, τ_s and τ_r respectively. This relationship was as follows: $\phi_f = \tau_s/\tau_r$ (1.14). For a multiexponential fluorescence decay, it is possible to calculate a mean or intensity–weighted lifetime which can be used as an approximation of τ_s in equation 1.14. The intensity–weighted mean lifetime $<\tau>$, is given by the following equation:

$$<\tau> = (\Sigma\alpha_i\tau_i^2)/(\Sigma\alpha_i\tau_i), \qquad (5.1)$$

where the α_is are the preexponential terms and the τ_is are the individual decay time components (Ross et al., 1989). In the case of holo cod III PV and holo F102W, the 21% longer mean (intensity–weighted) lifetime of the decay parameters in F102W ($<\tau>$ = 4.00 ns in holo F102W vs $<\tau>$ = 3.31 ns in holo PV) is not sufficiently great enough to account for the considerably greater ϕ_f. One explanation is that the Trp in cod III PV may be involved in an interaction leading to a significant degree of static quenching which would decrease ϕ_f but would not affect the lifetime values (Szalay & Szollosy, 1964). The specific molecular

interaction leading to static quenching is not readily apparent by an examination of the crystal structure. An alternative explanation is that the radiative lifetime, τ_r, is different for the Trp in the two proteins. Similar ideas have been proposed to account for discrepancies between the apo and holo cod III PV fluorescence parameters in Chapter 4. If a calculation is made to estimate τ_r using equations 3.2 and 3.3, τ_r (holo cod III PV) = 22 ns versus τ_r (holo F102W) = 16 ns. Such differences in the radiative lifetimes may be expected if the electronic polarization, or the dipolar environment of the Trp in the two proteins, were different (Privat et al., 1979). Specifically, differences may exist with respect to how the helix dipoles are oriented relative to the Trp which is situated just outside of the EF–loop at the start of the F–helix. As the interhelical angles in the two proteins appear to be virtually the same (Table 5.3), the different electronic/dipolar environment may originate from other local and specific differences.

An examination of the crystal structures and primary sequences (Figure 5.2) reveals that position–85 in the sequence differs with respect to the presence/absence of an aromatic Phe residue in close proximity to position–102. The residue in position–85 is a Leu in F102W but a Phe in cod III PV. As the residue in position–85 occurs less than 6 Å from position–102 in both proteins, it is possible that it may have an influence on the electronic interactions of Trp–102. Despite these more local electronic differences, the overall conformational heterogeneity of the two holo proteins is virtually indistinguishable.

5.3.3 Spectral Comparison of Apo (Ca^{2+}–Free) Proteins

Treatment of the holo proteins with trichloroacetic acid (TCA) resulted in greater than 96% decalcification. Atomic absorption measurements typically gave

TABLE 5.3

A comparison[a] of the interhelical angles in oncomodulin[b] and carp pI 4.25 parvalbumin[c].

Helices[d]	Oncomodulin	Parvalbumin
A–B	152.7°	158.6°
C–D_1	108.4°	105.6°
C–D_2	111.1°	110.2°
D_1–D_2	126.7°	129.3°
E–F	96.1°	99.1°

[a]The comparison was done by Dr. F. Ahmed, Division of Biological Sciences, NRCC.
[b]Ahmed et al., 1989.
[c]Kumar et al., Brookhaven Protein Data Bank.
[d]Helix A = residues 7–18; helix B = residues 25–34; helix C = residues 40–50; helix D_1 = residues 60–65; helix D_2 = residues 65–70; helix E = residues 79–89; helix F = residues 99–108.

0.03–0.08 mol Ca^{2+}/mol protein. Upon decalcification, dramatic changes were observed in the absorption and steady–state fluorescence emission spectra of cod III PV. In Figure 5.3 B it can be seen that decalcification resulted in a complete loss of the 289 nm subsidiary peak of the absorption spectrum, as well as a reduction in the defined spectral structure. The corrected fluorescence emission spectrum showed that Ca^{2+} removal prompted a substantial red–shift (λ_{max} (holo) = 321 nm versus λ_{max}(apo) = 337 nm), a broadening of the spectrum and a quenching of the Trp fluorescence (Figure 5.4). In general, a red–shifted fluorescence emission indicates the transfer of Trp from a relatively apolar, solvent–shielded environment to a more polar, solvent–accessible environment (Van Durren, 1961). Upon decalcification

the ϕ_f decreased from 0.14 ± 0.01 to 0.09 ± 0.01 when excited at 295 nm, 20°C.

In contrast, decalcification of F102W resulted in only minor changes in the absorption spectrum (Figure 5.3 B), with only a slight loss of the features associated with both Phe and Trp absorption. Unlike cod III PV, the fluorescence emission spectrum did not undergo a shape change nor a shift in the position of λ_{max} (Figure 5.4). However the ϕ_f did decrease upon Ca^{2+} removal from 0.24 ± 0.01 (holo) to 0.19 ± 0.01 (apo). Thus the influence of decalcification on the environment of the Trp in these two proteins is markedly different. The more polar environment of the Trp in apo cod III PV may suggest the F–helix, of which it is a part, may be better able to dissociate from the core of the molecule upon decalcification. Other studies using high resolution ^{1}H–NMR and optical stopped–flow techniques have suggested that hydrophobic residues in the F–helix, especially Val–99, Phe–102, Leu–105 and Val–106 in the carp pI 4.25 β–parvalbumin, are essential in stabilization of the protein structure (Corson et al., 1986). Because the F–helix of F102W contains a greater number of polar and/or charged residues (Figure 5.2), it was unexpected that it experienced a <u>less</u> dramatic change upon decalcification when compared to cod III PV. In addition, the presence of a Lys residue in position–27 of PV has been found to contribute to protein stability by formation of an ion pair bond with the C–terminal carboxyl function (Corson et al., 1986). Because F102W (as well as native oncomodulin) has a Gln residue in position–27 it is unable to form this bond and thus, should have a protein structure which is destabilized relative to PV.

Williams et al. (1986) found that upon decalcification the α–parvalbumins retained a large extent of both the secondary and tertiary structure typical of their holo forms. In contrast, the β–parvalbumins lost practically all of their tertiary structure and resembled random coils upon decalcification. In agreement, the

fluorescence results suggest that in the absence of Ca^{2+}, the PV molecule has additional conformational heterogeneity, at least in the region probed by Trp–102. Further, cod III PV appears to experience much greater perturbations upon decalcification in the region of Trp–102 when compared to F102W. Thus it appears that the magnitude of the conformational changes induced by Ca^{2+} may be an important difference between the two proteins. The lack of major conformational changes upon metal–ion binding to, or removal from F102W in the region probed by Trp–102 may be consistent with its putative function as a modulator protein. One would envision a modulator protein to be able to reversibly respond to ions in a manner which has a minimum entropy requirement. The fluorescence results presented herein suggest that although oncomodulin may possess the greatest degree of primary sequence homology with the β–parvalbumin subfamily, it may behave more like an α–parvalbumin upon decalcification.

Time–resolved fluorescence of the apo proteins showed that three lifetime components were required to adequately describe the decay. Log plots comparing the fluorescence decay curves of holo and apo cod III PV are given in Figure 5.8 and the residual plots for the best fit exponential decay functions corresponding to the apo protein decay are given in Figure 5.9. The appearance of a short 200 – 400 ps component, which disappeared upon Ca^{2+} reconstitution, indicated that both proteins experienced a greater degree of conformational heterogeneity in the absence of Ca^{2+}. This third component comprised only 1 – 4% of the total fluorescence. The values of the three lifetime components were very similar for the two apo proteins (See Table 5.2). Despite the similarity of the lifetime values, greater differences were observed in the preexponential terms. The fractional fluorescence and relative concentration of the longest decay time component were significantly

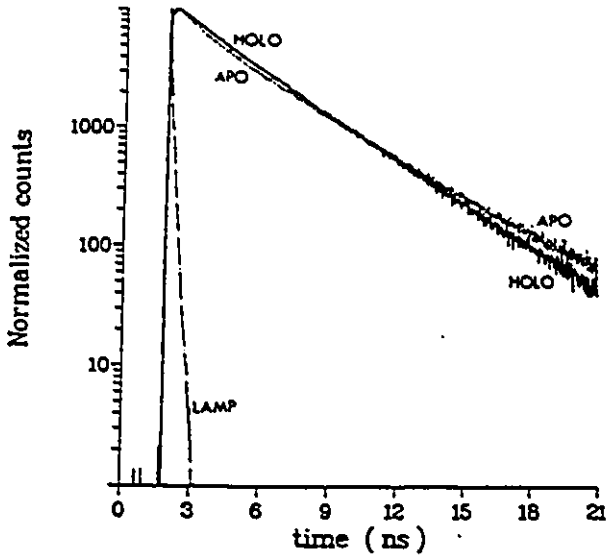

Figure 5.8: Log plots of the fluorescence decay curves of holo and apo cod III parvalbumin, as well as the instrument response function. $\lambda_{ex} = 295$ nm; $\lambda_{em} = 345$ nm.

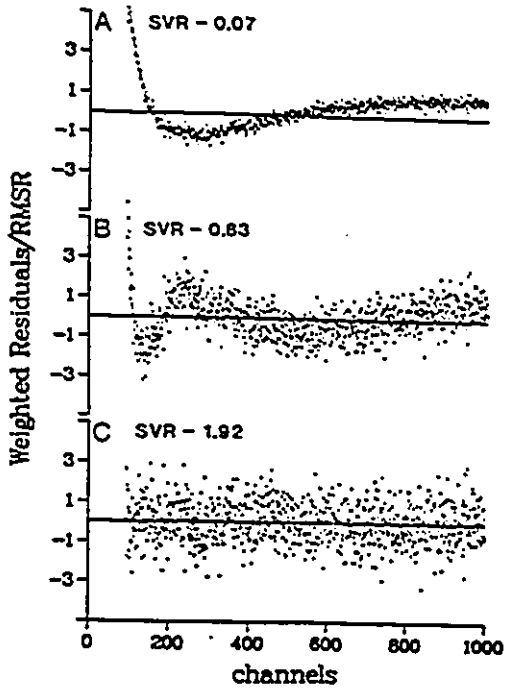

Figure 5.9: Weighted residual plots for the calculated best–fit emission decay curve corresponding to the experimentally measured decay curve of apo cod III parvalbumin. Panels A–C correspond to the plots for the decay fitted to single–, double–, and triple–exponential decay components, respectively. The SVR values are also shown.

less for apo cod III PV compared to apo F102W (F_1 = 0.59 (apo PV) vs F_1 = 0.79 (apo F102W); c_1 = 0.31 (apo PV) vs c_1 = 0.60 (apo F102W) at 320 nm (Figure 5.10 A – D)). Upon decalcification the middle decay time component of apo cod III PV became relatively more prevalent. A striking difference between the apo proteins was the concentration of the third component (c_3 = 0.28 (apo PV) vs c_3 = 0.08 (apo F102W). The results demonstrate that significantly greater conformational changes in the region probed by Trp–102 occur upon decalcification of cod III PV when compared to F102W. This is further supported by the DAS (Figures 5.10 A and B) which show that the λ_{max} of all three components in apo cod III PV experienced a 10–15 nm red–shift upon decalcification. This is in contrast to the DAS of apo F102W which have λ_{max} occurring in the identical positions as the holo protein (See Table 5.2). A feature which is consistent in both apo proteins is that the DAS of component 1 is red–shifted by 5 nm relative to the other component spectra. This suggests that the conformation associated with the longest lived decay component is such that the Trp residue exists in a relatively more polar environment compared to the shorter decay time components. The same is true for the DAS of the holo proteins (Figures 5.7 A and B), except that wavelength differences between the λ_{max} of the component spectra are not as great (See Table 5.2).

Although the ϕ_f decreased for both proteins upon decalcification, a greater degree of quenching was observed for cod III PV (36% decrease of ϕ_f (PV) vs 21% decrease ϕ_f (F102W)). The ϕ_f of apo F102W (0.19 ± 0.01) was more than double that of apo cod III PV (0.09 ± 0.01), even though the lifetime values of the three components were strikingly similar (Table 5.2). Consistent with the rationalization suggested for the holo proteins, a change in the radiative lifetime, τ_r, best explains

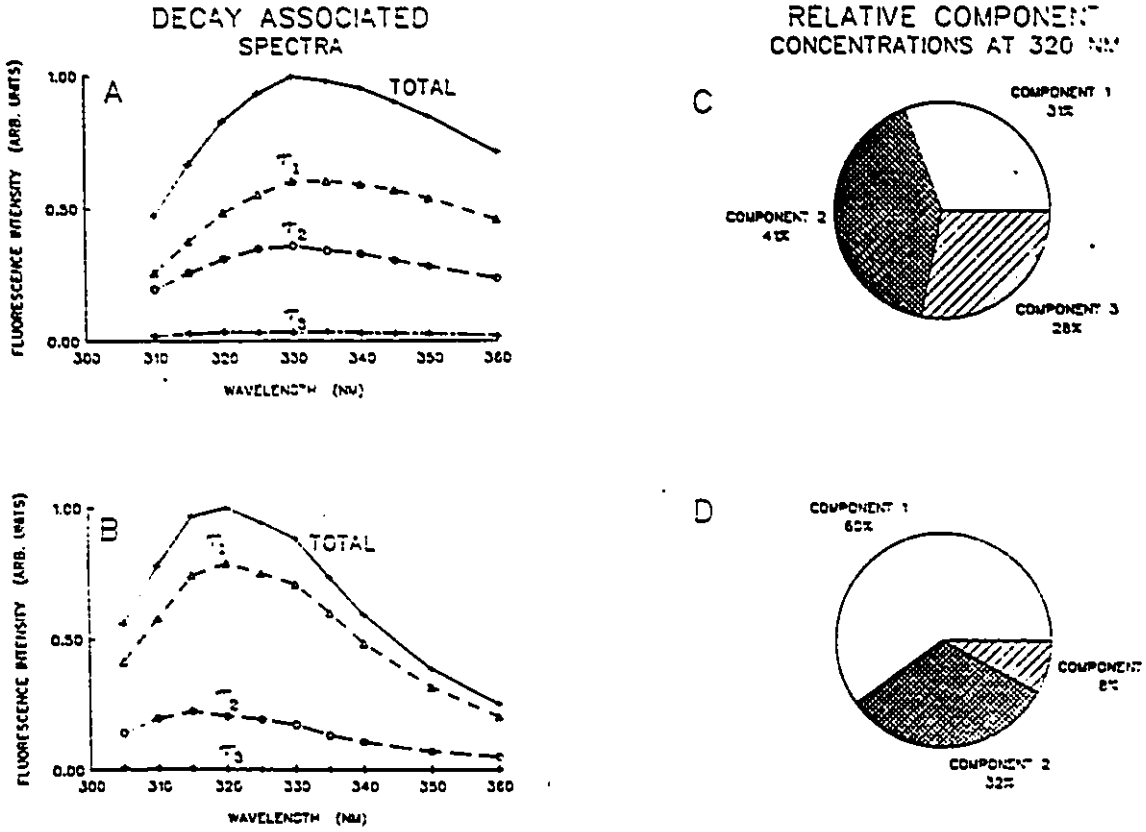

Figure 5.10: Decay–associated spectra for (A) apo–TCA cod III parvalbumin and (B) apo–TCA F102W oncomodulin mutant. The spectra sum to the corresponding corrected steady–state spectral intensities normalized to a value of one unit at the emission maximum. Standard errors are within the contours of the plotted symbols. The relative component concentrations at 320 nm of (C) apo–TCA cod III parvalbumin and (D) apo–TCA F102W are also shown.

the data. Calculation of τ_r revealed a considerable difference between the two apo proteins (τ_r (apo PV) = 26 ns vs τ_r (apo F102W) = 17 ns). In addition, when the τ_r of each apo protein was compared to the respective holo protein (Table 5.2), cod III PV experienced much greater changes upon decalcification.

Addition of Ca^{2+} to the apo–TCA PV restored the shape, wavelength position and greater than 96% of the fluorescence intensity (Figure 5.11, Spectrum 2). Addition of Ca^{2+} to apo–TCA F102W restored 100% of the spectral features (Figure 5.12, Spectrum 1). Thus the conformational changes associated with decalcification were largely reversible for both proteins. If conformational changes are at the root of the ability of oncomodulin to function as a modulator, then the features of these changes are that they are subtle, localized and reversible. In fact, the non–modulatory PV appears to undergo much more dramatic conformational changes upon decalcification in the region probed by Trp–102.

In Figures 5.11 and 5.12 are included the spectral response of Mg^{2+} addition to the apo forms of both cod III PV and F102W, respectively. These spectra clearly demonstrate that the Ca^{2+}–specificity of the conformational changes may have little to do with the ability of a protein to function as a modulator. Addition of Mg^{2+} to apo cod III PV had essentially no effect upon the spectral properties (Figure 5.11, Spectrum 3). In chapter 4, data have been presented which show how this protein may have been mistaken as a Ca^{2+}/Mg^{2+} protein. In fact, F102W displayed a larger response to Mg^{2+} than did parvalbumin, albeit a small one (Figure 5.12, Spectrum 3) which may be due to the fact the apo protein was less disrupted and was more poised to bind a divalent cation with moderate affinity. Thus the feature of being able to respond to Ca^{2+} instead of Mg^{2+} may not be as important as the detailed nature of the conformational changes that are induced

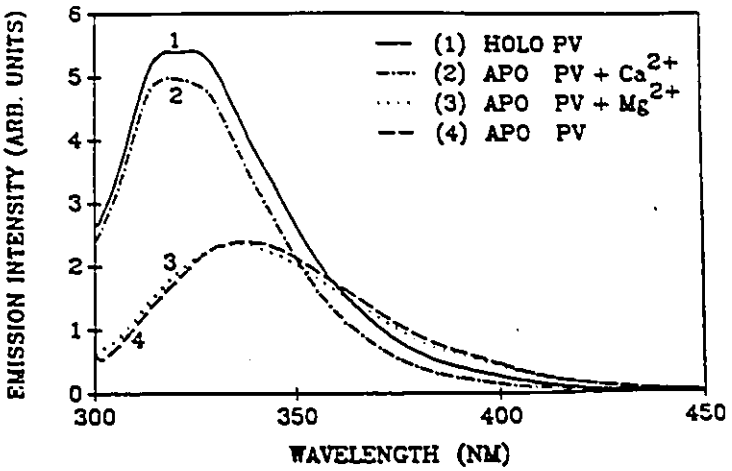

Figure 5.11: Corrected steady–state fluorescence emission spectra of apo cod III parvalbumin showing the response of the protein to Ca^{2+} and Mg^{2+} addition. The protein concentration was approximately 20 μM. $CaCl_2$ (aq) was added to a final concentration of 2.5 mM and $MgCl_2$ (aq) was added to a final concentration of 5 mM.

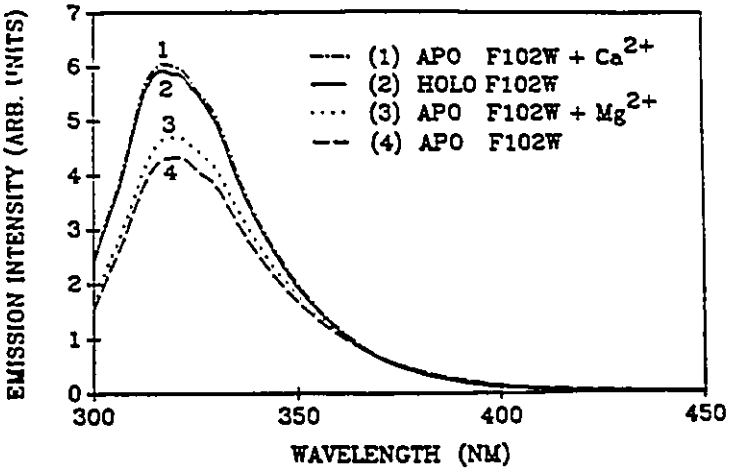

Figure 5.12: Corrected steady–state fluorescence emission spectra of the apo F102W oncomodulin mutant showing the response of the protein to Ca^{2+} and Mg^{2+} addition. The protein concentration was approximately 20 μM. $CaCl_2$ (aq) was added to a final concentration of 2.5 mM and $MgCl_2$ (aq) was added to a final concentration of 5 mM.

upon Ca^{2+}–binding to these two proteins.

Ca^{2+} titration of the apo proteins revealed that the magnitude of the response of each protein to substoichiometric amounts of Ca^{2+} was different. For F102W, one equivalent of Ca^{2+} produced 88% of the maximal response whereas only 73% of the total response was experienced upon addition of one equivalent of Ca^{2+} to apo cod III PV (Figure 5.13). From earlier work it was suggested that in oncomodulin the EF–site is a Ca^{2+}/Mg^{2+} parvalbumin–like site which possesses a greater affinity for Ca^{2+} compared to the weaker CD–site, which was thought to be Ca^{2+}–specific (MacManus et al., 1984). It was also suggested that the CD–site was most likely involved in manifesting the regulatory properties of the protein. If this is true, the titration data displayed in Figure 5.13 would suggest that the major conformational changes in oncomodulin are controlled by Ca^{2+}–binding to the EF–site, and not the CD–site. As the EF–sites of both the parvalbumins and oncomodulin are believed to have Ca^{2+}–binding affinity constants of at least 10^6 M^{-1} (Kretsinger, 1980; Williams et al., 1987), it is unlikely that the Ca^{2+} in the EF–site is removed under physiological conditions. The spectral results reported here suggest the Ca^{2+} bound to the higher affinity site in oncomodulin (presumably the EF–site, Williams et al., 1987) plays a strong role in maintaining the structural integrity of the protein in a similar manner to what has already been suggested for parvalbumin (Nelson et al., 1976).

A major difference between the two proteins was the observable response to the second equivalent of Ca^{2+}. Binding of the second Ca^{2+} equivalent produced an additional 12% of the total response for F102W and 21% of the total response for cod III PV (Figure 5.13). The PV titration curve displayed a slight break at 1 mol Ca^{2+}: 1 mol protein which suggested the affinity for Ca^{2+} in the two sites may be

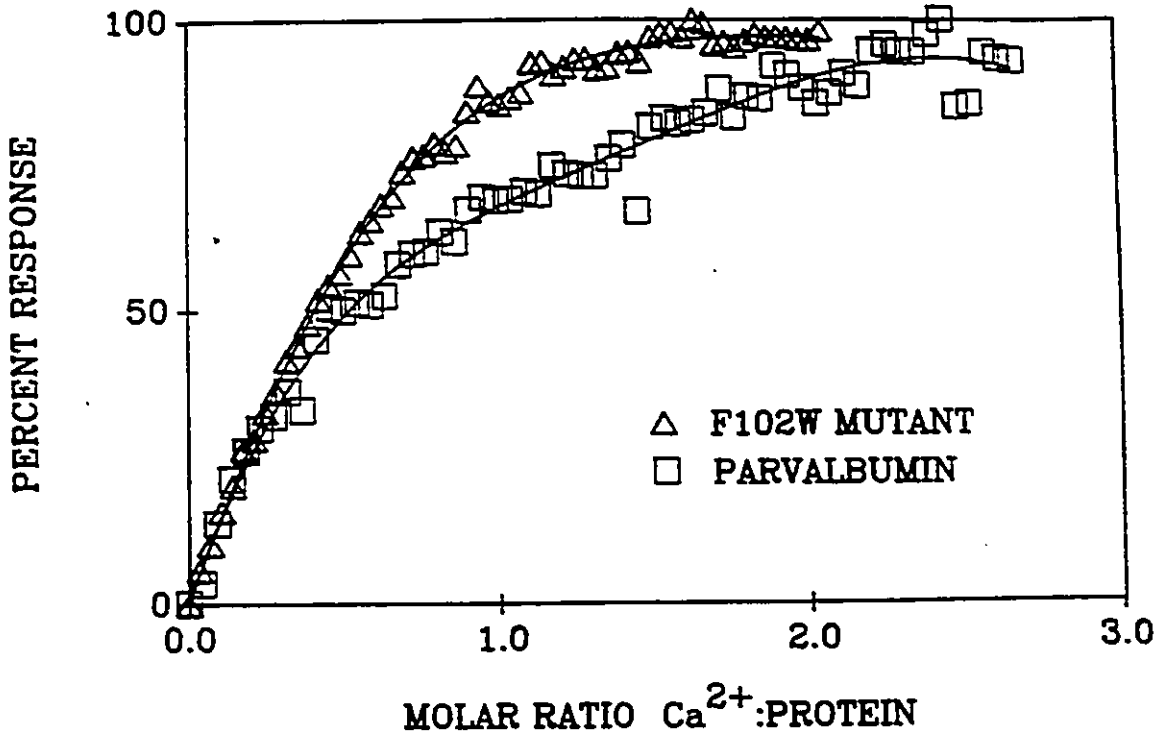

Figure 5.13: Ca^{2+} titration of apo–TCA cod III parvalbumin (□) and apo–TCA F102W oncomodulin mutant (△) plotted in terms of the fluorescence intensity change upon Ca^{2+} addition. For parvalbumin the intensities were monitored at 325 nm, while for F102W, they were monitored at 318 nm. Two μL aliquots of 1 mM $CaCl_2$ (aq) were added to 1.5 mL of a stirred solution of apoprotein.

different. It is interesting that the F102W titration curve reached a plateau value at a molar ratio of 1.5. This latter observation demonstrated that the filling of the lower affinity binding site in F102W had only a minor effect upon the fluorescence properties of the Trp probe in position–102. It is notable that only one equivalent of Ca^{2+} was required to induce the full conformational response at position–18 in oncomodulin (Mutus et al., 1985a); no conformational response was detected in this region upon the addition of the second Ca^{2+} equivalent. This site occurs on the side of the molecule opposite the two Ca^{2+}–binding sites in the non–functional AB–loop.

In contrast, Trp–102 in PV was capable of detecting conformational changes associated with the binding of the first and second equivalents of Ca^{2+} to a greater extent. However, it has been shown that the effects of the two Ca^{2+} ions are different. The binding of the first equivalent of Ca^{2+} is mainly responsible for the wavelength shift, while the second equivalent is important in locking the protein into its final conformation and hence restoring the full intensity of the Trp emission (Chapter 4).

On the basis of the results presented in this chapter, it would appear as if Ca^{2+}–binding to the putative regulatory CD–site in oncomodulin has only a minor role in altering the conformational properties of the protein. However, it should be emphasized that these results reflect events that are limited to the region probed by Trp–102. Examination of a number of site–specific mutants of oncomodulin revealed that the binding of the second equivalent of Ca^{2+} could produce more significant changes (44% of the total fluorescence response) only very locally in the EF–loop. This was demonstrated with the oncomodulin mutant K96W, the results

of which are presented and discussed in Chapter 6. These latter results imply that after the binding of Ca^{2+} to the stronger EF–site, the binding of the second equivalent of Ca^{2+} to the weaker CD–site induces conformational changes in the vicinity of the distant EF–site. A complex interplay between the two Ca^{2+}–binding sites has been reported for a number of calcium–binding proteins (Sekharudu & Sundaralingam, 1988) and has specifically been suggested in oncomodulin using high resolution ^1H–NMR spectroscopy and optical stopped–flow techniques (Golden et al., 1989). Details regarding the interaction of the two binding sites, as probed by fluorescence spectroscopy, are described in Chapter 6.

5.4 Chapter Summary and Conclusions

The calcium–induced conformational changes of the 108–amino acid residue proteins, cod III parvalbumin and oncomodulin, were compared using tryptophan as a sensitive spectroscopic probe. As native oncomodulin is devoid of tryptophan, a site–specific mutant was studied in which tryptophan was placed in the identical position (residue 102) as the single tryptophan residue in cod III parvalbumin. The results showed that in the region probed by tryptophan–102, cod III parvalbumin experienced significantly greater changes in conformation upon decalcification compared to the oncomodulin mutant, F102W. Addition of one equivalent of Ca^{2+} produced greater than 90% of the total fluorescence response in F102W while in cod III parvalbumin, only 74% of the total was observed. Cod III parvalbumin displayed a negligible response upon Mg^{2+} addition. In contrast, F102W did respond to Mg^{2+}, but the response was considerably less when compared to Ca^{2+} addition. Time–resolved fluorescence showed that the tryptophan in both proteins

existed in at least two conformational states in the presence of Ca^{2+}, and at least three conformational states in its absence. Differences in the absorption and fluorescence emission spectra and the radiative lifetimes indicated that the local electronic environment of the tryptophan was significantly different in the two proteins, especially upon decalcification. This suggested that the orientation and/or interactions of the tryptophanyl indole with the hydrophobic core of these two proteins were different, as well as the magnitude of the perturbations produced by Ca^{2+} removal. Collectively these results demonstrate that both cod III parvalbumin and oncomodulin undergo Ca^{2+}–specific conformational changes. However, oncomodulin is distinct from cod III parvalbumin in terms of the electronic environment of the hydrophobic core, the magnitude of the Ca^{2+}–induced conformational changes and the number of calcium ions required to modulate the major conformational changes. If the CD–site of oncomodulin does possess a lower Ca^{2+} affinity constant (compared to the EF–site), it is likely that this is the site that will be exchanging Ca^{2+} under physiological conditions. The data presented in this chapter suggest that conformational changes associated with Ca^{2+} binding to the CD–site in oncomodulin are very subtle in the region probed by Trp–102. Thus the presence of modulator abilities in oncomodulin, but their absence in parvalbumin, cannot be simply explained in terms of either the magnitude or Ca^{2+} specificity of the conformational response. It appears more likely that very subtle or local differences may be the answer. The description of highly localized Ca^{2+}–specific conformational changes associated with three specific regions of the Ca^{2+}–binding sites in oncomodulin is presented in Chapter 6. In this chapter, the examination of five spectrally informative site–specific mutants of oncomodulin not only permits a rationalization of the fluorescence properties of the

native tumour protein, but also reveals significant conformational changes associated with the binding of the second equivalent of Ca^{2+}.

5.5 References

Ahmed, F., Przybylska, M., Rose, D. R., Birnbaum, G. I. & MacManus, J. P. (1989) Crystal structure of oncomodulin. Proceedings of the Annual Meeting of the American Crystallographic Association, Seattle Washington, July 23–29, PB33, 112.

Axelsen, P. H. & Prendergast, F. G. (1989) Molecular dynamics of tryptophan in ribonuclease–T1. II. Correlations with fluorescence. Biophys. J. 56, 43–66.

Birdsall, W. J., Levine, B. A., Williams, R. J. P., Demaille, J. G., Haiech, J. & Pechere, J.–F. (1979) Calcium and magnesium binding by parvalbumin. A proton magnetic resonance spectral study. Biochimie 61, 741–750.

Boynton, A. L., MacManus, J. P. & Whitfield, J. F. (1982) Stimulation of liver cell DNA synthesis by oncomodulin, an MW 11 500 calcium–binding protein from hepatoma. Exp. Cell Res. 138, 454–458.

Catalan, J., Perez, P. & Acuna, A. U. (1986) Indole spectroscopy: The location of the ^1L_a and ^1L_b electronic states and the absorption spectrum. J. Mol. Struct. 142, 179–182.

Chen, L. X.–Q., Longworth, J. W. & Fleming, G. R. (1987) Picosecond time–resolved fluorescence of ribonuclease T_1. A pH and substrate analogue binding study. Biophys. J. 51, 865–873.

Corson, D. C., Williams, T. C., Kay, L. E. & Sykes, B. D. (1986) ^1H NMR spectroscopic studies of calcium–binding proteins. 1. Stepwise proteolysis of the C–terminal α–helix of a helix–loop–helix metal–binding domain. Biochem. 25, 1817–1826.

Creed, D. (1984) The photophysics and photochemistry of the near–UV absorbing amino acids—I. Tryptophan and its simple derivatives. Photochem. Photobiol. 39, 537–562.

Demchenko, A. P. (1986) In: Ultraviolet Spectroscopy of Proteins, (Springer, Berlin).

Elsayed, S. & Bennich, H. (1975) The primary structure of allergen M from cod. Scand. J. Immunol. 4, 203–208.

Godzik, A. & Sander, C. (1989) Conservation of residue interactions in a family of Ca–binding proteins. Protein Engineering 2, 589–596.

Golden, L. F., Corson, D. C., Sykes, B. D., Banville, D. & MacManus, J. P. (1989) Site specific mutants of oncomodulin: ^1H NMR and optical stopped flow studies of the effect on the metal binding properties of an $Asp^{59} \rightarrow Glu^{59}$ substitution in the calcium specific site. J. Biol. Chem. IN PRESS.

Haiech, J., Klee, C. B. & Demaille, J. G. (1981) Effects of cations on affinity of calmodulin for calcium: Ordered binding of calcium ions allows the specific activation of calmodulin–stimulated enzymes. Biochem. 20, 3890–3897.

Heizmann, C. W. (1984) Parvalbumin, an intracellular calcium–binding protein; distribution, properties and possible roles in mammalian cells. Experientia 40, 910–921.

Hutnik, C. M. L., MacManus, J. P., Banville, D. & Szabo, A. G. (1989) Comparison of metal ion–induced conformational changes in parvalbumin and oncomodulin as probed by the intrinsic fluorescence of tryptophan–102. J. Biol. Chem. SUBMITTED.

Ilich, P., Axelsen, P. H. & Prendergast, F. G. (1988) Electronic transitions in molecules in static external fields. I. Indole and Trp–59 in ribonuclease T_1. Biophys. Chem. 29, 341–349.

Joassin, L. & Gerday, Ch. (1977) The amino acid sequence of the major parvalbumin of the whiting (*Gadus merlangus*). Comp. Biochem. Physiol. 57B, 159–161.

Klee, C. B. & Vanaman, T. C. (1982) Calmodulin. Adv. Protein Chem. 35, 213–321.

Knutson, J. R., Beechem. J. M. & Brand, L. (1983) Simultaneous analysis of multiple fluorescence decay curves: A global approach. Chem. Phys. Lett. 102, 501–507.

Kretsinger, R. H. (1980) Structure and evolution of calcium–modulated proteins. CRC Crit. Rev. Biochem. 8, 119–174.

Kyte, J. & Doolittle, R. F. (1982) A simple method for displaying the hydropathic character of a protein. J. Mol. Biol. 157, 105–132.

Lakowicz, J. R. (1983) In: Principles of Fluorescence Spectroscopy, (Plenum Press, New York).

Lumry, R. & Hershberger, M. (1978) Status of indole photochemistry with special reference to biological applications. Photochem. Photobiol. 27, 819–840.

MacManus, J. P. (1979) Occurrence of a low–molecular–weight calcium–binding protein in neoplastic liver. Cancer Research 39, 3000–3005.

MacManus, J. P. (1981) The stimulation of cyclic nucleotide phosphodiesterase by a M_r 11 500 calcium binding protein from hepatoma. FEBS Lett. 126, 245–249.

MacManus, J. P., Brewer, L. M. & Whitfield, J. F. (1985) The widely–distributed tumour protein, oncomodulin, is a normal constituent of human and rodent placentas. Cancer Letters 27, 145–151.

MacManus, J. P., Hutnik, C. M. L., Sykes, B. D., Szabo, A. G., Williams, T. C. & Banville, D. (1989) Characterization and site–specific mutagenesis of the calcium–binding protein oncomodulin produced by recombinant bacteria. J. Biol. Chem. 264, 3470–3477.

MacManus, J. P., Szabo, A. G. & Williams, R. E. (1984) Conformational changes induced by binding of bivalent cations to oncomodulin, a parvalbumin–like tumour protein. Biochem. J. 220, 261–268.

MacManus, J. P., Watson, D. C. & Yaguchi, M. (1983a) The complete amino acid sequence of oncomodulin — a parvalbumin–like calcium–binding protein from Morris hepatoma 5123tc. Eur. J. Biochem. 136, 9–17.

MacManus, J. P., Watson, D. C. & Yaguchi, M. (1983b) A new member of the troponin C superfamily: Comparison of the primary structures of rat oncomodulin and rat parvalbumin. Biosci. Rep. 3, 1071–1075.

MacManus, J. P. & Whitfield, J. F. (1983) Oncomodulin: A calcium–binding protein from hepatoma. In: Calcium and Cell Function, Ed.: W. Y. Cheung (Academic Press, New York) Vol. 4, pp. 411–440.

Moeschler, H. J., Schaer, J.–J. & Cox, J. A. (1980) A thermodynamic analysis of the binding of calcium and magnesium ions to parvalbumin. Eur. J. Biochem. 111, 73–78.

Mutus, B., Flohr, E. J. & MacManus, J. P. (1985a) Ca^{2+}–specific fluorescence changes in *N*–dansylaminoethyl–labelled oncomodulin. Can. J. Biochem. Cell Biol. 63, 998–1002.

Mutus, B., Karuppiah, N., Sharma, R. K. & MacManus, J. P. (1985b) The differential stimulation of brain and heart cyclic–AMP phosphodiesterase by oncomodulin. Biochem. Biophys. Res. Commun. 131, 500–506.

Mutus, B., Palmer, E. J. & MacManus, J. P. (1988) Disulfide–linked dimer of oncomodulin: Comparison to calmodulin. Biochem. 27, 5615–5622.

Nelson, D. J., Opella, S. J. & Jardetzky, O. (1976) ^{13}C Nuclear magnetic resonance study of molecular motions and conformational transitions in muscle calcium binding parvalbumins. Biochem. 15, 5552–5560.

Palmer, E. J., MacManus, J. P. & Mutus, B. (1989) Inhibition of glutathione reductase by oncomodulin. Arch. Biochem. Biophys. IN PRESS.

Privat, J.–P., Wahl, P. & Auchet, J.–C. (1979) Rates of deactivation processes of indole derivatives in water–organic solvent mixtures — Application to tryptophyl fluorescence of proteins. Biophys. Chem. 9, 223–233.

Redinbaugh, M. G. & Turley, R. B. (1986) Adaptation of the bicinchoninic acid protein assay for use with microtiter plates and sucrose gradient fractions. Anal. Biochem. 153, 267–271.

Ricci, R. W. & Nesta, J. M. (1976) Inter– and intramolecular quenching of indole fluorescence by carbonyl compounds. J. Phys. Chem. 80, 974–980.

Ross, J. B. A., Laws, W. R., Rousslang, K. W. & Wyssbrod, H. R. (1989) Tyrosine fluorescence and phosphorescence from proteins and polypeptides. In: Fluorescence Spectroscopy, Biochemical Applications, Ed.: J. R. Lakowicz Vol. 2, IN PRESS.

Schauerte, J. A. & Gafni, A. (1989) Long–lived tryptophan fluorescence in phosphoglycerate mutase. Biochem. 28, 3948–3954.

Sekharudu, Y. C. & Sundaralingam, M. (1988) A structure–function relationship for the calcium affinities of regulatory proteins containing 'EF–hand' pairs. Protein Engineering 2, 139–146.

Skalski, N., Rayner, D. M. & Szabo, A. G. (1980) Ground–state complexes between polar solvents and 1–methylindole: The origin of the Stokes' shift in their fluorescence spectra. Chem. Phys. Lett. 70, 587–590.

Strynadka, N. C. J. & James, M. N. G. (1989) Crystal structures of the helix–loop–helix calcium–binding proteins. Annu. Rev. Biochem. 58, 951–998.

Szalay, L. & Szollosy, L. (1964) Investigations on the connection of polarization and foreign quenching in fluorescent solutions. Acta Phys. Chem. 10, 3–8.

Tanaka, T. & Hidaka, M. (1980) Hydrophobic regions function in calmodulin–enzymes(s) interactions. J. Biol. Chem. 255, 11078–11080.

Tournon, J., Kuntz, E. & El–Bayoumi, M. A. (1972) Fluorescence quenching in phenylalanine and model compounds. Photochem. Photobiol. 16, 425–433.

Van Durren, B. L. (1961) Solvent effects in the fluorescence of indole and substituted indoles. J. Org. Chem. 26, 2954–2960.

Williams, T. C., Corson, D. C., Oikawa, K., McCubbin, W. D., Kay, C. M. & Sykes, B. D. (1986) ^{1}H NMR spectroscopic studies of calcium–binding proteins. 3. Solution conformations of rat apo–α–parvalbumin and metal–bound rat α–parvalbumin. Biochem. 25, 1835–1846.

Williams, T. C., Corson, D. C., Sykes, B. D. & MacManus, J. P. (1987) Oncomodulin. ^{1}H NMR and optical stopped–flow spectroscopic studies of its solution conformation and metal–binding properties. J. Biol. Chem. 262, 6248–6256.

Wnuk, W., Cox, J. A. & Stein, E. A. (1982) Parvalbumins and other soluble high–affinity calcium–binding proteins from muscle. Calcium Cell Function 2, 243–278.

Chapter 6

PROBING THE BINDING SITES IN ONCOMODULIN — METAL ION INDUCED CONFORMATIONAL EFFECTS

6.1 Introduction

In Chapter 5, oncomodulin was introduced as a small, acidic calcium–binding protein having a parvalbumin–like structure, but certain calmodulin–like modulator functions. As a definite link between calcium–dependent conformational changes and modulator functions has been established for calmodulin (Van Eldik et al., 1982), the possibility was examined in Chapter 5 that differences in Ca^{2+}–induced conformational responses existed in oncomodulin and parvalbumin. Such differences could be the reason why oncomodulin does possess certain modulator functions, but parvalbumin does not.

The comparison of Ca^{2+}–induced conformational changes was performed by making use of the fluorescence properties of a single tryptophan residue which occurs naturally in position–102 of cod III parvalbumin, and which was placed in the same position in a site–specific mutant of oncomodulin, F102W. In Figure 5.1 it was shown that the tryptophan probe was positioned within the hydrophobic core of the protein, situated approximately 11 Å equidistant from both metal–binding sites. In the region probed by tryptophan–102, oncomodulin was shown to be less conformationally variable, and to possess a more limited conformational response upon Ca^{2+}–binding when compared to cod III parvalbumin. The conformational responses in both oncomodulin and cod III parvalbumin were shown to be Ca^{2+}–specific.

As the lower affinity CD–site (Williams et al., 1987) in oncomodulin is thought to be the most likely site involved in manifesting the regulatory properties of the protein (MacManus et al., 1984), it was curious that only minor fluorescence changes (< 12%) were experienced by tryptophan–102 upon the addition of a second

equivalent of Ca^{2+} to the apoprotein solution. As dramatic effects on cell function could result depending upon whether oncomodulin was turned "on" or "off", it was initially surprising that only minor changes could be found associated with the interaction of oncomodulin with a second equivalent of Ca^{2+}. This second equivalent would presumably bind to the putative regulatory CD–site. However, as the Trp–102 probe is located in the hydrophobic core, it is possible that this region is not directly involved in manifesting the regulatory properties. These results suggested that another region of the protein may be the more likely locus of important conformational changes induced by the binding of the second Ca^{2+} equivalent. However, previous studies had shown that another site located in the non–metal ion binding AB–loop on the opposite face of oncomodulin relative to the two Ca^{2+}–binding loops was also unaffected by the binding of the second equivalent of Ca^{2+} (Mutus et al., 1985). These studies showed that the second equivalent of Ca^{2+} had no detectable conformational influence in the region probed by the fluorescent reagent *N*–dansylaziridine conjugated to Cys–18 (Mutus et al., 1985).

Previous studies had also shown that the fluorescence emission of the tyrosine residues in native oncomodulin was sensitive to Ca^{2+}–induced conformational changes (MacManus et al., 1984). These residues are located in the vicinity of the CD–site, where the amide carbonyl of tyrosine–57 functions as a calcium ligand in the CD–loop and tyrosine–65 lies in the flanking D–helix of this loop (See Figure 5.2). However, as the measured fluorescence signal was the sum of emissions from two probed positions, and no attempt was made to monitor fluorescence changes upon Ca^{2+} titration of the apoprotein, it was largely speculation that led to the conclusion that the region probed by tyrosine–65 was

experiencing the most significant Ca^{2+}–specific conformational changes (MacManus et al., 1984). The assignment was made based upon the influence of Ca^{2+}–binding on the fluorescence excitation spectrum of oncomodulin and by an examination of the phenylalanine residues in a model of oncomodulin which was built based upon carp pI 4.25 parvalbumin coordinates (Moews & Kretsinger, 1975). In the presence of Ca^{2+}, but not Mg^{2+}, the fluorescence excitation spectrum of oncomodulin possessed an increase in both structure and intensity at the high energy end (blue–edge) relative to the spectrum of the apoprotein. Examination of the molecular model of oncomodulin suggested that Tyr–65 was the residue responsible for the excitation spectral changes owing to its location and orientation relative to the Phe residues (most likely Phe–49 or Phe–47); Tyr–57 was considered to be ill–positioned to account for the spectroscopic observations (MacManus et al., 1984).

The purpose of the present study was to examine in detail the nature of localized metal ion–induced conformational changes in the two binding loops of oncomodulin. Specifically, a search was made for significant conformational effects associated with the binding of the second Ca^{2+} equivalent. This was investigated by an examination of the fluorescence properties of five site–specific mutants in which Phe and Trp had been selectively placed. The first two mutations involved the substitution of Phe in placed of each tyrosyl residue (Y57F and Y65F). Because emission from Phe is not observed when this residue is excited at 280 nm (See Section 1.3), these mutations allowed each site probed by the remaining Tyr residue to be examined individually. As Trp is much more sensitive than Tyr to the polarity of its surrounding environment (See Section 1.3.1), the second set of mutations involved the substitution of Trp for Tyr in positions 57 and 65 (Y57W and Y65W). Since Tyr–57 and Tyr–65 are largely associated with the CD–loop, it

was desirable to select a position in the EF–loop for the installation of another Trp probe. As the amide carbonyl of Lys–96 functions in the EF–loop as a Ca^{2+}–binding ligand in the analogous position as Tyr–57 in the CD–loop (Figure 5.2), the final mutant was created by substitution of Trp for Lys in position–96 (K96W). Figure 6.1 highlights the positions of these mutations relative to the two calcium–binding loops.

6.2 Materials and Methods

Materials. All materials were the same as described in Sections 4.2 and 5.2. In addition, L–tyrosine was purchased from Aldrich Chemical Co., Milwaukee, Wisconsin.

Methods. The mutagenesis, plasmid characterization by DNA sequencing and expression of recombinant oncomodulin were performed by Dr. D. Banville at the Biotechnology Research Institute in Montreal, Quebec, and the proteins were purified to homogeneity and provided by Dr. J. MacManus, Division of Biological Sciences, NRC. Additional information regarding these procedures is given in Section 5.2. Native rat oncomodulin from Morris hepatoma 5123tc was also purified (MacManus, 1980) and provided by Dr. MacManus.

As described in Section 5.2, proteins were decalcified by precipitation with trichloroacetic acid (TCA) (Haiech et al., 1981) and concentrations of the mutant proteins were determined using the Pierce bicinchoninic acid (BCA) protein assay reagent. The steady–state and time–resolved spectroscopic data were collected as described in Chapter 2 and Section 4.2.5. Fluorescence quantum yields (ϕ_f) were measured at 20°C using L–tyrosine (recrystallized three times from water prior to use) for the Tyr–containing mutants and N–acetyltryptophanamide (NATA) for

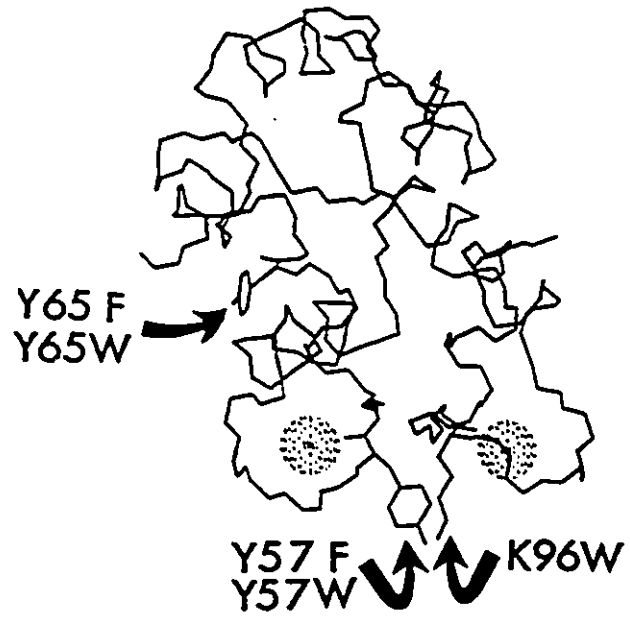

Figure 6.1: X–ray crystallographic structure of oncomodulin highlighting the native residues tyrosine–57, tyrosine–65 and lysine–96, and the identity of the point mutations at each position. The atomic spheres of the calcium ions are also shown in the CD–site at the bottom, left–hand side of the figure, and the EF–site, at the bottom right–hand side of the figure.

the Trp–containing mutants as the quantum yield standards. Each standard was dissolved in the same buffer as the protein solutions, pH 7, and was bubbled with nitrogen gas for 10 minutes prior to measurement. When the ϕ_f was being measured, the absorbance of all solutions at the excitation wavelength was less than 0.10. All spectroscopy was done with protein samples dissolved in 10 mM cacodylate buffer containing 150 mM KCl, pH 7.

6.3 Results

6.3.1 Bacterial Versus Native Protein

Previous analysis showed that the bacterial recombinant oncomodulin (BRONCO) was identical to the native hepatoma protein in all residues, but with 50–60% of the expressed protein still retaining the initiation amino acid N–formyl–methionine (MacManus et al., 1989). Thus in addition to BRONCO, a recombinant protein known as MAP–BRONCO (methionine amino peptidase–bacterial recombinant oncomodulin) was also examined which possessed the homogeneous N–terminal serine residue. The ultraviolet absorption spectra of native tumour oncomodulin, BRONCO and MAP–BRONCO were identical with the characteristic fine structure associated with Phe being apparent in the region 260–280 nm (Figure 6.2). The corrected steady–state fluorescence emission spectra, normalized at the emission maxima, (Figure 6.3) and quantum yields of fluorescence (ϕ_f) (Table 6.1) of these proteins were also very similar, with the spectra of the bacterial proteins being identical to the spectrum of L–tyrosine. Although there was a slight increase in the emission of the native tumour oncomodulin at the low energy end (red–edge) of the spectrum, none of the spectra showed any evidence of

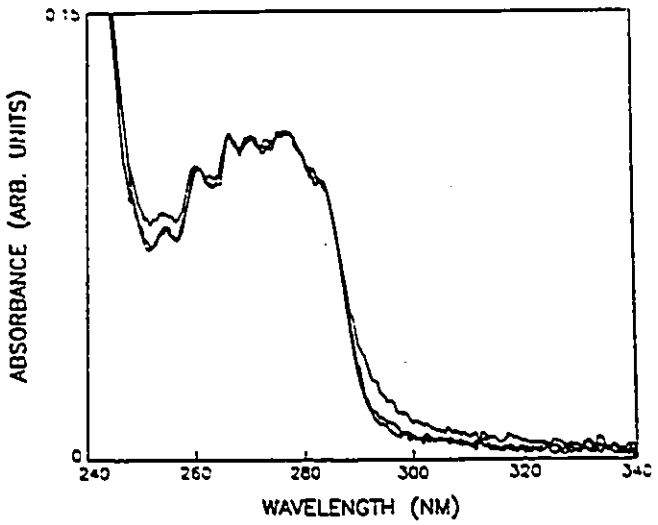

Figure 6.2: Superimposition of the ultraviolet absorption spectra of holo native tumour oncomodulin, bacterial recombinant oncomodulin (BRONCO), and methionine amino peptidase–bacterial recombinant oncomodulin (MAP–BRONCO). The proteins were in 10 mM cacodylate buffer containing 150 mM KCl, pH 7.0.

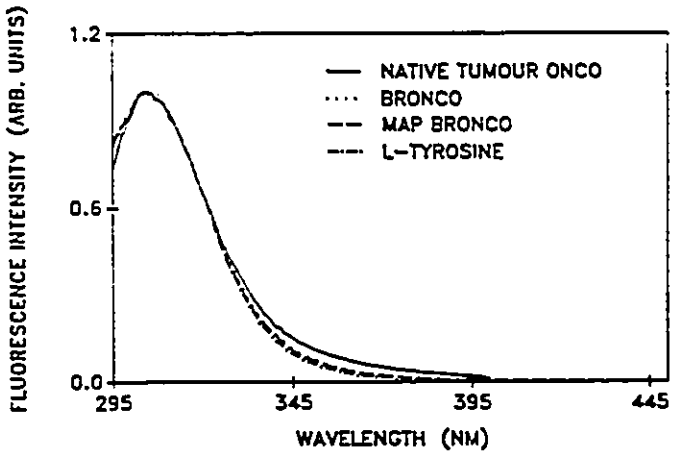

Figure 6.3: Corrected steady–state fluorescence emission spectra of native tumour oncomodulin, bacterial recombinant oncomodulin (BRONCO), methionine amino peptidase–bacterial recombinant oncomodulin (MAP–BRONCO) and L–tyrosine all normalized to a value of 1 at the emission maximum. The protein concentrations were 20 – 40 μM, λ_{ex} = 280 nm, excitation and emission slits = 4 nm, 20°C. The proteins were in the same buffer as described in Figure 6.2.

TABLE 6.1

Quantum yield summary of the tyrosine-containing oncomodulin proteins. λ_{ex} = 280 nm; 20°C. All values were obtained relative to L-tyrosine measured under identical conditions. The errors quoted are standard errors of the mean obtained from at least three determinations of the ϕ_f of each sample. The protein concentrations were 20–40 μM and Ca^{2+}(aq) and Mg^{2+}(aq) were added to a final concentration of 2.5 mM and 5 mM, respectively.

Protein	Holo	Apo	Apo + Ca^{2+}	Apo + Mg^{2+}
Native oncomodulin	0.052 ± 0.004	0.037 ± 0.003	0.052 ± 0.004	0.046 ± 0.004
BRONCO	0.055 ± 0.002	0.036 ± 0.002	0.054 ± 0.005	0.047 ± 0.003
MAP-BRONCO	0.052 ± 0.003	0.036 ± 0.002	0.052 ± 0.003	0.044 ± 0.003
Y57F	0.016 ± 0.004	0.023 ± 0.003	0.018 ± 0.004	0.023 ± 0.003
Y65F	0.072 ± 0.002	0.041 ± 0.003	0.074 ± 0.003	0.057 ± 0.005

any shoulder, or significant signal in this region (330–370 nm). Upon decalcification, the ϕ_f of all three proteins decreased by 32% from a mean value of

0.053 ± 0.001 to a mean value of 0.036 ± 0.001 when excited at 280 nm (See Table 6.1). Addition of a 100–fold excess of Ca^{2+} (aq) to the apoprotein solutions restored 100% of the fluorescence intensity at the wavelength of maximum emission, λ_{max} = 304 nm. In contrast, addition of a 200–fold excess of Mg^{2+} (aq) to the apoprotein solutions restored only 61% of the fluorescence intensity which was lost upon decalcification. These spectral changes are shown for BRONCO in Figure 6.4. The mean value of the ϕ_f for the Mg^{2+}–substituted proteins was 0.046 ± 0.002. Each apoprotein responded to metal ion titration in a similar manner. Ca^{2+} titration revealed that greater than 94% of the total fluorescence change was complete upon addition of the first equivalent of Ca^{2+} (Figure 6.5). Mg^{2+} titration revealed a much more gradual response, with plateau fluorescence values occurring only after the addition of 3–4 equivalents of Mg^{2+} (Figure 6.6).

6.3.2 The Tyrosine–Containing Mutant Proteins

The substitution of Phe into the place of each tyrosyl residue allowed the site probed by each of these latter residues to be examined independently by excitation at 280 nm. The absorption spectra of the holo (Ca^{2+}– containing) mutant proteins both showed increased intensity of the structured Phe bands in the region of 260–280 nm relative to the intensity of the Tyr absorption maximum at 280 nm (Figures 6.7 A and B). The enhancement of these Phe absorption bands was more pronounced for Y65F when compared to Y57F. Decalcification resulted in a further decrease of the extinction in the region of 280–290 nm which enhanced the Phe absorption bands to an even greater extent (Figure 6.7 A and B). This latter effect may be the result of a reduction in the amount of scattered light generated by the sample as witnessed in the closer–to–baseline tail of the spectra in the region

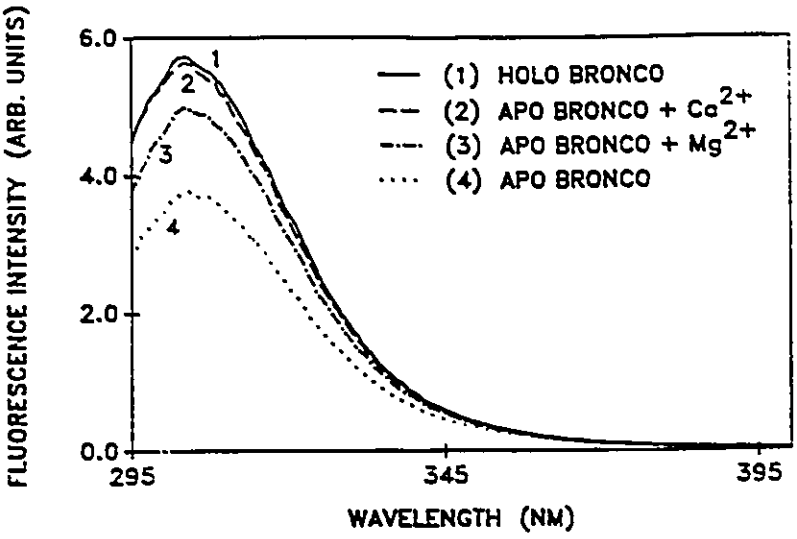

Figure 6.4: Corrected steady–state fluorescence emission spectra of bacterial recombinant oncomodulin (BRONCO) showing the response of the apo (Ca^{2+}–free) protein to Ca^{2+} (aq) and Mg^{2+} (aq) addition. The protein concentration was approximately 25 μM. $CaCl_2$ was added to a final concentration of 2.5 mM and $MgCl_2$ was added to a final concentration of 5 mM.

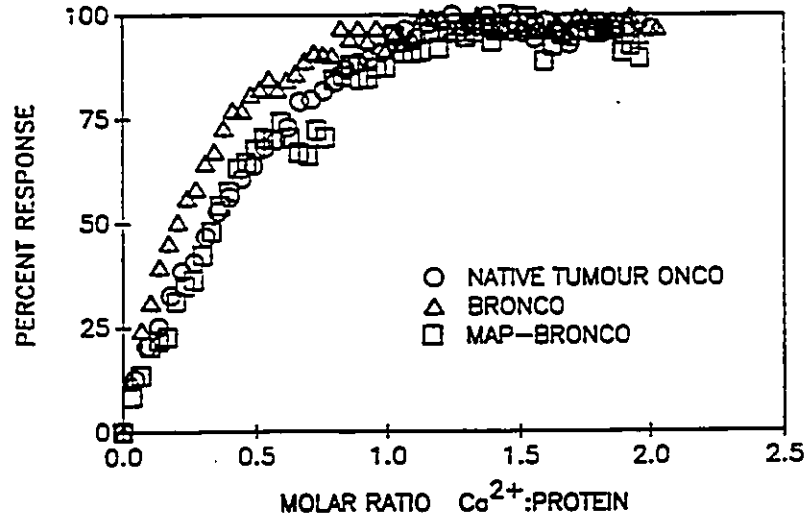

Figure 6.5: Ca^{2+} titration curves of apo (Ca^{2+}–free) native tumour oncomodulin (○), bacterial recombinant oncomodulin (BRONCO, △) and methioninc amino peptidase–bacterial recombinant oncomodulin (MAP–BRONCO, □), plotted in terms of the fluorescence intensity change upon Ca^{2+} titration. λ_{ex} = 280 nm; λ_{em} = 306 nm, 20°C. Two μL aliquots of 1 mM $CaCl_2$ were added to 1.5 mL of a stirred solution of apoprotein.

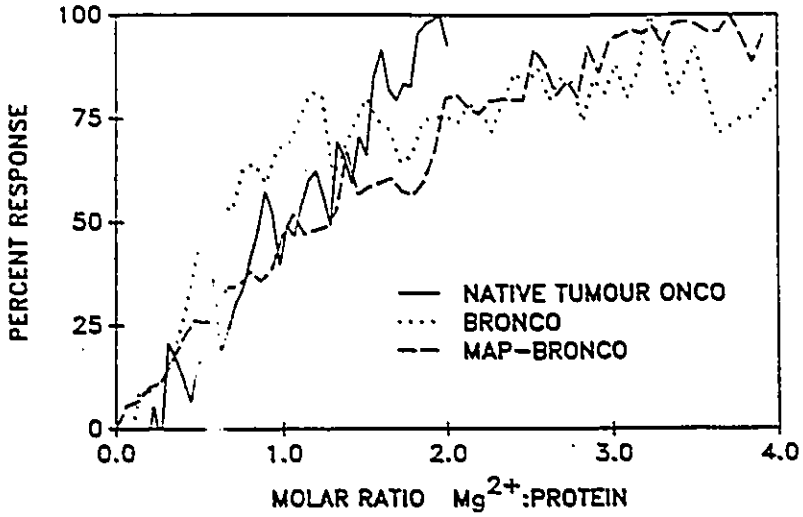

Figure 6.6: Mg^{2+} titration of apo (Ca^{2+}–free) native tumour oncomodulin (——), bacterial recombinant oncomodulin (BRONCO, ·····) and methionine amino peptidase–bacterial recombinant oncomodulin (MAP–BRONCO, — —), plotted in terms of the fluorescence intensity change upon Mg^{2+} addition. λ_{ex} = 280 nm; λ_{em} = 306 nm; 20°C. Two μL aliquots of 2 mM $MgCl_2$ were added to 1.5 mLs of a stirred solution of apoprotein.

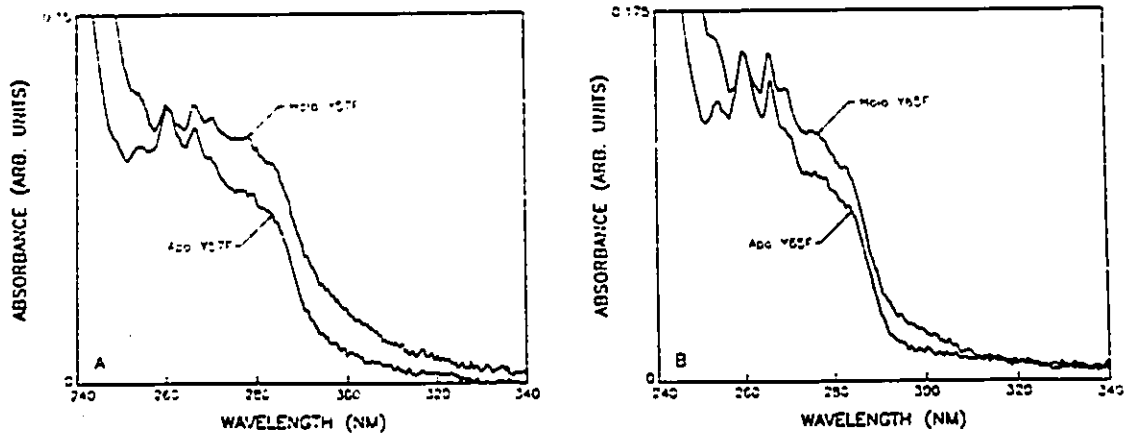

Figure 6.7: Ultraviolet absorption spectra of holo and apo (A) Y57F and (B) Y65F oncomodulin mutant proteins. The proteins were in 10 mM cacodylate buffer, containing 150 mM KCl, pH 7.0. The holo solutions also contained 1 μM $CaCl_2$ (aq).

290–320 nm.

The corrected steady–state fluorescence emission spectra of both the holo and apo (Ca^{2+}–free) mutant proteins had λ_{max} in the identical position as BRONCO (λ_{max} = 304 nm). Decalcification of Y65F resulted in a 55% decrease in the fluorescence intensity whereas the spectrum of Y57F experienced an 85% increase in fluorescence intensity at 304 nm upon decalcification (Figure 6.8). The ϕ_f of Y65F (0.072 ± 0.005) was approximately 5 times greater than the ϕ_f for Y57F (0.016 ± 0.006) (See Table 6.1). The fluorescence excitation spectra of the two mutant proteins showed opposite effects upon decalcification. In the absence of Ca^{2+}, the spectrum of Y57F showed a greater extent of structure and intensity at the blue–edge of the spectrum whereas the opposite was true for Y65F (Figures 6.9 A and B). Ca^{2+} titration of the changes in the fluorescence excitation spectrum of Y65F (λ_{ex} = 245nm; λ_{em} = 306nm) revealed that greater than 84% of the fluorescence changes were complete upon addition of one Ca^{2+} equivalent (Figure 6.10). Mg^{2+} addition had no effect upon the fluorescence excitation spectra of either Y65F or Y57F. Ca^{2+} and Mg^{2+} titration of apo Y65F produced changes in the fluorescence emission spectrum (λ_{ex} = 280 nm; λ_{em} = 306 nm) which followed similar patterns when compared to that of BRONCO (Figures 6.11 and 6.12, respectively). However, a greater percentage of the fluorescence change was complete after addition of one equivalent of Ca^{2+} to BRONCO (97%) when compared to Y65F (81%). Further, the changes upon Mg^{2+} titration of Y65F did not plateau, even after addition of 4 metal ion equivalents. The titration curves of Y57F were similar in shape to Y65F, but were considerably more noisy owing to the weak fluorescence of this protein.

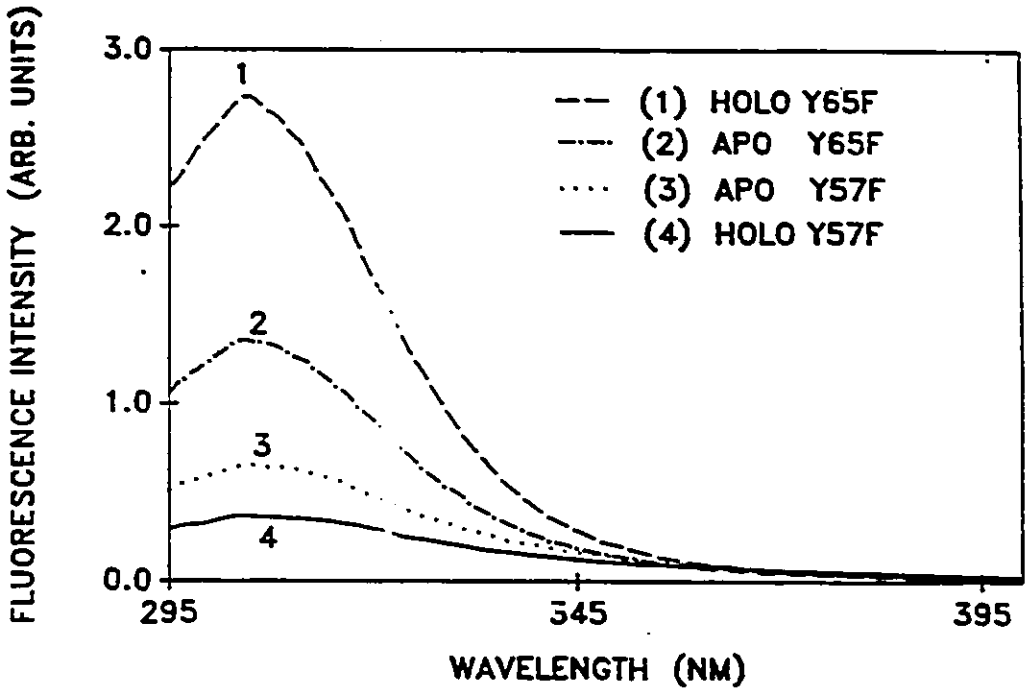

Figure 6.8: Corrected steady–state fluorescence emission spectra of Y57F and Y65F oncomodulin mutant proteins in the absence (apo) and presence (holo) of Ca^{2+}. Decalcification of Y65F resulted in a 55% decrease in the fluorescence intensity (Spectrum (1) → (2)), whereas the spectrum of Y57F experienced an 85% increase in fluorescence intensity at 304 nm upon decalcification (Spectrum (4) → (3)). The protein concentrations were approximately 25 μM, λ_{ex} = 280 nm, excitation and emission slits = 4 nm, 20°C. The proteins were in the same buffer as described in Figure 6.7.

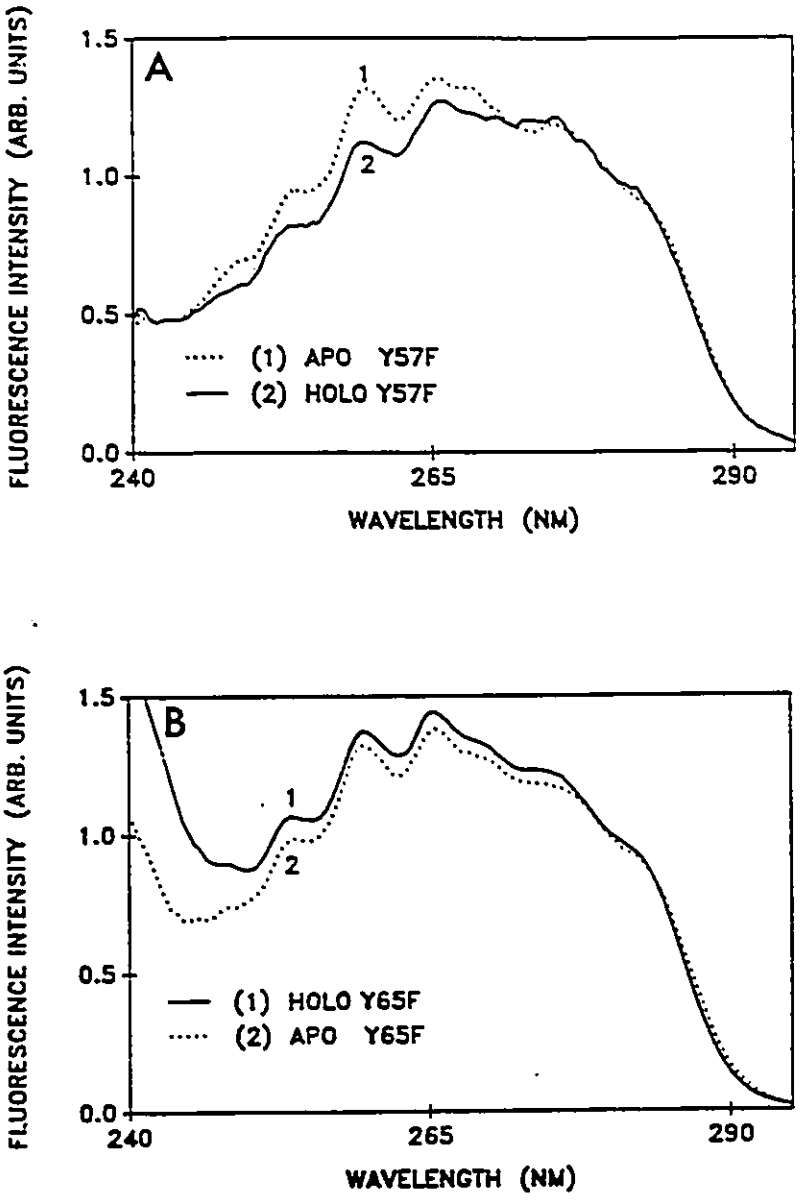

Figure 6.9: Uncorrected fluorescence excitation spectra of apo (Ca^{2+}–free) and holo (A) Y57F and (B) Y65F oncomodulin mutant proteins. The spectra of the holo proteins are shown with solid lines, while those of the apo proteins are shown with dotted lines. Decalcification promoted opposite trends in the spectral intensity in the region of 240 – 260 nm. The protein concentrations were approximately 25 μM. The proteins were dissolved in 10 mM cacodylate buffer, containing 150 mM KCl, pH 7.0. λ_{em} = 306 nm, excitation and emission slits = 4 nm, 20°C.

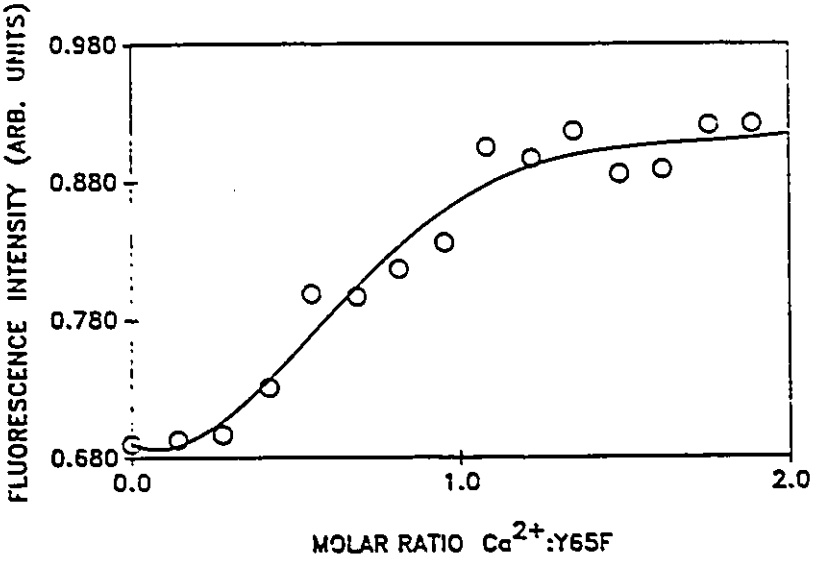

Figure 6.10: Changes in the fluorescence excitation spectrum of apo (Ca^{2+}–free) Y65F monitored at an excitation wavelength = 245 nm and an emission wavelength = 306 nm upon Ca^{2+} titration. The line drawn through the data points was the "best–fit" line obtained upon 5th order polynomial regression analysis.

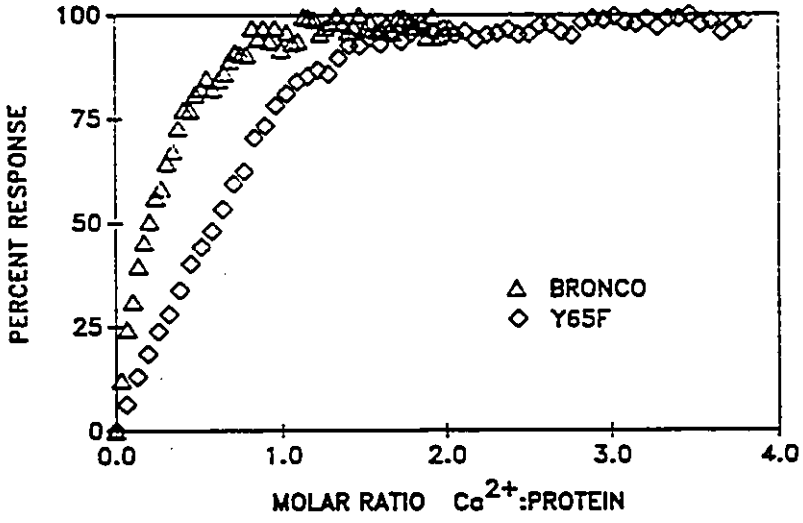

Figure 6.11: Ca^{2+} titration curves of apo (Ca^{2+}–free) bacterial recombinant oncomodulin (BRONCO, △) and Y65F oncomodulin mutant protein (◇) plotted in terms of the fluorescence intensity change upon Ca^{2+} (aq) addition. Two μL aliquots of 1 mM $CaCl_2$ were added to 1.5 mL of a stirred solution of apoprotein. λ_{ex} = 280 nm; λ_{em} = 306 nm, 20°C.

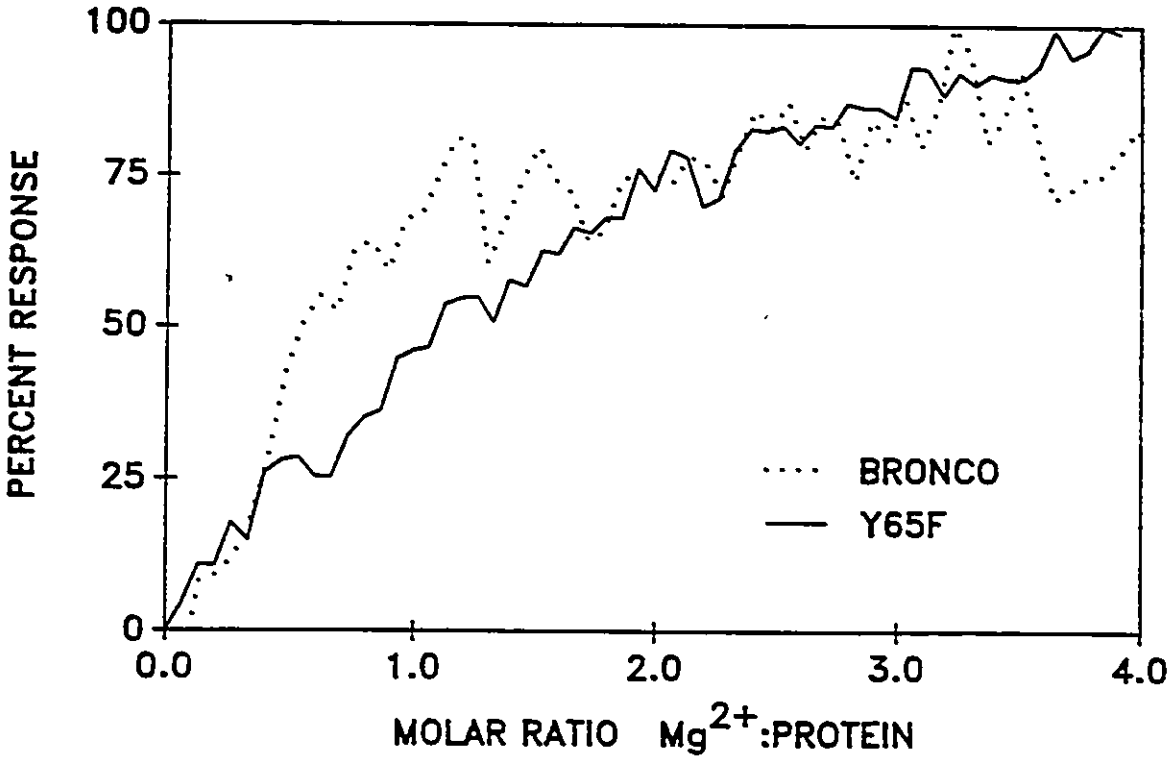

Figure 6.12: Mg^{2+} titration curves of apo (Ca^{2+}–free) bacterial recombinant oncomodulin (BRONCO, dotted line) and Y65F oncomodulin mutant protein (solid line) plotted in terms of the fluorescence intensity change upon Mg^{2+} (aq) addition. Two μL aliquots of a 2 mM $MgCl_2$ solution were added to 1.5 mL of a stirred apo protein solution. λ_{ex} = 280 nm; λ_{em} = 306 nm; 20°C.

Time–resolved fluorescence revealed that all of the tyrosine–containing proteins were best fit by a triple exponential decay function either in the presence or absence of Ca^{2+}. In Table 6.2 the fluorescence decay parameters obtained at an excitation wavelength of 284 nm and an emission wavelength of 310 nm are shown, together with the intensity–weighted (mean) lifetime. The intensity–weighted mean lifetime ($<\tau>$) was calculated using equation 5.1. The lifetime values of Y65F more closely resembled those of BRONCO when compared to the values of Y57F. The intensity–weighted lifetime, $<\tau>$, of Y65F decreased by approximately 18% upon decalcification, whereas the ϕ_f decreased to a much greater degree (43%). The fractional fluorescence of the longest lived decay component (F_1) decreased in both BRONCO and Y65F upon Ca^{2+} removal, whereas the F_2 and F_3 values for the middle and shortest lived decay components, respectively, increased. The fluorescence parameters of Y57F were significantly different when compared to the other two proteins. Instead of quenching, decalcification induced an enhancement of the tyrosine fluorescence. The ϕ_f increased by 53%, whereas the mean lifetime increased by only 4%. The lifetime values of the longest and middle decay components were significantly less both in the presence and absence of Ca^{2+} when compared to BRONCO and Y65F.

6.3.3 The Tryptophan–Containing Mutant Proteins

The absorption spectra of Y57W, Y65W and K96W were similar both in the absence and presence of Ca^{2+} (Figures 6.13 A and B). The spectra of holo Y57W and Y65W possessed a slight shoulder at 292 nm; such a feature was absent in the absorption spectrum of K96W. Decalcification in all cases promoted a small

TABLE 6.2

Various steady-state and time-resolved fluorescence decay parameters of the tyrosine-containing recombinant oncomodulin proteins BRONCO, Y57F and Y65F. λ_{ex} = 284 nm; λ_{ex} = 310 nm; 20°C.

Sample[a]	ϕ_c[b]	SVR[c]	SIGMA[c]	τ_1 (ns)	τ_2 (ns)	τ_3 (ns)	F_1[d]	F_2	F_3	<τ>[e] (ns)	<τ> Holo / <τ> Apo	ϕ_c Holo / ϕ_c Apo
Holo BRONCO	0.055 ± 0.003	2.00	1.04	3.19 ± 0.02	1.04 ± 0.05	0.322 ± 0.015	0.71	0.21	0.08	2.51	1.23	1.53
Apo BRONCO	0.036 ± 0.002	1.96	1.05	2.87 ± 0.03	1.13 ± 0.04	0.289 ± 0.011	0.58	0.32	0.10	2.04		
Holo Y57F	0.015 ± 0.004	1.89	1.14	2.95 ± 0.06	0.81 ± 0.03	0.278 ± 0.010	0.28	0.48	0.24	1.28	0.96	0.65
Apo Y57F	0.022 ± 0.003	1.85	0.99	3.07 ± 0.03	0.85 ± 0.04	0.245 ± 0.007	0.48	0.33	0.19	1.33		
Holo Y65F	0.072 ± 0.002	1.99	1.02	3.22 ± 0.02	1.58 ± 0.05	0.058 ± 0.009	0.80	0.19	0.01	2.89	1.21	1.76
Apo Y65F	0.041 ± 0.003	1.92	1.01	2.90 ± 0.02	1.11 ± 0.06	0.267 ± 0.011	0.68	0.22	0.10	2.39		

[a] All protein samples were in 10 mM cacodylate, 150 mM KCl, pH 7.0. In addition, 1 μM $CaCl_2$ was added to the holo samples to ensure complete occupancy of the metal-binding sites.
[b] The ϕ_c values were measured relative to L-tyrosine, λ_{ex} = 280 nm.
[c] SVR refers to the serial variance ratio which is a statistical parameter defined in equation 2.8. The SIGMA statistical parameter is defined in equation 2.7. "Ideal" statistical fits correspond to an SVR = 2 and SIGMA = 1.
[d] F_i denotes the fractional fluorescence of the ith decay time component.
[e] <τ> is the mean or intensity-weighted lifetime (defined in equation 3.1).

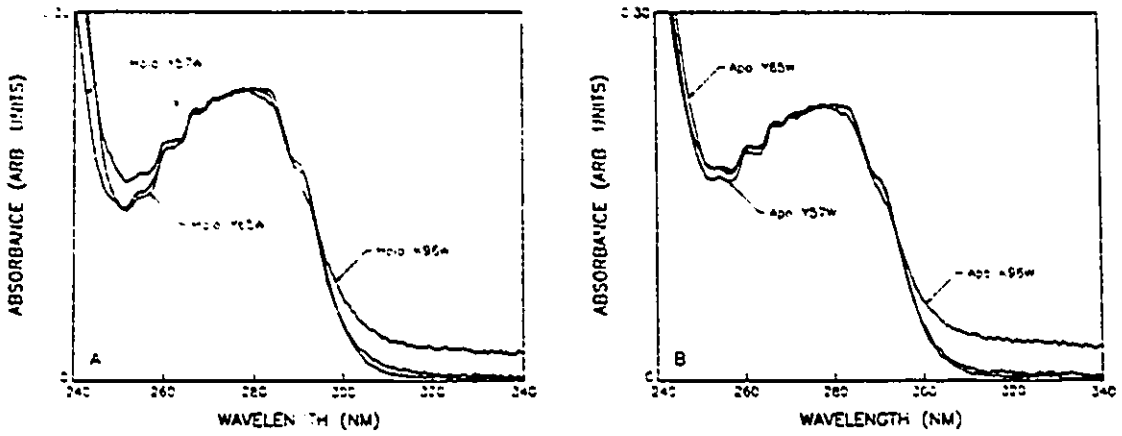

Figure 6.13: Ultraviolet absorption spectra of (A) holo and (B) apo (Ca^{2+}–free) Y57W, Y65W, and K96W oncomodulin mutant proteins. The proteins were in 10 mM cacodylate buffer, containing 150 mM KCl, pH 7.0. The holo solutions also contained 1 μM $CaCl_2$.

increase in intensity in the region of 260–280 nm of the absorption spectra. The spectra of both holo and apo K96W showed increased absorbance in the red–edge tail (in the region 300 – 340 nm) indicating a more significant extent of light scattering when compared to the spectra of the other two proteins.

Selective excitation of the single Trp residues at 295 nm showed that only Trp in position–57 was perturbed to a significant extent upon decalcification (Figure 6.14). The ϕ_f of Y57W increased from 0.078 ± 0.003 to 0.133 ± 0.003 (1.7–fold) upon Ca^{2+} removal. Although slight, decalcification resulted in a decrease in the fluorescence emission of Trp in positions 65 and 96. The ϕ_f of Y65W decreased by 9% from 0.157 ± 0.003 to 0.143 ± 0.002, and the ϕ_f of K96W decreased by 6% from 0.084 ± 0.004 to 0.079 ± 0.003 upon Ca^{2+} removal. The λ_{max} of the emission spectra of Y65W and K96W were slightly blue–shifted by 3–4 nm upon decalcification while in contrast, no change was observed in the wavelength position of the emission maximum of Y57W. In all cases, addition of Ca^{2+} to the apoproteins restored 100% of the fluorescence intensity, while Mg^{2+} addition had only a minor influence when compared to the intensity of the apoprotein (Figure 6.14).

Upon excitation of both Tyr–65 and Trp–57 in Y57W at 280 nm, similar results were obtained when compared to 295 nm excitation (Figures 6.14 A and 6.15 A). No significant shoulder at 304 nm was evident. In contrast, excitation of Y65W at 280 nm revealed notable intensity changes at 304 nm, even though minor changes were noted at 350 nm (Figure 6.15 B). The 304 nm intensity was greatest in the presence of Ca^{2+}, while Mg^{2+} addition produced intensity values intermediate between the intensities observed for the holo and apo proteins.

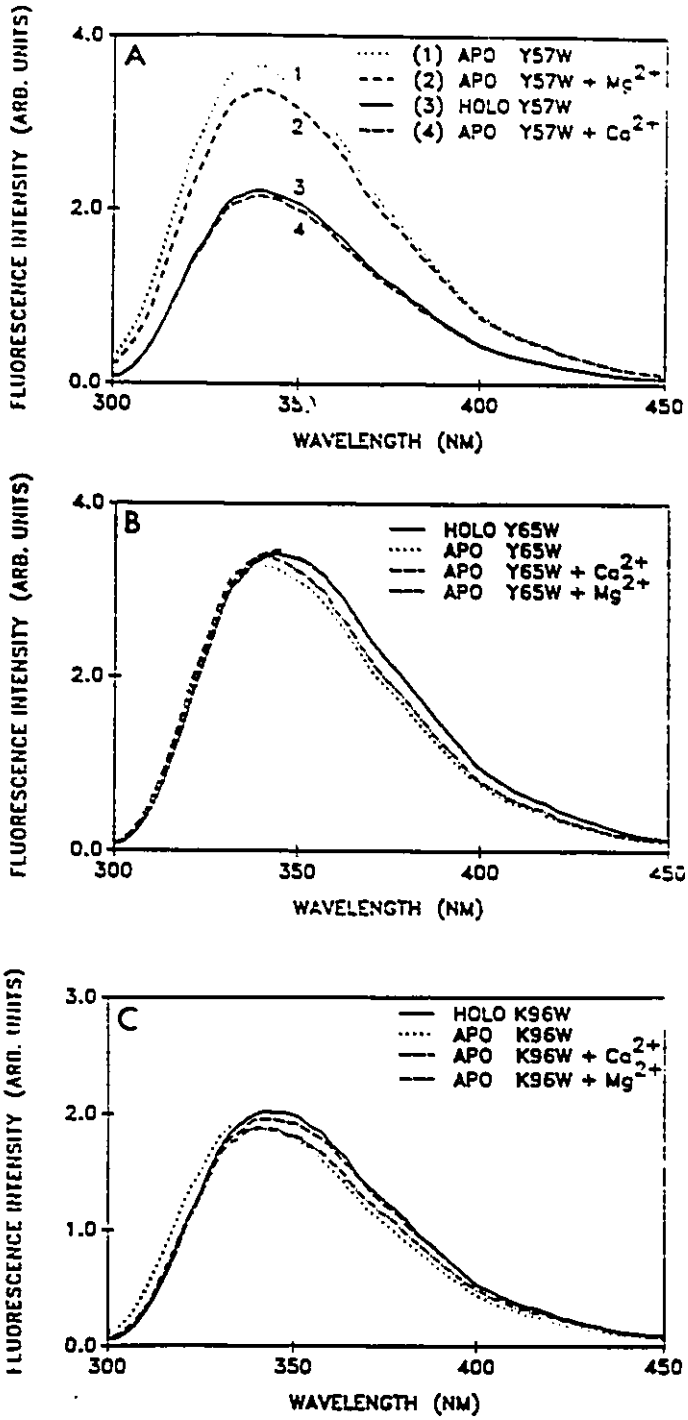

Figure 6.14: Corrected steady–state emission spectra of (A) Y57W, (B) Y65W, and (C) K96W showing the response of the proteins to Ca^{2+} (aq) and Mg^{2+} (aq) addition when excited at 295 nm. The protein concentration was approximately 25 μM. $CaCl_2$ was added to a final concentration of 2.5 mM and $MgCl_2$ was added to a final concentration of 5 mM. Excitation and emission slits = 4 nm, 20°C. The only protein to show a major effect upon decalcification was Y57W, in which decalcification promoted a 1.7–fold increase in the quantum yield of fluorescence (Spectrum (3) → (1) in A).

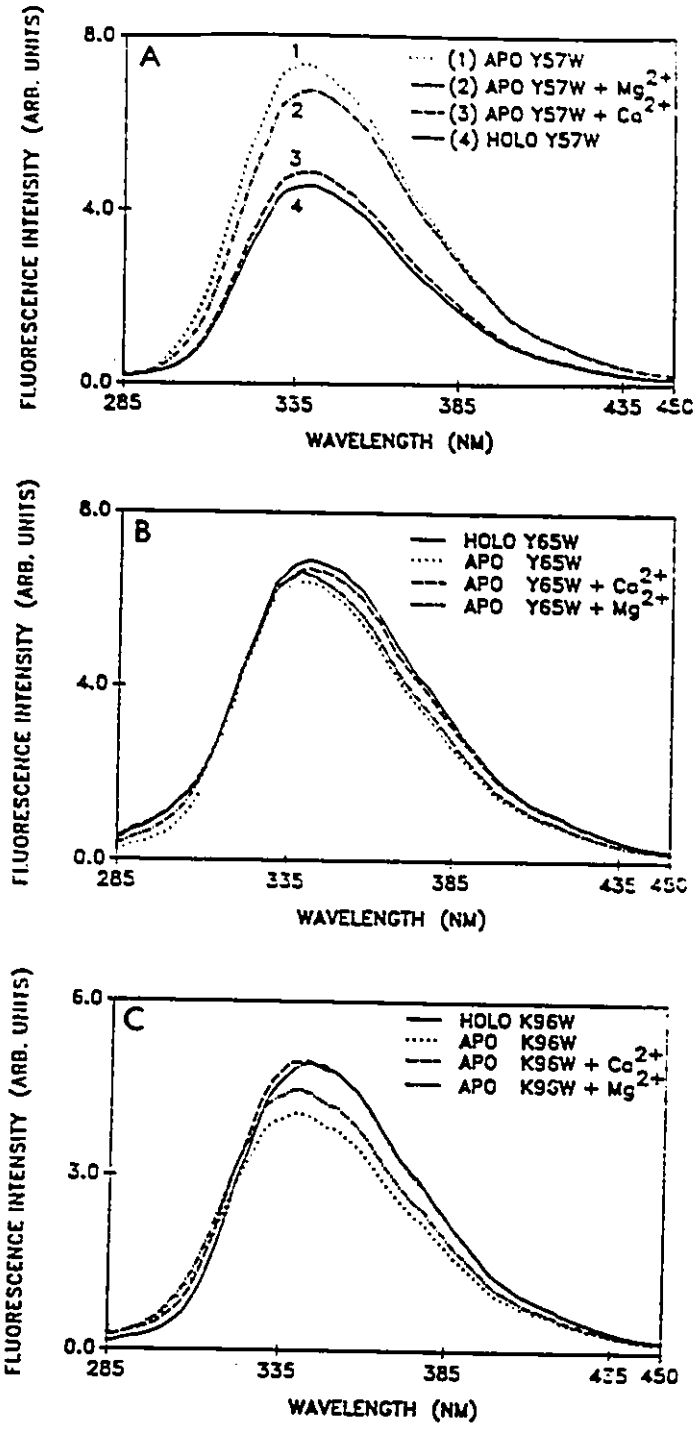

Figure 6.15: Corrected steady–state emission spectra of (A) Y57W, (B) Y65W, and (C) K96W showing the response of the proteins to Ca^{2+} (aq) and Mg^{2+} (aq) addition when excited at 280 nm. The protein concentration was approximately 25 μM. $CaCl_2$ was added to a final concentration of 2.5 mM and $MgCl_2$ was added to a final concentration of 5 mM. Excitation and emission slits = 4 nm, 20°C.

Excitation of K96W at 280 nm produced a more quantitatively dramatic result when compared to the same protein excited at 295 nm (Figures 6.14 C and 6.15 C). Compared to the 6% decrease in fluorescence intensity upon decalcification at λ_{ex} = 295 nm, an 18% decrease was observed when λ_{ex} = 280 nm. While Ca^{2+} addition to K96W restored 100% of the fluorescence intensity, Mg^{2+} addition restored only 44% of the fluorescence intensity which was lost upon Ca^{2+} removal (λ_{ex} = 280 nm). The λ_{max} upon excitation at 280 nm was essentially identical for all three proteins both in the absence and presence of Ca^{2+}, with Y57W being only slightly blue–shifted (by 3–4 nm) relative to Y65W and K96W.

Ca^{2+} titration revealed that the various apoproteins experienced different fractional changes in the fluorescence at various substoichiometric amounts of Ca^{2+} (Figures 6.16 and 6.17). For example, even with a Trp substituted in position 65, the Tyr in position 57 could be titrated and showed that greater than 86% of the changes were complete at one equivalent of Ca^{2+} (Y65W λ_{ex} = 280 nm, λ_{em} = 300 nm in Figure 6.16, solid line). The Trp in position 65 showed similar results (Y65W λ_{ex} = 295 nm, λ_{em} = 350 nm in Figure 6.16, dotted line). Direct excitation of Trp in position 96 showed that 72% of the total fluorescence change was complete upon addition of one Ca^{2+} equivalent (K96W λ_{ex} = 295 nm, λ_{em} = 350 nm in Figure 6.16, dashed line), whereas only 56% of the change was complete when the protein was excited at 280 nm (K96W λ_{ex} = 280 nm, λ_{em} = 350 nm in Figure 6.16, dashed–dotted line). Upon addition of one equivalent of Ca^{2+} to Y57W, 95% of the total fluorescence change was complete and this response was identical when the protein was excited at either 280 nm or 295 nm. In Figure 6.17 the Ca^{2+} titration curves for the three Trp–containing mutant proteins obtained at wavelengths of maximal fluorescence response are shown. Upon comparison, one Ca^{2+} equivalent had the greatest influence on the fluorescence response of Y57W (dotted curve),

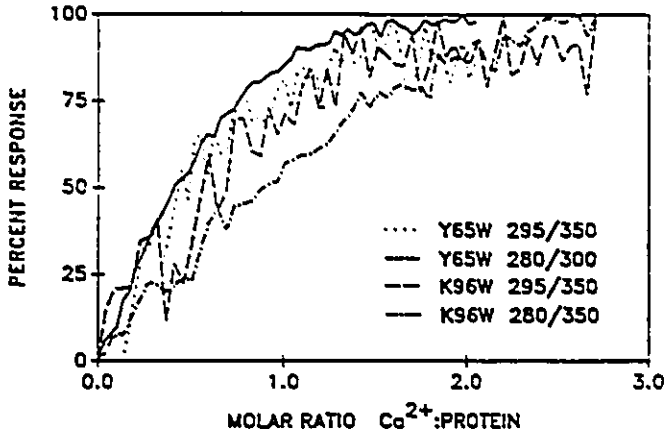

Figure 6.16: Ca^{2+} titration of apo (Ca^{2+}–free) Y65W and K96W plotted in terms of the fluorescence intensity changes at particular excitation and emission wavelengths. The effects of direct excitation of Trp–65 (Y65W, λ_{ex} = 295 nm; λ_{em} = 350 nm) are shown with the dotted line. The effects of excitation of Tyr–57 in Y65W (λ_{ex} = 280 nm; λ_{em} = 300 nm) are shown with the solid line. The effects of direct excitation of Trp–96 (K96W, λ_{ex} = 295 nm; λ_{em} = 350 nm) are shown with the dashed line and the effects of exciting both Tyr and Trp in K96W (λ_{ex} = 280 nm; λ_{em} = 350 nm) are shown with the dashed–dotted line.

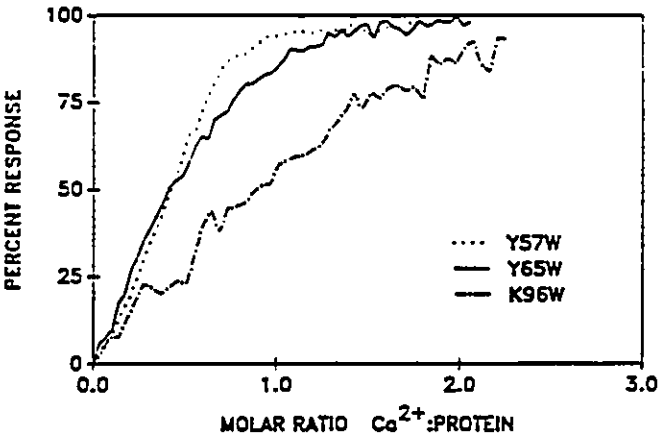

Figure 6.17: Ca^{2+} titration of apo (Ca^{2+}–free) Y57W (dotted line), Y65W (solid line) and K96W (dashed–dotted line) plotted in terms of the fluorescence intensity changes at the excitation and emission wavelengths of maximum fluorescence response. For Y57W, λ_{ex} = 295 nm, λ_{em} = 350 nm; for Y65W, λ_{ex} = 280 nm, λ_{em} = 300 nm; for K96W, λ_{ex} = 280 nm, λ_{em} = 350 nm.

followed by Y65W (solid curve), and lastly, by K96W (dashed–dotted curve).

Time–resolved fluorescence of the three Trp–containing oncomodulin mutant proteins revealed that the fluorescence decay of both the holo and apo proteins obeyed triple exponential decay kinetics. The various fluorescence parameters are summarized in Table 6.3. The longest lived decay component, τ_1, ranged between 5 – 6 ns, while the middle decay component, τ_2, ranged between 1.6 – 2.3 ns, and the shortest lived decay component, τ_3, had a value ranging between 0.1 and 0.5 ns.

In holo Y57W, the middle decay component (τ_2 = 1.61 ns) had both the greatest contribution to the total fluorescence (Figure 6.18A) as well as the greatest component concentration (75% in Figure 6.18C). Decalcification resulted in a decrease in the fractional contribution of this component to the fluorescence, a substantial blue–shift in the DAS of this component from 338 nm (holo) to 331 nm (apo), and a decrease in the relative component concentration to 51% (Figures 6.18 B and D). The λ_{max} of the short lifetime component in both holo and apo Y57W occurred relatively blue–shifted at 330 nm. Given that $\phi_f = \tau_s/\tau_r$, where τ_s and τ_r are the singlet and radiative lifetimes, respectively, upon decalcification the 24% increase in the mean lifetime $<\tau>$ did not parallel the 71% increase in ϕ_f. Assuming that the τ_r for each lifetime component was the same in a given protein, it was possible to calculate the value of τ_r using equation 3.3. When this was done, τ_r = 23 ns for holo Y57W and τ_r = 18 ns for apo Y57W.

In Y65W the longest lived decay component dominated the fluorescence emission both in the absence and presence of Ca^{2+}, despite the relatively larger concentration of the middle lifetime component (Figure 6.19). The λ_{max} of the longest decay component occurred at a relatively long wavelength position of 344 – 349 nm, which contrasted the blue–shifted emission of both the middle and shortest

TABLE 6.3

Various steady-state and time-resolved fluorescence decay parameters of the tryptophan-containing oncomodulin mutants Y57W, Y65W and K96W. λ_{ex} = 295 nm; 20°C.

Sample[a]	ϕ_f	λ_{max}^{ss}[b] (nm)	SVR[c]	τ_1[d] (ns)	τ_2 (ns)	τ_3 (ns)	λ_{max}^{1}[e] (nm)	λ_{max}^{2} (nm)	λ_{max}^{3} (nm)	F_1[f]	F_2	F_3	C_1[f]	C_2	C_3	τ_r[g] (ns)	<r>[h] (ns)
Holo Y57W	0.078 ± 0.003	339	1.98	6.17 ± 0.02	1.61 ± 0.01	0.374 ± 0.015	345	338	330	0.29	0.67	0.04	0.09	0.75	0.17	23.4	2.903
Apo Y57W	0.133 ± 0.003	340	1.98	5.25 ± 0.01	2.05 ± 0.02	0.504 ± 0.009	344	331	330	0.51	0.44	0.05	0.24	0.51	0.25	18.3	3.603
Holo Y65W	0.157 ± 0.003	343	1.90	5.13 ± 0.01	1.97 ± 0.01	0.167 ± 0.005	349	338	338	0.54	0.44	0.02	0.25	0.51	0.24	14.2	3.666
Apo Y65W	0.143 ± 0.002	340	1.89	4.05 ± 0.01	2.03 ± 0.01	0.213 ± 0.006	344	336	337	0.57	0.41	0.02	0.32	0.47	0.21	16.1	3.138
Holo K96W	0.084 ± 0.004	342	1.94	5.85 ± 0.02	2.30 ± 0.04	0.113 ± 0.003	347	332	340	0.84	0.15	0.02	0.41	0.18	0.41	24.0	5.240
Apo K96W	0.079 ± 0.003	339	1.89	5.06 ± 0.02	1.95 ± 0.01	0.373 ± 0.006	339	332	332	0.63	0.32	0.05	0.29	0.39	0.32	29.7	3.825

[a] All protein samples were in 10 mM cacodylate, 150 mM KCl, pH 7.0. In addition, 1 μM $CaCl_2$ was added to the holo samples to ensure complete occupancy of the metal-binding sites.

[b] λ_{max}^{ss} represents the wavelength of maximum intensity in the corrected steady-state fluorescence emission spectrum.

[c] SVR represents the serial variance ratio. It is a statistical parameter reflecting the goodness of fit. An SVR = 2 corresponds to an ideal statistical fit of the data (see Section 2.3.2). The SVR values shown reflect the statistics obtained upon global analysis of 10 data sets.

[d] The errors quoted for the lifetime values represent the standard errors for lifetime recovery from a given global set.

[e] λ_{max}^{i} represents the wavelength of the maximum intensity emission of the various components when excited at 295 nm. These values are obtained from the DAS.

[f] F_i and C_i denotes the fractional fluorescence and relative concentrations, respectively, of the various decay time components at 330 nm. The c_i's were calculated based upon their proportionality to the normalized preexponential times.

[g] τ_r represents the radiative lifetime and was calculated assuming that it was the same for all of the decay components in a given protein sample.

[h] <r> is the mean or intensity-weighted lifetime.

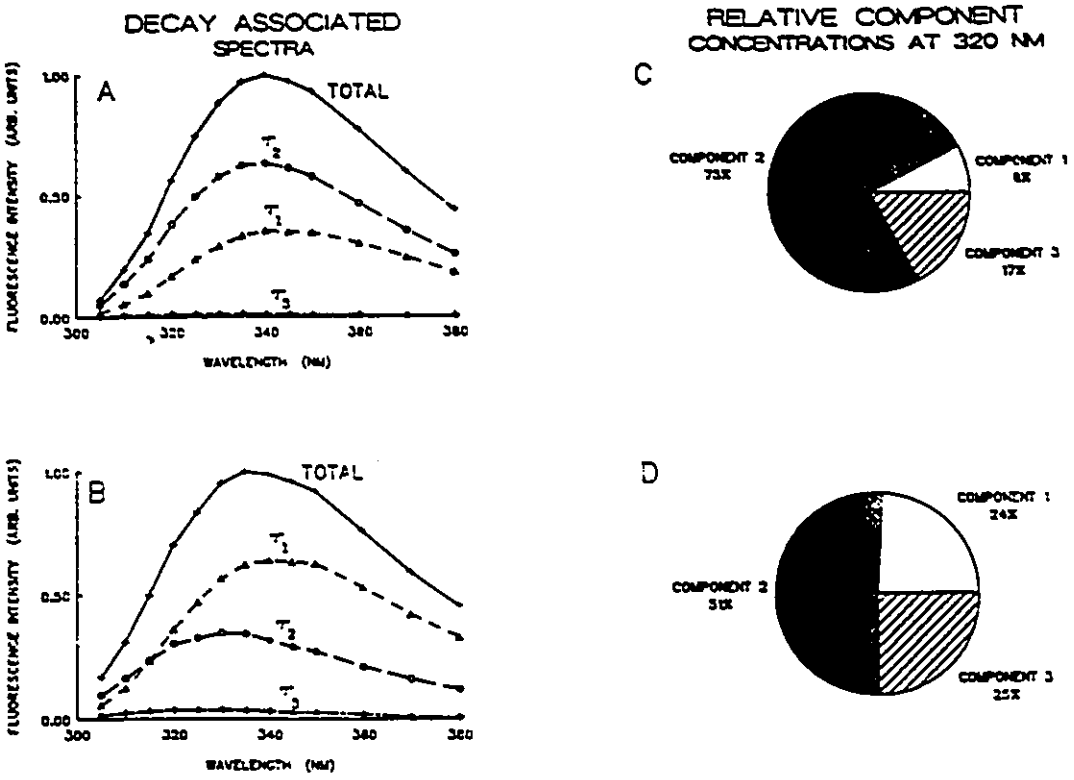

Figure 6.18: Decay–associated spectra for (A) holo Y57W and (B) apo (Ca^{2+}–free) Y57W oncomodulin mutant protein. The spectra sum to the corresponding corrected steady–state spectral intensities normalized to a value of one unit at the emission maximum. Standard errors are within the contours of the plotted symbols. The relative components concentrations at 320 nm of (C) holo Y57W and (D) apo Y57W are also shown.

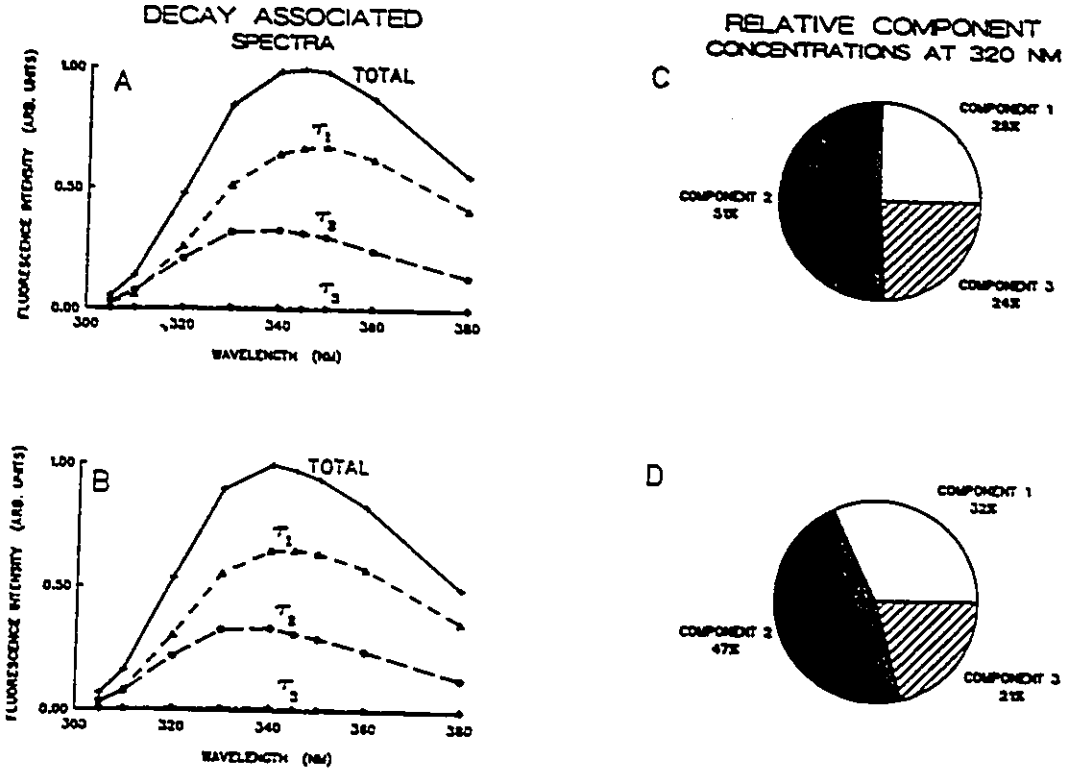

Figure 6.19: Decay–associated spectra for (A) holo Y65W and (B) apo (Ca^{2+}–free) Y65W oncomodulin mutant protein. The spectra sum to the corresponding corrected steady–state spectral intensities normalized to a value of one unit at the emission maximum. Standard errors are within the contours of the plotted symbols. The relative components concentrations at 320 nm of (C) holo Y65W and (D) apo Y65W are also shown.

decay components (336 – 338 nm) both in the absence and presence of Ca^{2+}.

Decalcification did not alter the fractional fluorescences, the relative component concentrations, or the DAS to any great extent in Y65W. The mean lifetime was decreased by 14% from 3.67 ns to 3.14 ns upon Ca^{2+} removal and, within relatively good agreement, paralleled the 9% decrease in ϕ_f. Calculation of the τ_rs showed that decalcification had virtually no effect upon this parameter (Table 6.3).

Although the ϕ_f of K96W decreased by only 6% upon decalcification, a 27% decrease in the mean lifetime was observed. In addition, the DAS of the longest and shortest decay components experienced substantial blue–shifts upon decalcification (λ^1_{max} (holo K96W) = 347 nm vs λ^1_{max} (apo K96W) = 339 nm; λ^3_{max} (holo K96W) = 340 nm vs λ^3_{max} (apo K96W) = 332 nm). The middle decay time component experienced both a greater fractional fluorescence and component concentration upon decalcification, despite no change in the position of λ_{max} of the DAS of this component (Figure 6.20). The radiative lifetime of holo K96W (34 ns) was considerably longer than that of the other proteins, and was decreased by 13% upon decalcification. The large 27% decrease in the mean lifetime was not accounted for in either the change in ϕ_f (6% decrease) or the change in τ_r (13% decrease).

6.4 Discussion

6.4.1 Bacterial Versus Native Protein

In an earlier study it had been reported, based upon amino acid analysis and ^{1}H–NMR spectroscopy, that 50–60% of the bacterially expressed oncomodulin still retained the initiation amino acid N–formyl–methionine (MacManus et al., 1989). However, UV and ^{1}H–NMR spectroscopies demonstrated that the recombinant protein folded in an identical manner to the native protein. Further, the two

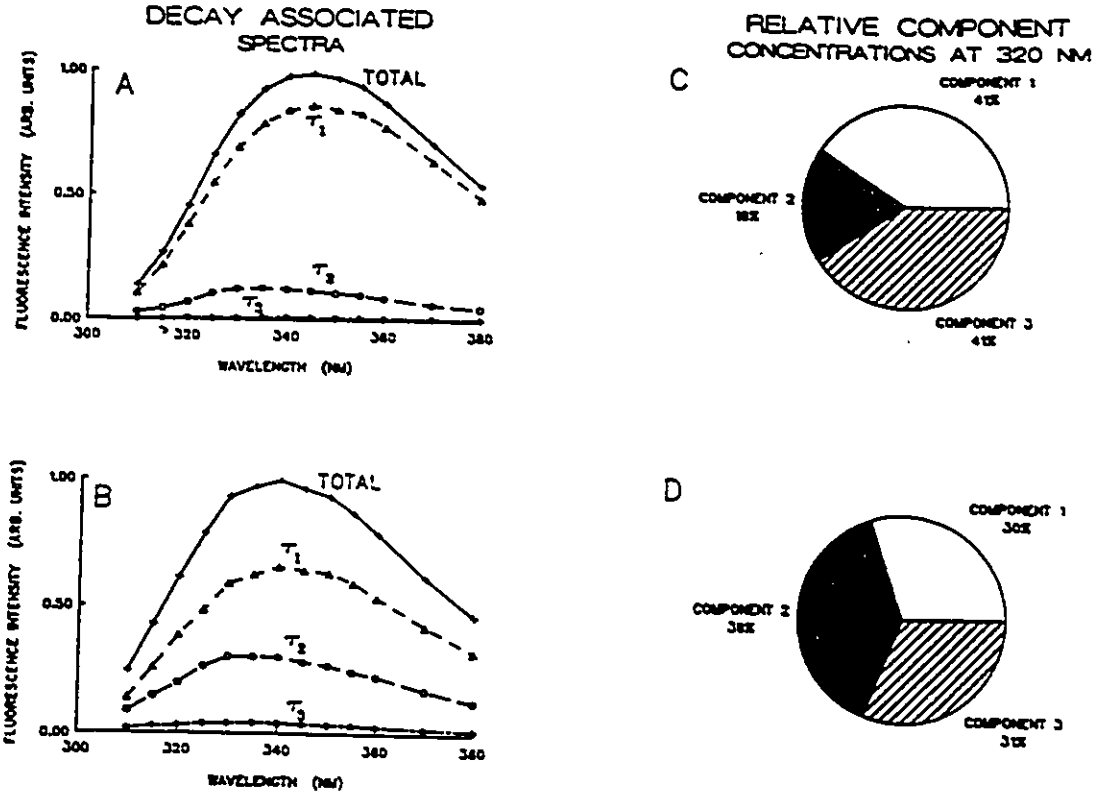

Figure 6.20: Decay–associated spectra for (A) holo K96W and (B) apo (Ca^{2+}–free) K96W oncomodulin mutant protein. The spectra sum to the corresponding corrected steady–state spectral intensities normalized to a value of one unit at the emission maximum. Standard errors are within the contours of the plotted symbols. The relative components concentrations at 320 nm of (C) holo K96W and (D) apo K96W are also shown.

proteins were found to be immunologically identical (MacManus et al., 1989). In the present study, the absorption spectra, fluorescence emission spectra, and quantum yields of fluorescence of the bacterial recombinant oncomodulin (BRONCO) were identical to the native tumour protein. In addition, both apo (Ca^{2+}–free) proteins responded to metal ion titration in an identical manner. Spectral comparison of BRONCO with another bacterially expressed oncomodulin known as MAP–BRONCO further confirmed that the heterogeneous amino terminus did not influence the spectrally–determined metal ion binding properties of the protein. This latter protein was expressed in the presence of an excess of the enzyme methionine amino peptidase and hence the N–formyl methionine amino terminus was completely cleaved. The identical ϕ_fs measured for all three proteins in the absence and presence of either Ca^{2+} or Mg^{2+} (See Table 6.1) provided a sensitive measure indicating the identical nature of these proteins.

The fluorescence emission spectra of all the proteins, including the native tumour oncomodulin, showed no evidence of an additional contribution to the fluorescence at longer wavelengths (Figure 6.3). Previously such a contribution was noted in native tumour oncomodulin and was assigned to tyrosinate fluorescence (MacManus et al., 1984). The previous appearance of a fluorescence band centered at 345 nm was most likely due to the presence of a Trp–containing contaminant which was more effectively removed in the present study due to the inclusion of HPLC in the purification procedures. A similar situation was reported for the brain S_{100b} protein where the initial report of tyrosinate fluorescence (Mani et al., 1982) was subsequently shown to be due to Trp contamination (Baudier & Gerard, 1983). When compared to the bacterially expressed proteins and L–tyrosine, the native

tumour oncomodulin did show some slight evidence of an increased contribution at longer wavelengths (Figure 6.3). This may suggest that even with an HPLC separation, it is exceedingly difficult to purify proteins from a mammalian source to complete homogeneity, and that exceptional care must be placed in assigning long wavelength fluorescence in non–tryptophan containing proteins to tyrosinate.

Titration of all three proteins with Ca^{2+}, revealed that greater than 90% of the total fluorescence response was complete upon the addition of one Ca^{2+} equivalent (Figure 6.5). This suggests that binding of Ca^{2+} to the higher affinity EF–site (Williams et al., 1987; MacManus et al., 1984) promotes the majority of conformational changes experienced in the regions probed by the tyrosine residues in positions 57 and 65. However, as the fluorescence signals measured in these proteins originate from both locations it is not possible to determine whether both sites are affected to the same degree. The bulk of the conformational change produced upon binding of only one Ca^{2+} equivalent may not be confined to the regions associated with the binding loops. Only one mole Ca^{2+}/mole oncomodulin was required to produce a maximal response of the fluorescent reagent *N*–dansylaziridine when attached to cysteine–18 in the AB–loop, which is located on the other side of the molecule relative to the two Ca^{2+}–binding sites (Mutus et al., 1985).

Circular dichroism had shown that native tumour oncomodulin experienced changes in the secondary structure which were complete upon the addition of only one equivalent of Mg^{2+} (MacManus et al., 1984). However, Mg^{2+} titration of the three apoproteins in the present study showed that $3 - 4$ Mg^{2+} equivalents were required to achieve plateau values (Figure 6.6). In addition, the Mg^{2+} titration curves were much noisier compared to the Ca^{2+} titration curves. These results can be rationalized in two ways. If indeed the EF–site in oncomodulin is a

parvalbumin–like Ca^{2+}/Mg^{2+}–site (MacManus et al., 1984), then the affinity of the site for Mg^{2+} is much less when compared to Ca^{2+}. Because of this, upon the addition of one molar equivalent of Mg^{2+}(aq) to the apoprotein solution, only a small fraction of the Mg^{2+} ions will be bound to the EF–site. It may be that only in the presence of excess of Mg^{2+} (aq) will the majority of protein molecules have a Mg^{2+} ion specifically bound to the EF–site, thus promoting a fluorescence change. An alternative explanation is that Mg^{2+} binds non–specifically to the protein at 3 or more sites and it is this binding which is affecting the fluorescence properties. Given that magnesium affinity constants (K_{Mg}) in the highly homologous parvalbumins have been found to be up to four orders of magnitude less than the corresponding calcium affinity constants (K_{Ca}) (Moeschler et al., 1980), it is possible that a similar situation exists for the EF–site in oncomodulin. This would be compatible with the former interpretation. In any case, based upon the titration data and the ϕ_fs, it is clear that Mg^{2+} binding to oncomodulin in no way mimics the effects of Ca^{2+}, and as previously suggested (MacManus et al., 1984), the conformational response of oncomodulin is definitely Ca^{2+}–specific. Similar results were reported for ram testis and octopus calmodulins where it was found that, at physiological ionic strength (150 mM KCl), Mg^{2+}–binding did not seem to exert a major influence on conformation (Kilhoffer et al., 1981).

6.4.2 The Tyrosine–Containing Mutant Proteins

The replacement of each Tyr residue by Phe permitted a detailed assessment of the origin of the fluorescence changes observed in the native protein. In addition, the impact of metal ion binding on the environment associated with each site (positions 57 and 65) was revealed. As expected, owing to the loss of one Tyr

residue and the gain of one Phe residue, the absorption spectra of both mutants, Y57F and Y65F, displayed an increased intensity of the Phe bands in the region 260 – 280 nm relative to the tyrosine absorption maximum at 280 nm (Figure 6.7). This Phe–associated structure appeared to be more more pronounced for Y65F when compared to Y57F.

A relatively low ϕ_f was measured for Y57F (ϕ_f = 0.016, Table 6.2). A possible explanation for this low ϕ_f is the involvement of Tyr–65 in a hydrogen–bonding interaction in the holoprotein. It has been shown that hydrogen bonding provides an effective static quenching mechanism of Tyr fluorescence (Chignell & Gratzer, 1968). Decalcification of Y57F resulted in a 53% <u>increase</u> in the ϕ_f (ϕ_f (holo Y57F) = 0.016 vs ϕ_f (apo Y57F) = 0.023). This suggested that Ca^{2+}–binding promoted a conformational change that diminished the interaction of Tyr–65 with the nearby protein moiety responsible for its quenching in the presence of Ca^{2+}.

The effect of decalcification on the ϕ_f of Y65F was opposite to that of Y57F, with the ϕ_f <u>decreasing</u> by 43% upon Ca^{2+} removal (ϕ_f (holo Y65F) = 0.072 vs ϕ_f (apo Y65F) = 0.041). As a number of acidic residues in both the CD– and EF–sites would no longer be bound to Ca^{2+} upon decalcification, a number of potential hydrogen–bonding partners would be present in the vicinity of Tyr–57. If a hydrogen bond involving Tyr–57 was formed in the decalcified Y65F, this would explain the observed decrease in the ϕ_f. As Tyr–57 was much more fluorescent that Tyr–65 in both the absence and presence of Ca^{2+} (Figure 6.8), the fluorescence of Tyr–57 dominates the intrinsic fluorescence properties of the native, two–tyrosine containing protein. As the ϕ_f values were measured under conditions wherein the absorbance of the proteins at the excitation wavelength (280 nm) was very close to

0.10, the assumption may be made that there was approximately double the concentration of each mutant relative to BRONCO owing to the loss of one Tyr residue. If this assumption is valid, then the sum of each mutant ϕ_f divided by two, should equal the ϕ_f of BRONCO. The average ϕ_f of Y57F and Y65F of 0.044 was 21% less than the 0.055 value for BRONCO. This discrepancy may be explained by different extinction coefficients for the two mutants at 280 nm, or by the possibility that the loss of a phenolic hydroxyl in one, or both of the positions is itself producing conformational changes that are disturbing the photophysical properties of the remaining Tyr. Although the differences in absorption characteristics of the two mutants in Figure 6.7, and the relatively small 2% difference in molecular volume of Tyr (193.6 $Å^3$) and Phe (189.9 $Å^3$) (Zamyatnin, 1972) suggest the first alternative may be likely, the metal ion titration curves of Y65F in particular displayed a diminished response relative to that of BRONCO (Figures 6.11 and 6.12). This latter observation suggests that a loss of the phenolic hydroxyl in position–65 may be affecting the affinity of Ca^{2+} and Mg^{2+} for the higher affinity metal–ion binding site.

The initial conclusions that oncomodulin experienced Ca^{2+}–specific conformational changes were based upon an examination of the fluorescence excitation spectrum. It was found that Ca^{2+}, but not Mg^{2+} addition to apo–oncomodulin, could produce an increase in both the structure and intensity at the blue–edge of the fluorescence excitation spectrum. This was interpreted as being due to a Ca^{2+}–induced conformational change that increased the efficiency of energy transfer from Phe to Tyr (MacManus et al., 1984). At the time, based upon the examination of a model of oncomodulin, it was suggested that Phe–49 (or less likely Phe–47) was transferring its excitation energy to Tyr–65. Tyr–57 was ruled

out from functioning in this interaction due to the lack of any Phe residues in a correct position for efficient energy transfer. However, the fluorescence excitation spectra of Y57F and Y65F revealed that the opposite situation was the case (Figure 6.9). In the presence of Ca^{2+}, it was the excitation spectrum of Y65F which experienced increased intensity at the high–energy end, which implied that Tyr–57 was the residue responsible for the changes observed in the native protein. This result emphasizes that although static structures of protein molecules are informative, a lack of appreciation for fact that they are only time–averaged representations can lead to misconceptions regarding their solution structures. It is now well accepted that proteins are dynamic structures and that the motions of these molecules are central to their biological function (Williams, 1989). The fluorescence excitation spectra of the oncomodulin mutant proteins displayed that the molecules must be sufficiently flexible in order to permit the interaction between an apparently distantly located Phe and Tyr–57. As this interaction was completely absent upon the addition of Mg^{2+}, and the CD–site had already been pinpointed as the lower affinity, Ca^{2+}–specific site (MacManus et al., 1984), a titration of the fluorescence excitation spectrum at λ_{ex} = 245 nm, λ_{em} = 306 nm was performed in hope that the conformational impact of the second Ca^{2+} equivalent might be apparent in this particular parameter. However, as seen in Figure 6.10, although a slight lag in response was observed upon the first few additions, 84% of the maximal change in the fluorescence excitation spectrum was complete after the addition of only one equivalent of Ca^{2+}. This Ca^{2+}–specific conformational response was largely dependent upon the filling of the higher affinity site in oncomodulin.

The fluorescence decay parameters of Y65F were similar to those of

BRONCO, both in the absence and presence of Ca^{2+} (Table 6.2). The most significant difference was in the fractional fluorescence and value of the shortest lifetime component in the holo proteins (τ_3 (holo Y65F) = 0.058 ns vs τ_3 (holo BRONCO) = 0.322 ns; F_3 (holo Y65F) = 0.01 vs F_3 (holo BRONCO) = 0.08). In both proteins, the decrease in the ϕ_f upon decalcification was approximately double the decrease in the mean lifetime (Table 6.2). As Tyr–57 has been shown to dominate the fluorescence of BRONCO, these results suggest that decalcification resulted in a significant degree of static quenching of this tyrosyl residue. A similar situation has been reported for the single Tyr residue in octopus calmodulin (Kilhoffer et al., 1980). In addition to hydrogen bond formation (Cowgill, 1967), quenching of Tyr emission may be mediated by the interaction with a variety of amino acid side chains, with the latter functioning as either proton acceptors or donors (Cowgill, 1976). In addition, the carbonyl group of the peptide bond has been singled out as an efficient quencher of Tyr emission (Cowgill, 1967). Owing to the relatively large number of possible quenching interactions, it is difficult to identify the specific source within any given protein. Nonetheless, the results demonstrate that the conformational effects of decalcification are apparent in the region probed by Tyr–57.

The complexity of the influence of the protein environment on the fluorescence properties of Tyr is demonstrated by the observation that unlike Tyr–57, Tyr–65 experienced a greater degree of quenching in the presence of Ca^{2+}. Despite virtually no change in the mean lifetime (4% increase), the ϕ_f increased by 53% upon decalcification of Y57F. A static quenching mechanism has been used to explain a similar discrepancy between the lifetime and quantum yield data for octopus calmodulin (Kilhoffer et al., 1981). The significantly shorter lifetime values

for the first and second decay components in Y57F demonstrate that the environment of Tyr–65 is significantly different from that of Tyr–57, both in the absence and presence of Ca^{2+}. In the case of Tyr–65, the effect of decalcification appears to be limited to the influence on the longest lived decay component (Table 6.2). However it is clear that both positions are capable of reporting Ca^{2+}–induced changes in their environment.

6.4.3 The Tryptophan–Containing Mutant Proteins

The absorption spectra of all three Trp–containing mutants lacked a sharp 292 nm subsidiary peak, which was the first indication that the Trp residues in the three locations resided in relatively polar environments (Andrews & Forster, 1972). Decalcification did not alter this feature to any significant extent (Figure 6.13).

The steady–state fluorescence emission spectra of all of the Trp–containing mutants possessed emission maxima in the range of 339 – 343 nm, both in the absence and presence of Ca^{2+} (Figures 6.14 and 6.15). This offered additional evidence that the Trp in all the proteins resided in polar, solvent–accessible environments (Van Durren, 1961). Whereas Trp–57 emission was significantly affected by decalcification, relatively minor changes were experienced by either Trp–65 or Trp–96 when excited at 295 nm (Figure 6.14). The results from the Y65W mutant were initially regarded as a disappointment, because instead of amplifying the fluorescence signal associated with conformational changes experienced in position–65, the fluorescence intensity changes of Trp in this location were smaller than those of Tyr upon decalcification. However, when Y65W was excited at 280 nm, it was the only mutant to display a significant extent of tyrosine emission at 304 nm (Figure 6.15B). In most proteins containing Tyr and Trp,

rarely is Tyr emission observed because the relative positions of the absorption and fluorescence spectra favour a resonance energy transfer process (Teale, 1960). The efficiency of the process is dependent on the mutual distance and orientation of the residues involved; a highly efficient transfer is characterized by effective stacking interactions between the indole and phenol sidechains which in turn, optimizes both the dipole orientations and the through–space interactions (Longworth, 1971). The changes of the Tyr emission produced by decalcification and subsequent Ca^{2+} and Mg^{2+} addition, suggested that the environment of Tyr–57 was behaving in a similar manner as in the native protein, and that substitution of a bulky Trp residue in position–65 did not affect these interactions (the molecular volume of Trp (227.8 $Å^3$) is 15% larger than that of Tyr (193.6 $Å^3$)). It was interesting that although Tyr–57 was not able to efficiently transfer its excitation energy to Trp–65, the reverse situation was observed when the positions of the residues were reversed. Upon excitation at 280 nm, Y57W showed no similar evidence of Tyr emission (Figure 6.15A). These results would suggest that the substitution of Trp into one, or both of the positions (57 and 65) was altering either the distance and/or orientation of the ring systems relative to each other. However, it is not possible to rule out the situation in which Tyr–65 was more highly quenched than Tyr–57 by a mechanism other than energy transfer. Such a possibility would also prevent tyrosine emission from being observed when Y57W was excited at 280 nm. Despite the large intensity changes experienced by Y57W upon decalcification, no change in the position of λ_{max} was observed. On the other hand, the fluorescence spectra of both Y65W and K96W experienced a 3 – 4 nm blue–shift upon Ca^{2+} removal which indicates that the Trp environments may have become slightly less polar in the absence of Ca^{2+} (See Table 6.3).

While comparable changes in the emission intensity were observed upon excitation of Y57W and Y65W at both 295 nm and 280 nm, much larger differences were noted in the emission spectra of K96W when excited at the two wavelengths (Figures 6.14 C and 6.15 C). Instead of a 6% decrease in intensity observed upon decalcification with λ_{ex} = 295 nm, an 18% decrease was observed when the excitation wavelength was 280 nm. These data demonstrate that although the Trp in position–96 does respond to Ca^{2+}–induced changes, the largest effect of Ca^{2+} at this position is to alter the position of this Trp relative to Tyr in position–57. The crystal structure shows that both positions, although residing in two separate binding loops, lie in very close proximity to each other (Figure 6.1). Thus Ca^{2+} has an important effect of altering the position of the two binding loops relative to each other. The most dramatic evidence of this effect was obtained upon an examination of the Ca^{2+} titration curves. In Figure 6.16 it can be seen that when Trp–96 was directly excited at 295 nm (λ_{em} = 350), 72% of the total fluorescence response was complete upon the addition of one equivalent of Ca^{2+}. In contrast, when the emission of Trp–96 was measured after exciting both Tyr and Trp at 280 nm (λ_{em} = 350 nm), only 56% of the total response was observed upon addition of one Ca^{2+} equivalent. This dramatically contrasts the results obtained upon titration of either Y57W or Y65W (Figure 6.17). Addition of one Ca^{2+} equivalent promoted greater than 95% of the total fluorescence change in Y57W, and greater than 86% in Y65W. Further, monitoring the Tyr–57 emission or the Trp–65 emission in Y65W produced identical titration curves (Figure 6.16). These results provide the best indication of the effects of the second equivalent of Ca^{2+} on the conformational properties of oncomodulin. Although the filling of the higher affinity site (presumably the EF–site, Williams et al., 1987) produces the bulk of the

conformational changes associated with both the CD– and EF–sites, the second Ca^{2+} equivalent has a very subtle effect of positioning the two loops relative to each other. Although it may be argued that the considerably bulkier, and differently charged Trp residue (cf. molecular volumes of Trp (227.8 $\AA^3$) vs Lys (168.6 $\AA^3$)), may alter the affinity of Ca^{2+} for the EF–site, it is unlikely that this single change would have such a drastic effect owing to the largely solvent exposed position of the side chain. However in the absence of binding constant determinations, this possibility cannot be dismissed.

The fluorescence decay behaviour of all three Trp–containing mutants was best described by a triple exponential decay function. The results are summarized in Table 6.3. By combining the steady–state and the time–resolved fluorescence data it was possible to contruct decay–associated spectra (DAS). DAS represent the relative contributions of individual lifetime components, as a function of wavelength, to the total fluorescence. Thus DAS are capable of revealing differences in Trp environments of single Trp–containing proteins (Knutson et al., 1982).

Dramatic differences were observed in Y57W upon decalcification. The fractional contribution to the total fluorescence of the middle lifetime component was greatly reduced, and the DAS of this component significantly blue–shifted (λ^2_{max} (holo Y57W) = 338 nm vs λ^2_{max} (apo Y57W) = 331 nm)) upon decalcification (Figure 6.18). The blue–shift in the DAS indicated that the environment of the Trp associated with the middle decay time component was relatively less polar upon decalcification. Calculation of the relative component concentrations at 320 nm revealed that decalcification resulted in a decrease in the amount of this second decay component. Although the mean lifetime increased by 24% upon Ca^{2+} removal, this did not account for the 71% increase in ϕ_f. This

discrepancy can be rationalized in two ways. First, the Trp in holo Y57W may be involved in a particular static quenching mechanism (Szalay & Szollosy, 1964). However, because interactions with the terminal carboxylic and amino groups, the peptide bonds, the carboxylic/carbonyl groups of Asp and Glu, the amino groups of Lys and Arg, and a whole range of solvent interactions have all been recognized as potential sources of Trp emission quenching (for a review, see Creed, 1984), it is virtually impossible to attempt to identify the source of such a mechanism in holo Y57W. An alternative explanation which explains the discrepancy is that the radiative lifetime, τ_r, changes upon decalcification. Calculation of the radiative lifetimes shows that the value decreases from 23 ns to 18 ns upon Ca^{2+} removal, which in accordance with model compound studies would suggest that decalcification was accompanied by a transfer of the indole from a more polar to a less polar environment (Privat et al., 1979). The blue–shift in the λ_{max} of the middle decay component, which dominates the fluorescence in the holo protein would be consistent with this interpretation. However the fact that the steady–state λ_{max} remains unchanged suggests that perhaps the radiative lifetimes of all three components in Y57W are not equivalent, or that upon decalcification, both a change in the τ_r and specific quenching mechanisms are simultaneously operating. Owing to the complexity of the photophysics associated with the free Trp zwitterion (Creed, 1984), such a situation is conceivable.

In contrast to Y57W, the fluorescence decay behaviour of Y65W was affected to a lesser extent by decalcification. The fractional fluorescences, relative component concentrations and DAS of the various components were remarkably similar (Figure 6.19). The largest difference was a decrease of the value of the longest lived decay component from 5.13 ns to 4.05 ns upon Ca^{2+} removal. The

14% decrease in the mean lifetime was in reasonable agreement with the 9% decrease in ϕ_f upon decalcification. These results suggest that although position–65 does experience some perturbation upon decalcification, the magnitude of such effects are much less compared to position–57. Similar conclusions were made upon examination of the single Tyr–containing mutants, Y57F and Y65F. The Ca^{2+}–induced conformational changes are localized more towards the region between the two Ca^{2+}–binding loops.

This latter conclusion is consistent with the results obtained with K96W. Decalcification produced blue–shifts of 8 nm in the λ_{max} of both the longest and shortest decay time components (Figure 6.20), which indicated that in the conformations associated with these particular decay components, the Trp existed in a relatively less polar environment in the absence of Ca^{2+}. Although the ϕ_f decreased by only 6% upon decalcification, the mean lifetime decreased by 27%. The relative concentration of the second component increased from 18% to 39% upon Ca^{2+} removal. It is interesting that the mean lifetimes of both holo and apo K96W were significantly longer than those of either Y57W or Y65W (Table 6.3). Calculation of the radiative lifetimes showed that both apo and holo K96W had significantly longer values. These results demonstrate that although the Trp residues in positions 57 and 96 are sensitive to Ca^{2+}–induced changes, the nature of the environment of these two residues is considerably different. Although the residues occupy analogous positions as binding ligands in the two loops, the immediate electronic environment of the two residues is markedly different. Although it may not be possible to identify the origin of the photophysical behaviour associated with each Trp residue, it is clear from these results that the region located between the two binding loops is significantly affected by the binding

of Ca^{2+} ions. Trp in position 57, but not 65 is highly sensitive to the filling of the first Ca^{2+}–binding site, and Trp in position 96 is capable of sensing highly localized conformational changes produced upon the binding of the second Ca^{2+} equivalent.

6.5 Chapter Summary and Conclusions

Oncomodulin is a 108–residue, oncodevelopmental protein containing two calcium–binding sites known as the CD– and EF–loops. The protein contains no tryptophan and only two tyrosine residues, one which functions as a calcium ligand in the CD–loop (Tyr–57) and one which lies in the flanking D–helix of this loop (Tyr–65). Site–specific mutagenesis of oncomodulin was used to generate five spectrally informative mutants. The recombinant protein was spectroscopically indistinguishable from the native tumour protein, both in the absence and presence of a partially retained N–formylmethionine amino terminus. In contrast to earlier reports, no tyrosinate fluorescence was found associated with either the native or recombinant proteins. The single Tyr–containing mutants demonstrated that position 57 was perturbed to a significantly greater extent than position 65 upon calcium–binding. Although both tyrosine residues responded to decalcification, the fluorescence response was in opposite directions, with the more dominant Tyr–57 accounting for the majority of the intrinsic fluorescence observed in native oncomodulin. The substitution of tryptophan for each tyrosyl residue revealed that both positions resided in highly polar, conformationally heterogeneous environments. The environment of Trp–57 was modulated by Ca^{2+}–binding to a much greater extent compared to that of Trp–65. This modulation of position–57 was apparent even when Trp was substituted into the nearby position–65. Only one

equivalent of Ca^{2+} was required to produced greater than 90% of the changes in positions 57 and 65 in the CD–loop. In contrast, substitution of Trp in place of Lys–96 in the EF–loop, showed that the second Ca^{2+} equivalent had an important role in modulating the conformation of this position, especially with respect to its interactions with Tyr–57 in the CD–loop. Thus highly localized and very subtle conformational effects characterize the influence of the binding of the second equivalent of Ca^{2+} to oncomodulin.

6.6 References

Andrews, L. J. & Forster, L. S. (1972) Protein difference spectra. Effect of solvent and charge on tryptophan. Biochem. 11, 1875–1879.

Baudier, J. & Gerard, D. (1983) The S100–b protein: Tyrosine residues do not exhibit an abnormal fluorescence spectrum. J. Neurochem. 40, 1765–1767.

Chignell, D. A. & Gratzer, W. B. (1968) Solvent effects on aromatic chromophores and their relation to ultraviolet difference spectra of proteins. J. Phys. Chem. 72, 2934–2941.

Cowgill, R. W. (1967) Fluorescence and protein structure. X. Reappraisal of solvent and structural effects. Biochim. Biophys. Acta 133, 6–18.

Cowgill, R. W. (1976) In: Biochemical Fluorescence: Concepts 2, Eds.: R. F. Chen and H. Edelhoch (Marcel Dekker, New York) pp. 441–486.

Creed, D. (1984) The photophysics and photochemistry of the near–UV absorbing amino acids — I. Tryptophan and its simple derivatives. Photochem Photobiol. 39, 537–562.

Haiech, J., Klee, C. B. & Demaille, J. G. (1981) Effects of cations on affinity of calmodulin for calcium: Ordered binding of calcium ions allows the specific activation of calmodulin–stimulated enzymes. Biochem. 20, 3890–3897.

Kilhoffer, M.–C., Demaille, J. G. & Gerard, D. (1981) Tyrosine fluorescence of ram testis and octopus calmodulins. Effects of calcium, magnesium, and ionic strength. Biochem. 20, 4407–4414.

Kilhoffer, M.–C., Gerard, D. & Demaille, J. G. (1980) Terbium binding to octopus calmodulin provides the complete sequence of ion binding. FEBS Lett. 120, 99–103.

Knutson, J. R., Walbridge, D. G. & Brand, L. (1982) Decay–associated fluorescence spectra and the heterogeneous emission of alcohol dehydrogenase. Biochem. 21, 4671–4679.

Longworth, J. W. (1971) In: Excited States of Proteins and Nucleic Acids, Eds.: R. F. Steiner and I. Weinryb (Plenum Press, New York) pp. 319–484.

MacManus, J. P. (1980) The purification of a unique calcium–binding protein from Morris hepatoma 5123 tc. Biochim. Biophys. Acta 621, 296–304.

MacManus, J. P., Hutnik, C. M. L., Sykes, B. D., Szabo, A. G., Williams, T. C. & Banville, D. (1989) Characterization and site–specific mutagenesis of the calcium–binding protein oncomodulin produced by recombinant bacteria. J. Biol. Chem. 264, 3470–3477.

MacManus, J. P., Szabo, A. G. & Williams, R. E. (1984) Conformational changes induced by binding of bivalent cations to oncomodulin, a parvalbumin–like tumour protein. Biochem. J. 220, 261–268.

Mani, R. S., Boyes, B. E. & Kay, C. M. (1982) Physicochemical and optical studies on calcium– and potassium–induced conformational changes in bovine brain S–100b protein. Biochem. 21, 2607–2612.

Moeschler, H. J., Schaer, J.–J. & Cox, J. A. (1980) A thermodynamic analysis of the binding of calcium and magnesium ions to parvalbumin. Eur. J. Biochem. 111, 73–78.

Moews, P. C. & Kretsinger, R. H. (1975) Refinement of the structure of carp muscle calcium–binding parvalbumin by model building and difference fourier analysis. J. Mol. Biol. 91, 201–228.

Mutus, B., Flohr, E. J. & MacManus, J. P. (1985) Ca^{2+}–specific fluorescence changes in *N*–dansylaminoethyl–labelled oncomodulin. Can. J. Biochem. Cell Biol. 63, 998–1002.

Privat, J. P., Wahl, P. & Auchet, J. C. (1979) Rates of deactivation processes of indole derivatives in water–organic solvent mixtures — Application to tryptophyl fluorescence of proteins. Biophys. Chem. 9, 223–233.

Szalay, L. & Szollosy, L. (1964) Investigations on the connection of polarization and foreign quenching in fluorescent solutions. Acta Phys. Chem. 10, 3–8.

Teale, F. W. J. (1960) The ultraviolet fluorescence of proteins in neutral solution. Biochem. J. 76, 381–388.

Van Durren, B. L. (1961) Solvent effects in the fluorescence of indole and substituted indoles. J. Org. Chem. 26, 2954–2960.

Van Eldik, L. J., Zendegui, J. G., Marshak, D. R. & Watterson, D. M. (1982) Calcium–binding proteins and the molecular basis of calcium action. Int. Rev. Cytol. 77, 1–61.

Williams, R. J. P. (1989) NMR studies of mobility within protein structure. Eur. J. Biochem. 183, 479–497.

Williams, T. C., Corson, D. C., Sykes, B. D. & MacManus, J. P. (1987) Oncomodulin. ^{1}H NMR and optical stopped–flow spectroscopic studies of its solution conformation and metal–binding properties. J. Biol. Chem. 262, 6248–6256.

Zamyatnin, A. A. (1972) Protein volume in solution. Prog. Biophys. Mol. Biol. 24, 107–123.

Chapter 7

CONCLUSIONS AND FUTURE EXPERIMENTS

7.1 Conclusions

The intrinsic fluorescence properties of twelve native and bacterial recombinant metalloproteins were examined in this thesis. The following conclusions can be made:

1) In all cases, the quantum yields of fluorescence, the emission maxima and/or the fluorescence decay kinetics of the single tryptophan or tyrosine amino acid probes in the proteins were affected by the binding of metal ions. These changes in fluorescence can be rationalized in terms of metal ion–induced protein conformational changes.

2) As can be seen in Table 7.1, with the exception of apoazurin, all of the examined single tryptophan–containing proteins exhibited multiexponential fluorescence decay kinetics and hence, were conformationally heterogeneous. In most cases, this conformational heterogeneity was dramatically affected by the binding of a metal ion to the protein matrix. The range of decay times shown in Table 7.1 illustrates the great sensitivity of the fluorescence properties of tryptophan to its microenvironment.

3) The efficiency of tryptophan fluorescence varied widely from one protein to another, with quantum yields of fluorescence ranging from 0.018 to 0.33. From an examination of the available crystal structures, it was clear that no simple relationship was apparent between the surface exposure of the tryptophyl side chains and the magnitude of the quantum yields of fluorescence. In addition, tryptophan residues situated in identical locations within highly homologous proteins possessed significantly different quantum yields. Thus the efficiency of tryptophan emission is extremely sensitive to the local microenvironment provided by the protein matrix.

TABLE 7.1

Survey of the intrinsic fluorescence decay (λ_{ex} = 295 nm; 20°C) of the single tryptophan–containing proteins examined in this thesis.

Protein	τ_1(ns)	τ_2(ns)	τ_3(ns)
Pae apoazurin[a]	5.11		
Pfl apoazurin	5.10		
Pae holoazurin	4.89	0.36	0.098
Pfl holoazurin	4.91	0.52	0.105
Pae Cu(I) azurin	4.76	0.47	0.061
Pfl Cu(I) azurin	4.98	0.37	0.063
Pfl Co(II) azurin	4.88	2.08	0.136
Pfl Ni(II) azurin	4.90	1.01	0.094
Holo cod III parvalbumin[b]	3.55	1.54	
Holo F102W onco mutant	4.19	1.89	
Apo cod III parvalbumin	4.39	2.17	0.361
Apo F102W onco mutant	4.11	2.00	0.222
Holo Y57W onco mutant[b]	6.17	1.61	0.374
Apo Y57W onco mutant	5.25	2.05	0.504
Holo Y65W onco mutant	5.13	1.97	0.167
Apo Y65W onco mutant	4.05	2.03	0.213
Holo K96W onco mutant	5.85	2.30	0.113
Apo K96W onco mutant	5.06	1.95	0.373

[a]All the fluorescence decay results shown for azurin and azurin derivatives were measured at an emission wavelength = 310 nm.

[b]The fluorescence decay results for parvalbumin and the oncomodulin mutant proteins were obtained upon global analysis of 10 data sets measured at 10 emission wavelengths spanning the emission spectrum.

4) Although it is difficult to comment on the relationship between the spectroscopic information and the absolute structure of the proteins in the absence of other information, the results of this thesis show that fluorescence spectroscopy

can provide information allowing the assessment of relative local changes in protein conformation induced by the binding of metal ions. The limitation of being able to probe only the environment in which the intrinsic tryptophyl or tyrosyl probe is naturally located can be removed by the examination of bacterial recombinant proteins. By site–specific mutagenesis, it is possible to place highly sensitive single tryptophan probes in any site of interest.

5) Perhaps of all the spectroscopic techniques, fluorescence spectroscopy possesses the most stringent requirement for homogeneous protein samples and care in sample preparation. The high sensitivity of fluorescence renders the method intolerant of sample contamination. Monitoring the protein samples by both SDS–PAGE and isoelectric focusing was shown to be a minimum prerequisite for fluorescence measurements.

7.1.1 Critical Comments

In this thesis, information about the influence of metal ion binding upon the conformational distribution of a variety of metalloproteins was reported. This information was obtained through a steady–state and time–resolved study of the intrinsic fluorescence properties of single–tyrosine and single–tryptophan containing proteins. With this technique, covalent modification of the proteins was not required in order to obtain the information, and with the aid of protein engineering, a number of different regions of the same protein could be probed in a highly specific, and highly sensitive manner. An example of the specificity and sensitivity was observed with the oncomodulin mutant proteins, Y57W and K96W. It was shown that although positions 57 and 96 were located within 5 Å from one another, tryptophan probes in these positions displayed dramatically different fluorescence

properties suggesting important differences existed in the microenvironments of these probes. Given this information, it is not surprising that, as concluded in Section 7.1, no simple relationship could be determined between the surface exposure of the Trp residues and the magnitude of the quantum yields of fluorescence. The results presented in this thesis emphasize that the latter parameter is very sensitive to the local microenvironment of the Trp probe. The approach of comparing an identically–situated Trp probe in highly homologous proteins, or an identical Trp probe in different regions of the same protein provides a sound method of beginning to understand the relationship between probe location and fluorescence properties in a protein. By combining fluorescence spectroscopy with protein engineering it becomes possible to probe adjacent environments within a particular protein allowing more to be learned about the photophysical properties of both Trp and Tyr in proteins with respect to the detailed effects of their microenvironments.

The sensitivity of the technique also permits reliable data to be obtained from relatively small amounts of sample which is a bonus when working with biological samples that are difficult to obtain. The fact that the samples can be recovered intact after a fluorescence study provides another advantage of the technique.

Although the high sensitivity of fluorescence may be regarded as an advantage when extracting detailed information from small amounts of sample, it can simultaneously be regarded as a disadvantage. Extreme care and adequate time must be taken in obtaining homogeneous samples as even trace amounts of a highly fluorescent contaminant can lead to invalid results. Another disadvantage is the amount of attention that must be applied to instrumental details. Fluorescence

spectroscopy is a deceptively simple method owing to the ease with which data can be generated. However, as described in Chapter 2, the quality of the data depends a great deal upon the instrumental set–up. In addition, the data must be corrected to account for a number of instrumental factors. Unfortunately, it is not a rare event to discover that a reported "molecular phenomenon" is in reality an "instrumental phenomenon". For example, it was shown that the anomalous report of long–wavelength fluorescence (at wavelengths > 600 nm) of tyrosine and tryptophan (Macias et al., 1987) was due to second order diffraction characteristics of the grating monochromator, and not the electronic properties of the molecules (Hutnik & Szabo, 1988).

Unlike two–dimensional NMR which can provide an absolute global solution structure of small proteins, fluorescence is able to provide local information about differences in the conformational properties of one protein relative to another, or one form of a protein relative to another (for example, parvalbumin in the absence and presence of calcium ions) with a minimum of calculation and experimental time. However, reliable intrinsic fluorescence measurements are generally restricted to proteins containing only single tyrosine or tryptophan residues. The complexity of the data obtained from proteins containing two or more tryptophan residues requires additional investigations in order to obtain conformational information (examples are provided in a review by Beechem and Brand (1985)).

However, even in the presence of multiple amino acid probes, measurement of protein fluorescence can provide a highly sensitive method of determining the extent of protein perturbations induced by various molecular phenomena, examples including ligand binding, metal–ion interactions, protein denaturation, and protein folding. Unlike NMR which provides motion–averaged protein structures,

time–resolved spectroscopy of single tryptophan–containing proteins can provide information about different conformational states of a protein molecule. In addition, as described below, additional information about proteins can be obtained by a special application of time–resolved fluorescence spectroscopy.

In this thesis, an analysis of the time–resolved decay of the total fluorescence intensity of specifically situated tryptophan and tyrosine probes was reported. This decay was directly related to the photophysical properties of these molecules. However, if the time–resolved decay of the polarized components of the light intensity is examined, it is possible to obtain dynamic information about the rotational properties of the fluorescent molecule. Using this latter technique and the information presented in this thesis, additional information regarding nanosecond–picosecond segmental dynamics of the proteins can be obtained. Such future experiments are outlined in Section 7.2.

7.2 Future Experiments

In a time–resolved fluorescence anisotropy decay experiment, measurements are made of the intensity of light emitted parallel ($I_{\parallel}$) and perpendicular ($I_{\perp}$) to the polarization of the excitation beam. The following equations illustrate the relationship between these intensities and a number of relevant physical parameters (Cross & Fleming, 1984):

$$I_{\parallel}(t) = 1/3[S(t)(1 + 2\,r(t))], \qquad (7.1)$$

$$I_{\perp}(t) = 1/3[S(t)(1 - r(t))], \qquad (7.2)$$

$$S(t) = \sum_i \alpha_i \exp[-t/\tau_i], \qquad (7.3)$$

$$r(t) = \sum_j \beta_j \exp[-t/\phi_j], \qquad (7.4)$$

where S(t) is the time–resolved decay of the total intensity (measured as described in this thesis), r(t) is the anisotropy decay, α_i are wavelength–dependent weighting factors for the total intensity of the emission and β_j are functions of the excitation wavelength and related to the angle between the absorption and emission dipoles of the molecules and the principle diffusion axes of the molecule. ϕ_j is the rotational correlation time of the particle and for spheres this value is given by the Stokes–Einstein relationship: $\phi = \eta V/kT$, where η is the viscosity, V is the volume, k is Boltzmann's constant, and T is the absolute temperature (Weber, 1953). From equations 7.1 – 7.4 it can be seen that by an analysis of the anisotropy decay of a fluorophore, information about viscosity– and temperature–dependent rapid motions can be obtained. The rotational correlation times which are measured may reflect not only the global motions of the protein as a whole, but may also reflect localized rapid motions that are characteristic of specific segments within the protein molecule. The ability to measure subnanosecond motions of tryptophan in proteins allows anisotropy decay analysis to be one of the few experimental techniques available which can yield data to support (or refute) theoretical conclusions obtained from molecular dynamics calculations (Karplus & McCammon, 1981).

All of the single tryptophan–containing proteins examined in this thesis are

ideal candidates for anisotropy decay experiments. The presence of a single, highly sensitive fluorophore minimizes uncertainties arising from a heterogeneous population of fluorophores. The availability of crystal structures for representatives in both the azurin and parvalbumin families, as well as the availability of a crystal structure of oncomodulin, provides time–averaged information about the tryptophan environments which can aid in the rationalization of the photophysical data. By probing different regions in the oncomodulin mutant proteins, local motions which are most affected by metal ion binding may be revealed. It would be of particular interest to measure the anisotropy decay of these proteins as a function of temperature. By comparing the results obtained over a range of temperatures, additional information regarding influences upon both the global and segmental dynamics of the proteins may be obtained.

Additional information about rapid fluctuations of the protein matrices can be obtained by performing a completely different set of experiments. In equation 1.4 of this thesis, it was shown that one of the factors affecting the rate of non–radiative deactivation of a fluorophore is the rate of collisional interactions between the fluorophore and quencher molecules. A wide variety of neutral and charged molecules exist which can function as quenchers of tryptophan fluorescence upon collision (Eftink & Ghiron, 1981; Steiner & Kirby, 1969). By performing quenching studies with both neutral and charged quenchers, a quantitative assessment can be made of the relative solvent accessibility of the tryptophan residues in the proteins listed in Table 7.1. It is anticipated that largely solvent exposed residues will have much larger bimolecular quenching rate constants in the presence of the neutral quencher acrylamide when compared to more buried residues. In addition, the bimolecular quenching rate constants may provide a

measure of the relative dynamic properties of the protein matrix, as more rapidly fluctuating structures are expected to allow quenchers to diffuse more readily to the location of internally located residues. With the use of charged quenchers, the local electrostatic environment of surface exposed tryptophan residues may also be revealed.

Thus by the extension of the time–resolved fluorescence studies reported in this thesis to include anisotropy decay analysis, low temperature analysis, and diffusional quenching experiments, additional details describing the motions and flexibility that govern the conformational heterogeneity of the protein may be obtained.

7.3 References

Beechem, J. M. & Brand, L. (1985) Time–resolved fluorescence of proteins. Ann. Rev. Biochem. 54, 43–71.

Cross, A. J. & Fleming, G. R. (1984) Analysis of time–resolved fluorescence anisotropy decays. Biophys. J. 46, 45–56.

Eftink, M. R. & Ghiron, C. (1981) Fluorescence quenching studies with proteins. Anal. Biochem. 114, 199–227.

Hutnik, C. M. L. & Szabo, A. G. (1988) Long–wavelength fluorescence of tyrosine and tryptophan: A classic example of second order diffraction. Biochem. Int. 16, 587–591.

Karplus, M. & McCammon, J. A. (1981) The internal dynamics of globular proteins. CRC Crit. Rev. Biochem. 9, 293–349.

Macias, P., Pinto, M. C. & Gutierrez–Merino, C. (1987) Long–wavelength fluorescence of tyrosine and tryptophan solutions. Biochem. Int. 15, 961–969.

Steiner, R. F. & Kirby, E. P. (1969) The interaction of the ground and excited states of indole derivatives with electron scavengers. J. Phys. Chem. 73, 4130–4135.

Weber, G. (1953) Rotational brownian motion and polarization of the fluorescence of solutions. Adv. Prot. Chem. 8, 415–459.

Appendix A

CURRICULUM VITAE

N A M E

CINDY MARY–LYNN HUTNIK

PERSONAL DATA

Date of birth	February 08, 1962
Place of birth	Windsor, Ontario
Citizenship	Canadian

ACADEMIC BACKGROUND

Sept 1985–Dec 1989	*DOCTOR OF PHILOSOPHY (BIOCHEMISTRY)* University of Ottawa/National Research Council Thesis submitted – December 1989
1981–1985	*BACHELOR OF SCIENCE (HONOURS BIOCHEMISTRY)* University of Windsor
1981	*HONOURS SECONDARY SCHOOL DIPLOMA* Vincent Massey Secondary School Windsor, Ontario

MEMBERSHIP TO PROFESSIONAL BODIES

Canadian Society for Chemistry (ACIC)
Biophysical Society (American)
Spectroscopy Society of Canada
Biophysical Society of Canada

SCHOLARSHIPS AND AWARDS

NSERC Visiting Scientist in a Government Laboratory Post–doctoral Fellowship		1990
Medical Research Council— Canadian Hypertension Society Post–doctoral Fellowship		Declined
NSERC 1967 Science and Engineering Scholarship		1985–1989
Supplementary Merit Scholarship	U. Ottawa	1985–1989
Boehringer Mannheim Canada Graduate Student Award	CFBS meeting Calgary, Al.	1989
Harold Lamport Poster Competition—American Biophysical Society	Cincinnati, Ohio	1989
Talbot Travel Award—American Biophysical Society	Cincinnati, Ohio	1989
NATO–ASI Travel Award	Barga, Italy	1988
NSERC Postgraduate Scholarship		Declined
U. Ottawa Entrance Scholarship	U. Ottawa	Declined
Ontario Graduate Scholarship		Declined
Connaught Scholarship	U. Toronto	Declined
NSERC Summer Research Award		1985
The Presidents Medal (Top graduating university student)	U. Windsor	1985
The Board of Governors Medal (Top chemistry graduate)	U. Windsor	1985
The Society of Chemical Industry Merit Award		1985
U. Windsor In–Course Scholarship	U. Windsor	1985
NSERC Summer Research Award		1984

Allied Chemical Ltd. Scholarship (Top 3rd yr chemistry student)		1984
Chemical Institute of Canada Prize		1984
U. Windsor In–Course Scholarship	U. Windsor	1984
NSERC Summer Research Award		1983
JW Price Memorial Scholarship (Top 2nd yr chemistry student)	U. Windsor	1983
Archimedes Award		1983
Freshman Chemistry Award	U. Windsor	1982
U. Windsor Alumni Scholarship	U. Windsor	1981–1985
U. Windsor Entrance Scholarship	U. Windsor	Declined
U. Western Ontario Entrance Scholarship	(London)	Declined
McMaster Entrance Scholarship	(Hamilton)	Declined
Ontario Scholar		1981
Chemical Institute Of Canada Prize		1981
Carter Scholarship (Top city student)		1981
IBM Proficiency Award		1981
Academic Award (each of five yrs for maintaining A+ average)		1981
Bronze, silver and gold awards (extracurricular activities)		1981
Subject proficiency awards for obtaining top average in each of Calculus, Algebra, Functions & Relations, English, Chemistry & Biology		1981
Editor of the Year		1981

EXTRACURRICULAR ACTIVITIES

President Biochemistry Graduate Students Association	U. Ottawa	1988–1989
Graduate student representative Department of Biochemistry	U. Ottawa	1985–1989
Secretary Health Sciences Graduate Students Association	U. Ottawa	1986–1988
President of Chemistry Club	U. Windsor	1984–1985

PRESENTATIONS

HUTNIK, C.M., MacManus, J.P., Szabo, A.G. and Banville, D. "Probing the metal ion binding properties of oncomodulin using spectroscopy and site–specific mutagenesis", 32nd Annual Meeting of the Canadian Federation of Biological Societies, Calgary, Alberta, June, 1989.

HUTNIK, C.M. "The distinct effects of calcium and magnesium on the conformational properties of parvalbumin: A spectroscopic study", 33rd Annual Meeting of the American Biophysical Society, Cincinnati, Ohio, February, 1989.

HUTNIK, C.M., Szabo, A.G., MacManus, J.P. and Banville, D. "Cation–induced conformational changes of calcium–binding proteins: A time–resolved fluorescence spectroscopic study", 35th Canadian Spectroscopy Symposium, Ottawa, Ontario, Canada, August, 1988.

HUTNIK, C.M. and Szabo, A.G. "Protein Conformation and Dynamics: A time–resolved fluorescence spectroscopic study", NATO–ASI—The Enzyme Catalysis Process: Energetics Structure and Dynamics, Il Ciocco, Barga, Italy, July, 1988.

HUTNIK, C.M. and Szabo, A.G. "Fluorescence quenching studies of calcium–binding proteins: Dynamics of the protein matrix", 31st Annual Meeting of the Canadian Federation of Biological Societies, Quebec City, Quebec, Canada, June, 1988.

HUTNIK, C.M. and Szabo, A.G. "Conformational heterogeneity of homologous azurins and their metallo–derivatives: A time–resolved fluorescence study", SPIE's O–E Lase '88, Los Angeles, California, USA, January, 1988.

HUTNIK, C.M. "The blue–copper protein controversy: Conformational heterogeneity versus apo contamination", Department of Chemistry and Biochemistry, University of Windsor, Windsor, Ontario, Canada, November, 1987.

HUTNIK, C.M. and Szabo, A.G. "The Interrelationship between protein function and protein structure and dynamics using time–resolved fluorescence", Protein Engineering Workshop, Biotechnology Research Institute, Montreal, Quebec, Canada, May, 1987.

HUTNIK, C.M. "Protein dynamics and azurin", Protein Biochemistry and Spectroscopy Seminar Series, Division of Biological Sciences, National Research Council of Canada, Ottawa, Ontario, Canada, November, 1986.

PUBLICATIONS (Full Papers)

HUTNIK, C.M.L. and Szabo, A.G. (1988) "Long–wavelength fluorescence of tyrosine and tryptophan: A classic example of second order diffraction", *Biochemistry International* 16 (4), 587–591.

HUTNIK, C.M.L. and Szabo, A.G. (1988) "Conformational heterogeneity of homologous azurins and their metallo–derivatives: A time–resolved fluorescence study", in *Time–Resolved Laser Spectroscopy in Biochemistry*, J.R. Lakowicz, ed., SPIE Proceedings, Volume 909, 301–302.

MacManus, J.P., *HUTNIK, C.M.L.*, Sykes, B.D., Szabo, A.G., Williams, T. and Banville, D. (1989) "Characterization and site specific mutagenesis of the calcium–binding protein oncomodulin produced by recombinant bacteria", *Journal of Biological Chemistry* 264, 3470–3477.

HUTNIK, C.M.L. and Szabo, A.G. (1989) "Confirmation that multiexponential fluorescence decay behaviour of holoazurin originates from conformational heterogeneity", *Biochemistry* 28, 3923–3934.

HUTNIK, C.M.L. and Szabo, A.G. (1989) "A time–resolved fluorescence study of azurin and metallo azurin derivatives", *Biochemistry* 28, 3935–3939.

HUTNIK, C.M.L., MacManus, J.P. and Szabo, A.G. (1989) "A calcium–specific conformational response in parvalbumin", *Biochemistry* (Accepted with minor revision).

HUTNIK, C.M.L., MacManus, J.P., Banville, D. and Szabo, A.G. (1989) "Comparison of metal ion–induced conformational changes in parvalbumin and oncomodulin as probed by the intrinsic fluorescence of tryptophan–102", *Journal of Biological Chemistry* (Accepted with minor revision).

HUTNIK, C.M.L., MacManus, J.P., Banville, D. and Szabo, A.G. (1989) "The origin and relevance of Ca^{2+}–specific fluorescence changes in oncomodulin using site–specific mutagenesis. I. Tyrosine–containing mutants", *Biochemistry* (Submitted).

HUTNIK, C.M.L., MacManus, J.P., Banville, D. and Szabo, A.G. (1989) "The origin and relevance of Ca^{2+}–specific fluorescence changes in oncomodulin using site–specific mutagenesis. II. Tryptophan–containing mutants", *Biochemistry* (Submitted).

HUTNIK, C.M.L. and Szabo, A.G. (1989) "Acrylamide quenching of Trp–102 in cod III parvalbumin: Static quenching versus non–linear diffusion", *Biophysical Journal* (In preparation).

PUBLICATIONS (Abstracts)

MacManus, J.P., Hogue, C., *HUTNIK, C.M.L.*, Banville, D. and Szabo, A.G. (1990) "Fluorescent monitoring of metal–binding to tryptophan mutants of oncomodulin", Seventh International Symposium on Calcium–Binding Proteins in Health and Disease (Banff, Alberta: March, 1990).

HUTNIK, C.M.L., MacManus, J.P., Banville, D. and Szabo, A.G. (1989) "Probing the metal ion induced properties of oncomodulin using site–specific mutagenesis and spectroscopy", CFBS Proceedings (Calgary, Alberta: June, 1989), Volume 32, 273.

Szabo, A.G., *HUTNIK, C.M.L.*, Krajcarski, D.T. and Willis, K. (1989) "Time–resolved fluorescence of mutant proteins", CFBS Proceedings (Calgary, Alberta: June, 1989), Volume 32, 540.

HUTNIK, C.M.L. (1989) "The distinct effects of calcium and magnesium on the conformational properties of parvalbumin: A spectroscopic study", Biophysical Journal, 55, 516a.

HUTNIK, C.M.L., Szabo, A.G., MacManus, J.P. and Banville, D. (1988) "Cation–induced conformational changes of calcium–binding proteins: A time–resolved fluorescence spectroscopic study", 35th Canadian Spectroscopy Symposium, Ottawa, Ontario, Canada, August, 1988.

HUTNIK, C.M.L. and Szabo, A.G. (1988) "Protein conformation and dynamics: A time–resolved fluorescence spectroscopic study", NATO–ASI–The Enzyme Catalysis Process: Energetics Structure and Dynamics, Il Ciocco, Barga, Italy, July, 1988.

HUTNIK, C.M.L. and Szabo, A.G. (1988) "Fluorescence quenching studies of calcium–binding proteins: Dynamics of the protein matrix", CFBS Proceedings (Quebec City, Quebec: June, 1988), Volume 31, 540.

WORK EXPERIENCE

ACADEMIC INSTRUCTION:

Undergraduate Laboratory Demonstrator	3rd year Physical Biochemistry	1986–1989
Undergraduate Laboratory Demonstrator	3rd year Analytical Chemistry	1985

Teaching Assistant	1st year Calculus	1985

RESEARCH:

The purification of bovine brain calcineurin	U. Windsor	1985
^{19}F–NMR studies of fetuin	U. Windsor	1984
The immobilization of glucose oxidase on polyacrylamide beads	U. Windsor	1983